

Macroscopic aspects of ferromagnetic nematic phases, tetrahedral order in ferrogels, and magnetorheological fluids

Der Universität Bayreuth
zur Erlangung des Grades
„Doktor der Naturwissenschaften“ (Dr. rer. nat.)
genehmigte Abhandlung

vorgelegt von

Tilen Potisk
geboren in Kranj, Slowenien

1. Gutachter:	Prof. Dr. H. R. Brand
2. Gutachter:	Priv.-Doz. Dr. A. Menzel
Tag der Einreichung:	20. 5. 2019
Tag des Kolloquiums:	26. 7. 2019

Contents

Summary	ii
Zusammenfassung	v
1 Introduction	1
1.1 Ferrofluids	1
1.2 Nematic liquid crystals	2
1.3 Ferromagnetic nematics	4
1.4 Tetrahedral order	6
1.5 Ferrogels	8
1.6 Magnetorheological fluids	9
1.7 Macroscopic dynamics	10
2 Overview of the publications	15
2.1 Magneto-optic dynamics of a ferromagnetic nematic liquid crystal	15
2.2 Effects of flow on the dynamics in a ferromagnetic nematic liquid crystal	20
2.3 Dynamic interplay of nematic, magnetic, and tetrahedral order in ferromagnetic nematics	24
2.4 Influence of tetrahedral order on ferromagnetic gels	27
2.5 A continuum model of magnetic field induced viscoelasticity in magnetorheological fluids	29
2.6 References	35
2.7 Publications	42
Acknowledgement	121
Erklärung	123

Summary

This thesis deals with the construction of macroscopic models for several magnetic macroscopic phases. The results are applied to the available experimental data or simple experimental suggestions are made for detecting static or dynamic aspects of each phase. The considered magnetic systems are ferromagnetic nematic liquid crystals, tetrahedral ferromagnetic gels and magnetorheological fluids. A common feature in the description of these systems is the inclusion of an independent dynamic equation for the magnetization. This is a variable that changes sign under time reversal. Such behavior introduces profound consequences on the static as well as dynamic phenomena, which are not possible in nonmagnetic systems. The approach used in this thesis is macroscopic dynamics which is based on linear irreversible thermodynamics. The equations are nevertheless highly nonlinear as the transport tensors are generally dependent on the variables. Macroscopic dynamics provides a systematic description valid on length and time scales much larger than the ones characteristic for microscopic degrees of freedom. It can be applied to many different systems and to different geometries.

In the Introduction various macroscopic phases are presented that can be seen as basic ingredients of the magnetic phases we model. The first two sections deal with ferrofluids and nematic liquid crystals, which are used in the synthesis of ferromagnetic nematics described in the following section. The next two sections present tetrahedral order and ferrogels, since a part of the thesis is devoted to describe the effects of the tetrahedral order in ferrogels as well as in ferromagnetic nematics. Next we consider the magnetorheological fluids. At the end of the Introduction, a section is devoted to a short introduction to macroscopic dynamics, which was the main approach used in this thesis to derive the dynamic equations.

Fairly recently ferromagnetic nematic liquid crystals were experimentally realized for the first time. This is considered to be the first room temperature ferromagnetic liquid. This discovery gives a way to study interesting phenomena in ferromagnetism. A magnetic domain, for example, can flow, which is not possible in solid ferromagnets. Several experiments were performed on this phase to characterize the optical response to external magnetic fields. Owing to the spontaneous magnetization there are various effects not present in usual nematic liquid crystals. One such effect is the dissipative cross-coupling between the magnetization and the director field. We have shown that the presence of such dynamic coupling is crucial to explain the experimentally investigated initial behavior of the phase difference of the transmitted light across a sample of a ferromagnetic nematic and secondly, it is the simplest possible mechanism to explain the linear dependence of the reorientation relaxation rate on the applied magnetic field. The determination of the dissipative cross coupling has already been proven to be robust when comparing results for different concentrations and when a different nematic liquid crystal is used as a solvent. The values of other reversible and dissipative transport coefficients still have to be determined. We have made simple suggestions for measuring certain combinations of the dynamic coefficients using simple shear flow. We extended the notion of the Miesowicz viscosities to ferromagnetic nematics and we showed that due to the additional orientational order of ferromagnetic nematics, there are nine such viscosities in contrast to three in usual nematics. Furthermore, it was shown that an application of a small magnetic field can shift the critical shear rate of the tumbling regime.

With the advent of certain bent-core liquid crystals it has become clear that the usual description using a director field does not account for all experimental observations such as the

isotropic to isotropic phase transition, shifts of the temperature of the phase transition linear in an electric field, *etc.* The simplest possible mechanism to account for these properties is the presence of a tetrahedral order. A characteristic property of such an order is that it breaks the inversion symmetry of the phase. If orientational order is present in addition to the tetrahedral order, helical configurations of either hand existing simultaneously can be found. This is a remarkable property, as the molecules are not chiral, which one might be tempted to think due to the helix formation. We have derived static and dynamic equations for a hypothetical phase where the tetrahedral order is combined with the ferromagnetic nematic phase. The motivation for such a study comes from the recent successful experimental realizations of ferromagnetic fluid phases as well as the distinct features of bent-core liquid crystals. The ground state of this hypothetical phase would break time reversal symmetry, due to the spontaneous magnetization, as well as parity due to the tetrahedral structure. We find several interesting static as well as dynamic effects. The presence of the spontaneous magnetization promotes the formation of helices through a linear gradient term in the free energy. Especially intriguing are the dynamic effects of a temperature gradient. We find that it can drive reversible director rotations and it is only possible if both time reversal and parity are broken.

Experimentally it is known that certain phases made from bent-core molecules produce macroscopic chiral domains of either hand. An existing model accounts for these observations by the simultaneous presence of the tetrahedral order and a transient network. A natural question arises on the effects when one combines tetrahedral order with the ferromagnetic gel phases. From the applications point of view, ferrogels are commonly considered as actuators or in medicine for drug release mechanism. The reason behind this is that they can be manipulated strongly using external magnetic fields. We find that the presence of tetrahedral order in ferromagnetic gels gives unique properties when dealing with mechanical forces. A uniaxial compression for example, produces interesting spatially modulated patterns of the magnetization that can only arise when tetrahedral order is present. Different spatial patterns occur when the gel is sheared. For a transient network, we furthermore find that a temperature gradient along the spontaneous magnetization induces shear stresses, which could be measured by mechanical means. If the external temperature gradient is applied perpendicularly to the magnetization the value of the induced shear stress depends on the angle between the gradient and the orientation of the tetrahedral structure. In principle one could then determine the orientation of the tetrahedral structure, which is not possible using light scattering experiments as they are optically isotropic.

Lastly, we deal with magnetorheological fluids. These fluids are useful in vibration control, for example as part of the suspension systems in cars, dampers or clutches. They have an extremely important ability of magnetic field induced transitions from a liquid-like behavior in the off state to a solid-like behavior when an external magnetic field is applied. Knowing the dynamics of such a system is therefore of practical importance. We show that a dynamic interplay of magnetization and the strain field is enough to explain many features of magnetorheological fluids, such as the magnetic field dependence of the yield stress. This is made possible by a quadratic dependence of the elastic moduli on the magnetization. We also find that the flow curves exhibit a steep increase for low shear rates and a peak structure at intermediate shear rates and higher magnetic fields. This also indicates that shear thinning, which is usually observed in magnetorheological fluids, is captured by this model. We furthermore find specific frequency dependent behavior of the storage and loss moduli. For instance, the loss modulus

appears to have a maximum and a minimum at intermediate frequencies. For the minimum we also predict a shift to higher frequencies as one increases the external magnetic field. All these phenomena can be accounted for already on the macroscopic level without considering microscopic features of magnetorheological fluids.

Zusammenfassung

Diese Dissertation befasst sich mit der Herleitung einer makroskopischen Beschreibung für mehrere magnetische makroskopische Phasen. Die Ergebnisse werden mit den verfügbaren experimentellen Daten verglichen und wir machen einfache experimentelle Vorschläge zur Messung statischer oder dynamischer Aspekte jeder Phase. Die betrachteten magnetischen Systeme sind ferromagnetische nematische Flüssigkristalle, tetrahedrale ferromagnetische Gele und magnetorheologische Flüssigkeiten. Ein gemeinsames Merkmal in der Beschreibung dieser Systeme ist die Einbeziehung einer unabhängigen dynamischen Gleichung für die Magnetisierung. Diese ist eine Variable, die das Vorzeichen unter Zeitumkehr ändert. Ein solches Verhalten führt zu tiefgreifenden Folgen für die statischen und dynamischen Phänomene, die in nichtmagnetischen Systemen nicht möglich sind. In dieser Dissertation wird die Methode der makroskopischen Dynamik verwendet, die auf linearer, irreversibler Thermodynamik basiert. Die Gleichungen sind jedoch stark nichtlinear, weil generell die Transporttensoren von den Variablen abhängig sind. Die makroskopische Dynamik liefert eine systematische Beschreibung, die auf Längen- und Zeitskalen gültig ist, welche viel größer sind als die für mikroskopische Freiheitsgrade charakteristischen Skalen. Man kann deswegen die makroskopische Dynamik auf viele verschiedene Systeme und auf verschiedene Geometrien anwenden.

In der Einführung werden verschiedene makroskopische Phasen vorgestellt, die als Bestandteile der magnetischen Phasen, die wir modellieren, angesehen werden können. In den ersten zwei Abschnitten geht es um Ferrofluide und nematische Flüssigkristalle, die bei der Synthese der ferromagnetischen nematischen Flüssigkristalle verwendet werden. Die ferromagnetischen nematischen Flüssigkristalle werden dann im folgenden Abschnitt beschrieben. Die nächsten zwei Abschnitte präsentieren tetrahedrale Ordnung und Ferrogele, da ein Teil der Dissertation der Beschreibung der Auswirkungen von tetrahedralear Ordnung sowohl auf Ferrogele als auch auf ferromagnetische nematische Flüssigkristalle gewidmet ist. Dann betrachten wir magnetorheologische Flüssigkeiten. Das Ende dieses Kapitels widmet sich einer kurzen Einführung in die makroskopische Dynamik, die der Hauptzugang in dieser Dissertation war, um die dynamischen Gleichungen herzuleiten.

Vor kurzem wurden ferromagnetische nematische Flüssigkristalle erstmals experimentell realisiert. Diese gelten als die erste ferromagnetische Flüssigkeiten bei Raumtemperatur. Diese Entdeckung ermöglicht es, interessante Phänomene im Ferromagnetismus zu studieren. Eine magnetische Domäne kann beispielsweise fließen, was in festen Ferromagneten nicht möglich ist. Für diese Phase wurden mehrere Experimente durchgeführt, um die optische Antwort auf äußere Magnetfelder zu charakterisieren. Aufgrund der spontanen Magnetisierung gibt es verschiedene Effekte, die in üblichen nematischen Flüssigkristallen nicht vorhanden sind. Ein solcher Effekt ist die dissipative Kreuzkopplung zwischen der Magnetisierung und dem Direktorfeld. Wir haben gezeigt, dass das Vorhandensein einer solchen dynamischen Kopplung entscheidend ist, um das Anfangsverhalten der Phasendifferenz des durchgehenden Lichts für eine Probe der ferromagnetischen nematischen Flüssigkristalle zu erklären. Weiterhin ist es der einfachste Mechanismus die lineare Abhängigkeit der Relaxationsrate der Orientierung vom Magnetfeld zu erklären. Die Bestimmung der dissipativen Kreuzkopplung hat sich bereits beim Vergleich der Ergebnisse für unterschiedliche Konzentrationen und bei der Verwendung anderer nematischer Flüssigkristalle als Lösungsmittel als robust erwiesen. Die Werte anderer reversibler und dissipativer Transportkoeffizienten müssen noch ermittelt werden. Wir haben

einfache Vorschläge für die Messung bestimmter Kombinationen der dynamischen Koeffizienten mit einfacher Scherströmung gemacht. Wir haben die Miesowicz Viskositäten auf ferromagnetische nematische Flüssigkristalle verallgemeinert und gezeigt, dass es aufgrund der zusätzlichen Orientierungsordnung der ferromagnetischen nematischen Flüssigkristalle neun solche Viskositäten gibt, im Gegensatz zu drei in gewöhnlichen nematischen Flüssigkristallen. Weiterhin kann man zeigen, dass eine Anwendung eines kleinen Magnetfeldes die kritische Scherrate des Tumbling-Regimes verschieben kann.

Es ist mit dem Aufkommen bestimmter Flüssigkristallphasen, die von bent-core Molekülen gebildet werden, klar geworden, dass die übliche Beschreibung des Systems mit einem Direktorfeld nicht alle experimentellen Beobachtungen, wie zum Beispiel einen isotrop zu isotrop Phasenübergang, Verschiebung der Temperatur des Phasenübergangs linear in einem elektrischen Feld, *usw.*, beschreiben kann. Der einfachste Mechanismus, diese Eigenschaften zu berücksichtigen, ist die Gegenwart einer tetrahedralen Ordnung. Eine charakteristische Eigenschaft einer solchen Ordnung ist die Brechung der Inversionssymmetrie in einer solchen Phase. Wenn zusätzlich zur tetrahedralen Ordnung eine Orientierungsordnung vorhanden ist, können gleichzeitig Helices beider Händigkeiten gefunden werden. Dies ist eine bemerkenswerte Eigenschaft, weil die Moleküle nicht chiral sind, was man aufgrund der Helixbildung denken könnte. Wir haben statische und dynamische Gleichungen für eine Phase hergeleitet, in der die tetrahedrale Ordnung mit der ferromagnetischen nematischen Phase kombiniert ist. Die Motivation für eine solche Studie ergibt sich aus den jüngsten erfolgreichen experimentellen Realisierungen ferromagnetischer Flüssigkristallphasen sowie den Besonderheiten von bent-core-Flüssigkristallen. Der Grundzustand dieser hypothetischen Phase würde die Zeitumkehrsymmetrie, aufgrund der spontanen Magnetisierung, sowie die Parität, aufgrund der tetrahedralen Struktur, brechen. Wir finden mehrere interessante statische und dynamische Effekte. Das Vorhandensein der spontanen Magnetisierung verursacht die Bildung von Helices durch einen linearen Gradiententerm in der freien Energie. Besonders faszinierend sind die dynamischen Effekte eines Temperaturgradienten. Wir zeigen, dass ein Temperaturgradient zu reversiblen Direktor-Rotationen führen kann; dies ist nur möglich, wenn beide, die Zeitumkehr und die Parität, gebrochen sind.

Experimentell ist bekannt, dass bestimmte Phasen aus bent-core Molekülen makroskopische chirale Domänen beider Hände erzeugen. Ein bestehendes Modell erklärt diese Beobachtungen durch das gleichzeitige Vorhandensein einer tetrahedralen Ordnung und eines transienten Netzwerks. Eine natürliche Frage stellt sich bzgl. der neu auftretenden Effekte, wenn man tetrahedrale Ordnung mit ferromagnetischen Gelphasen kombiniert. Aus der Sicht der Anwendungen werden Ferrogele häufig als Aktuatoren oder in der Medizin als Vehikel zur Medikamentenfreisetzung ins Auge gefasst. Der Grund dafür ist, dass sie mit externen Magnetfeldern leicht manipuliert werden können. Wir finden, dass das Vorhandensein von tetrahedraler Ordnung in ferromagnetischen Gelen einzigartige Eigenschaften zeigt, wenn man mechanische Kräfte anlegt. Eine uniaxiale Kompression erzeugt zum Beispiel interessante räumlich modulierte Muster der Magnetisierung, die nur existieren, wenn tetrahedrale Ordnung vorhanden ist. Verschiedene räumliche Muster treten auf, wenn man das Gel schert. Für ein transientes Netzwerk finden wir weiterhin, dass ein Temperaturgradient parallel zur spontanen Magnetisierung Scherspannungen induziert, die man mechanisch messen kann. Wenn der äußere Temperaturgradient senkrecht zur Magnetisierung angelegt wird, hängt der Wert der induzierten Scherspannung vom Winkel zwischen dem Gradienten und der Ausrichtung der tetrahedralen Struktur ab. Prinzipiell kann man dann die Ausrichtung der tetrahedralen Struktur messen, was mit Licht-

streuexperimenten nicht möglich ist, weil tetrahedrale Strukturen optisch isotrop sind.

Schließlich beschäftigen wir uns mit magnetorheologischen Flüssigkeiten. Diese Flüssigkeiten sind für das Gebiet der Schwingungskontrolle nützlich, zum Beispiel als Teil der Federungssysteme in Fahrzeugen, als Dämpfer oder Kupplungen. Sie zeigen die überaus interessante Eigenschaft eines Übergangs von einem flüssigkeitsähnlichen Verhalten im aus-Zustand zu einem festen Verhalten, wenn man ein externes Magnetfeld anlegt. Es ist deswegen von praktischer Bedeutung die Dynamik solcher Systeme zu verstehen. Wir zeigen, dass ein dynamisches Zusammenspiel der Magnetisierungsvariablen und des Dehnungsfeldes ausreicht, viele Eigenschaften magnetorheologischer Flüssigkeiten zu beschreiben, zum Beispiel die Magnetfeldabhängigkeit des yield stress. Dies wird durch eine quadratische Abhängigkeit der elastischen Moduln von der Magnetisierung ermöglicht. Wir zeigen, dass die Strömungskurven einen steilen Anstieg für niedrige Scherraten und eine Peakstruktur bei mittleren Scherraten und höheren Magnetfeldern aufweisen. Dies zeigt auch, dass Scherverdünnung, die normalerweise in magnetorheologischen Flüssigkeiten beobachtet wird, von diesem Modell erfasst wird. Des Weiteren finden wir spezifisches frequenzabhängiges Verhalten der Speicher- und Verlustmoduln. Zum Beispiel, hat der Verlustmodul ein Maximum und ein Minimum bei mittleren Frequenzen. Für das Minimum sagen wir eine Verschiebung zu höheren Frequenzen vorher, wenn man das äußere Magnetfeld erhöht. Alle diese Phänomene können bereits auf makroskopischer Ebene beschrieben werden, ohne die mikroskopischen Eigenschaften magnetorheologischer Flüssigkeiten zu berücksichtigen.

Chapter 1

Introduction

In this chapter I give a short overview of the basic physical systems and concepts, which were the main focus of this work. I start with ferrofluids and nematic liquid crystals, which are the basic ingredients for the synthesis of ferromagnetic nematic liquid crystal phases, presented in the following section. I continue with a description of the tetrahedral order which we combined with the ferromagnetic nematic phase and ferrogels. In Sec. 1.6 I also give a short overview of the properties of magnetorheological fluids. At the end of this chapter in Sec. 1.7 I present the concepts of macroscopic dynamics, which is the main approach used in this thesis to derive the governing equations.

1.1 Ferrofluids

Ferrofluids are suspensions of ferromagnetic nanoparticles in a carrier liquid, which is typically water or an organic solvent [1,2]. A common choice for the magnetic nanoparticles are usually iron oxides (such as magnetite or hematite) or cobalt with a particle diameter of about 10 nm [2].

An external magnetic field aligns the magnetic moments in the direction parallel to the imposed field. The initial magnetic susceptibility is orders of magnitude higher than in usual paramagnetic liquids, which means ferrofluids exhibit liquid as well as superparamagnetic behavior [3]. After the field is switched off the magnetization relaxes by rotation of the particles itself (Brownian relaxation) or by rotation of the magnetic moment within the particle (Neel relaxation) [4]. Usual ferrofluids exhibit a complex combination of both processes. For smaller sized magnetic particles the Neel relaxation is much faster than the Brownian relaxation, while for larger sized particles, the Brownian relaxation dominates and the particles are also referred to as magnetically hard. The field of ferrofluid research developed quickly after first stable ferrofluids were synthesized in the 1960's [5]. The magnetic particles have a tendency to agglomerate, largely due to the attractive van der Waals interactions and also due to magnetic dipole forces. To inhibit this agglomeration, one can either charge the particles, thereby introducing a strong enough electrostatic repulsion, or coat the particles using special organic molecules, also called surfactants. These molecules induce steric repulsion, which keeps the particles apart and stabilizes the suspension [3,6].

The application of a magnetic field leads to a significant rise of the viscosity. This was first measured in ferrofluids composed of magnetite nanoparticles [7], followed soon afterwards by

diluted cobalt based ferrofluids [8]. On the theoretical side this effect was first studied in Ref. [4], while the dynamics of ferrofluids was modeled macroscopically in Ref. [9]. In Refs. [10, 11] the (reversible) coupling of the magnetization to the symmetric velocity gradient was crucial to explain the experimental data. By measuring this coupling one can also estimate the length of magnetic chains, which is typically between 2 and 5 particle diameters.

Ferrofluids are used in various areas of applications such as in computer hard drives, where ferrofluid seals prevent debris from entering the devices. They can be used as dampers. In biomedical applications they are used as a contrast fluid in magnetic resonance imaging [12]. They even have the potential to be used in cancer treatment by the use of magnetic hyperthermia. This technique utilizes oscillating magnetic fields, which cause the particles to heat up and in turn damage the tumor without heating the surrounding tissue. Ferrofluids have been shown to be useful in magnetically controlled drug targeting, where drugs are bound with magnetic particles and released at the area of interest [13, 14].

1.2 Nematic liquid crystals

Certain organic compounds show a series of intermediate phases (mesophases) between the liquid and the solid state [15]. Such a material can flow like an ordinary liquid, but can also show additional orientational or partial positional order, which indicates solid-like properties. Consequently, these phases are also called liquid crystals.

The molecules that form these liquid crystals are usually highly anisotropic in the form of rod-like or disk-like molecules. There are many different mesophases, since there are numerous combinations that orientational and positional symmetries can be broken. The classification of different types of phases was first done in 1922 by Friedel [16], where liquid crystals were divided into three different classes; nematics, cholesterics and smectics. The simplest possible phase is the nematic phase, which is characterized by a long-range orientational order, while the positions of the molecules are still random, Fig. 1.1. This orientational order is for uniaxial nematics described by the so called director \mathbf{n} , with the additional identification of head-tail symmetry $\mathbf{n} \leftrightarrow -\mathbf{n}$ for non-polar materials. For biaxial nematics an additional director is needed \mathbf{l} , with the equivalent symmetry $\mathbf{l} \leftrightarrow -\mathbf{l}$. It should be noted, that biaxiality can be induced in uniaxial nematics by large external fields. Throughout this thesis we discard any biaxiality. The strength of the nematic ordering is described by the scalar order parameter $S = \frac{1}{2}(3\langle \cos^2 \theta \rangle - 1)$, with θ the angle between the molecular axis and the director and $\langle . \rangle$ the thermal average. It takes the values between $-1/2$ and 1 with 1 corresponding to the case where all the molecules point along the director and 0 in the isotropic phase, where the molecules are oriented randomly. In usual nematics $S \sim 0.5 - 0.6$ at room temperature [15]. Very often the director and the scalar order parameter are combined into a symmetric traceless tensorial order, which reads for uniaxial nematics $Q_{ij} = \frac{1}{2}S(3n_i n_j - \delta_{ij})$, with δ_{ij} being the Kronecker delta. Throughout this work we assume the scalar order parameter to be constant, which is a valid assumption if one is far away from the isotropic-nematic phase transition or sufficiently far away from defects. We therefore use the director \mathbf{n} to characterize the orientational order and ensure all equations are invariant with respect to the head-tail symmetry.

Cholesterics are chiral liquid crystals, which break the inversion symmetry and have a strong tendency to form helical structures. Chiral nematics for example can be obtained by doping

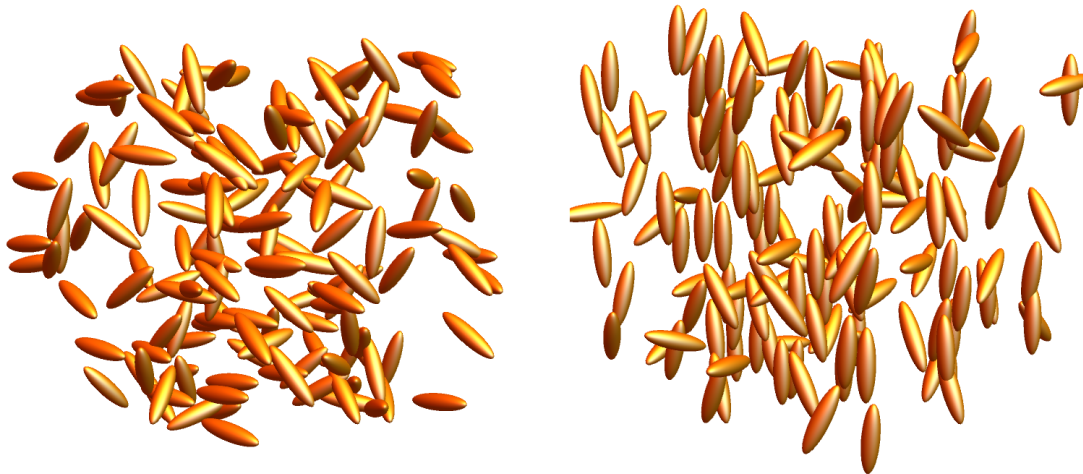


Figure 1.1: A schematic of a liquid crystal in the isotropic phase (left) and in the nematic phase (right) with $S \approx 0.8$.

nematic liquid crystals by chiral molecules. The pitch of the helices is frequently on the order of several 100 nanometers, which is the reason they often appear colorful due to Bragg reflection being in the visible spectrum of light. The pitch is sensitive to temperature, external fields and concentration of the chiral dopant.

Smectic phases are characterized in addition to the orientational order by some degree of positional order. In the smectic-A (SmA) phase for example, the translational order is broken once and the molecules form layers, with the director \mathbf{n} on average parallel to the layer normal. In the smectic-C (SmC) phase, the director is tilted with respect to the layer normal.

The continuum (static) theory of liquid crystals started in the 1930's with the works of Oseen [17] and Zocher [18], which was later developed further by Frank [19] and Ericksen [20]. Later on Ericksen derived the dynamic theory for nematic liquid crystals [21], which was completed by Leslie [22]. The set of these equations together with the constitutive relations form the so called Ericksen-Leslie theory. In the 1970's the linear hydrodynamic approach was used to derive the dynamic equations [23, 24]. The advantages of this approach is that there is a clear distinction between reversible and irreversible processes [25] and it can be easily extended to nonlinear descriptions [26] and to more complex systems. This approach will also be described at the end of this chapter.

Liquid crystals in sufficiently thick layers appear turbid. Their scattering cross section is of the order of 10^6 higher than in usual isotropic liquids [15]. In fact, when liquid crystals were first discovered by Reinitzer [27] and Lehmann [28], they observed a cloudy phase above the melting temperature of cholesterol. As they heated this phase further it transformed into a transparent liquid. First detailed experiments on light scattering were done by Chatelain [29]. It was later understood that the dominant contribution to the scattering of light in nematic liquid crystals is caused by the thermal fluctuations of the director field \mathbf{n} [30]. This is because fluctuations of the orientation are strongly related to the fluctuations of the dielectric tensor, which causes the scattering.

Due to their anisotropic optical properties and high sensitivity to external electric fields, liquid crystals are of great importance in display devices. In liquid crystal displays (LCDs) a nematic liquid crystal is placed between two parallel layers located between two polarizers. The polarizers are crossed and the ground state assumes a twist of 90 degrees across the cell. Such a slow rotation of the director acts as a waveguide [31] and allows the light to pass through. If a strong enough electric field of order of 1 V is applied perpendicularly to the layers, the director field aligns along the electric field and the device is no longer transparent.

Recently, cholesteric liquid crystals were proposed to be used in security applications, such as the authentication of people. The idea behind this makes use of colored patterns coming from Bragg reflections of shells of cholesteric liquid crystals [32].

1.3 Ferromagnetic nematics

Ferromagnetism is a phenomenon well known in solids. In 1970 an idea to generate a liquid ferromagnet was proposed by Brochard and de Gennes [33]. The claim was that by introduction of ferromagnetic nanoparticles in a nematic liquid crystal one could induce a phase showing simultaneously ferromagnetic and nematic ordering. The synthesis and experimental characterizations of magnetic fluids combined with nematic phases followed soon afterwards [34–39]. These experimental works did not lead to ferromagnetic nematic phases, as the particles were too large and not well enough characterized. In more concentrated systems, phase separation and segregation as well as aging were the big problems. Such phases are called ferronematics, where the spontaneous magnetization is zero. They respond superparamagnetically to the external magnetic field, and typically show a substantial lowering of the critical magnetic field of the Fredericks transition [40, 41]. Ferronematics have recently also been synthesized using spindle-like magnetic particles with the magnetic moments oriented perpendicularly to their main axes [42].

Only rather recently the group of Lisjak and Mertelj successfully experimentally realized ferromagnetic nematic phases [43] and characterized their macroscopic properties [44, 45]. A key step in obtaining a ferromagnetic phase was to use platelet-like magnetic nanoparticles, Fig. 1.2. They used barium hexaferrite particles ($\text{BaSc}_x\text{Fe}_{12-x}\text{O}_{19}$) with a diameter of 70 nm and thickness of 5 nm, which were covered by dodecylbenzenesulphonic acid (DBSA). This is a common surfactant used in colloidal suspensions to ensure that the molecules of the nematic liquid crystal prefer a perpendicular (homeotropic) orientation with respect to the platelets. This shape, together with homeotropic anchoring, induces a quadrupolar distortion of the nematic director field around the platelets, which prevents aggregation in the direction of the director. Furthermore, the magnetic interaction prefers parallel orientation of the dipoles, resulting in ferromagnetism [46].

Magnetic particles were then suspended in a nematic liquid crystal (common choices are 5CB [43, 44, 47, 48], E7 [49], 7CB [49], 8CB [45]) above the nematic-isotropic phase transition temperature. The suspension was then filled in a liquid crystal cell between two parallel glass plates 20 micrometers apart, with rubbed surfaces, so that the preferred orientation of the nematic liquid crystal was parallel to the plates (planar orientation). During the filling a small magnetic field of 8 mT was applied parallel to the rubbing direction to ensure a monodomain sample. Typical values of the magnetization are 50 A/m - 300 A/m [43–45, 49], which is

equivalent to a magnetic field of 0.06 mT to 0.38 mT.

Static measurements were performed on a sample of a ferromagnetic nematic confined between two parallel plates, about $20\ \mu\text{m}$ apart. The sample was put between two crossed polarizers and the intensity of the transmitted light was measured. Measurements revealed a strong magneto-optic response at very small magnetic fields of order 5 mT [43, 44]. This is due to the linear coupling of the spontaneous magnetization with the magnetic field and a static coupling between the director and the magnetization. Furthermore, shear flow experiments revealed a strong magnetoviscous effect, where the effective viscosity could be doubled using magnetic fields of order 20 mT.

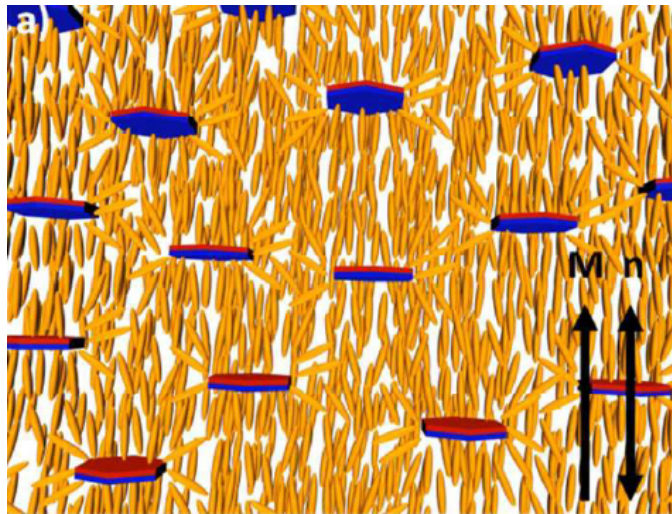


Figure 1.2: A microscopic picture of a ferromagnetic nematic. Taken from Ref. [49].

On the theoretical side, ferronematics were first considered in Ref. [33], where the free energy was derived by considering orientational distortions induced in a nematic liquid crystals by a magnetic grain. In addition a strong anchoring of the director \mathbf{n} and the local magnetization \mathbf{M} was assumed. It was soon shown that such an approximation is not applicable in thermotropic ferronematics [35]. A finite anchoring of the director to the magnetic grains has been considered in Refs. [50, 51], thereby treating \mathbf{n} and \mathbf{M} as independent variables. Macroscopically ferromagnetic nematics were modeled by assuming the magnetization is already relaxed to the value and the direction set by the external magnetic field in Ref. [52]. The dynamic effects in such a system are technically also present in usual nematic liquid crystals, but there is a much higher chance they would be observed in ferronematics. A model, taking into account the magnetization as an independent dynamic variable Ref. [53] followed soon afterwards. Suspensions of magnetic particles in a liquid crystal were also studied microscopically using molecular dynamics simulations [54].

Since the discovery of ferromagnetic nematics in 2013, additional ferromagnetic fluid phases have been synthesized. We first mention the biaxial ferromagnetic nematic [48]. There a conical anchoring of the nematic molecules on the surfaces of the platelets was achieved, which gave rise to a rich variety of domain structures. Secondly, ferromagnetic cholesteric liquid crystals have been synthesized using platelet shaped particles [47, 55, 56].

Since the director and the magnetization are coupled, \mathbf{n} is also coupled indirectly to the

external magnetic field and the magnetization to the external electric field. The former can be detected in the form of the magneto-optic effect, while the latter is called converse magnetoelectric effect [43]. Ferromagnetic nematics can be manipulated using a very weak external magnetic field. Consequently they have a potential use in magneto-optic devices, or as a visualization of small magnetic fields [57]. An advantage of the magnetic field compared to the use of the electric fields, is that the former can be applied without any contact and in any direction, whereas the use of the latter is limited by the geometry of the electrodes.

1.4 Tetrahedral order

In a certain class of liquid crystals formed by bent-core [58–70] or ferrocene-type molecules [71, 72], unusual properties have been observed. Examples are isotropic-isotropic phase transitions, where the higher temperature is the truly isotropic liquid, while the other is only optically isotropic, but has lower symmetry. In such liquid crystals it is possible to induce nematic order linearly in an electric field as well as shift the phase transition temperature up to 10 K linearly in an electric field. Some compounds, composed of achiral bent-core molecules, show a spontaneous formation of left and right handed domains [58, 62, 68].

A candidate to model such a behavior is the presence of tetrahedral order [73–77], which can be represented by 4 vectors spanning a tetrahedron. The tetrahedral order parameter T_{ijk} is a fully symmetric third rank tensor [78, 79]

$$T_{ijk} = T_0 \sum_{\beta=1}^4 n_i^\beta n_j^\beta n_k^\beta, \quad (1.1)$$

where T_0 is the strength of the tetrahedral order and n_i^β are the four vectors spanning a tetrahedron, Fig. 1.3. The symmetry of a tetrahedron contains four proper threefold axes (n_i^β),

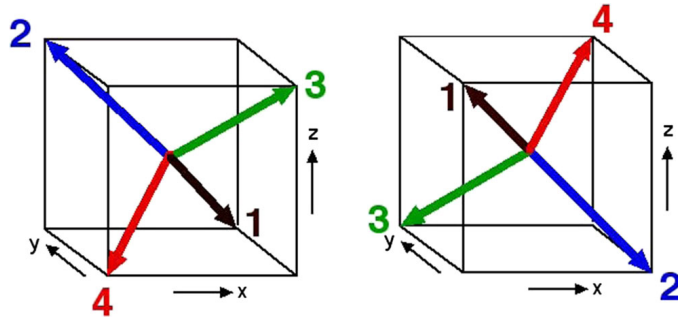


Figure 1.3: A schematic of the tetrahedral structure, (right) the mirror image. Taken from Ref. [74].

and three improper fourfold axes (x , y and z in Fig. 1.3). A special property of the tetrahedral symmetry is that it breaks the inversion symmetry, *i.e.*, a spatially inverted structure is different from the original one. An external electric field orients the tetrahedral structure so that one of the tetrahedral vectors is along the electric field. The lowest possible term is cubic in the electric field [79]

$$f_{\text{el}} = -\xi_1 T_{ijk} E_i E_j E_k \quad (1.2)$$

A magnetic field \mathbf{H} alone can not orient the tetrahedral structure, but there is an orienting effect if an electric field is imposed in addition [80]

$$f_{\text{el}} = -\xi_2 T_{ijk} E_i H_j H_k. \quad (1.3)$$

In Ref. [73–75] a mechanism was proposed to explain the spontaneous formation of macroscopic domains of either hand in systems composed of achiral bent-core molecules. It turns out the presence of the nematic (quadrupolar) in addition to the tetrahedral (octupolar) order can give rise to ambidextrous helicity and ambidextrous chirality. It should be emphasized that this phenomenon is different from the formation of helices in chiral nematic liquid crystal, where the macroscopic chirality originates from the chirality of the molecules. Using a Landau description it can be shown that in the ground state the director can either point along one of the tetrahedral vectors or along one of the improper $\bar{4}$ axes. In the former case the phase is of polar C_{3v} symmetry, while the latter is the nonpolar D_{2d} phase. A special feature of this phase is the presence of a linear gradient term of the director field f_l in the free energy

$$f_l = \xi T_{ijk} n_i \nabla_j n_k. \quad (1.4)$$

Such a term is only possible due to the broken inversion symmetry of the tetrahedral order. This term gives rise to helices of both hand as shown in Fig. 1.4. There is also additional

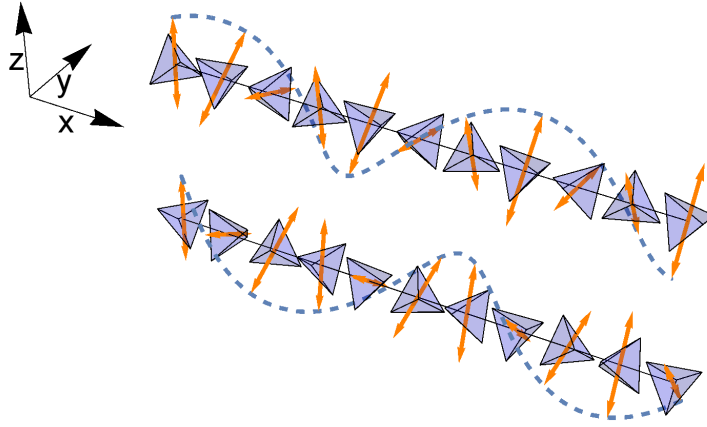


Figure 1.4: Helical configurations of opposite hands. The orange double-headed arrows represent the director field and the blue tetrahedra the tetrahedral structure.

complexity in the static response of the structure to an applied external electric field. The nematic dielectric anisotropy favors a parallel (or perpendicular) orientation of \mathbf{n} with respect to the field, while the tetrahedral vectors try to orient along the field. This leads to a field dependent orientation of the structure [74].

The tetrahedral structure breaks the rotational symmetry three times and therefore gives rise to three additional hydrodynamic variables. It was found [81] that electric field or gradients

of temperature or concentration lead to an induced reversible flow. The tetrahedral symmetry leads to one additional transport parameter in the viscosity tensor compared to ordinary fluids.

Tetrahedral order has also been considered in active matter in models of self propulsion in two dimensions [82–84]. The dynamical model included an equation for the velocity of the center of gravity, and equations for the second rank and third rank tensor, describing the weak deformation of a circular shape of the cell. Because of the couplings between these dynamic variables one deduces, for example, the migration-induced deformation and vice-versa deformation-induced migration.

1.5 Ferrogels

Magnetic gels or elastomers are composed of magnetic particles embedded in a polymer gel and therefore include properties of ferrofluids as well as gels. The elastic response as well as the properties of such a material can be then controlled using an external magnetic field. Experimentally, research on magnetic gels started in the 1990's [85, 86], when isotropic gels were successfully prepared. As in ferrofluids, in such a gel the magnetic moments of particles are oriented randomly in the absence of an external magnetic field. A superparamagnetic response is observed when a magnetic field is applied. A first attempt to produce anisotropic magnetic gels was reported in Ref. [87], where micrometer sized particles were used. In 2003 uniaxial magnetic gels were synthesized by two groups [88, 89], where the gels were prepared in the presence of an external magnetic field. During the crosslinking process the magnetic particles oriented themselves along the magnetic field and formed columns larger than the mesh size of the network. This led to a nonzero frozen-in magnetization even if a magnetic field is switched off. Such gels can be oriented by homogeneous magnetic fields, which is in contrast to isotropic gels, which can only deform in a magnetic field gradient. In Ref. [88] a high concentration ferrofluid was used in the synthesis and an anisotropic mechanical and swelling behavior was observed. In contrast, in Ref. [89] a lower concentrated ferrofluid was used. Anisotropic magnetic as well as anisotropic optical properties but no anisotropic mechanical properties were observed.

Isotropic ferrogels were first modeled theoretically macroscopically in Ref. [90]. A contribution linear in the magnetic field was found for the low frequency regime of the sound spectrum that depends on the angle between the field and the wave vector. In addition, several reversible and dissipative couplings are found between the elastic strain, magnetization and flow. Furthermore if a magnetic field gradient and oscillating temperature gradient is imposed, a shear deformation perpendicular to both, the field and the temperature gradient is created. Interesting properties of magnetic gels such as nonaffine deformations and buckling of magnetic particle chains have been experimentally analyzed and numerically described using a mesoscopic approach [91, 92].

A macroscopic theory for uniaxial magnetic gels was presented in [93]. Therein it was predicted that a constant shear flow induces a rotation of the magnetization out of the shear plane. This effect is due to the variable of relative rotations between the elastic network and the magnetization, which is absent in isotropic gels. Another effect special for uniaxial magnetic gels is magnetic field induces strain. Here an oscillating magnetic field applied perpendicularly to the magnetization induces relative rotations, which in turn induce shear strains.

Since the shape of the ferrogel can be controlled by an external magnetic field, they

have the potential to be used as magnetic actuators, where the gels contract, elongate or rotate. Ferrogels can also be made from biocompatible materials, which makes them safe for medical applications. Examples are hyperthermia [94] or drug release mechanisms [95, 96]. The drug release mechanism makes use of an imposed oscillatory magnetic field. During the remagnetization and relaxation, the heat dissipation increases the temperature of the gel, which in turn causes swelling or shrinking of the gel [97] and consequently drug release. Due to their ability to contract or elongate, ferrogels are also considered as candidates for artificial muscles [98].

1.6 Magnetorheological fluids

Many fluids experience significant changes upon application of an external electric or magnetic field. Examples are rapid and reversible acquisition of solid-like properties and huge increase of the viscosity. The effects of external electric or magnetic fields on the viscosity of normal fluids were studied already by König [99], while the research on electrically polarized liquids started with the works of Duff [100] and Quincke [101], who studied liquids such as ether, carbon disulphide and benzene mixed with glass spheres. Winslow [102] found that the effective viscosity of these so called electrorheological fluids can be varied by orders of magnitude using an external electric field. More specifically the viscosity varied with the square of the applied electric field. When an electric field was applied to the initial undisturbed suspension, fibrous particle chains appeared in the direction of the applied field.

In 1948 Rabinow [103] introduced magnetorheological fluids, which are colloidal suspensions of micrometer sized magnetizable particles in a carrier fluid. MR fluids are different from ferrofluids in the diameter of the particles and the fact that ferrofluids stay fluid even in strong magnetic fields [6], though they do share a magnetic field dependent viscosity. The most common choices of materials for magnetic particles are iron oxides, carbonyl iron or iron cobalt with a diameter ranging between 1 to 100 micrometers, suspended in a mineral oil or a silicone oil. As for ferrofluids, the magnetic particles are coated with surfactants such as oleic or citric acid to prevent the agglomeration process.

In an external magnetic field, the particles get magnetized and as the magnetic interaction energy overcomes the thermal energy, the dipole forces promote the formation of chains. If the concentration is high enough thick columnar structures are formed in the direction of the magnetic field, see Fig. 1.5. The formation of these gap-spanning columns is fast, usually on the order of milliseconds. When the magnetic field is switched off, the magnetic particles diffuse, which leads back to an isotropic state, though in certain cases a small hysteresis was observed, where the chains persisted even at zero magnetic field [104]. This is in part due to colloidal van der Waals forces and remnant magnetization of the magnetic particles used [105].

The structural changes are responsible for the resistance of the system to external shear stress, which gives it solid-like properties. When a critical shear stress, also called the static yield stress, is applied, the structures break and the material starts to flow. The yield stress can reach up to 100 kPa at a magnetic field of 1 T. A further increase in the shear yield stress has been reported [106–108] by uniaxially compressing the system along the direction of the magnetic field.

On the theoretical side, several microscopic and macroscopic models have been developed

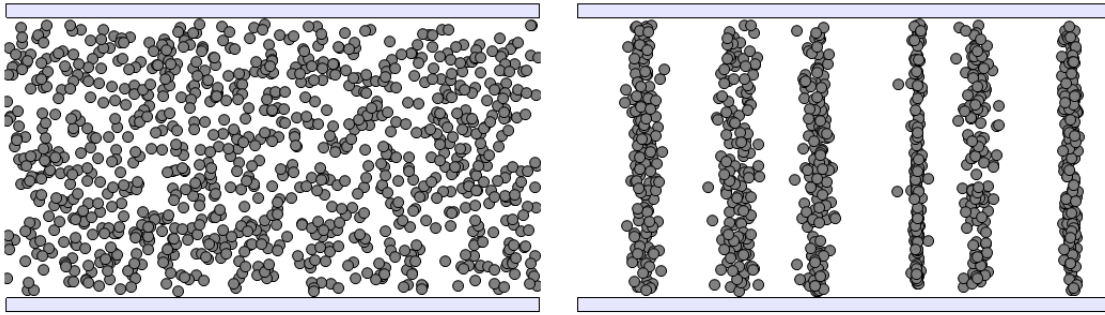


Figure 1.5: A schematic of a magnetorheological fluid in the isotropic phase (left). When a magnetic field is applied, columns of magnetizable particles are formed (right), which are positioned aperiodically and can be of various thicknesses.

to study the magnetic field dependence of the yield stress. Due to the similar form of the interaction between the particles, certain models made for electrorheological fluids [109, 110] can be applied to magnetorheological fluids as well. Microscopic models typically assume the formation of single chain structures [111–115], which deform affinely when the system is sheared. The yield stress is then proportional to the maximal interparticle force. Certain refinements of such a model can be done by taking into account the actual crystal structures formed by the particles [116]. The dynamics of MR fluids was studied microscopically by the simulation of individual particles [117] or single chains [118, 119]. The independent droplet model was used in Ref. [120] to describe the shear-thinning behavior.

Macroscopically the static behavior of magnetorheological fluids was modeled using a director-like degree of freedom [121–123]. In [124] the yield stress was calculated for a fluid with lamellar structure. The formation of the columnar structures was modeled using a variant of a two-fluid approach, treating the fluid and the magnetic phases separately. Therein it was found that an application of an external field leads to thin columns of particles [125–127].

The main limitations of using magnetorheological suspensions is the fact that the particles tend to sediment, which is no surprise as they are composed of micron sized particles. With such a suspension the gravitational forces become important. It should be therefore emphasized that we assume throughout this work that the experiments are done on a timescale shorter than the sedimentation time. MR fluids are used in automobile industry as an active control of suspension and vibrations (shock absorbers) as well as for clutches. Other examples are seismic vibration dampers and magnetic seals.

1.7 Macroscopic dynamics

While microscopic theories and simulations thrive when the number of constituent parts is small, these techniques are generally not feasible for a macroscopic system where the number of degrees of freedom is of the order of Avogadro’s constant. In a macroscopic description we are saved by the fact that there is only a small number of degrees of freedom that relax to

equilibrium in time proportional to some power of the wave-number [24]. These degrees of freedom are the variables that constitute the hydrodynamic theory of a system and formally obey

$$\lim_{\mathbf{k} \rightarrow \mathbf{0}} \omega(\mathbf{k}) = 0, \quad (1.5)$$

where ω and \mathbf{k} are the frequency and the wave-vector of a disturbance.

There are three basic classes of macroscopic variables. The first class is connected with the variables corresponding to global conservation laws. Examples are the conservation of mass, linear momentum and energy. These variables cannot be created or destroyed and can only be transported [24, 128]. The second class contains variables connected with spontaneously broken continuous symmetries. The energy functional is invariant with respect to the symmetry operation, but the macroscopic state itself is not. Using the Goldstone theorem it can be proven that the frequency of the disturbance of such variables vanishes at zero wave-number, which makes such a variable hydrodynamic. Examples are the changes of the director \mathbf{n} from the equilibrium direction, the direction of the magnetization in ferromagnetic systems \mathbf{m} , uniform displacements along the layer normal in smectic-A liquid crystals, the relative velocity in superfluid systems, the elastic strain tensor ε_{ij} in elastic systems, *etc.* [129]. It should be emphasized that in the presence of external electric or magnetic fields, several of these variables are strictly speaking no longer hydrodynamic. In certain systems there are in addition microscopic variables that relax on timescales much larger than the rest of the microscopic degrees of freedom and it is therefore sensible to include these in the macroscopic description. They constitute the class of slowly relaxing variables. Examples are the magnetization modulus, nematic scalar order parameter, strength of the tetrahedral order, relative rotations in a nematic elastomer, *etc.* The inclusion of such variables in a dynamic description falls outside the realm of the strictly hydrodynamic approach and one has to present experimental or microscopic arguments to justify their inclusion.

One of the advantages of the hydrodynamic method is its applicability to different systems and different geometries. A price one has to pay are the unknown phenomenological coefficients that come up as generalized susceptibilities and transport parameters in statics and dynamics. These have to be either measured or estimated from microscopic theories.

The hydrodynamic description is based on local thermodynamic equilibrium [130]. One starts by writing the total energy E as a function of the relevant variables,

$$E = \varepsilon V = E(V, M, \mathbf{G}, S, Mx_\alpha, M\nabla_i x_\alpha), \quad (1.6)$$

where the mass M , the volume V , the momentum \mathbf{G} , and the entropy S are related to their volume densities $\rho = M/V$, $\mathbf{g} = \mathbf{G}/V$, $\sigma = S/V$ and x_α are assumed to be additional intensive variables that can for example be connected with spontaneous symmetry breaking. The local formulation of the first law of thermodynamics (Gibbs relation) establishes the relation between the change of the energy density and the variables:

$$d\varepsilon = Td\sigma + \mu d\rho + \mathbf{v} \cdot d\mathbf{g} + \sum_{\alpha} F_{\alpha} dx_{\alpha}, \quad (1.7)$$

where the temperature T , the velocity \mathbf{v} , the chemical potential μ , and F_{α} are the thermodynamic conjugates (thermodynamic forces) to the corresponding macroscopic variables. These conjugate quantities express how much the energy density changes when the thermodynamic variable is

changed when the others are kept constant. The thermal equilibrium is a state with maximal entropy, $d\sigma = 0$ [131], from which one obtains the vanishing of all the thermodynamic forces, $F_\alpha = 0$. The statics of the system is obtained by writing the thermodynamic forces in terms of the relevant macroscopic variables. The obtained energy density must respect all fundamental invariance principles, such as invariance with respect to parity, time reversal, translational and rotational symmetry, *etc.*

The general dynamic equation for the variables y_α takes the form

$$\left(\frac{\partial}{\partial t} + v_j \nabla_j \right) y_\alpha + J_\alpha = 0. \quad (1.8)$$

It is instructive to split the currents J_α further into dissipative (D) and reversible (R) parts, $J_\alpha = J_\alpha^R + J_\alpha^D$. This separation is done based on the behavior of the currents under the time reversal operation. Dissipative currents have the opposite behavior and reversible currents behave in the same way under time reversal as the time derivative of the dynamic variables, \dot{y}_α . To put these statements in a perspective we write down the conservation laws for the mass density, energy density and momentum density [129],

$$\dot{\rho} + \nabla_i(\rho v_i) = 0, \quad (1.9)$$

$$\dot{\varepsilon} + \nabla_i([\varepsilon + p]v_i) + \nabla_i j_i^\varepsilon = 0, \quad (1.10)$$

$$\dot{g}_i + \nabla_j(p\delta_{ij} + g_i v_j + \sigma_{ij}) = 0, \quad (1.11)$$

with j_i^ε the energy density current, σ_{ij} the stress tensor and p the pressure,

$$p = -\frac{\partial E}{\partial V} = -\varepsilon + T\sigma + \mu\rho + \mathbf{v} \cdot \mathbf{g}. \quad (1.12)$$

The conservation of angular momentum is ensured by the following condition [24, 128, 132]:

$$\sigma_{ij} - \sigma_{ji} = 2\nabla_l \phi_{ijl}, \quad (1.13)$$

with $\phi_{ijl} = -\phi_{jil}$. To symmetrize a general stress tensor, one can use the rotational invariance of the energy density (1.7). As a result one typically reduces the number of phenomenological coefficients, *e.g.* from two to one in the flow alignment tensor of nematic liquid crystals [23, 133]. For uniaxial nematic liquid crystal the flow alignment was derived also microscopically [134].

To derive the dissipative parts of the currents one first sets up the so called dissipation function R . Formally R is proportional to the source term in the dynamic equation for the entropy density

$$\dot{\sigma} + \nabla_i j_i^\sigma = \frac{2R}{T}, \quad (1.14)$$

where j_i^σ is the current of the entropy density. It is positive for irreversible processes and zero for reversible currents. It is interpreted as half the rate at which energy is dissipated into microscopic degrees of freedom. It should be pointed out here that having written down the dynamic equation for the entropy density, there is no need to write down the equation for the energy density as they are related through the Gibbs relation. The second law of thermodynamics requires $R > 0$, while for reversible currents $R = 0$ must be satisfied. For the dissipative processes the Gibbs relation then leads to

$$2R = -j_i^{\sigma D} \nabla_i T - \sigma_{ij}^D A_{ij} + J_\alpha^D F_\alpha > 0, \quad (1.15)$$

where $2A_{ij} = \nabla_i v_j + \nabla_j v_i$ is the symmetrized gradient of the velocity field. In Eq. (1.15) the antisymmetric part of the gradient of the velocity field does not show up, as solid body rotations do not produce entropy. In Eq. (1.15) we have also omitted any pure divergence contributions. For reversible processes the condition,

$$-j_i^{\sigma R} \nabla_i T - \sigma_{ij}^R A_{ij} + J_\alpha^R F_\alpha = 0, \quad (1.16)$$

holds. Equation (1.16) also reveals the equilibrium conditions, $F_\alpha = 0$, $A_{ij} = 0$ and $\nabla_i T = 0$. An assumption used in linear irreversible thermodynamics is the linear expansion of currents in terms of the thermodynamic forces [130, 135],

$$J_\alpha^R = \gamma_{\alpha\beta}^R F_\beta, \quad (1.17)$$

$$J_\alpha^D = \gamma_{\alpha\beta}^D F_\beta, \quad (1.18)$$

where the transport (pseudo-)tensors $\gamma_{\alpha\beta}^R$ and $\gamma_{\alpha\beta}^D$ should obey the correct symmetries and can be constructed using the available invariants of the system. These invariants are, for example for nematic liquid crystals, the transverse Kronecker delta $\delta_{ij}^\perp = \delta_{ij} - n_i n_j$, the Levi-Civita symbol ϵ_{ijk} and the director n_i .

Another way to derive the dissipative parts of the currents is to set up a dissipation function as a positive quadratic form in the thermodynamic forces. The currents are then obtained by taking variational derivatives of the dissipation function with respect to the corresponding thermodynamic force, $J_\alpha = \frac{\delta R}{\delta F_\alpha}$. It should be emphasized that the obtained equations are generally not linear since the dynamic coefficients can depend on macroscopic variables. An analogous potential to derive reversible currents does not exist.

Chapter 2

Overview of the publications

In this chapter I briefly describe each publication in chronological order and present the main results. At the end I append all of the publications in the same order.

2.1 Magneto-optic dynamics of a ferromagnetic nematic liquid crystal

As mentioned in the Introduction, the synthesis of truly ferromagnetic nematic liquid crystals was a challenge for over forty years since their prediction in 1970 [33]. One of the main reasons for the successful experimental realization in 2013 [43] was the platelet shape of the magnetic particles. Such a shape allowed for a stable suspension and consequently it opened the possibility to perform experiments on the phase. A series of static experiments were first performed, where the magneto-optic response was measured as a function of the magnetic field [43, 44]. In publications [136] and [137], we model the static as well as dynamic magneto-optic experiments performed on a sample of ferromagnetic nematic liquid crystals.

We first describe the experimental set-up, see Fig. 2.1. The sample of a ferromagnetic nematic, using 5CB [136] or E7 [137] as a nematic solvent, was confined between two parallel glass plates, approximately $20\ \mu\text{m}$ apart. It was then placed between two crossed polarizers, such that the director was initially at 45 degrees with respect to the polarizer axes. The intensity of the transmitted light was then measured dynamically at different values of the applied magnetic field. Due to the uniaxial symmetry of the nematic solvent, ferromagnetic nematics are birefringent as well. The effects of biaxiality on the optics, which occur out of equilibrium when $\mathbf{n} \nparallel \mathbf{M}$, are discarded in our analysis. The transmitted light intensity is then related to the phase difference of the ordinary and extraordinary rays of light,

$$I \sim \sin^2 \left(\frac{\phi}{2} \right). \quad (2.1)$$

To present our data we used the normalized phase difference, $r = 1 - \phi/\phi_0$, where ϕ_0 is the phase difference in the absence of a magnetic field.

We first modeled the phase difference of the transmitted light as a function of the magnetic field. We started with the expression for the free energy

$$f = -\mu_0 \mathbf{M} \cdot \mathbf{H} - \frac{1}{2} A_1 (\mathbf{M} \cdot \mathbf{n})^2 + \frac{1}{2} A_2 (|\mathbf{M}| - M_0)^2 + f^F, \quad (2.2)$$

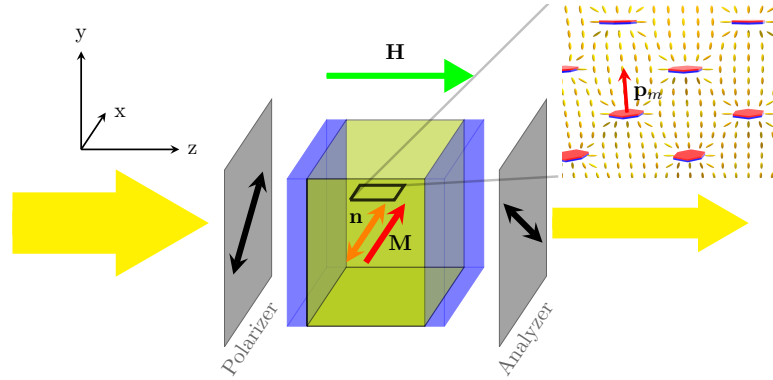


Figure 2.1: Experimental set-up used for the magneto-optic measurements. The thick yellow arrows indicate the direction of the light passing through the polarizer and the analyzer. The outgoing arrow is smaller, indicating the transmitted light intensity is smaller than that of the incoming light. In the absence of an applied magnetic field (\mathbf{H} , z direction), the equilibrium director (\mathbf{n}) and magnetization (\mathbf{M}) fields are only slightly pretilted from the x direction. Inset: distortion of the NLC director (ellipsoids, schematic) prevents flocculation of the suspended nanoplatelets carrying a magnetic moment \mathbf{p}_m parallel to \mathbf{n} in equilibrium. Figure taken from Ref. [136].

where μ_0 is the magnetic constant, $\mathbf{H} = H\hat{\mathbf{e}}_z$ is the applied magnetic field, and $A_{1,2} > 0$ are constants. The first term represents the coupling of the magnetization and the external magnetic field. Since the applied magnetic field is large compared to the equivalent field originating from the magnetization, $H \gg M_0$, the local magnetic field is equal to \mathbf{H} , which is fixed externally, and is thus independent of the $\mathbf{M}(\mathbf{r})$ configuration. The second term describes the static coupling between the director field and the magnetization. The third term describes the energy connected with the deviation of the modulus of the magnetization from M_0 . The last term f^F is the Frank elastic energy associated with director distortions [15]

$$f^F = \frac{1}{2}K_1(\nabla \cdot \mathbf{n})^2 + \frac{1}{2}K_2[\mathbf{n} \cdot (\nabla \times \mathbf{n})]^2 + \frac{1}{2}K_3[\mathbf{n} \times (\nabla \times \mathbf{n})]^2, \quad (2.3)$$

with positive elastic constants for splay (K_1), twist (K_2), and bend (K_3). The free energy is minimized by varying the director field and the magnetization field.

In equilibrium the magnetic field distorted director and magnetization field are both lying within the xz plane, $\mathbf{n} = \sin \theta \hat{\mathbf{e}}_x + \cos \theta \hat{\mathbf{e}}_z$, and $\mathbf{M} = \sin \psi \hat{\mathbf{e}}_x + \cos \psi \hat{\mathbf{e}}_z$. The phase difference can be then calculated from the director field using

$$\phi = k_0 \int_0^d (n_e(z) - n_o) dz \quad (2.4)$$

where $k_0 = 2\pi/\lambda$ is the wave-number of the light with the wavelength λ , d is the cell thickness, n_o is the ordinary refractive index and n_e is the refractive index experienced by the extraordinary ray, defined by

$$n_e^{-2} = n_{e0}^{-2} \sin^2 \theta(z) + n_o^{-2} \cos^2 \theta(z), \quad (2.5)$$

with n_{e0} the so called extraordinary refractive index.

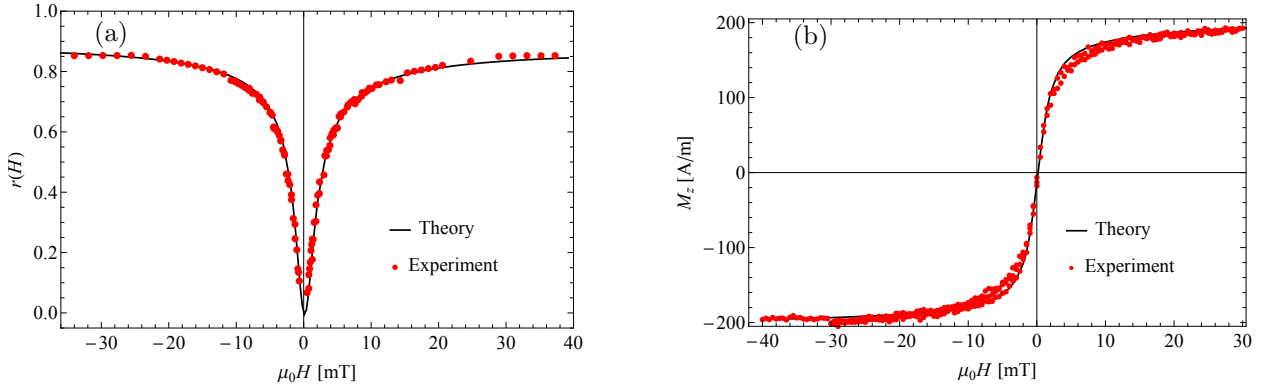


Figure 2.2: Comparison of experimental and theoretical static results: (left) normalized phase difference $r(H)$ and (right) magnetization component M_z as functions of the magnetic field μ_0H . Figure taken from Ref. [137].

The experimental and theoretical results are shown in Fig. 2.2. One can see that very small magnetic fields of order 5 mT already produce a significant magneto-optic effect. It should be mentioned that the magnetic anisotropy was not included in the description, as it becomes important at larger fields of order 0.5 T.

Experimental measurements of the dynamics of the magneto-optic effect show that the reorientation process of the ferromagnetic nematic is quite fast, on the order of less than a second, Fig. 2.4. We have modeled the measurements using just the dynamic variables of the director and the magnetization and we discarded the velocity field. The evolution of these two fields can be derived by the macroscopic dynamic approach presented in the Introduction, which takes into account also the behavior of magnetization under time reversal,

$$\dot{n}_i + Y_i^R + Y_i^D = 0, \quad (2.6)$$

$$\dot{M}_i + X_i^R + X_i^D = 0, \quad (2.7)$$

with $Y_i^{R,D}$ and $X_i^{R,D}$ the quasi-currents, which have been explicitly split into reversible (R) and irreversible (D) parts. At this point we write down only the dissipative parts of the currents as they were sufficient to explain the experimental results:

$$X_i^D = b_{ij}^D h_j^M + \chi_{ji}^D h_j^n, \quad (2.8)$$

$$Y_i^D = \frac{1}{\gamma_1} h_i^n + \chi_{ij}^D h_j^M, \quad (2.9)$$

with

$$\chi_{ij}^D = \chi_1^D \delta_{ik}^\perp M_k n_j + \chi_2^D \delta_{ij}^\perp M_k n_k, \quad (2.10)$$

$$b_{ij}^D = b_{\parallel}^D n_i n_j + b_{\perp}^D \delta_{ij}^\perp. \quad (2.11)$$

In Eqs. (2.8) and (2.9) the thermodynamic forces h_i^n and h_i^M are obtained by variational derivatives of the free energy Eq. (2.2), with respect to the director and the magnetization, respectively.

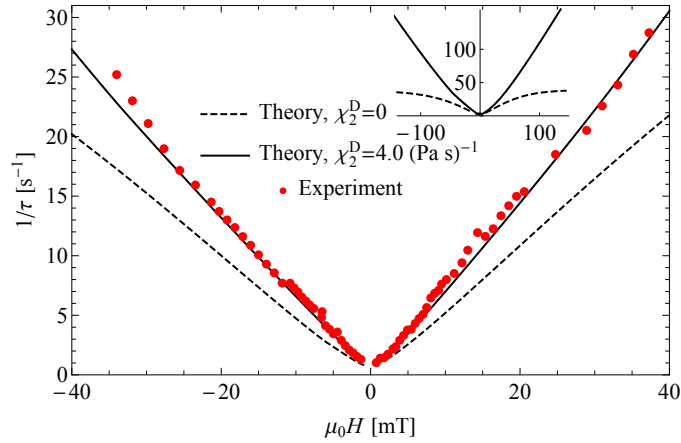


Figure 2.3: The overall relaxation rate, $1/\tau(H)$, as a function of the magnetic field $\mu_0 H$, extracted from the experimental data and the theoretical results using the fitting function Eq. (2.12). Inset: without the dynamic cross-coupling, the relaxation rate levels off already at low fields (dashed). Figure taken from Ref. [137].

We show [136,137] that the inclusion of the dissipative cross-coupling between the magnetization and the director field, described by χ_{ij}^D , is crucial to explain the experimental data. One of the experimental observations that demonstrates the importance of this dynamic cross-coupling is a linear dependence of the overall relaxation rate as a function of the magnetic field, see Fig. 2.3. To extract the relaxation rates from the numerical and experimental data we used a squared sigmoidal model function for the time dependence of the phase difference:

$$f(t) = C' \left[1 - \frac{1 + C}{1 + C \exp(-2t/\tau)} \right]^2. \quad (2.12)$$

In the absence of χ_2^D , the relaxation rate levels off already at low fields, see Inset of Fig. 2.3, as expected since the transient angle between \mathbf{M} and \mathbf{n} gets larger.

The second proof can be found in the initial dynamics of the phase difference. We show that the dynamic cross-coupling χ_2^D induces a director field rotation along the field direction, which is linear in time and linear in the magnetic field,

$$n_z(t) \approx \varphi_s + \chi_2^D M_0 \mu_0 H t. \quad (2.13)$$

This in turn means a linear-quadratic initial dependence of the phase difference in time and in magnetic field. In the lowest order of t , for the phase difference one gets a linear term that is proportional to the pretilt angle and a quadratic term which does not vanish if the pretilt is zero:

$$\begin{aligned} r(H) &\approx r_0 \left[(\chi_2^D M_0 \mu_0 H)^2 t^2 + 2\varphi_s \chi_2^D M_0 \mu_0 H t \right] \\ &\equiv k^2 t^2 + pt. \end{aligned} \quad (2.14)$$

The determination of the dissipative cross-coupling χ_2^D from the initial dynamics of the phase difference has already been shown to be robust and reliable, even at different concentrations of magnetic particles and for different nematic solvents [49].

A comparison of the numerical and experimental results of the dynamics of the normalized phase difference is shown in Fig. 2.4. In addition we calculated the dynamics of the normalized magnetization,

$$M_z/M_0 = \frac{1}{d} \int_0^d \cos \psi \, dz. \quad (2.15)$$

Analysis of the initial dynamics of M_z/M_0 yields a linear response in time:

$$M_z/M_0 \approx \varphi_s + b_{\perp}^D \mu_0 H t, \quad (2.16)$$

which can be seen in the Inset of Fig. 2.4. The vertical component of the magnetization M_z is typically measured using a vibrating sample magnetometer, which requires several tenths of a second for a single measurement. This limits the use of this technique for the dynamic measurements in a ferromagnetic nematic liquid crystal.

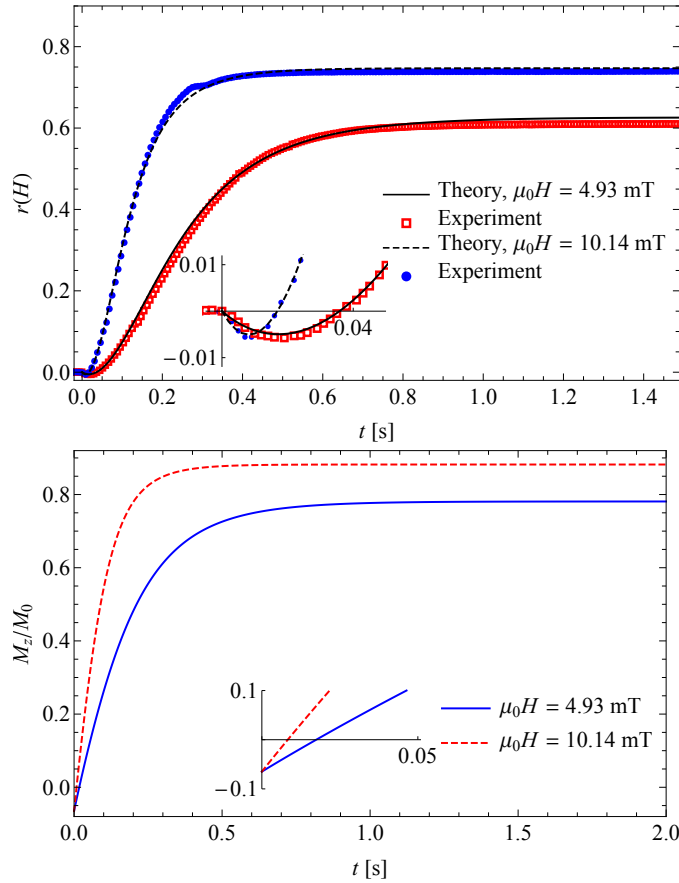


Figure 2.4: Top: time evolution of the measured normalized phase difference, $r(H)$, fitted by the dynamic model Eqs. (2.6)-(2.11). The linear-quadratic onset of $r(H)$ is in accord with the analytic result given in Eq. (2.14). Bottom: the corresponding theoretical time evolution of M_z/M_0 , initially growing linearly as given in Eq. (2.16). Figure taken from Ref. [137].

Apart from the comparison to the experimental results we make several theoretical predictions. We studied the fluctuation modes of the coupled director and magnetization dynamics. We found four different fluctuation modes. Two of these are the analogues of the splay-bend mode

in usual nematics and the other two are the twist-bend modes, see Fig. 2.5. The modes can be further separated into faster (optic) modes and slower (acoustic) modes. Using the common light scattering geometries for nematic liquid crystals it is impossible to detect only a single mode in ferromagnetic nematic. One will always detect a complicated combination of two modes. This is, according to our predictions, not the case at very large fields, when the modes become decoupled and one observes only the slower mode. We also predict that the relaxation rate of the slower mode $1/\tau_\alpha^t$ saturates at a finite value as one increases the field, whereas the faster modes $1/\tau_\alpha^p$ grows linearly with the field, where $\alpha = 1$ for the splay-bend mode and $\alpha = 2$ for the twist-bend mode,

$$\frac{1}{\tau_\alpha^p} = \frac{A_1(b_\perp^D - \chi_2^D M_0)^2 + (\chi_2^D M_0)^2(K_\alpha q_\perp^2 + K_3 q_x^2)}{b_\perp^D} + \frac{b_\perp^D}{M_0} \mu_0 H, \quad (2.17)$$

$$\frac{1}{\tau_\alpha^t} = \frac{A_1 M_0^2 + (K_\alpha q_\perp^2 + K_3 q_x^2)}{\gamma_1} \left(1 - \frac{(\chi_2^D M_0)^2 \gamma_1}{b_\perp^D} \right). \quad (2.18)$$

At a critical field $\mu_0 H = \mu_0 H^c = -\frac{A_1 M_0 K_\alpha q_z^2}{K_\alpha q_z^2 + A_1 M_0^2}$, where $q_z = \pi/d$, the dynamics of the acoustic modes slows down. If the field is more negative than this critical field, the magnetization and with it the director starts to reverse.

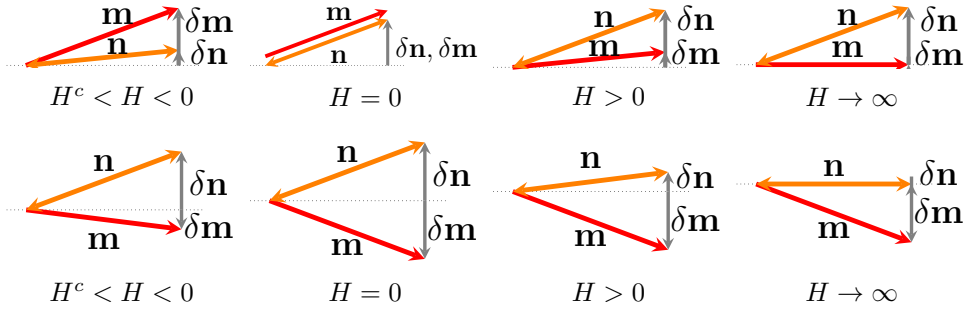


Figure 2.5: A schematic of the magnetic field dependence of the slower (top) and the faster (bottom) mode. The vectors $\delta \mathbf{n}$ and $\delta \mathbf{m}$ represent the deviations of the director and the magnetization orientation from the equilibrium.

2.2 Effects of flow on the dynamics in a ferromagnetic nematic liquid crystal

In order to understand the dynamic behavior of a system better one needs to study its rheological properties. A common technique used in rheology is to study the effects of an imposed shear rate. In a ferromagnetic nematic, the orientations of the molecules and the platelets are influenced by a shear flow, which in turn influences the measured viscosity. In Ref. [45] measurements have been done on a sample of ferromagnetic nematic using a cone-plate rheometer. It was found for example that an imposed magnetic field of order of 20 mT enhances the viscosity by two times.

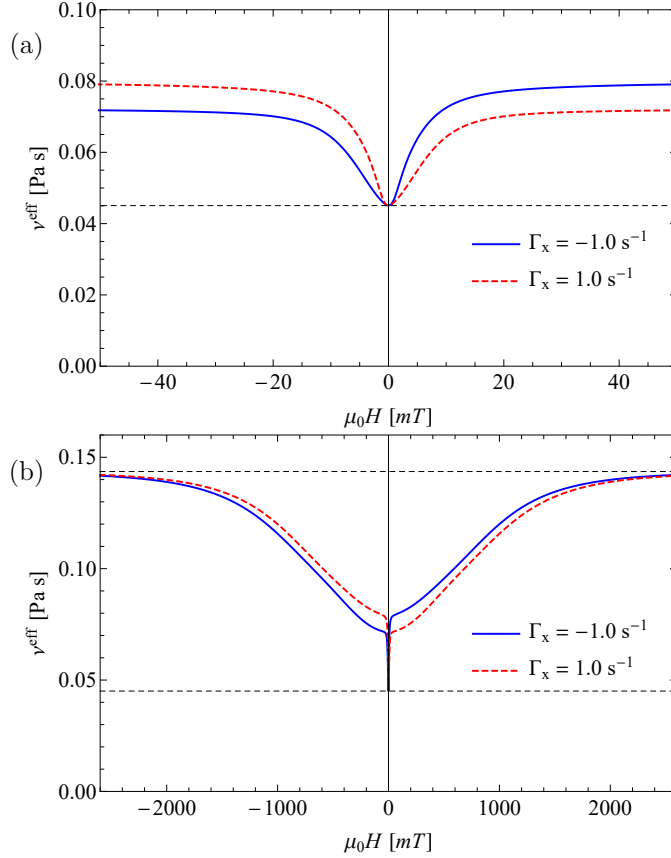


Figure 2.6: The behavior of the effective viscosity for (a) small and (b) large values of the applied magnetic field at oppositely equal shear rates. The dashed lines represent two of the Miesowicz viscosities (η_{xx} and η_{zz}). Figure taken from Ref. [138].

We study the Couette flow of a ferromagnetic nematic between two parallel plates. Several theoretical predictions on the effects of flow were made by studying the dynamic interplay of the director field, the magnetization and the velocity field [53],

$$\left(\frac{\partial}{\partial t} + v_j \nabla_j\right) M_i + \epsilon_{ijk} M_j \omega_k + X_i^R + X_i^D = 0, \quad (2.19)$$

$$\left(\frac{\partial}{\partial t} + v_j \nabla_j\right) n_i + \epsilon_{ijk} n_j \omega_k + Y_i^R + Y_i^D = 0, \quad (2.20)$$

$$\rho \left(\frac{\partial}{\partial t} + v_j \nabla_j\right) v_i + \nabla_j (\sigma_{ij}^R + \sigma_{ij}^D + \sigma_{ij}^{th}) - \nabla_i p = 0, \quad (2.21)$$

where $Y_i^{R,D}$, $X_i^{R,D}$ and $\sigma_{ij}^{R,D}$ are the reversible and the dissipative currents for the director, the magnetization and the velocity field. We shall not write down all the currents explicitly, but we mention the analogue of the flow alignment tensor for the magnetization, described by the tensor c_{ijk}^R [53],

$$X_i^R = \dots - c_{ijk}^R A_{jk}, \quad (2.22)$$

$$\sigma_{ij}^R = \dots - c_{kij}^R h_k^M, \quad (2.23)$$

where ... contains all the other parts of the currents, $2A_{ij} = \nabla_i v_j + \nabla_j v_i$ is the symmetrized velocity gradient and h_i^M is the thermodynamic force, defined by $h_i^M = \frac{\delta \varepsilon}{\delta M_i}$. The tensor c_{ijk}^R contains 6 coefficients

$$\begin{aligned} c_{ijk}^R &= c_1^R M_i n_j n_k + c_2^R (\delta_{ij} M_k + \delta_{ik} M_j) + c_3^R M_i \delta_{jk} \\ &+ c_4^R n_i M_p n_p \delta_{jk} + c_5^R (n_i M_j n_k + n_i M_k n_j) + c_6^R n_i M_p n_p n_j n_k. \end{aligned} \quad (2.24)$$

Our numerical results on the viscosity as a function of the applied magnetic field agree qualitatively well with experiments. One observes a quick increase of the viscosity for low magnetic fields, Fig. 2.6. A further increase is observed at fields of order 1 T, when the diamagnetic energy becomes important.

We also calculate analytically the distortion of the director and the magnetization as a function of the imposed shear rate and the magnetic field. The angles are defined by $\mathbf{n} = \cos \theta \hat{\mathbf{e}}_x + \sin \theta \hat{\mathbf{e}}_z$ and $\mathbf{m} = \cos \psi \hat{\mathbf{e}}_x + \sin \psi \hat{\mathbf{e}}_z$. The solution at large values of the applied magnetic field is,

$$\theta^\pm(z) = \pm \frac{\pi}{2} - C \Gamma_x \mp \left(\frac{\pi}{2} \mp C \Gamma_x \right) \frac{\cosh [q(z - d/2)]}{\cosh (qd/2)}, \quad (2.25)$$

where

$$q^2 = q_0^2 \frac{\mu_0 |H| M_0}{A_1 M_0^2 + \mu_0 |H| M_0}, \quad (2.26)$$

with $q_0 = \sqrt{A_1 M_0^2 / K}$, and C is a constant determined by the dynamic and the static parameters [138]. We point out that Eq. (2.25) also predicts the fact that the director can rotate by more than $\pi/2$ in the middle of the cell. These results could be used in future experiments on shear flow, while simultaneously measuring the magneto-optic response.

In a complex fluid, such as a nematic liquid crystal, there are more dynamical coefficients compared to ordinary fluids. A simple way to determine some of the additional viscosities in a nematic is to measure the so called Miesowicz viscosities [139, 140], where one fixes the director by external fields and imposes a simple shear flow. Depending on the direction of the shear plane, the velocity and the director, there are three different limiting cases for the Miesowicz viscosities in a nematic. In a ferromagnetic we find 9 different viscosities, which is due to the additional variable of spontaneous magnetization, see Fig. 2.7. If the director is fixed along the z axis, for example, the Miesowicz viscosities take the following form

$$\eta_{zx} = \nu_3 + \frac{\gamma_1}{4} (1 + \lambda)^2 - \frac{(c^D)^2}{b_\perp^D} + \frac{M_0^2 (1 - 2c_2^R - 2c_5^R)^2}{4b_\parallel^D}, \quad (2.27)$$

$$\eta_{zy} = \nu_3 + \frac{\gamma_1}{4} (1 + \lambda)^2 - \frac{(c^D)^2}{b_\perp^D}, \quad (2.28)$$

$$\begin{aligned} \eta_{zz} &= \nu_3 + \frac{1}{4} \left(1 - \frac{(\chi_2^D)^2 M_0^2 \gamma_1}{b_\perp^D} \right)^{-1} \\ &\times \left[\gamma_1 (1 + \lambda)^2 - 4(c^D)^2 + \frac{M_0^2}{b_\perp^D} (1 + 2c_2^R) (1 + 2c_2^R - 2\chi_2^D \gamma_1 (1 + \lambda)) \right]. \end{aligned} \quad (2.29)$$

We furthermore study the flow alignment, which is a phenomenon well known in usual nematic liquid crystals, where the director is tilted by a finite angle with respect to the velocity

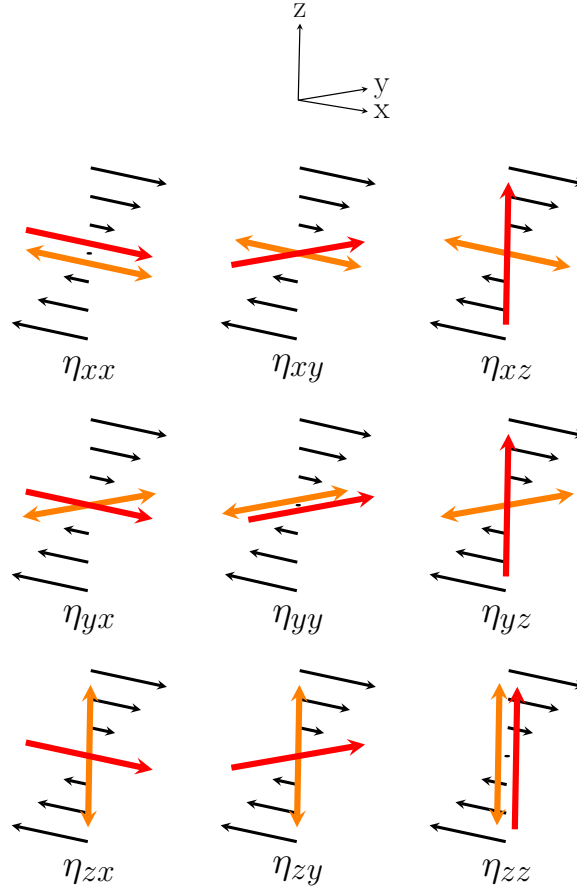


Figure 2.7: Miesowicz viscosities in a ferromagnetic nematic where the director is indicated by yellow double-headed arrows. Figure taken from Ref. [138].

field. In ferromagnetic nematics we have an additional dynamic equation for the magnetization and a different dynamic coupling to the velocity field. This not only leads to different stationary directions of the magnetization and the director, but both of them can move out of the shear (xz) plane, see Fig. 2.8. We studied the case, where the magnetic field is pointing along the x axis. The solution for the angle ψ is

$$\sin \psi^\pm = -\frac{\Gamma_x^H}{\Gamma_x} \pm \sqrt{\left(\frac{\Gamma_x^H}{\Gamma_x}\right)^2 + \frac{2c_2^R - 1}{4c_2^R}}, \quad (2.30)$$

where $\Gamma_x^H = \frac{b_1^D}{4c_2^R M_0^2} \mu_0 H M_0$ is the characteristic shear rate determined by the magnetic field. In the absence of the magnetic field and in the large shear rate limit, the stationary solution exists if $|\lambda| \geq 1$ and $|c_2^R| \geq \frac{1}{2}$. In usual nematic liquid crystals, if $|\lambda| < 1$, the stationary solution does not exist and the system shows a tumbling behavior. In such a system flow alignment can be recovered if a sufficiently large electric field is applied, see Refs. [141, 142]. In Ref. [138], we show that in ferromagnetic nematics this can be achieved by using low magnetic fields.

Lastly the effects of flow on the switch-ON dynamics are investigated. In this case flow is generated by the reorientation of the director field and the magnetization field. An inclusion of only the reversible couplings of \mathbf{n} and \mathbf{M} has shown a very small influence on the reorientation

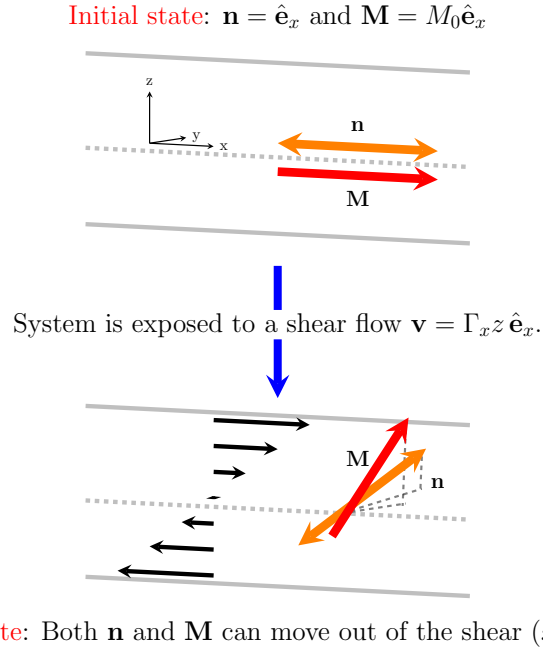


Figure 2.8: A schematic of the director field and the magnetization under imposed shear flow.

dynamics, which is typically observed in usual nematics. On the other hand the dissipative cross-coupling of \mathbf{n} to the velocity field can have a strong effect. Such a coupling induces a nonzero rotation of the director out of the shear plane, which could potentially be detected using polarizing microscopy techniques.

2.3 Dynamic interplay of nematic, magnetic, and tetrahedral order in ferromagnetic nematics

As mentioned in the Introduction, there is a class of liquid crystals, formed by bent-core molecules, which can show rather unusual properties. The simplest candidate to explain the properties is the inclusion of the tetrahedral order, described by the fully symmetric third rank tensor T_{ijk} , Eq. (1.1). Due to the recent successes in the synthesis of ferromagnetic liquid crystal phases, such as ferromagnetic nematics and ferromagnetic cholesterics, a natural question arises: how does tetrahedral order influence these phases? We studied the macroscopic aspects of this hypothetical phase and focused on the effects unique to phases with the simultaneous nematic, magnetic and tetrahedral order.

Such a phase has an interesting ground state, which breaks the inversion symmetry due to the tetrahedral order and the time reversal symmetry due to the spontaneous magnetization. To find the ground state of this phase we minimized the Landau energy. At this point we mention only the cross-coupling term F^{QTM} between the tetrahedral, quadrupolar and magnetic order parameter,

$$F^{QTM} = c_1 Q_{il} M_j M_m T_{ilk} T_{jmk} + \frac{c_2}{2} (Q_{ij} M_m + Q_{im} M_j) M_l T_{ilk} T_{jmk}. \quad (2.31)$$

To calculate the ground state we assume the director is fixed with respect to the tetrahedral structure and then vary the direction of the magnetization. There are five different solutions of the angles that correspond to the minimum of the free energy. For one of the solutions, the director and the magnetization are parallel, see Fig. 2.9. For the next two possibilities the magnetization is in the plane perpendicular to the director. In the last two solutions the angle between the director and the magnetization depends on the values of the coefficients in the Landau energy. We studied the case $\mathbf{n} \parallel \mathbf{M}$, which is an analogue of the D_{2d} phase, mentioned in the Introduction.

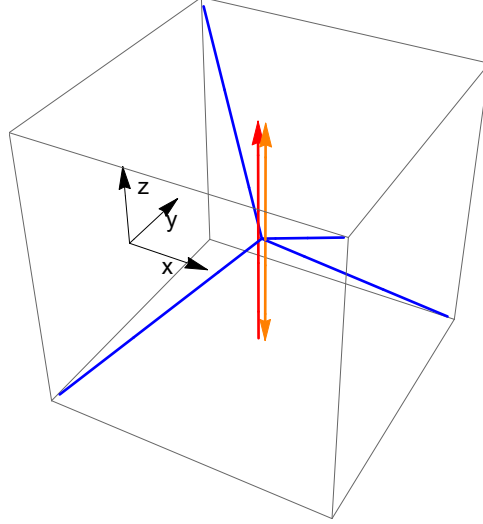


Figure 2.9: The ground state of the system showing the magnetization (red) and the director (orange) along one of the improper $\bar{4}$ axes of the tetrahedron (blue). Figure taken from Ref. [143].

To describe the system macroscopically one must first recognize the relevant macroscopic variables. Apart from the usual variables connected with global conservation laws (energy density ε , mass density ρ , linear momentum \mathbf{g} , concentration c), we have additional variables connected with the broken rotational symmetries and variables that are slowly relaxing. The magnetic order can be described by the modulus $M \equiv |\mathbf{M}|$ and its orientation $\mathbf{m} = \mathbf{M}/M$. The modulus is a slowly relaxing variable, while the orientation \mathbf{m} belongs to the class of hydrodynamic variables connected with spontaneous symmetry breaking. Rotations of the tetrahedral structure can be described by a projection, $\delta\Gamma_i$, with [74]

$$\delta\Gamma_i = \frac{1}{4\tilde{\alpha}} \epsilon_{ipq} T_{pkl} \delta T_{qkl}, \quad (2.32)$$

where δT_{qkl} is the deviation of the tetrahedral order parameter from the equilibrium one, $\delta T_{qkl} = T_{qkl} - T_{qkl}^{\text{eq}}$. We use the normalization [74, 77] $T_{ikl} T_{jkl} = \tilde{\alpha} \delta_{ij}$, with $\tilde{\alpha} = (32/27)T_0^2$. Since we assume rigid coupling between the director, the magnetization and the tetrahedral order, we will use as hydrodynamic variables the director variations δn_i and the rotations around it $\delta\Omega = n_i \delta\Gamma_i$. The material tensors are constructed using the invariants n_i , δ_{ij}^\perp , ϵ_{ijk} and T_{ijk} . The magnetization does not define an extra, independent preferred direction, and is used when its specific time-reversal behavior is crucial.

An interesting consequence of the broken inversion symmetry with the additional orientational order, is the presence of a linear gradient term:

$$f_{\text{lin}} = \xi^M T_{ijk} M_i \nabla_j m_k + \xi^n T_{ijk} n_i \nabla_j n_k. \quad (2.33)$$

It contains a linear gradient term already present in the D_{2d} phase and in addition a term for the magnetization field. As a consequence the ground state might not be homogeneous. It can be shown that a helical state, where the director and the magnetization rotate around one of the (other) improper $\bar{4}$ axes, has lower energy than the homogeneous state. The energy reduction of the two linear gradient terms is

$$\Delta f = \tilde{T}_0^2 \frac{(\xi^n + \xi^M M_0)^2}{2(K_2 + K_2^m)}, \quad (2.34)$$

which yields for the helical wave vector

$$q_0 = -\tilde{T}_0 \frac{(\xi^n + \xi^M M_0)}{K_2 + K_2^m}, \quad (2.35)$$

with $\tilde{T}_0 = 4T_0/3\sqrt{3}$. Provided the domains are large enough, the optical observation of the domains of opposite handedness would demonstrate the presence of a tetrahedral order. It should also be noted that there is no restriction on the sign of the coefficients ξ^M and ξ^n . If the signs happen to be opposite this could lead to helical domains with large wavelengths.

It should be mentioned that $\delta\Omega$ is not a scalar, but transforms as a vector component. This is also apparent from the dynamic equation for $\delta\Omega$

$$\left(\frac{\partial}{\partial t} + v_j \nabla_j \right) \Omega - m_i \omega_i + Z = 0, \quad (2.36)$$

where the quasi-current Z contains besides the term proportional to h^Ω , the thermodynamic conjugate of $\delta\Omega$, also a reversible and a dissipative coupling to the velocity field.

We find that temperature or concentration gradients generate director rotations,

$$\dot{n}_i \sim Y_i^{nR} = \dots + \xi_{ji}^{Tn} \nabla_j T + \xi_{ji}^{cn} \nabla_j c, \quad (2.37)$$

where $\xi_{ij}^{T,cn} = \xi^{T,cn} M_k n_r \varepsilon_{ipr} T_{jpk}$. For the case $\mathbf{m} \parallel \hat{\mathbf{e}}_z$ and $\mathbf{n} \parallel \hat{\mathbf{e}}_z$ one gets explicitly

$$\dot{n}_i \sim Y_x^{nR} = \dots + \xi^{Tn} M_0 \tilde{T}_0 \nabla_x T + \xi^{cn} M_0 \tilde{T}_0 \nabla_x c, \quad (2.38)$$

$$\dot{n}_i \sim Y_y^{nR} = \dots - \xi^{Tn} M_0 \tilde{T}_0 \nabla_y T - \xi^{cn} M_0 \tilde{T}_0 \nabla_y c, \quad (2.39)$$

$$\dot{n}_i \sim Y_z^{nR} = \dots + 0. \quad (2.40)$$

Similarly temperature or concentration gradients produce dissipative magnetization currents,

$$\dot{m}_i \sim X_i^{mD} = \dots + M_j T_{ijk} (\tilde{\psi}^{TD} \nabla_j T + \tilde{\psi}^{cD} \nabla_j c). \quad (2.41)$$

2.4 Influence of tetrahedral order on ferromagnetic gels

Spontaneous formation of chiral domains of either handedness is a phenomenon that has been observed in bent-core liquid crystals. A distinct property is that the compounds are composed of achiral molecules. As mentioned in the introduction, this can arise as a consequence of the simultaneous tetrahedral as well as orientational order (*e.g.* nematic or magnetic). This can also be explained in terms of the ambidextrous chirality, which is based on the existence of a pseudo-scalar quantity due to the special structure of the phase and not because of the chirality of molecules.

Another mechanism for the chiral symmetry breaking was proposed recently, which takes into account the simultaneous presence of the tetrahedral order and of a transient network. The motivation for the inclusion of the latter was that for certain experiments clusters or agglomerates of substantial size were reported. It was shown that a linear gradient term coupling the tetrahedral order and elastic strain leads to ambidextrous helicity [76].

Here we consider the effects of tetrahedral order on ferromagnetic gels. Ferromagnetic gels have been successfully experimentally realized already in 2003 [88, 89]. They are distinguished from other magnetic gels by a spontaneous magnetization and consequently a strong linear response to a magnetic field. As a consequence many reversible and dissipative effects arise that are not present in superparamagnetic gels. A natural question is what are the effects of the tetrahedral order on, for example, the elastic response of a magnetic gel.

A Landau energy analysis yields two energetic minima, when varying the orientation of the magnetization with respect to the tetrahedral order. The magnetization points either along one of the tetrahedral vectors or along one of the improper $\bar{4}$ axes. The former is of C_{3v} symmetry, while the later is similar to the tetrahedral nematics with D_{2d} symmetry. For the dynamic

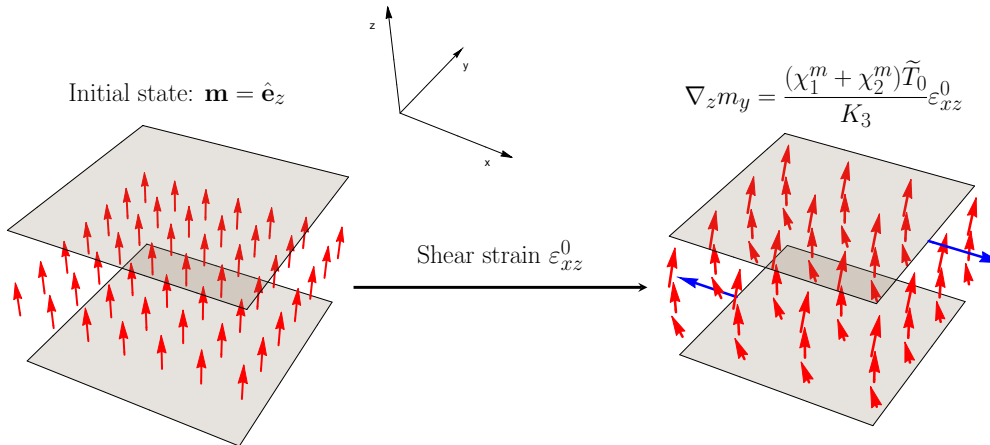


Figure 2.10: A shear strain of the initial homogeneous state leads to a nonuniform rotation of the magnetization (red arrows) within the shear plane (xz).

variables we chose the magnetization \mathbf{M} , which is split into equations for its modulus M and the orientation $\delta\mathbf{m}$. Next, we have similarly as in tetrahedral ferromagnetic nematics, the rotations around the magnetization $\delta\Omega = m_i \delta\Gamma_i$ with $\delta\Gamma_i$ defined in Eq. (2.32). We include also

the strain field $2\varepsilon_{ij} = \nabla_i u_j + \nabla_j u_i$, with u_i the displacement field of the network. In addition, we consider the relative rotations between the elastic network and the magnetization direction. This is a variable that plays an important role in the description of nematic gels [144, 145].

In our paper we consider static experiments that are unique for a ferromagnetic gel with the additional tetrahedral order. In particular we study the effects of imposed external strains on the orientation of the magnetization. The corresponding term in the free energy f is

$$f \sim \chi_{ijkl}^m \varepsilon_{ij} \nabla_l m_k, \quad (2.42)$$

with $\chi_{ijkl}^m = \delta_{kp}^\perp (\chi_1^m [T_{ipl} m_j + T_{jpl} m_i] + \chi_2^m T_{ijp} m_l)$. A straightforward calculation then shows that an external shear strain gives rise to an inhomogeneous rotation of the magnetization out of the shear plane, Fig. 2.10,

$$\nabla_z m_y = A \varepsilon_{xz}^0 \quad \text{and} \quad \nabla_z m_x = A \varepsilon_{yz}^0 \quad (2.43)$$

with $A = (\chi_1^m + \chi_2^m) \tilde{T}_0 / K_3$.

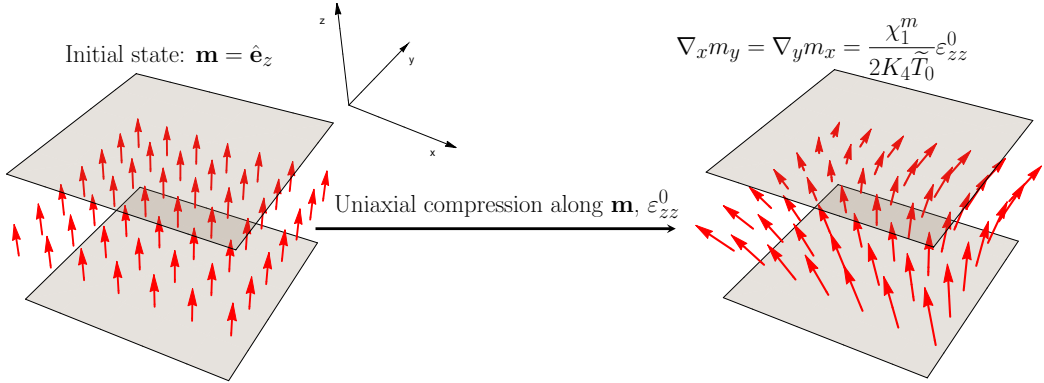


Figure 2.11: A uniaxial compression of the initial homogeneous state leads to a spatial pattern of the magnetization (red arrows).

Similarly, a uniaxial compression along the magnetization leads to linear deviations of the magnetization in the transverse plane, Fig. 2.11,

$$\nabla_x m_y = \nabla_y m_x = \frac{\chi_1^m}{2K_4 \tilde{T}_0} \varepsilon_{zz}^0. \quad (2.44)$$

We investigated the effects of the transient elasticity. In this case the strain field is relaxing, rather than diffusing. We find that an applied temperature gradient along the magnetization leads to induced elastic stresses in the plane perpendicular to the gradient. If the applied gradient is perpendicular to the magnetization, it induces shear stresses that depend on the orientation of the tetrahedral structure, see Fig. 2.12. By changing the direction of the temperature gradient one could, in principle, detect the orientation of the tetrahedral structure. This finding is important, as it opens the door for experiments investigating a particular orientation of the structure without the need of both magnetic and electric fields. As a prospect it will be interesting to investigate the rotations around the magnetization, which couple dynamically (neglecting the inhomogeneous stress forces) only to flow.

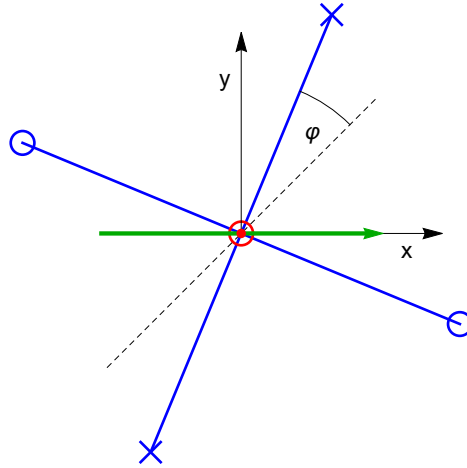


Figure 2.12: The red circle in the middle indicates the magnetization perpendicular to the drawing plane, while the temperature gradient (green arrow) is along the x-axis. The blue lines show the projections of the tetrahedral vectors (where circles and the crosses represent vectors pointing out or into the plane, respectively). Figure taken from Ref. [146].

2.5 A continuum model of magnetic field induced viscoelasticity in magnetorheological fluids

Magnetorheological fluids experience significant changes when an external magnetic field is applied. Examples are fast and reversible acquisition of solid-like properties and a strong magnetoviscous effect. This makes them suitable for many applications, like shock absorbers, dampers or clutches. It is of practical importance to construct a macroscopic model, which is able to reproduce the behavior of MR fluids in many different geometries and on macroscopic length and time scales that are actually used in applications.

We have constructed a basic model, which takes into account the variables of the strain field and the magnetization. The motivation behind the inclusion of these variables is the following. Under the application of an external magnetic field, columns of magnetic particles are formed. They are the underlying reason for the observed solid-like properties. We model the magnetic properties by the magnetization, which is a variable included already in ferrofluids, while the solid-like properties are captured by the strain field ε_{ij} . To discuss the rheological behavior of the MR fluid we include the equation for the linear momentum.

The statics of the MR fluid can be split into the magnetic part, which describes the induced magnetization, and the elastic energy associated with the deformation of the columns. It is described by the energy density $\epsilon(\varepsilon_{ij}, \mathbf{M}, \mathbf{g})$

$$\epsilon = \epsilon_0 - \mu_0 H_i M_i + \frac{1}{2} \alpha \mathbf{M}^2 + \frac{1}{4} \beta (\mathbf{M}^2)^2 + \frac{1}{2} c_{ijkl} \varepsilon_{ij} \varepsilon_{kl} - \frac{1}{2} \gamma_{ijkl} \varepsilon_{ij} M_k M_l + \frac{1}{2\rho} \mathbf{g}^2. \quad (2.45)$$

The coupling to an external magnetic field, $\sim \mu_0 \mathbf{H}$, ensures the induced magnetization to be parallel to the field, while the next two terms describe the energy associated with the magnitude of the magnetization (modulus) $M \equiv \sqrt{\mathbf{M}^2}$. The elastic energy is described by the term $\sim c_{ijkl}$. To ensure that elasticity vanishes, when there are no columns, the phenomenological coefficients

of c_{ijkl} are proportional to \mathbf{M}^2 ,

$$c_{ijkl} = c_1 \mathbf{M}^2 \delta_{ij} \delta_{kl} + c_2 \mathbf{M}^2 (\delta_{ik} \delta_{jl} + \delta_{il} \delta_{kj}), \quad (2.46)$$

with c_1 corresponding to compressible and c_2 to shear strains. In the statics we have included a magnetostriction term $\sim \gamma_{ijkl}$, which produces as one of the consequences, the tilting of the chains or compression induced magnetization,

$$\gamma_{ijkl} = \gamma_1 \delta_{ij} \delta_{kl} + \gamma_2 (\delta_{ik} \delta_{jl} + \delta_{il} \delta_{kj}). \quad (2.47)$$

As mentioned we model the dynamic interplay of the linear momentum, the magnetization and the strain field, which is described by the following equations

$$\frac{d}{dt} g_i + \nabla_j (p \delta_{ij} - \psi_{ij} + \sigma_{ij}^{th} + \sigma_{ij}) = 0, \quad (2.48)$$

$$\frac{d}{dt} M_i + \epsilon_{ijk} M_j \omega_k + X_i = 0, \quad (2.49)$$

$$\frac{d}{dt} \varepsilon_{ij} + \varepsilon_{kj} \nabla_i v_k + \varepsilon_{ki} \nabla_j v_k - A_{ij} + Y_{ij} = 0, \quad (2.50)$$

where ψ_{ij} is the elastic stress. The viscoelastic properties of MR fluids are captured by considering a relaxing strain variable. In Eq. (2.50) this is contained by the term $Y_{ij} \sim (1/\tau)_{ijkl} \psi_{kl}$, where $(1/\tau)_{ijkl}$ takes the form

$$(1/\tau)_{ijkl} = \frac{1}{\tau_1 M_0^2} \delta_{ij} \delta_{kl} + \frac{1}{\tau_2 M_0^2} (\delta_{ik} \delta_{jl} + \delta_{jk} \delta_{il}). \quad (2.51)$$

We first studied the influence of a static shear deformation. The upper plate is moved along the x axis, perpendicularly to the columns. This is a common experimental technique to determine the stress-strain curves. Experimental results show that the elastic stress first increases linearly with the shear strain Γ . If one increases the strain further a saturation in the elastic stress is observed. In our model, the elastic stress is simply

$$\psi_{xz} = c_2 \mathbf{M}^2 \Gamma - \gamma_2 M_x M_z, \quad (2.52)$$

where the magnetization \mathbf{M} is determined from

$$\mu_0 H = \alpha M_z + c_2 \Gamma^2 M_z - \gamma_2 \Gamma M_x, \quad (2.53)$$

$$0 = \alpha M_x + c_2 \Gamma^2 M_x - \gamma_2 \Gamma M_z. \quad (2.54)$$

The elastic shear stress was calculated as a function of the shear strain, see Fig. 2.13. We find a quadratic dependence of the static yield stress ψ_{xz}^{yield} as a function of the magnetic field, in accordance with the experiments,

$$\psi_{xz}^{yield} \approx \frac{3\sqrt{3}}{16} \sqrt{\alpha c_2} \left(1 - \frac{3}{16} \frac{\gamma_2^2}{\alpha c_2} \right) \frac{\mu_0^2 H^2}{\alpha^2}. \quad (2.55)$$

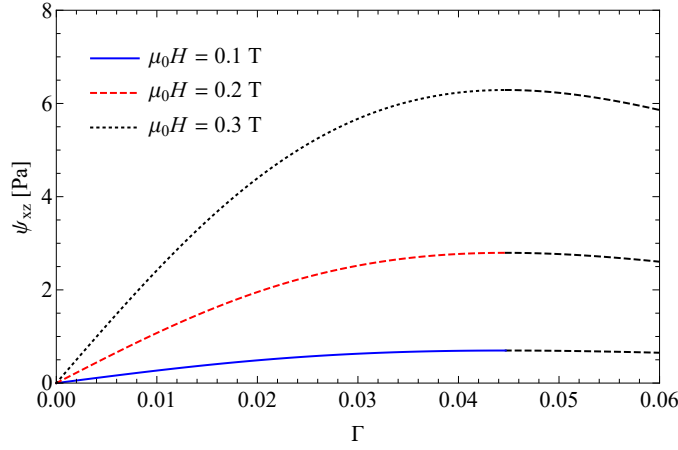


Figure 2.13: The elastic shear stress as a function of the shear strain $\gamma_2 = 0$ at three different values of the applied magnetic field. The black dashed parts of the curves represent the unstable regime, where the elastic shear stress decreases with the shear strain. Figure taken from Ref. [147].

A desirable property of MR fluids is a large yield stress. This can to some extent be achieved by a large magnetic field, however at large magnetic fields the magnetization saturates and with it also the yield stress. It was found that compressing the MR fluid uniaxially along the columns increases the shear yield stress, which can be understood by the fact that the compression makes the columns thicker, which can better resist the forces, compare Fig. 2.14. We have found that the magnetostriction coefficient $\sim \gamma_1$ accounts for these experimental findings. As a result of the compression, the magnetization M_z increases due to the magnetostrictive coupling $\sim \gamma_1$ (M_x vanishes in the $\gamma_2 = 0$ approximation),

$$M_z \approx \frac{\mu_0 H}{(\alpha + c_2 \Gamma^2)} + \frac{\gamma_1}{\bar{c}_1 \mu_0 H} P. \quad (2.56)$$

This leads to an increase of the yield stress linearly in the pressure for small pressures,

$$\psi_{xz}^{yield}(P) = \psi_{xz}^{yield}(0) + kP, \quad (2.57)$$

where $\psi_{xz}^{yield}(0)$ is the static yield stress without compression, and the slope k is

$$k \approx \frac{9}{32} \frac{\gamma_1}{\bar{c}_1} \sqrt{\frac{3c_2}{\alpha}}. \quad (2.58)$$

Dynamically, we have investigated the rheology of MR fluids under the influence of a steady shear and an oscillatory shear. We assume simple shear with a linear velocity profile of the form $\mathbf{v} = \dot{\gamma}z\hat{\mathbf{e}}_x$, where the so-called shear rate is constant for a steady shear flow, $\dot{\gamma} = \dot{\gamma}_0$, and time-dependent for oscillatory flow, $\dot{\gamma} = \dot{\gamma}_0 \cos(\omega t)$, with ω the oscillatory frequency.

The quantity of interest is the total stress tensor, the momentum density current in Eq. (2.48), contains the elastic stress tensor ψ_{ij} , as well as the dissipative and reversible phenomenological parts σ_{ij}^D and σ_{ij}^R ,

$$-\sigma_{xz}^{\text{tot}} = \nu_2 \dot{\gamma} + 2c_2 M^2 \varepsilon_{xz} + \frac{1}{2} (1 - 2c_2^R) \mu_0 H M_x + 2c_2^R M_x M_z (\alpha + \beta \mathbf{M}^2 + 4c_2 \varepsilon_{xz}^2). \quad (2.59)$$

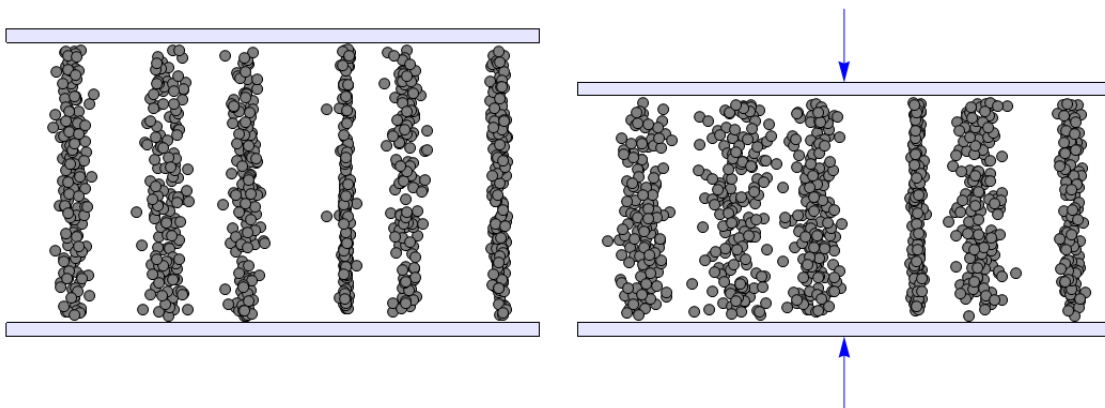


Figure 2.14: A schematic of the MR fluid in the uncompressed (left) and compressed state (right). The columns are thicker when the MR fluid is compressed, which corresponds in our model to a higher value of magnetization, Eq. (2.56).

We could produce flow curves, *i.e.* shear stress as a function of the shear rate, that are characterized by a fast initial increase at small shear rates, a peak at intermediate shear rates and a linear increase at large shear rates, see Fig. 2.15. The peak structure arises due to the fast increase of the elastic stress for small shear rates. At intermediate shear rates the magnetization starts to vanish quickly with the shear rate, which decreases the elastic stress contribution. Finally the flow curves converge to a linear increase of the shear stress with the shear rate given by the suspension viscosity ν_2 .

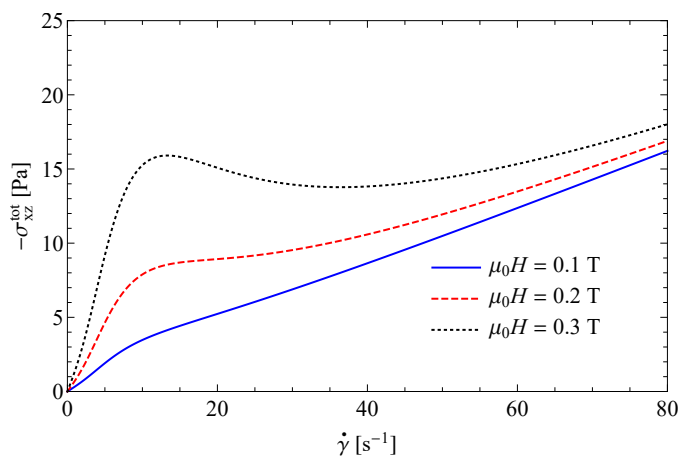


Figure 2.15: The shear stress $-\sigma_{xz}^{tot}$ as a function of the steady shear rate at three different values of the applied magnetic field. Figure taken from Ref. [147].

In the oscillatory shear mode, we were interested in the complex shear modulus $G = G' + iG''$, defined as the ratio of the shear stress σ_{xz}^{tot} , Eq. (2.59), and the imposed strain $-\gamma \equiv \dot{\gamma}/i\omega$, $G = \sigma_{xz}^{tot}/\gamma$. The real, G' , and the imaginary part, G'' , are the storage and the loss modulus, describing the reactive and dissipative response, respectively.

Experimental results show that the storage modulus is larger than the loss modulus at

intermediate frequencies and that both increase with increasing magnetic field, which we could qualitatively reproduce, see Fig. 2.16. This means that the system behaves more like a solid than a liquid, which is expected, since a small amplitude shear oscillation can only slightly influence the strength of the columns. For smaller frequencies, the numerical results show that the system behaves, as expected, more like a liquid than a solid, Fig. 2.16.

For low frequencies, the storage modulus increases quickly with frequency and then saturates for larger frequencies. This can be seen in Fig. 2.16. The initial rise of the storage modulus is quadratic in the frequency

$$G' \approx \left(\frac{\alpha}{4} (1 + 2c_2^R)^2 \tau_m^2 + c_2 \tau_{el}^2 \right) M_0^2 \omega^2, \quad (2.60)$$

while for larger frequencies the plateau value

$$G'_\infty = \left(\frac{\alpha}{4} (1 + 2c_2^R)^2 + c_2 \right) M_0^2 \quad (2.61)$$

is reached.

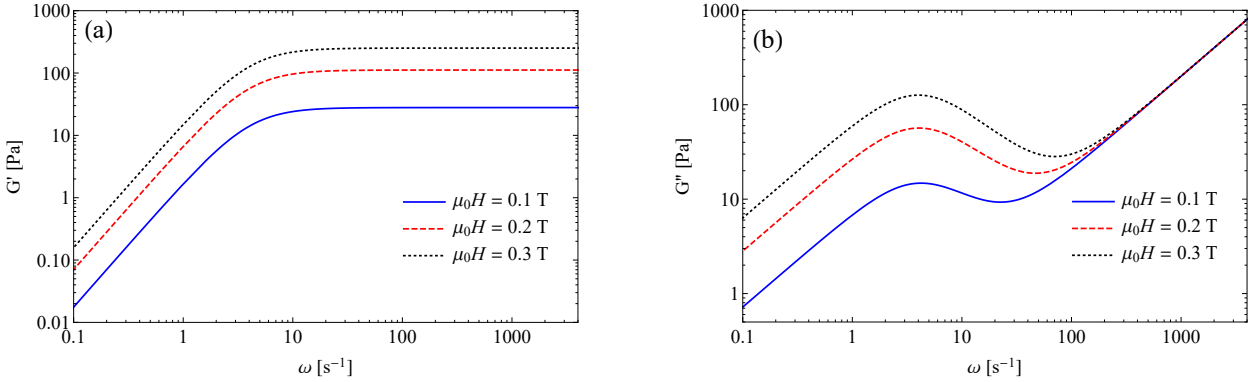


Figure 2.16: Storage modulus G' (left) and loss modulus G'' as a function of the frequency at three different values of the applied magnetic field. Figure taken from Ref. [147].

The loss modulus on the other hand, has a slightly more complicated behavior. Experimentally one has observed a maximum and a minimum in the frequency dependence of the loss modulus [148, 149]. We find that the frequency of the minimum ω_{\min} shifts linearly with the field, which is a testable prediction,

$$\omega_{\min} \approx \frac{M_0}{\sqrt{\nu_2}} \sqrt{\frac{4c_2^2}{\tau_2} + \frac{1}{4} (1 + 2c_2^R)^2 b^D \alpha^2}. \quad (2.62)$$

We found that a simple relation exists for the master curves g' and g'' of G' and G'' , respectively. The storage modulus has to be rescaled by a factor of $\mu_0 H^2$, $g'(\omega) = G'(\omega)/\mu_0 H^2$, while the viscosity term needs to be subtracted first from the loss modulus, $g''(\omega) = (G''(\omega) - \nu_2 \omega)/\mu_0 H^2$. Since the characteristic time scales, τ_m and τ_{el} are independent of magnetic field, the master curves are obtained without the need to rescale the frequency variable.

We also discussed the dependence of the absolute value of the complex shear modulus $|G| = \sqrt{(G')^2 + (G'')^2}$ on the frequency. After the initial linear increase, governed by the loss

modulus there is a plateau at intermediate frequencies, which is basically given by the plateau of the storage modulus G'_∞ , Eq. (2.61), since the loss modulus G'' is much smaller there. For high frequencies the loss modulus is dominating again, and $|G|$ increases linearly with the frequency.

This scenario applies to the case of (almost) equal elastic and magnetic time scales. If these time scales are sufficiently well separated, a somewhat different behavior of $|G|$ is found. After the very steep initial rise a very narrow plateau is found at rather low frequencies, which is approximately of height $c_2 M_0^2$ (for $\tau_{el} \ll \tau_m$) and $\frac{1}{4}(1 + 2c_2^R)^2 \alpha M_0^2$ (for $\tau_{el} \gg \tau_m$). At intermediate frequencies $|G|$ slowly increases to the combined plateau G'_∞ , Eq. (2.61), and finally converges to the asymptotic behavior independent of the relaxation times.

2.6 References

- [1] S. Odenbach, *Magnetoviscous Effects in Ferrofluids*, Lecture Notes in Physics Monographs 71, (Springer, Berlin, 2002).
- [2] R.E. Rosensweig, *Ferrohydrodynamics* (Cambridge University Press, Cambridge, 1985).
- [3] S. Odenbach, J. Phys.: Condens. Matter **16**, R1135 (2004).
- [4] M.I. Shliomis, Sov. Phys. Usp. **17**, 153 (1974).
- [5] S.S. Papell, U.S. Patent No. 3 215 572 (1965).
- [6] C. Scherer and A.M.F. Neto, Braz. J. Phys. **35**, 718 (2005).
- [7] R.E. Rosensweig, R. Kaiser, and G. Miskolczy, J. Colloid Interface Sci. **29**, 680 (1969).
- [8] J.P. McTague, J. Chem. Phys. **51**, 133 (1969).
- [9] H.-W. Müller and M. Liu, Phys. Rev. E **64**, 061405 (2001).
- [10] S. Odenbach and H.-W. Müller, Phys. Rev. Lett. **89**, 037202 (2002).
- [11] S. Odenbach and H.-W. Müller, J. Magn. Magn. Mater. **289**, 242 (2005).
- [12] Q.A. Pankhurst, J. Connolly, S.K. Jones, and J. Dobson, J. Phys. D: Appl. Phys. **36**, R167 (2003).
- [13] A.S. Lübke, C. Alexiou, and C. Bergemann, J. Surg. Res. **95**, 200 (2001).
- [14] R. Jurgons, C. Seliger, A. Hilpert, L. Thrams, S. Odenbach, and C. Alexiou, J. Phys.: Condens. Matter **18**, S2893 (2006).
- [15] P.G. de Gennes and J. Prost, *The Physics of Liquid Crystals* (Clarendon Press, Oxford, 1993).
- [16] G. Friedel, Ann. Phys. (Paris) **18**, 273 (1922).
- [17] C.W. Oseen, Trans. Faraday Soc. **29**, 883 (1933).
- [18] H. Zocher, Trans. Faraday Soc. **29**, 945 (1933).
- [19] F.C. Frank, Faraday Soc. Disc. **25**, 19 (1958).
- [20] J.L. Ericksen, Arch. Rat. Mech. Anal. **9**, 371 (1962).
- [21] J.L. Ericksen, Arch. Rat. Mech. Anal. **4**, 231 (1960).
- [22] F.M. Leslie, Arch. Rat. Mech. Anal. **28**, 265 (1968).
- [23] D. Forster, T.C. Lubensky, P.C. Martin, J. Swift, and P.S. Pershan, Phys. Rev. Lett. **26**, 1016 (1971).

- [24] P.C. Martin, O. Parodi, and P. Pershan, *Phys. Rev. A* **6**, 2401 (1972).
- [25] H.R. Brand, H. Pleiner, and D. Svenšek, *Rheol. Acta* **57**, 773 (2018).
- [26] H. Pleiner and H.R. Brand, *Phys. Rev. A* **25**, 995 (1982).
- [27] R. Reinitzer, *Monatsh. Chem.* **9**, 421 (1888).
- [28] O. Lehmann, *Z. Phys. Chem.* **4**, 462 (1889).
- [29] P. Chatelain, *Acta Crystallogr.* **1**, 315 (1948).
- [30] P.G. de Gennes, *C. R. Acad. Sci. (Paris)* **B266**, 15 (1968).
- [31] P. Yeh and C. Gu, *Optics of Liquid Crystal Displays*, (Wiley, New York, 1999).
- [32] Y. Geng, J. Noh, I. Drevenšek-Olenik, R. Rupp, G. Lenzini, and J.P.F. Lagerwall, *Sci. Rep.* **6**, 26840 (2016).
- [33] F. Brochard and P.G. de Gennes, *J. Phys. (France)* **31**, 691 (1970).
- [34] J. Rault, P.E. Cladis, and J. Burger, *Phys. Lett. A* **32**, 199 (1970).
- [35] S.-H. Chen and N. Amer, *Phys. Rev. Lett.* **51**, 2298 (1983).
- [36] P. Kopčanský, N. Tomašovičová, M. Koneracká, V. Závášová, M. Timko, A. Džarová, A. Šprincová, N. Éber, K. Fodor-Csorba, T. Tóth-Katona, A. Vajda, and J. Jadzyn, *Phys. Rev. E* **78**, 011702 (2008).
- [37] E. Ouskova, O. Buluy, C. Blanc, H. Dietsch and A. Mertelj, *Mol. Cryst. Liq. Cryst.* **525**, 104 (2010).
- [38] O. Buluy, S. Nepijko, V. Reshetnyak, E. Ouskova, V. Zadorozhnyi, A. Leonhardt, M. Ritschel, G. Schönhense, and Y. Reznikov, *Soft Matter* **7**, 644 (2011).
- [39] N. Podoliak, O. Buchnev, D.V. Bavykin, A.N. Kulak, M. Kaczmarek, T.J. Sluckin, *J. Colloid Interface Sci.* **386**,158 (2012).
- [40] N. Tomašovičová, M. Timko, Z. Mitróvá, M. Koneracká, M. Rajnak, N. Éber, T. Tóth-Katona, X. Chaud, J. Jadzyn, and P. Kopčanský, *Phys. Rev. E* **87**, 014501 (2013).
- [41] N. Podoliak, O. Buchnev, O. Buluy, G. D'Alessandro, M. Kaczmarek, Y. Reznikov, and T.J. Sluckin, *Soft Matter* **7**, 4742 (2011).
- [42] N. Tomašovičová, S. Burylov, V. Gdovinová, A. Tarasov, J. Kovac, N. Burylova, A. Voroshilov, P. Kopčanský, and J. Jadzyn, *J. Mol. Liq.* **267**, 390 (2018).
- [43] A. Mertelj, D. Lisjak, M. Drofenik and M. Čopič, *Nature* **504**, 237 (2013).
- [44] A. Mertelj, N. Osterman, D. Lisjak and M. Čopič, *Soft Matter* **10**, 9065 (2014).

- [45] R. Sahoo, M.V. Rasna, D. Lisjak, A. Mertelj, and S. Dahra, *Appl. Phys. Lett.* **106**, 161905 (2015).
- [46] A. Mertelj and D. Lisjak, *Liq. Cryst. Rev.* **5**, 1 (2017).
- [47] Q. Zhang, P.J. Ackerman, Q. Liu, and I.I. Smalyukh, *Phys. Rev. Lett.* **115**, 097802 (2015).
- [48] Q. Liu, P.J. Ackerman, T.C. Lubensky, and I.I. Smalyukh, *Proc. Natl. Acad. Sci.* **113**, 10479 (2016).
- [49] N. Sebastian, N. Osterman, D. Lisjak, M. Čopič, and A. Mertelj, *Soft Matter* **14**, 7180 (2018).
- [50] S.V. Burylov and Y.L. Raikher, *Mol. Cryst. Liq. Cryst.* **258**, 107 (1995).
- [51] S.V. Burylov and Y.L. Raikher, *Mol. Cryst. Liq. Cryst.* **258**, 123 (1995).
- [52] E. Jarkova, H. Pleiner, H.-W. Müller, A. Fink, and H.R. Brand, *Eur. Phys. J. E* **5**, 583 (2001).
- [53] E. Jarkova, H. Pleiner, H.-W. Müller, and H.R. Brand, *J. Chem. Phys.* **118**, 2422 (2003).
- [54] S.D. Peroukidis and S.H.L. Klapp, *Soft Matter* **12**, 6841 (2016).
- [55] P.J. Ackerman and I.I. Smalyukh, *Nat. Mater.* **16**, 426 (2017).
- [56] P. Medle Rupnik, D. Lisjak, M. Čopič, S. Čopar, and A. Mertelj, *Sci. Adv.* **3**, e1701336 (2017).
- [57] P. Medle Rupnik, D. Lisjak, M. Čopič, and A. Mertelj, *Liq. Cryst.* **42**, 1684 (2015).
- [58] G. Pelzl, A. Eremin, S. Diele, H. Kresse, and W. Weissflog, *J. Mat. Chem.* **12**, 2591 (2002).
- [59] W. Weissflog, M.W. Schröder, S. Diele, and G. Pelzl, *Adv. Mat.* **15**, 630 (2003).
- [60] V. Bourny, V. Lorman, J. Pavel, B. Mettout, and H.T. Nguyen, *Ferroelectrics* **276**, 127 (2002).
- [61] M.W. Schroeder, S. Diele, G. Pelzl, and W. Weissflog, *ChemPhysChem* **2004**, 99 (2004).
- [62] T. Niori, J. Yamamoto, and H. Yokoyama, *Mol. Cryst. Liq. Cryst.* **409**, 475 (2004).
- [63] D. Wiant, J.T. Gleeson, N. Eber, K. Fodor-Csorba, A. Jakli, and T. Toth-Katona, *Phys. Rev. E* **72**, 041712 (2005).
- [64] J. Harden, B. Mbang, N. Eber, K. Fodor-Csorba, S. Sprunt, J.T. Gleeson, and A. Jakli, *Phys. Rev. Lett.* **97**, 157802 (2006).
- [65] D. Wiant, S. Stojadinovic, K. Neupane, S. Sharma, K. Fodor-Csorba, A. Jakli, J.T. Gleeson, and S. Sprunt, *Phys. Rev. E* **73**, 030703 (2006).

- [66] D. Wiant, K. Neupane, S. Sharma, J.T. Gleeson, S. Sprunt, A. Jakli, N. Pradhan, and G. Iannacchione, *Phys. Rev. E* **77**, 061701 (2008).
- [67] T. Ostapenko, D.B. Wiant, S.N. Sprunt, A. Jakli, and J.T. Gleeson, *Phys. Rev. Lett.* **101**, 247801 (2008).
- [68] Y. Jang, R. Balachandran, C. Keith, A. Lehmann, C. Tschierske, and J.K. Vij, *Soft Matter* **8**, 10479 (2012).
- [69] F. Vita, I.F. Placentino, C. Ferreo, G. Singh, E.T. Samulski, and O. Francescangeli, *Soft Matter* **9**, 6475 (2013).
- [70] M. Jasinski, D. Pocięcha, H. Monobe, J. Szczytko, and P. Kaszynski, *J. Am. Chem. Soc.* **136**, 14658 (2014).
- [71] O.N. Kadkin, E.H. Kim, Y.J. Rha, S.Y. Kim, J. Taem and M.-G. Choi, *Chem. Eur. J.* **15**, 10343 (2009).
- [72] E.H. Kim, O.N. Kadkin, S.Y. Kim, J. Taem and M.-G. Choi, *Eur. J. Inorg. Chem.* **2011**, 2933 (2011).
- [73] H.R. Brand, H. Pleiner and P.E. Cladis, *Physica A* **351**, 189 (2005).
- [74] H.R. Brand and H. Pleiner, *Eur. Phys. J. E* **31**, 37 (2010).
- [75] H. Pleiner and H.R. Brand, *Eur. Phys. J. E* **37**, 11 (2014).
- [76] H.R. Brand and H. Pleiner, *Eur. Phys. J. E* **40**, 34 (2017).
- [77] H. Pleiner and H.R. Brand, *Braz. J. Phys.* **46**, 565 (2016).
- [78] L.G. Fel, *Phys. Rev. E* **52**, 702 (1995).
- [79] L.G. Fel, *Phys. Rev. E* **52**, 2692 (1995).
- [80] H.R. Brand, H. Pleiner and P.E. Cladis, *Eur. Phys. J. E* **7**, 163 (2002).
- [81] H.R. Brand, H. Pleiner and P.E. Cladis, *Eur. Phys. J. E* **11**, 283 (2003).
- [82] T. Ohta, T. Ohkuma, and K. Shitara, *Phys. Rev. E* **80**, 056203 (2009).
- [83] M. Tarama and T. Ohta, *Phys. Rev. E* **87**, 062912 (2013).
- [84] T. Hiraiwa, M.Y. Matsuo, T. Ohkuma, T. Ohta, and M. Sano, *EPL* **91**, 20001 (2010).
- [85] M. Zrinyi, *Trends in Polymer Science* **5**, 280 (1997).
- [86] M. Zrinyi, L. Barsi and A. Büki, *J. Chem. Phys.* **104**, 8750 (1996).
- [87] T. Mitsumata, K. Juliac, K. Furukawa, K. Iwakura, T. Taniguchi, and K. Koyoma, *Macromol. Rapid Commun.* **23**, 175 (2002).

- [88] Z. Varga, J. Fehér, G. Filipcsei and M. Zrínyi, *Macromol. Symp.* **200**, 93 (2003).
- [89] D. Collin, G.K. Auernhammer, O. Gavat, P. Martinoty, and H.R. Brand, *Macromol. Rapid Commun.* **24**, 737 (2003).
- [90] E. Jarkova, H. Pleiner, H.-W. Müller, and H.R. Brand, *Phys. Rev. E* **68**, 041706 (2003).
- [91] G. Pessot, P. Cremer, D.Y. Borin, S. Odenbach, H. Löwen, and A.M. Menzel, *J. Chem. Phys.* **141**, 124904 (2014).
- [92] S. Huang, G. Pessot, P. Cremer, R. Weeber, C. Holm, J. Nowak, S. Odenbach, A.M. Menzel, and G.K. Auernhammer, *Soft Matter* **12**, 228 (2016).
- [93] S. Bohlius, H.R. Brand, and H. Pleiner, *Phys. Rev. E* **70**, 061411 (2004).
- [94] M. Babincová, D. Leszczynska, P. Sourivong, P. Čičmanec and P. Babinec, *J. Magn. Magn. Mater.* **225**, 109 (2001).
- [95] N.S. Satarkar and J.Z. Hilt, *J. Control. Release* **130**, 246 (2008).
- [96] D. Müller-Schulte and T. Schmitz-Rode, *J. Magn. Magn. Mater.* **302**, 267 (2006).
- [97] T.-Y. Liu, S.-H. Hu, D.-M. Liu, S.-Y. Chen, and I.-W. Chen, *Nano Today* **4**, 52 (2009).
- [98] M. Zrínyi, *Coll. Polym. Sci.* **278**, 98 (2000).
- [99] W. König, *Ann. Phys. (Leipzig)* **25**, 618 (1885).
- [100] A.W. Duff, *Phys. Rev.* **4**, 23 (1896).
- [101] G. Quincke, *Ann. Phys. (Leipzig)* **62**, 1 (1897).
- [102] W.M. Winslow, *J. Appl. Phys.* **20**, 1137 (1949).
- [103] J. Rabinow, *AIEE Trans.* **67**, 1308 (1948).
- [104] M. Lopez-Lopez, P. Kuzhir, J. Caballero-Hernandez, L. Rodriguez Arco, J.D.G. Durán, and G. Bossis, *J. Rheol.* **56**, 1209 (2012).
- [105] P.P. Phulé, M.P. Mihalcin, and S. Genc, *J. Mater. Res.* **14**, 3037 (1999).
- [106] X. Tang, X. Zhang, R. Tao, and Y.M. Rong, *J. Appl. Phys.* **87**, 2634 (2000).
- [107] R. Tao, *J. Phys.: Condens. Matter* **13**, R979 (2001).
- [108] X.Z. Zhang, X.L. Gong, P.Q. Zhang, and Q.M. Wang, *J. Appl. Phys.* **96**, 2359 (2004).
- [109] J.W. Zhang, X.Q. Gong, C. Liu, W. Wen, and P. Sheng, *Phys. Rev. Lett.* **101**, 194503 (2008).
- [110] P. Sheng and W. Wen, *Solid State Commun.* **150**, 1023 (2010).

- [111] J.M. Ginder and L.C. Davis, *Appl. Phys. Lett.* **65**, 3410 (1994).
- [112] J.M. Ginder, in *Encyclopedia of Applied Physics*, Vol. 16 edited by G. L. Trigg (VCH, Weinheim, 1996), p. 487.
- [113] G. Bossis, E. Lemaire, O. Volkova, and H. Clercx, *J. Rheol.* **41**, 687 (1997).
- [114] G. Bossis, O. Volkova, S. Lacis, and A. Meunier, *Lect. Notes Phys.* **594**, 202 (2002).
- [115] D.J. Klingenberg and C.F. Zukoski, *Langmuir* **6**, 15 (1990).
- [116] G.L. Gulley and R. Tao, *Phys. Rev. E* **48**, 2744 (1993).
- [117] R.T. Bonnecaze and J.F. Brady, *J. Chem. Phys.* **96**, 2183 (1992).
- [118] S. Melle and J. E. Martin, *J. Chem. Phys.* **118**, 9875 (2003).
- [119] J.E. Martin, J. Odinek, T.C. Halsey, and R. Kamien, *Phys. Rev. E* **57**, 756 (1998).
- [120] T.C. Halsey, J. E. Martin, and D. Adolf, *Phys. Rev. Lett.* **68**, 1519 (1992).
- [121] P.O. Brunn and B. Abu-Jdayil, *Z. Angew. Math. Mech.* **78**, 97 (1998).
- [122] Y.M. Shkel and D.J. Klingenberg, *J. Rheol.* **43**, 1307 (1999).
- [123] A.T. Horvath, D.J. Klingenberg, and Y.M. Shkel, *Int. J. Mod. Phys. B* **16**, 2690 (2002).
- [124] R.E. Rosensweig, *J. Rheol.* **39**, 179 (1995).
- [125] K. von Pfeil, M.D. Graham, D.J. Klingenberg, and J.F. Morris, *Phys. Rev. Lett.* **88**, 188301 (2002).
- [126] K. von Pfeil, M.D. Graham, D.J. Klingenberg, and J.F. Morris, *J. Appl. Phys.* **93**, 5769 (2003).
- [127] K. von Pfeil and D.J. Klingenberg, *J. Appl. Phys.* **96**, 5341 (2004).
- [128] H. Pleiner and H. R. Brand, *Hydrodynamics and Electrohydrodynamics of Nematic Liquid Crystals*, in *Pattern Formation in Liquid Crystals*, edited by A. Buka and L. Kramer (Springer, New York, 1996).
- [129] D. Forster, *Hydrodynamic Fluctuations, Broken Symmetries and Correlation Functions* (W.A. Benjamin, Reading, Mass., 1975).
- [130] S.R. de Groot and P. Mazur, *Nonequilibrium Thermodynamics*, (North Holland, Amsterdam, 1962).
- [131] H.B. Callen, *Thermodynamics* (John Wiley, New York, 1985).
- [132] F.J. Belinfante, *Physica* **6**, 887 (1939).
- [133] D. Forster, *Ann. Phys. (N.Y.)* **84**, 505 (1974).

-
- [134] D. Forster, Phys. Rev. Lett. **32**, 1116 (1974).
- [135] L. Landau and E.M. Lifshitz, *Statistical Physics*, (Pergamon, New York, 1978).
- [136] T. Potisk, D. Svenšek, H.R. Brand, H. Pleiner, D. Lisjak, N. Osterman, and A. Mertelj, Phys. Rev. Lett. **119**, 097802 (2017).
- [137] T. Potisk, A. Mertelj, N. Sebastián, D. Lisjak, N. Osterman, H.R. Brand, H. Pleiner, and D. Svenšek, Phys. Rev. E **97**, 012701 (2018).
- [138] T. Potisk, H. Pleiner, D. Svenšek, and H.R. Brand, Phys. Rev. E **97**, 042705 (2018).
- [139] M. Miesowicz, Nature **136**, 261 (1935).
- [140] M. Miesowicz, Nature **158**, 27 (1946).
- [141] K. Skarp and T. Carlsson, Mol. Cryst. Liq. Cryst. **49**, 75 (1978).
- [142] T. Carlsson and K. Skarp, Mol. Cryst. Liq. Cryst. **78**, 157 (1981).
- [143] T. Potisk, H. Pleiner, and H.R. Brand, Phys. Rev. E **98**, 042703 (2018).
- [144] A. Menzel, H. Pleiner, and H.R. Brand, J. Appl. Phys. **105**, 013503 (2009).
- [145] A. Menzel, H. Pleiner, and H.R. Brand, Eur. Phys. J. E **30**, 371 (2009).
- [146] T. Potisk, H. Pleiner, and H.R. Brand, Eur. Phys. J. E **42**, 35 (2019).
- [147] T. Potisk, D. Svenšek, H. Pleiner, and H.R. Brand, J. Chem. Phys. **150**, 174901 (2019).
- [148] G. Wang, Y. Ma, G.H. Cui, N.N. Li, and X.F. Dong, Soft Matter **14**, 1917 (2018).
- [149] I. Arief and P.K. Mukhopadhyay, J. Alloys Compd. **696**, 1053 (2017).

2.7 Publications

Publication 1

Dynamic Magneto-optic Coupling in a Ferromagnetic Nematic Liquid Crystal

T. Potisk, D. Svenšek, H.R. Brand, H. Pleiner, D. Lisjak, N. Osterman, and A. Mertelj
Phys. Rev. Lett. **119**, 097802 (2017).

Dynamic Magneto-optic Coupling in a Ferromagnetic Nematic Liquid Crystal

Tilen Potisk,^{1,2,*} Daniel Svenšek,¹ Helmut R. Brand,² Harald Pleiner,³ Darja Lisjak,⁴
Natan Osterman,^{1,4} and Alenka Mertelj⁴

¹*Department of Physics, Faculty of Mathematics and Physics, University of Ljubljana, SI-1000 Ljubljana, Slovenia*

²*Theoretische Physik III, Universität Bayreuth, 95440 Bayreuth, Germany*

³*Max Planck Institute for Polymer Research, 55021 Mainz, Germany*

⁴*J. Stefan Institute, SI-1000 Ljubljana, Slovenia*

(Received 21 February 2017; published 1 September 2017)

Hydrodynamics of complex fluids with multiple order parameters is governed by a set of dynamic equations with many material constants, of which only some are easily measurable. We present a unique example of a dynamic magneto-optic coupling in a ferromagnetic nematic liquid, in which long-range orientational order of liquid crystalline molecules is accompanied by long-range magnetic order of magnetic nanoplatelets. We investigate the dynamics of the magneto-optic response experimentally and theoretically and find out that it is significantly affected by the dissipative dynamic cross-coupling between the nematic and magnetic order parameters. The cross-coupling coefficient determined by fitting the experimental results with a macroscopic theory is of the same order of magnitude as the dissipative coefficient (rotational viscosity) that governs the reorientation of pure liquid crystals.

DOI: 10.1103/PhysRevLett.119.097802

Fluids with an apolar nematic orientational ordering—nematic liquid crystals (NLCs)—are well known and understood, with properties useful for different types of applications [1]. As a contrast, the possible existence of fluids with a polar orientational order, thus of a lower symmetry than NLCs, has always been intriguing. An electrically polar nematic liquid was theoretically discussed [2] as early as the 1910s, but such a phase has never been observed. Similarly, vectorial magnetic ordering, i.e., ferromagnetism, is a phenomenon that occurs in solids and has been for the longest time considered hardly compatible with the liquid state.

Quite recently, however, ferromagnetic NLCs have been realized in suspensions of magnetic nanoplatelets in NLCs [3–5] and their macroscopic static properties were characterized in detail [6]. These systems possess two order parameters giving rise to two preferred directions—the nematic director \mathbf{n} (denoting the average orientation of liquid crystalline molecules) and the spontaneous magnetization \mathbf{M} (describing the density of magnetic moments of the nanoplatelets)—that are coupled statically as well as dynamically. As a consequence, optical and magnetic responses are coupled in these materials, which makes them particularly interesting in the multiferroic context: optical properties can be manipulated with a weak external magnetic field (a strong magneto-optic effect) and, conversely, the spontaneous magnetization can be reoriented by an external electric field (the converse magnetoelectric effect). Note that subjecting the liquid crystal to an external electric field is the usual means of controlling the nematic director in optical applications.

The search for a ferromagnetic nematic phase started when Brochard and de Gennes [7] suggested and discussed a ferromagnetic nematic phase combining the long-range

nematic orientational order with long-range ferromagnetic order in a fluid system. The synthesis and experimental characterization of ferronematics and ferrocholesterics, a combination of low-molecular-weight NLCs with magnetic liquids leading to a superparamagnetic phase, started immediately and continued thereafter [8–13] (also compare Ref. [14] for a recent review). These studies were making use of ferrofluids or magnetorheological fluids (colloidal suspensions of magnetic particles) [15]; their experimental properties [15,16] have been studied extensively in modeling [17–23] using predominantly macroscopic descriptions [17–22].

On the theoretical side, the macroscopic dynamics of ferronematics was given first for a relaxed magnetization [24] followed by taking into account the magnetization as a dynamic degree of freedom [25] as well as incorporating chirality effects leading to ferrocholesterics [26]. In parallel, a Landau description including nematic as well as ferromagnetic order has been presented [27].

In this Letter we describe experimentally and theoretically the dynamic properties of ferromagnetic NLCs, focusing on the coupled evolution of the magnetization and the director fields actuated by an external magnetic field. The dynamic coupling between \mathbf{M} and \mathbf{n} has been a complete blank to this day. It has been known that it is allowed by symmetry and the rules of linear irreversible thermodynamics, and was cast in a definite form theoretically [25] as a prediction. Here we demonstrate that these coupling terms influence decisively the dynamics. Quantitative agreement between the experimental results and the model is reached and a dissipative cross-coupling coefficient between the magnetization and the director is accurately evaluated. It is shown that this cross-coupling is crucial to account for the experimental

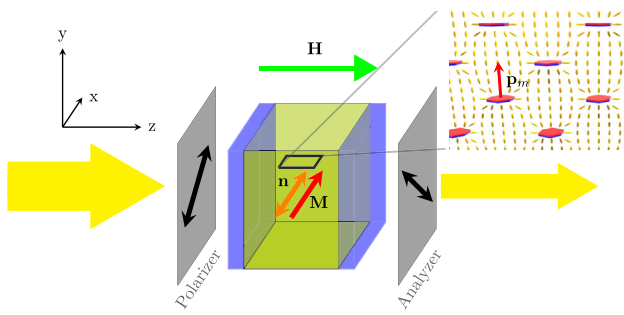


FIG. 1. Sketch of the experimental setup and definition of coordinate axes. The thick yellow arrows indicate the direction of the light passing through the polarizer and the analyzer. In the absence of an applied magnetic field (\mathbf{H} , z direction), the equilibrium director (\mathbf{n}) and magnetization (\mathbf{M}) fields are only slightly pretilted from the x direction. Inset: Distortion of the NLC director (ellipsoids, schematic) prevents flocculation of the suspended nanoplatelets carrying a magnetic moment \mathbf{p}_m parallel to \mathbf{n} in equilibrium.

results, thus underscoring the importance of such cross-coupling effects in this recent soft matter system.

The suspension of magnetic nanoplatelets in the NLC pentylcyanobiphenyl (5CB, Nematel) was prepared as described in Ref. [6]. The magnetic platelets with an average diameter of 70 nm and thickness of 5 nm, made of barium hexaferrite doped with scandium, were covered by the surfactant dodecylbenzenesulphonic acid (DBSA). The surfactant induced perpendicular anchoring of 5CB molecules on the platelet surface leading to parallel orientation of the platelet magnetic moments and the nematic director, Fig. 1 (inset). The volume concentration of the platelets in 5CB, determined by measuring the saturated magnetization of the suspension, was $\sim 3 \times 10^{-4}$, which corresponds to the magnetization magnitude of $M_0 \sim 50$ A/m. The suspension was put in a liquid crystal cell with thickness $d \sim 20 \mu\text{m}$, inducing planar homogeneous orientation of \mathbf{n} along the rubbing direction x , Fig. 1. During the filling process a magnetic field (not shown) of 8 mT was applied in the direction of the rubbing, so that a magnetic monodomain sample was obtained. In the absence of an external magnetic field the spontaneous magnetization \mathbf{M} was parallel to \mathbf{n} .

The suspension exhibits a strong magneto-optic effect. For example, when a magnetic field \mathbf{H} is applied perpendicularly to \mathbf{M} (z direction) it exerts a torque on the magnetic moments, i.e., on the platelets, and causes their reorientation. Because the orientations of the platelets and the director are coupled through the anchoring of the NLC molecules on the platelet's surface, \mathbf{n} also reorients, which is observed as an optic response. In Fig. 2 (left) the response of \mathbf{M} and \mathbf{n} is shown schematically. Note the small angle between \mathbf{M} and \mathbf{n} in equilibrium.

The reorientation of \mathbf{n} is detected optically by measuring the phase difference ϕ between transmitted extraordinary

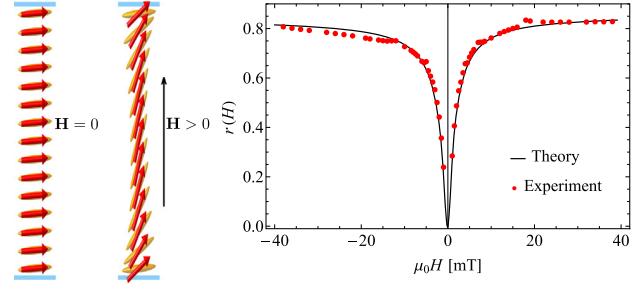


FIG. 2. Left: Response of the magnetization (red arrows) and the director (ellipsoids) to the external magnetic field \mathbf{H} applied in the z direction. Right: Equilibrium normalized phase difference $r(H)$ as a function of the magnetic field $\mu_0 H$, fitted by the static model.

and ordinary light [6], Fig. 1. The normalized phase difference $r(H) = 1 - \phi(H)/\phi_0$, where ϕ_0 is the phase difference at zero magnetic field, is shown in Fig. 2 (right) as a function of the applied magnetic field. While in ordinary nonpolar NLCs a finite threshold field needs to be exceeded to observe a response to the external field, in the ferromagnetic case the response is thresholdless.

The static response was quantitatively studied in Ref. [6]. Here we focus on the dynamics of the response. Figure 3 (top) shows two examples of the measured time dependence of the normalized phase difference $r(H)$. The time dependences of $r(H)$ acquired systematically for

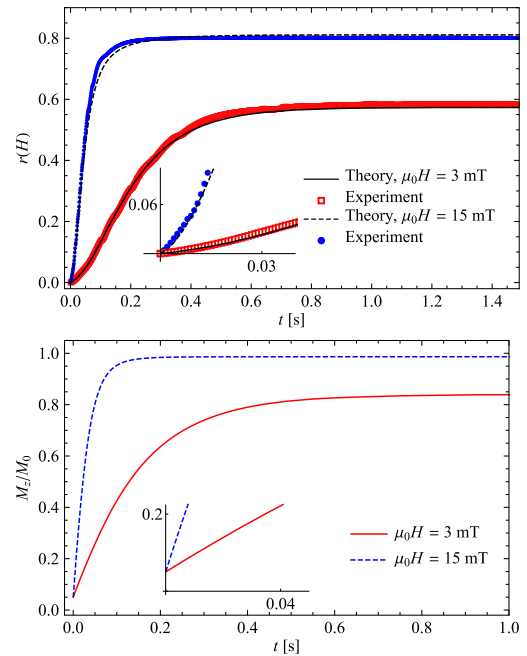


FIG. 3. Top: Time evolution of the normalized phase difference $r(H)$ fitted by the dynamic model Eqs. (2)–(11). The linear-quadratic onset of $r(H)$ is in accord with the analytic result given in Eq. (13). Bottom: The corresponding theoretical time evolution of M_z/M_0 , initially growing linearly as expected analytically.

several field strengths were fitted by a squared sigmoidal function,

$$f(t) = C' \left(1 - \frac{1 + C}{1 + C \exp(-2t/\tau)} \right)^2, \quad (1)$$

to obtain the characteristic switching time $\tau(H)$. Remarkably, its inverse shows a linear dependence on H , Fig. 4. Considering only a static (energetic) coupling between \mathbf{M} and \mathbf{n} one would expect that $1/\tau(H)$ saturates already at low fields as the transient angle between \mathbf{M} and \mathbf{n} gets larger.

In a minimal theoretical model we include the magnetization field $\mathbf{M}(\mathbf{r})$ and the director field $\mathbf{n}(\mathbf{r})$ and focus on the essential ingredients of their dynamics necessary to capture the experimental results. For a complete set of macroscopic dynamic equations for ferronematics, we refer to Ref. [25], and for ferromagnetic NLCs, to Ref. [28].

The statics is described by a free-energy density $f(\mathbf{M}, \mathbf{n}, \nabla \mathbf{n})$,

$$f = -\mu_0 \mathbf{M} \cdot \mathbf{H} - \frac{1}{2} A_1 (\mathbf{M} \cdot \mathbf{n})^2 + \frac{1}{2} A_2 (|\mathbf{M}| - M_0)^2 + f^F, \quad (2)$$

where μ_0 is the magnetic constant, $\mathbf{H} = H \hat{\mathbf{e}}_z$ is the homogeneous magnetic field fixed externally (since $H \gg M_0$), $A_{1,2} > 0$ will be assumed constant, and the Frank elastic energy of director distortions is [29]

$$f^F = \frac{1}{2} K_1 (\nabla \cdot \mathbf{n})^2 + \frac{1}{2} K_2 [\mathbf{n} \cdot (\nabla \times \mathbf{n})]^2 + \frac{1}{2} K_3 [\mathbf{n} \times (\nabla \times \mathbf{n})]^2, \quad (3)$$

with positive elastic constants for splay (K_1), twist (K_2), and bend (K_3). To a good approximation, one can assume that $|\mathbf{M}| = M_0$. We will, however, allow for small variations of $|\mathbf{M}|$ (large A_2), which is physically sound and technically convenient.

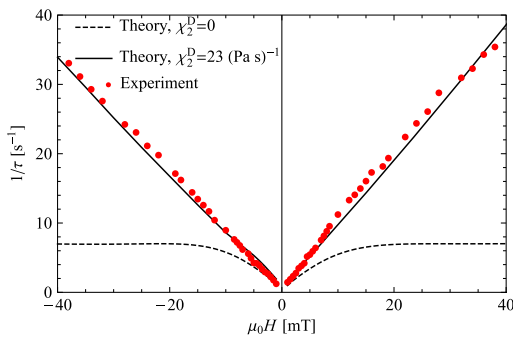


FIG. 4. The inverse of the switching time, $1/\tau(H)$, as a function of the magnetic field $\mu_0 H$, extracted from the experimental data and the theoretical results using the fitting function Eq. (1). Without the dynamic cross-coupling, $1/\tau(H)$ saturates already at low fields (dashed line).

At the cell plates, the director is anchored with a finite surface anchoring energy [30], $f^S = -\frac{1}{2} W (\mathbf{n}_S \cdot \mathbf{n})^2$, where W is the anchoring strength and $\mathbf{n}_S = \hat{\mathbf{e}}_z \sin \varphi_s + \hat{\mathbf{e}}_x \cos \varphi_s$ is the preferred direction specified by the director pretilt angle φ_s .

The total free energy is $F = \int f dV + \int f^S dS$, and the equilibrium condition requires $\delta F = 0$.

The dynamics is governed by the balance equations [25,31],

$$\dot{M}_i + X_i^R + X_i^D = 0, \quad (4)$$

$$\dot{n}_i + Y_i^R + Y_i^D = 0, \quad (5)$$

where the quasicharges have been split into reversible (X_i^R, Y_i^R) and irreversible, dissipative (X_i^D, Y_i^D) parts. The reversible (dissipative) parts have the same (opposite) behavior under time reversal as the time derivatives of the corresponding variables; i.e., Eqs. (4) and (5) are invariant under time reversal if and only if dissipative quasicharges are zero.

The quasicharges are expressed as linear combinations of conjugate quantities (thermodynamic forces), which in our case are the molecular fields

$$h_i^M \equiv \frac{\delta f}{\delta M_i} = \frac{\partial f}{\partial M_i}, \quad (6)$$

$$h_i^n \equiv \delta_{ik}^\perp \frac{\delta f}{\delta n_k} = \delta_{ik}^\perp \left(\frac{\partial f}{\partial n_k} - \partial_j \Phi_{kj} \right), \quad (7)$$

where $\Phi_{kj} = \partial f / \partial (\partial_j n_k)$ and $\delta_{ik}^\perp = \delta_{ik} - n_i n_k$ projects onto the plane perpendicular to the director owing to the constraint $\mathbf{n}^2 = 1$. These molecular fields can be viewed as exerting torques on \mathbf{M} and \mathbf{n} . In equilibrium they are zero, yielding the static solutions for \mathbf{M} and \mathbf{n} , Fig. 2. When they are nonzero, they generate quasicharges, which drive the dynamics through Eqs. (4) and (5). If there is no dynamic cross-coupling, h^M drives the dynamics of \mathbf{M} and h^n drives the dynamics of \mathbf{n} . In Fig. 4, $1/\tau(H)$ for this case is shown as the dashed line. The clear deviation from the experiments indicates the importance of the dynamic cross-coupling.

We will focus on the dissipative quasicharges as they have a direct relevance for the explanation of the experimental results discussed. The dissipative quasicharges read [25]

$$X_i^D = b_{ij}^D h_j^M + \chi_{ji}^D h_j^n, \quad (8)$$

$$Y_i^D = \frac{1}{\gamma_1} h_i^n + \chi_{ij}^D h_j^M, \quad (9)$$

where

$$\chi_{ij}^D = \chi_1^D \delta_{ik}^\perp M_k n_j + \chi_2^D \delta_{ij}^\perp M_k n_k, \quad (10)$$

$$b_{ij}^D = b_{\parallel}^D n_i n_j + b_{\perp}^D \delta_{ij}^\perp, \quad (11)$$

and we will everywhere disregard the biaxiality of the material tensors that takes place when $\mathbf{n} \nparallel \mathbf{M}$. We speculate that a possible origin of this dissipative dynamic coupling between \mathbf{M} and \mathbf{n} is a microscopic fluid flow localized in the vicinity of the rotating magnetic platelets.

The system Eqs. (4) and (5) is discretized in the z direction and solved numerically. By fitting the static data to the model, Fig. 2 (right), we extract the values for the anchoring strength $W \sim 2.3 \times 10^{-6}$ J/m², the pretilt angle $\varphi_s \sim 0.05$, and the static magnetic coupling coefficient $A_1 \sim 130\mu_0$. The agreement between the static experimental data and the model underscores that we have solid ground for the analysis of the dynamics.

In Fig. 3 (top) the measured time dependence of the normalized phase difference $r(H)$ is compared [6] to the model for two rather distinct values of the magnetic field. The fits are performed by varying the values of the dynamic parameters subject to stability restrictions, while keeping the values of W , φ_s , and A_1 fixed as determined from the statics. The model captures the dynamics very well for all times from the onset to the saturation. The extracted values of the dynamic parameters are $\gamma_1 \sim 0.03$ Pa s, $b_{\perp}^D \sim 7.8 \times 10^4$ A m/V s², and $\chi_2^D \sim 23$ (Pa s)⁻¹, which safely meets the positivity condition of the entropy production $|\chi_2^D| < \sqrt{b_{\perp}^D/(\gamma_1 M_0^2)} \sim 32$ (Pa s)⁻¹. The remaining two dynamic parameters do not affect the dynamics significantly and are set to $b_{\parallel}^D = b_{\perp}^D$ and $\chi_1^D = 0$.

Figure. 3 (bottom) shows the corresponding theoretical time dependence of the normalized z component of the magnetization, which is not measured due to insufficient time resolution of the vibrating sample magnetometer [6] (LakeShore 7400 Series VSM, several seconds are required for ambient magnetic noise averaging).

Initially, \mathbf{n} is homogeneous and aligned with \mathbf{M} , such that \mathbf{h}^n is zero and the director dynamics in Eq. (9) is due to \mathbf{h}^M alone. For small times when \mathbf{M} and \mathbf{n} are only slightly pretilted from the x direction, it thus follows from Eqs. (5) and (9) that

$$n_z(t) \approx \varphi_s + \chi_2^D M_0 \mu_0 H t, \quad (12)$$

and hence [6],

$$\begin{aligned} r(H) &= \frac{n_{0e}(n_{0e} + n_0)}{2n_0^2} [(\chi_2^D M_0 \mu_0 H)^2 t^2 + 2\varphi_s \chi_2^D M_0 \mu_0 H t] \\ &\equiv k^2 t^2 + p t, \end{aligned} \quad (13)$$

which is also revealed by Fig. 3 (top, inset); n_0 and n_{0e} are the ordinary and the extraordinary refractive indices. In principle, k^2 contains a small static coupling (A_1) correction linear in the pretilt, which is, however, within the error margin and is neglected. The initial dynamics of the director and the behavior of $r(H)$ are thus governed by the dissipative dynamic cross-coupling between director and magnetization, Eq. (9), described by the parameter χ_2^D .

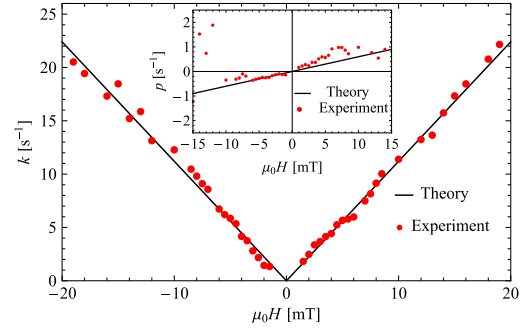


FIG. 5. The coefficients k and p (inset) of Eq. (13) as functions of $\mu_0 H$, extracted from the initial stage $r(H)$ measurements by the straight line fits.

Fitting Eq. (13) to the initial time evolution of measured normalized phase differences for several values of the magnetic field $\mu_0 H$, we determine the parameters k and p , Fig. 5, and extract therefrom values of the dissipative magnetization-director coupling parameter $\chi_2^D \sim (21 \pm 2)$ (Pa s)⁻¹ and the pretilt $\varphi_s \sim 0.05 \pm 0.03$.

The best match of $1/\tau(H)$, Fig. 4, extracted from the experimental data and the model via Eq. (1), allows for a robust evaluation of the dissipative magnetization-director coupling parameter: $\chi_2^D = (23 \pm 2)$ (Pa s)⁻¹. The theoretical results confirm that the linear shape of $1/\tau(H)$ is due precisely to this dissipative cross-coupling and would not take place if only the static coupling [the A_1 term in Eq. (2)] were at work, as demonstrated in Fig. 4 (dashed curve).

The coupling of \mathbf{M} and \mathbf{n} to flow was not taken into account. As flow is generated by gradients (i.e., divergence of the stress tensor), starting with a homogeneous configuration it is absent initially. To lowest order, Eq. (12) is thus unaffected by the flow coupling, irrespective of its details. Moreover, in ordinary NLCs the small backflow effect makes the response a little faster [32]. In a ferromagnetic NLC, additional couplings to the velocity field are possible. Nevertheless, the match of χ_2^D extracted from the initial (where flow is absent) and the overall dynamics speaks for only a minor flow coupling effect.

In summary, we have presented experimental and theoretical investigations of the magnetization and director dynamics in a ferromagnetic liquid crystal. We have demonstrated that a dissipative cross-coupling between the magnetization and the director, which has been determined quantitatively, is crucial to describe the experimental results. Such a coupling arises for all systems with macroscopic magnetization and director fields, and its presence dictated by symmetry has been pointed out before for ferronematics. Clearly its strength is expected to be higher in ferromagnetic systems of the type studied here. This coupling makes the response of such materials much faster, which is important for potential applications in magneto-optic devices, e.g., devices for magnetic field visualization [33]. Their main advantage compared to existing techniques is that both the magnitude and the direction of

the field can be simultaneously visualized. Further possible applications include remote optical sensing of magnetic fields and the use of a magnetic field to manipulate complex (patterned) structures in liquid crystals, e.g., for spatial light modulation [34,35]. An advantage of the magnetic field is that it can be applied in a noncontact way in any direction, whereas the application of the electric field is limited by the geometry of the electrodes. The main challenge is to produce a variety of suspensions with different magnetic and viscoelastic properties, stable in a wide temperature range.

We have laid here, in a pioneering step, the experimental and theoretical basis of a dynamic description. Naturally to include the coupling to flow is next. First experimental results in this direction have been described in Ref. [36], where it was shown that viscous effects can be tuned by an external magnetic field of about 10^{-2} T by more than a factor of 2, indicating a potential for applications in the field of smart fluids.

As ferromagnetic NLCs have two order parameters characterized by the magnetization and the director field, they offer the possibility to chiralize the material to obtain a ferromagnetic cholesteric NLC breaking parity and time-reversal symmetry in a fluid ground state. The formation of solitons in an unwound ferromagnetic cholesteric NLC has been recently realized and discussed in Refs. [35,37]. Another promising direction to pursue will be to produce a liquid crystalline version of uniaxial magnetic gels [38,39]. Cross-linking a ferromagnetic NLC gives rise to the possibility to obtain a soft ferromagnetic gel opening the door to a new class of magnetic complex fluids. This perspective looks all the more promising since recently [40,41] important physical properties of magnetic gels such as nonaffine deformations [40] and buckling of chains of magnetic particles [41] have been characterized well experimentally and modeled successfully.

Partial support through the Schwerpunktprogramm SPP 1681 of the Deutsche Forschungsgemeinschaft is gratefully acknowledged by H. R. B., H. P., T. P., and D. S., as well as the support of the Slovenian Research Agency, Grants No. N1-0019, J1-7435 (D. S.), No. P1-0192 (A. M. and N. O.), and No. P2-0089 (D. L.).

*tilen.potisk@uni-bayreuth.de

- [1] *Handbook of Liquid Crystals*, in Applications of Liquid Crystals, 2nd ed., edited by J. W. Goodby, P. J. Collings, T. Kato, C. Tschierske, H. Gleeson, and P. Raynes (Wiley-VCH, Weinheim, 2014), Vol. 8.
- [2] M. Born, in *Sitzungsberichte der Königlich Preussischen Akademie der Wissenschaften* (Verlag der Königl. Akademie der Wissenschaften, Berlin, 1916), pp. 614–650.
- [3] A. Mertelj, D. Lisjak, M. Drogenik, and M. Čopič, *Nature (London)* **504**, 237 (2013).
- [4] M. Shuai, A. Klitnick, Y. Shen *et al.*, *Nat. Commun.* **7**, 10394 (2016).
- [5] Q. Liu, P. J. Ackerman, T. C. Lubensky, and I. I. Smalyukh, *Proc. Natl. Acad. Sci. U.S.A.* **113**, 10479 (2016).
- [6] A. Mertelj, N. Osterman, D. Lisjak, and M. Čopič, *Soft Matter* **10**, 9065 (2014).
- [7] F. Brochard and P. G. de Gennes, *J. Phys. (Paris)* **31**, 691 (1970).
- [8] J. Rault, P. E. Cladis, and J. Burger, *Phys. Lett. A* **32**, 199 (1970).
- [9] S.-H. Chen and N. M. Amer, *Phys. Rev. Lett.* **51**, 2298 (1983).
- [10] P. Kopčanský, N. Tomašovičová, M. Koneracká *et al.*, *Phys. Rev. E* **78**, 011702 (2008).
- [11] E. Ouskova, O. Buluy, C. Blanc, H. Dietsch, and A. Mertelj, *Mol. Cryst. Liq. Cryst.* **525**, 104 (2010).
- [12] O. Buluy, S. Nepijko, V. Reshetnyak, E. Ouskova, V. Zadorozhnyi, A. Leonhardt, M. Ritschel, G. Schönhense, and Y. Reznikov, *Soft Matter* **7**, 644 (2011).
- [13] N. Podoliak, O. Buchnev, D. V. Bavykin, A. N. Kulak, M. Kaczmarek, and T. J. Sluckin, *J. Colloid Interface Sci.* **386**, 158 (2012).
- [14] Y. Reznikov, A. Glushchenko, and Y. Garbovskiy, in *Ferromagnetic and Ferroelectric Nanoparticles in Liquid Crystals*, edited by J. P. F. Lagerwall and G. Scalia, Liquid Crystals with Nano and Microparticles Vol. 2 (World Scientific, Singapore, 2016).
- [15] R. E. Rosensweig, *Ferrohydrodynamics* (Cambridge University Press, Cambridge, England, 1985).
- [16] S. Odenbach, *J. Phys. Condens. Matter* **16**, R1135 (2004).
- [17] S. V. Burylov and Y. L. Raikher, *Mol. Cryst. Liq. Cryst. Sci. Technol., Sect. A* **258**, 123 (1995).
- [18] H.-W. Müller and M. Liu, *Phys. Rev. E* **64**, 061405 (2001).
- [19] B. Huke and M. Lücke, *Rep. Prog. Phys.* **67**, 1731 (2004).
- [20] P. Ilg, E. Coquelle, and S. Hess, *J. Phys. Condens. Matter* **18**, S2757 (2006).
- [21] V. I. Zadorozhnyi, A. N. Vasilev, V. Yu. Reshetnyak, K. S. Thomas, and T. J. Sluckin, *Europhys. Lett.* **73**, 408 (2006).
- [22] S. Mahle, P. Ilg, and M. Liu, *Phys. Rev. E* **77**, 016305 (2008).
- [23] S. D. Peroukidis and S. H. L. Klapp, *Phys. Rev. E* **92**, 010501 (2015).
- [24] E. Jarkova, H. Pleiner, H.-W. Müller, A. Fink, and H. R. Brand, *Eur. Phys. J. E* **5**, 583 (2001).
- [25] E. Jarkova, H. Pleiner, H.-W. Müller, and H. R. Brand, *J. Chem. Phys.* **118**, 2422 (2003).
- [26] H. R. Brand, A. Fink, and H. Pleiner, *Eur. Phys. J. E* **38**, 65 (2015).
- [27] H. Pleiner, E. Jarkova, H.-W. Müller, and H. R. Brand, *Magnetohydrodynamics* **37**, 254 (2001).
- [28] T. Potisk *et al.* (to be published).
- [29] P. G. de Gennes and J. Prost, *The Physics of Liquid Crystals* (Clarendon Press, Oxford, 1995).
- [30] A. Rapini and M. Papoular, *J. Phys. Colloq.* **30**, C4-54 (1969).
- [31] H. Pleiner and H. R. Brand, in *Pattern Formation in Liquid Crystals*, edited by A. Buka and L. Kramer (Springer, New York, 1996).
- [32] D. Svenšek and S. Žumer, *Liq. Cryst.* **28**, 1389 (2001).

- [33] P. Medle Rupnik, D. Lisjak, M. Čopič, and A. Mertelj, *Liq. Cryst.* **42**, 1684 (2015).
- [34] A. J. Hess, Q. Liu, and I. I. Smalyukh, *Appl. Phys. Lett.* **107**, 071906 (2015).
- [35] P. J. Ackerman and I. I. Smalyukh, *Nat. Mater.* **16**, 426 (2017).
- [36] R. Sahoo, M. V. Rasna, D. Lisjak, A. Mertelj, and S. Dahra, *Appl. Phys. Lett.* **106**, 161905 (2015).
- [37] Q. Zhang, P. J. Ackerman, Q. Liu, and I. I. Smalyukh, *Phys. Rev. Lett.* **115**, 097802 (2015).
- [38] D. Collin, G. K. Auernhammer, O. Gavat, P. Martinoty, and H. R. Brand, *Macromol. Rapid Commun.* **24**, 737 (2003).
- [39] S. Bohlius, H. R. Brand, and H. Pleiner, *Phys. Rev. E* **70**, 061411 (2004).
- [40] G. Pessot, P. Cremer, D. Y. Borin, S. Odenbach, H. Löwen, and A. M. Menzel, *J. Chem. Phys.* **141**, 124904 (2014).
- [41] S. Huang, G. Pessot, P. Cremer, R. Weeber, C. Holm, J. Nowak, S. Odenbach, A. M. Menzel, and G. K. Auernhammer, *Soft Matter* **12**, 228 (2016).

Publication 2

Magneto-optic dynamics in a ferromagnetic nematic liquid crystal

T. Potisk, A. Mertelj, N. Sebastián, D. Lisjak, N. Osterman,
H.R. Brand, H. Pleiner, and D. Svenšek
Phys. Rev. E **97**, 012701 (2018).

Magneto-optic dynamics in a ferromagnetic nematic liquid crystalTilen Potisk,^{1,2,*} Alenka Mertelj,³ Nerea Sebastián,³ Natan Osterman,^{1,3} Darja Lisjak,³ Helmut R. Brand,² Harald Pleiner,⁴ and Daniel Svenšek¹¹*Department of Physics, Faculty of Mathematics and Physics, University of Ljubljana, SI-1000 Ljubljana, Slovenia*²*Department of Physics, University of Bayreuth, 95440 Bayreuth, Germany*³*J. Stefan Institute, SI-1000 Ljubljana, Slovenia*⁴*Max Planck Institute for Polymer Research, 55021 Mainz, Germany*

(Received 30 October 2017; published 5 January 2018)

We investigate dynamic magneto-optic effects in a ferromagnetic nematic liquid crystal experimentally and theoretically. Experimentally we measure the magnetization and the phase difference of the transmitted light when an external magnetic field is applied. As a model we study the coupled dynamics of the magnetization, \mathbf{M} , and the director field, \mathbf{n} , associated with the liquid crystalline orientational order. We demonstrate that the experimentally studied macroscopic dynamic behavior reveals the importance of a dynamic cross-coupling between \mathbf{M} and \mathbf{n} . The experimental data are used to extract the value of the dissipative cross-coupling coefficient. We also make concrete predictions about how reversible cross-coupling terms between the magnetization and the director could be detected experimentally by measurements of the transmitted light intensity as well as by analyzing the azimuthal angle of the magnetization and the director out of the plane spanned by the anchoring axis and the external magnetic field. We derive the eigenmodes of the coupled system and study their relaxation rates. We show that in the usual experimental setup used for measuring the relaxation rates of the splay-bend or twist-bend eigenmodes of a nematic liquid crystal one expects for a ferromagnetic nematic liquid crystal a mixture of at least two eigenmodes.

DOI: [10.1103/PhysRevE.97.012701](https://doi.org/10.1103/PhysRevE.97.012701)**I. INTRODUCTION**

In Ref. [1] Brochard and de Gennes suggested and discussed a ferromagnetic nematic phase combining the long-range nematic orientational order with long-range ferromagnetic order in a fluid system. The synthesis and experimental characterization of ferronematics and ferrocholesterics, a combination of low-molecular-weight nematic liquid crystals (NLCs) with magnetic liquids leading to a superparamagnetic phase, started immediately [2] and continued thereafter [3–9]. These studies made use of ferrofluids or magnetorheological fluids (colloidal suspensions of magnetic particles) [10]; their experimental properties [10,11] have been studied extensively in modeling [12–17] using predominantly macroscopic descriptions [12–14,16].

On the modeling side, the macroscopic dynamics of ferronematics was given first for a relaxed magnetization [18] followed by taking into account the magnetization as a dynamic degree of freedom [19] as well as incorporating chirality effects leading to ferrocholesterics [20]. In parallel a Landau description including nematic as well as ferromagnetic order has been presented [21].

Truly ferromagnetic NLCs have been generated [22] in 2013 followed by reports of further ferromagnetic NLCs in Refs. [23,24], and their macroscopic static properties were characterized in detail [25]. Quite recently ferromagnetic cholesteric liquid crystals have been synthesized and inves-

tigated [26–28]. For a review on ferromagnetic NLCs, see Ref. [29].

In the present paper we describe in detail experimentally and theoretically the static and dynamic properties of ferromagnetic NLCs [30]. We analyze the coupled dynamics of the magnetization and the director, initiated and controlled by an external magnetic field. We show experimentally and theoretically that dissipative dynamic coupling terms influence qualitatively the dynamics. Experimentally, this is done by measuring the temporal evolution of the normalized phase difference associated with the dynamics of the director. Quantitative agreement between the experimental results and the model is reached and a dissipative cross-coupling coefficient between the magnetization and the director is accurately evaluated. It is demonstrated that this cross-coupling is crucial to account for the experimental results thus underscoring the importance of such off-diagonal effects in this first multiferroic fluid system. We also make concrete theoretical predictions of how the reversible dynamic cross-coupling terms between magnetization and director influence the macroscopic dynamics and how these effects can be detected experimentally. The experimental and theoretical dynamic results discussed in some detail in this paper for low magnetic fields in ferromagnetic NLCs demonstrate the potential for applications of these materials in displays and magneto-optic devices as well as in the field of smart fluids.

The paper is organized as follows. In Sec. II we describe the experimental setup followed in Sec. III by the macroscopic model. The connection between the measurements and the model is established in Sec. IV. In Sec. V we analyze the

*tilen.potisk@uni-bayreuth.de

statics and in Secs. VI and VII we analyze in detail the coupled macroscopic dynamics of the magnetization and the director field when switching the external magnetic field on and off, respectively. Section VIII is dedicated to a theoretical analysis of fluctuations and light scattering and in the conclusions we give a summary of the main results and a perspective.

II. EXPERIMENTS

The experimental samples have been prepared along the lines described in detail in Refs. [22,25]. In brief, the $\text{BaSc}_x\text{Fe}_{12-x}\text{O}_{19}$ nanoplatelets were suspended in the liquid crystal mixture E7 (Merck, nematic-isotropic transition temperature $T_{\text{NI}} = 58^\circ\text{C}$). The suspension was filled in liquid crystal cells with rubbed surfaces (thickness $d = 20\ \mu\text{m}$, Instec Inc.), which induced homogeneous in-plane orientation of the NLC. The volume concentration of the magnetic platelets in the nematic low-molecular-weight liquid crystal E7 (Merck) has been estimated to be $\sim 1.3 \times 10^{-3}$ from the measurements of the magnetization magnitude [25] which was $M_0 \sim 200\ \text{A/m}$. E7 suspensions show long-term stability, with a homogeneous response to magnetic fields and no aggregates for a period of several months. A surfactant (dodecylbenzene sulfonic acid) was used for the treatment of the nanoplatelets, which favors a perpendicular orientation of the NLC molecules with respect to the nanoplatelets. Quantitative values for the Frank coefficients for E7 are available in the literature [31].

Dynamics of the director was measured by inducing director reorientation in planarly treated $20\text{-}\mu\text{m}$ cells (pretilt in the range $1^\circ\text{--}3^\circ$) when applying a magnetic field perpendicularly to the cell plates, Fig. 1 (top). Experiments were performed on monodomain samples (see Ref. [29] for a description of monodomain sample preparation) so that the director is initially at 45° with respect to the crossed polarizers, Fig. 1 (bottom). Using polarizing microscopy, the monochromatic light intensity transmitted through the sample was recorded with a complementary metal-oxide-semiconductor (CMOS) camera (IDS Imaging UI-3370CP, 997 fps) as a function of time on switching the magnetic field on and off. An interference filter (623.8 nm) was used to filter the light from the halogen lamp used in the microscope. The transmitted light intensity is related to the phase difference between the ordinary and the extraordinary light as will be explained below. The advantage of using polarization microscopy is that the measurements are performed in the homogeneous region of the sample without spacers or other impurities. Recording the image of the sample during the measurements also allows us to simultaneously monitor the homogeneity of the response.

With the use of a vibrating sample magnetometer [25] (LakeShore 7400 Series VSM) also the equilibrium z component of the magnetic moment of the sample is measured. We note that this technique is not suitable for measuring the magnetization dynamically, as several seconds per measurement are required for ambient magnetic noise averaging.

III. MACROSCOPIC MODEL

Throughout the present paper we take into account the magnetization \mathbf{M} and the director field \mathbf{n} as macroscopic variables; in the following we focus on the essential ingredients of their dynamics necessary to capture the experimental results

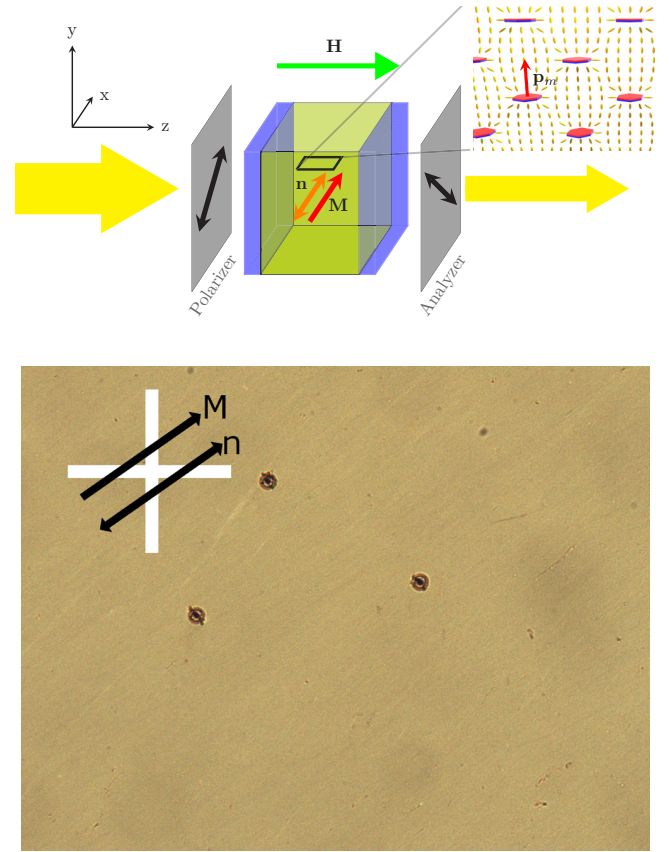


FIG. 1. Top: Sketch of the experimental setup and definition of coordinate axes [30]. The thick yellow arrows indicate the direction of the light passing through the polarizer and the analyzer. In the absence of an applied magnetic field (\mathbf{H} , z direction), the equilibrium director (\mathbf{n}) and magnetization (\mathbf{M}) fields are only slightly pretilted from the x direction. Inset: Distortion of the NLC director (ellipsoids, schematic) prevents flocculation of the suspended nanoplatelets carrying a magnetic moment \mathbf{p}_m parallel to \mathbf{n} in equilibrium. Bottom: Ferromagnetic E7 nematic $20\text{-}\mu\text{m}$ sample placed between crossed polarizers, with the director at an angle of 45° . Polarizing optical microscopy image width corresponds to $700\ \mu\text{m}$. The spheres are cell spacers.

we will discuss. That is we assume isothermal conditions and discard flow effects. For a complete set of macroscopic dynamic equations for ferronematics we refer to Ref. [19].

The static behavior is described by the free energy density $f(\mathbf{M}, \mathbf{n}, \nabla \mathbf{n})$,

$$f = -\mu_0 \mathbf{M} \cdot \mathbf{H} - \frac{1}{2} A_1 (\mathbf{M} \cdot \mathbf{n})^2 + \frac{1}{2} A_2 (|\mathbf{M}| - M_0)^2 + f^F, \quad (1)$$

where μ_0 is the magnetic constant, $\mathbf{H} = H \hat{\mathbf{e}}_z$ is the applied magnetic field, and $A_{1,2} > 0$ will be assumed constant. The first term represents the coupling of the magnetization and the external magnetic field. Since $H \gg M_0$, the local magnetic field is equal to \mathbf{H} , which is fixed externally and is thus independent of the $\mathbf{M}(\mathbf{r})$ configuration. The second term describes the static coupling between the director field and the magnetization (originating from the magnetic particles). The third term describes the energy connected with the deviation of the modulus of the magnetization from M_0 . The last term

is the Frank elastic energy associated with director distortions [32]

$$f^F = \frac{1}{2}K_1(\nabla \cdot \mathbf{n})^2 + \frac{1}{2}K_2[\mathbf{n} \cdot (\nabla \times \mathbf{n})]^2 + \frac{1}{2}K_3[\mathbf{n} \times (\nabla \times \mathbf{n})]^2, \quad (2)$$

with positive elastic constants for splay (K_1), twist (K_2), and bend (K_3). The saddle-splay elastic energy [32] is zero in the considered geometry. While it is a good approximation to assume that $|\mathbf{M}| = M_0$, we will take into account small variations of $|\mathbf{M}|$ (corresponding to large values of A_2).

The anchoring of the director at the plates is taken into account using a finite surface anchoring energy [33],

$$f^S = -\frac{1}{2}W(\mathbf{n}_S \cdot \mathbf{n})^2, \quad (3)$$

where W is the anchoring strength and $\mathbf{n}_S = \hat{\mathbf{e}}_z \sin \varphi_s + \hat{\mathbf{e}}_x \cos \varphi_s$ is the preferred direction specified by the director pretilt angle φ_s .

For the total free energy we have $F = \int f dV + \int f^S dS$ and the equilibrium condition requires $\delta F = 0$.

The macroscopic dynamic equations for the magnetization and the director read [19,34]

$$\dot{M}_i + X_i^R + X_i^D = 0, \quad (4)$$

$$\dot{n}_i + Y_i^R + Y_i^D = 0, \quad (5)$$

where the quasicurrents have been split into reversible (X_i^R, Y_i^R) and irreversible, dissipative (X_i^D, Y_i^D) parts. The reversible (dissipative) parts have the same (opposite) behavior under time reversal as the time derivatives of the corresponding variables, i.e., Eqs. (4) and (5) are invariant under time reversal only if the dissipative quasicurrents vanish.

The quasicurrents are expressed as linear combinations of conjugate quantities (thermodynamic forces); they take the form

$$h_i^M \equiv \frac{\delta f}{\delta M_i} = \frac{\partial f}{\partial M_i}, \quad (6)$$

$$h_i^n \equiv \delta_{ik}^\perp \frac{\delta f}{\delta n_k} = \delta_{ik}^\perp \left(\frac{\partial f}{\partial n_k} - \partial_j \Phi_{kj} \right), \quad (7)$$

with $\Phi_{kj} = \partial f / \partial (\partial_j n_k)$ and where the transverse Kronecker delta $\delta_{ik}^\perp = \delta_{ik} - n_i n_k$ projects onto the plane perpendicular to the director due to the constraint $\mathbf{n}^2 = 1$.

In Ref. [30] we focused on the dissipative quasicurrents as they had a direct relevance for the explanation of the experimental results discussed there. In the present paper we also include the reversible quasicurrents, which give rise to transient excursions of \mathbf{M} and \mathbf{n} out of the switching plane.

The dissipative quasicurrents take the form [19]

$$X_i^D = b_{ij}^D h_j^M + \chi_{ji}^D h_j^n, \quad (8)$$

$$Y_i^D = \frac{1}{\gamma_1} h_i^n + \chi_{ij}^D h_j^M, \quad (9)$$

with

$$\chi_{ij}^D = \chi_1^D \delta_{ik}^\perp M_k n_j + \chi_2^D \delta_{ij}^\perp M_k n_k, \quad (10)$$

$$b_{ij}^D = b_{\parallel}^D n_i n_j + b_{\perp}^D \delta_{ij}^\perp \quad (11)$$

Throughout the present paper we will discard the biaxiality of the material which arises for $\mathbf{n} \nparallel \mathbf{M}$.

The reversible quasicurrents are obtained by requiring that the entropy production $Y_i h_i^n + X_i h_i^M$ is zero [19]:

$$X_i^R = b_{ij}^R h_j^M + \chi^R \epsilon_{ijk} n_j h_k^n, \quad (12)$$

$$Y_i^R = (\gamma_1^{-1})_{ij}^R h_j^n + \chi^R \epsilon_{ijk} n_j h_k^M, \quad (13)$$

where [18]

$$b_{ij}^R = b_1^R \epsilon_{ijk} M_k + b_2^R \epsilon_{ijk} n_k n_p M_p + b_3^R (\epsilon_{ipq} M_p n_q n_j - \epsilon_{jpq} M_p n_q n_i), \quad (14)$$

$$(\gamma_1^{-1})_{ij}^R = (\gamma_1^{-1})_1^R \epsilon_{ijk} n_k n_p M_p + (\gamma_1^{-1})_2^R (\epsilon_{ijp} \epsilon_{ipk} n_k n_j - \epsilon_{jpk} n_k n_i) M_p. \quad (15)$$

For solving the system Eqs. (4) and (5) a simple numerical method was used. We first discretized space into slices of width $\Delta z = d/(N-1)$, where N is the number of discretization points. Empirically it was found that using $N = 50$ is already sufficient. After discretizing space one obtains N ordinary differential equations. Due to its simplicity, we use the Euler method. One step of the Euler method for the i th component of the director field at z is

$$n_i(t + \delta t, z) = n_i(t, z) - \delta t Y_i(t, z) + \mathcal{O}(\delta t^2), \quad (16)$$

where δt is the time step. An analogous equation holds for the magnetization field and the equations are solved simultaneously. Since the numerical scheme for the director field is not norm preserving, we normalize the director field after each time step: $n_i \rightarrow n_i / \sqrt{n_j n_j}$.

In the discrete version, the two surface points are best treated by satisfying the same dynamic equations Eqs. (4) and (5) as the internal points, with the addition of the surface anchoring energy Eq. (3) expressed as a volume density. The divergence part of the force Eq. (7) is then replaced by its surface flux (the volume density thereof again):

$$h_i^{n, \text{surf.}} = \delta_{ik}^\perp \left[\frac{\partial f}{\partial n_k} + \frac{1}{\Delta z} \left(v_j \Phi_{kj} + \frac{\partial f^S}{\partial n_k} \right) \right], \quad (17)$$

where \mathbf{v} is the surface normal pointing down (up) at the bottom (top) plate.

IV. CONNECTION BETWEEN MEASUREMENTS AND THE MODEL

In equilibrium the magnetic-field-distorted director and magnetization fields are lying in the xz plane, $\mathbf{n} = (\sin \theta, 0, \cos \theta)$ and $\mathbf{M} = M(\sin \psi, 0, \cos \psi)$. In the absence of the magnetic field, the director is tilted from the x axis by the pretilt φ_s , Eq. (3). The coordinate system used here is shown in Fig. 1. As explained earlier, the average z component of the magnetization, M_z , is measured by the vibrating sample magnetometer. In modeling, it is obtained by averaging the z component of the magnetization field,

$$M_z = \frac{1}{d} \int_0^d M \cos \psi(z) dz. \quad (18)$$

To derive the expression for the phase difference we start with an electric field \mathbf{E} , which is linearly polarized after the light passes through the polarizer,

$$\mathbf{E} = E_0 \mathbf{j} e^{i(\mathbf{k}_i \cdot \mathbf{r} - \omega t)}, \quad (19)$$

where E_0 is the electric field amplitude, \mathbf{j} the initial polarization, \mathbf{k}_i the wave vector, and ω the frequency of the incident light. In our case the wave vector points in the z direction, $\mathbf{k}_i = k_0 \hat{\mathbf{e}}_z$, with $k_0 = \frac{2\pi}{\lambda}$ being the wave number. The polarization of the light therefore lies in the xy plane and is described by the two-component complex vector $\mathbf{j} = j_x(z) \hat{\mathbf{e}}_x + j_y(z) \hat{\mathbf{e}}_y$. As the light passes through the sample also the components of this (Jones) polarization vector change and we analyze these changes using the Jones matrix formalism (assuming perfectly polarized light) [35].

The incident light first goes through the polarizer oriented at 45° with respect to the x axis, Fig. 1, and is linearly polarized with the initial Jones vector being $\mathbf{j} = \frac{1}{\sqrt{2}}(1, 1)^T$. The optical axis is parallel to the director and generally varies through the cell. For any ray direction we can decompose the polarization into a polarization perpendicular to the optical axis (ordinary ray) and a polarization which is partly in the direction of the optical axis (extraordinary ray). The ordinary ray experiences an ordinary refractive index n_o and the extraordinary ray experiences a refractive index n_e ,

$$n_e^{-2}(z) = n_o^{-2} \sin^2 \theta(z) + n_e^{-2} \cos^2 \theta(z), \quad (20)$$

where n_{e0} is the extraordinary refractive index.

To calculate the intensity of the transmitted light, one first divides the liquid crystal cell into N thin slices of width $h = d/N$ and describes the effect of each slice on the polarization by the phase matrix

$$\mathbf{W}(z) = \begin{pmatrix} e^{ik_0[n_e(z)-n_o]h/2} & 0 \\ 0 & e^{-ik_0[n_e(z)-n_o]h/2} \end{pmatrix}. \quad (21)$$

In the limit $N \rightarrow \infty$ we can express the transmission matrix of the liquid crystal cell as

$$\mathbf{T} = \begin{pmatrix} e^{i\phi/2} & 0 \\ 0 & e^{-i\phi/2} \end{pmatrix}, \quad (22)$$

where we have introduced the phase difference

$$\phi = k_0 \int_0^d [n_e(z) - n_o] dz. \quad (23)$$

In general, as we will see, the director can have also a nonzero component in the y direction. In this case the simple expression for the transmission matrix Eq. (22) does not hold anymore and must be generalized.

We start the derivation of the general transmission matrix by assuming a general orientation of the director,

$$\mathbf{n} = (\sin \theta \cos \varphi, \sin \theta \sin \varphi, \cos \theta). \quad (24)$$

The azimuthal angle of the director φ can vary through the cell and the transformation matrix at point z is

$$\mathbf{T}(z) = \mathbf{R}[-\varphi(z)] \mathbf{W}(z) \mathbf{R}[\varphi(z)], \quad (25)$$

where \mathbf{R} is the rotation matrix

$$\mathbf{R}(\varphi) = \begin{bmatrix} \cos(\varphi) & \sin(\varphi) \\ -\sin(\varphi) & \cos(\varphi) \end{bmatrix}. \quad (26)$$

Our goal is to find the transfer matrix for the whole cell,

$$\mathbf{T} = \overleftarrow{\prod}_{z \in [0, d]} \mathbf{T}(z), \quad (27)$$

where the arrow denotes the ordered product starting from $\mathbf{T}(0)$ at the right side. We first notice that

$$\mathbf{T}(z) \approx \mathbf{I} + i \frac{k_0[n_e(z) - n_o]h}{2} \begin{pmatrix} \cos[2\varphi(z)] & \sin[2\varphi(z)] \\ \sin[2\varphi(z)] & -\cos[2\varphi(z)] \end{pmatrix}, \quad (28)$$

where \mathbf{I} is the identity matrix. Consequently, we can write $\mathbf{T}(z)$ as an exponential,

$$\mathbf{T}(z) = \lim_{h \rightarrow 0} \exp[i\mathbf{A}(z)h], \quad (29)$$

where \mathbf{A} is defined by

$$\mathbf{A}(z) = \frac{k_0[n_e(z) - n_o]}{2} \begin{pmatrix} \cos[2\varphi(z)] & \sin[2\varphi(z)] \\ \sin[2\varphi(z)] & -\cos[2\varphi(z)] \end{pmatrix}. \quad (30)$$

We can now rewrite Eq. (27) as

$$\mathbf{T} = \lim_{h \rightarrow 0} \exp \left[i \sum_{z \in [0, d]} \mathbf{A}(z)h \right] = \exp \left[i \int_0^d \mathbf{A}(z) dz \right], \quad (31)$$

where we used

$$e^{\mathbf{A}h} e^{\mathbf{B}h} = e^{(\mathbf{A}+\mathbf{B})h} + \frac{1}{2}[\mathbf{A}, \mathbf{B}]h^2 + \mathcal{O}(h^3). \quad (32)$$

The exponential of the 2×2 matrix from Eq. (31) reads

$$\mathbf{T} = \begin{bmatrix} \cos(c) + i \frac{a}{c} \sin(c) & i \frac{b}{c} \sin(c) \\ i \frac{b}{c} \sin(c) & \cos(c) - i \frac{a}{c} \sin(c) \end{bmatrix}, \quad (33)$$

where $c = \sqrt{a^2 + b^2}$ with

$$a = \frac{k_0}{2} \int_0^d [n_e(z) - n_o] \cos[2\varphi(z)] dz, \\ b = \frac{k_0}{2} \int_0^d [n_e(z) - n_o] \sin[2\varphi(z)] dz. \quad (34)$$

We then let the light pass through an analyzer \mathbf{P}_α at an angle α ,

$$\mathbf{P}_\alpha = \begin{pmatrix} \cos^2 \alpha & \sin \alpha \cos \alpha \\ \sin \alpha \cos \alpha & \sin^2 \alpha \end{pmatrix}, \quad (35)$$

which gives for the final Jones vector ($\alpha = -45^\circ$)

$$\mathbf{j}' = \frac{ia \sin(c)}{\sqrt{2}c} \begin{pmatrix} 1 \\ -1 \end{pmatrix}. \quad (36)$$

This yields the measured normalized intensity

$$\frac{I}{I_0} = \mathbf{j}'^{*T} \mathbf{j}' = \frac{a^2}{c^2} \sin^2(c). \quad (37)$$

Next we evaluate the relation between the phase difference and the measured intensity. Let \mathbf{j} be the Jones vector after the liquid crystal cell,

$$\mathbf{j} = \begin{pmatrix} z_1 e^{i\phi} \\ z_2 \end{pmatrix}, \quad (38)$$

where z_1 and z_2 are real and $z_1^2 + z_2^2 = 1$. Generally $|z_1| \neq |z_2|$. After an analyzer with $\alpha = -45^\circ$ we have a Jones vector

$$\mathbf{j}' = \frac{1}{2}(z_1 e^{i\phi} - z_2) \begin{pmatrix} 1 \\ -1 \end{pmatrix} \quad (39)$$

and the intensity is related to the phase difference as

$$\frac{I}{I_0} = \frac{1}{2}[1 - 2z_1 z_2 \cos(\phi)]. \quad (40)$$

Only if the director is restricted to the xz plane, $z_1 = z_2$ and we have

$$\frac{I}{I_0} = \frac{1}{2}[1 - \cos(\phi)] = \sin^2\left(\frac{\phi}{2}\right), \quad (41)$$

such that the relation between the intensity and the phase difference is

$$\phi = m\pi \pm 2 \arcsin \left[\sqrt{\frac{I}{I_0}} \right], \quad (42)$$

where $m \in \mathbb{Z}$ and the sign \pm is determined by demanding that ϕ is sufficiently smooth. Generally, however, the quantity obtained from the measured intensity by Eq. (42) is not the phase difference. It is the phase difference only when the director field is in the xz plane. For the analysis of the dynamics not confined to the xz plane, Sec. VIC, we will therefore use the normalized intensity Eq. (37).

In the case when the dynamics is in the xz plane, to compare the numerical results with the experiments and also to compare the dynamics of the director with the dynamics of the magnetization, it is convenient to introduce the normalized phase difference

$$r(H) = 1 - \frac{\phi(H)}{\phi_0}, \quad (43)$$

where ϕ_0 is the phase difference at zero magnetic field. The normalized phase difference is zero at $t = 0$ and is always smaller or equal to 1. It can also assume negative values as we will see.

V. STATICS

In this section we present experimental and numerical results of statics and derive analytic formulas for the equilibrium configurations in the low and large external magnetic field limits.

In Fig. 2 we compare the numerical results of the equilibrium normalized phase difference to the experimental data. Below we will show in Eqs. (52) and (53) that the equilibrium normalized phase difference is quadratically dependent on the applied magnetic field at small magnetic fields. The normalized phase difference saturates quickly above $\mu_0 H = 10$ mT at a value which is less than 1, which means there is a limit to how much the director field deforms. We also observe that the dependence of the equilibrium normalized phase difference is not symmetric with respect to the $\mu_0 H = 0$ axis, which is seen in experiments as well. The reason for this is the nonzero pretilt at both glass plates.

From the fits to the model we extract values for the anchoring strength W , the pretilt angle φ_s , the Frank elastic constant $K \equiv K_1 = K_3$ in the one constant approximation, and

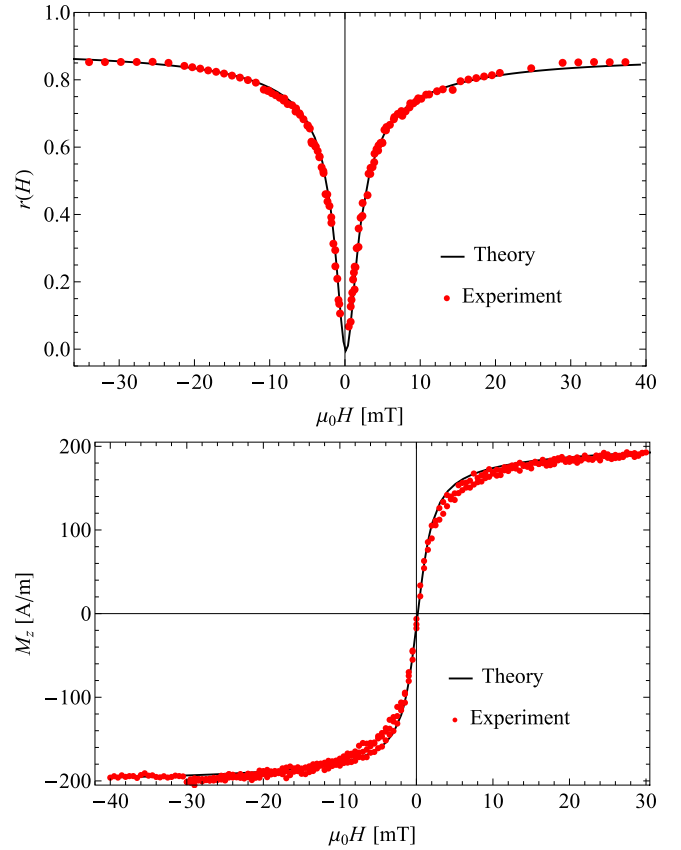


FIG. 2. Comparison of experimental and theoretical static results. Top: Normalized phase difference $r(H)$. Bottom: Magnetization component M_z as functions of the magnetic field $\mu_0 H$.

the static coupling coefficient A_1 :

$$W \sim 4 \times 10^{-5} \text{ J/m}^2, \quad (44)$$

$$\varphi_s \sim -0.05, \quad (45)$$

$$K \sim 17 \text{ pN}, \quad (46)$$

$$A_1 \sim 140\mu_0. \quad (47)$$

The extracted parameters Eqs. (44)–(47) correspond to the (local) minimum of the sum of squares of residuals between the numerical and experimental values of the normalized phase difference. This minimum was sought in sensible parameter ranges (for example, the Frank elastic constant was sought in the range between 5 and 25 pN). There are several indications that this minimum is at least very close to the global one. First, the extracted value of the Frank elastic constant is close to the value of K_3 in the pure E7 NLC. Second, the extracted pretilt is within the range specified by the cell provider. Moreover, the value of the static coupling is similar to that estimated for the ferromagnetic NLC based on pentylcyanobiphenyl (5CB) [25].

The limiting behaviors of the normalized phase difference and the normalized z component of the magnetization as the magnetic field goes to zero or infinity can be calculated analytically. In all cases the boundary condition is

$$K \frac{\partial \theta}{\partial z} v_z + \frac{\partial f^S}{\partial \theta} = 0, \quad (48)$$

where v_z is the z component of the surface normal pointing upwards at $z = d$ and downwards at $z = 0$.

A. Low magnetic fields

The free energy density in lowest order in deviations of magnetization and director field from the equilibrium is

$$f = \frac{1}{2}K \left(\frac{\partial \theta}{\partial z} \right)^2 + \frac{1}{2}A_1 M_0^2 (\theta - \psi)^2 + \mu_0 H M_0 \psi. \quad (49)$$

The equilibrium solutions for the angles are

$$\theta(z) = \frac{1}{2} \frac{\mu_0 H M_0}{K} z(z-d) - \frac{\mu_0 H M_0 d}{2W} + \frac{\pi}{2} - \varphi_s, \quad (50)$$

$$\psi(z) = \theta(z) - \frac{\mu_0 H M_0}{A_1 M_0^2}. \quad (51)$$

After inserting the solutions Eqs. (50) in equations for the normalized phase difference and magnetization, one gets

$$r(H) = r_0 \frac{\mu_0 H M_0 d^2}{6K} \times \left[\frac{\mu_0 H M_0 d^2}{20K} \left(1 + 10 \frac{\xi}{d} + 30 \frac{\xi^2}{d^2} \right) + \left(1 + 6 \frac{\xi}{d} \right) \varphi_s \right], \quad (52)$$

where $\xi = K/W$ is the so-called anchoring extrapolation length and $r_0 = n_{e0}(n_{e0} + n_o)/(2n_o^2)$. In the limit of infinite anchoring the normalized phase difference reads

$$r(H) = r_0 \frac{\mu_0 H M_0 d^2}{6K} \left(\frac{\mu_0 H M_0 d^2}{20K} + \varphi_s \right). \quad (53)$$

One can also observe that the location of the minimum of the normalized phase difference is shifted to a value $\mu_0 H_{\min}$ determined by the pretilt:

$$-\frac{10K\varphi_s(1+6\frac{\xi}{d})}{M_0 d^2(1+10\frac{\xi}{d}+30\frac{\xi^2}{d^2})} \xrightarrow{W \rightarrow \infty} -\frac{10K\varphi_s}{M_0 d^2}. \quad (54)$$

Equations (52) and (54) are useful for determining the anchoring strength W and the pretilt φ_s .

From the behavior of the normalized phase difference at low fields [Eqs. (52) and (53)] one cannot determine the value of the static coupling A_1 . It can, on the other hand, be determined from the low-field behavior of the magnetization. In Fig. 2 we see that the behavior is linear for low magnetic fields as can be shown analytically:

$$\frac{M_z}{M_0} = \varphi_s + \left(\frac{1}{A_1 M_0^2} + \frac{1}{12} \frac{d^2}{K} + \frac{d}{2W} \right) \mu_0 H M_0. \quad (55)$$

B. Large magnetic fields

In the large-magnetic-field limit we assume that both the polar angle of the director and the magnetization are either close to 0 if the applied magnetic field is positive (+) or close to π if the applied magnetic field is negative (-). The corresponding solutions will be denoted as $\theta^+(z), \theta^-(z), \psi^+(z), \psi^-(z), M_z^+, M_z^-, r^+$, and r^- .

The free energy in the case of a positive magnetic field is

$$f \approx \frac{1}{2}K \left(\frac{\partial \theta}{\partial z} \right)^2 + \frac{1}{2}A_1 M_0^2 (\theta - \psi)^2 + \frac{1}{2} \mu_0 H M_0 \psi^2. \quad (56)$$

The equilibrium solutions for the angles $\theta^+(z)$ and $\psi^+(z)$ are

$$\theta^+(z) = \frac{\frac{\pi}{2} - \varphi_s}{1 + q\xi \tanh(\frac{qd}{2})} \frac{\cosh[q(z - \frac{d}{2})]}{\cosh(\frac{qd}{2})}, \quad (57)$$

$$\psi^+(z) = \frac{\theta^+(z)}{1 + \frac{\mu_0 |H| M_0}{A_1 M_0^2}}, \quad (58)$$

where

$$q^2 = q_0^2 \frac{\mu_0 |H| M_0}{\mu_0 |H| M_0 + A_1 M_0^2} \quad (59)$$

with $q_0 = \sqrt{A_1 M_0^2 / K}$ (which is proportional to the inverse ‘‘magnetization coherence length’’ of the director).

The normalized z component of the magnetization for large fields is

$$\frac{M_z^+}{M_0} = 1 - \frac{[\frac{\pi}{2} - \varphi_s]^2 (qd + \sinh(qd)) A_1^2 M_0^4}{4qd [1 + q\xi \tanh(\frac{qd}{2})]^2 \cosh^2(\frac{qd}{2}) (A_1 M_0^2 + \mu_0 |H| M_0)^2} \quad (60)$$

and the normalized phase difference is

$$r^+(H) = 1 - \frac{n_o r_\infty k_0 d}{2\phi_0} \frac{[\frac{\pi}{2} - \varphi_s]^2}{[1 + q\xi \tanh(\frac{qd}{2})]^2} \frac{qd + \sinh(qd)}{2qd \cosh(\frac{qd}{2})^2} - \frac{n_o r_\infty k_0 d}{4\phi_0} (3r_\infty/4 - 1/3) \frac{[\frac{\pi}{2} - \varphi_s]^4}{[1 + q\xi \tanh(\frac{qd}{2})]^4} \frac{6qd + 8 \sinh(qd) + \sinh(2qd)}{8qd \cosh(\frac{qd}{2})^4}, \quad (61)$$

where $r_\infty = (n_{e0}^2 - n_o^2)/n_{e0}^2$.

It follows from symmetry that $\theta^-(\varphi_s) = \pi - \theta^+(-\varphi_s)$, $\psi^-(\varphi_s) = \pi - \psi^+(-\varphi_s)$, $M_z^-(\varphi_s) = -M_z^+(-\varphi_s)$, and $r^-(\varphi_s) = r^+(-\varphi_s)$.

Since the magnetization is not anchored at the boundary, in Eq. (60) it was sufficient to consider terms not higher than

$(\psi^+)^2$. On the other hand, due to the anchoring of the director field, in Eq. (61) we expanded the phase difference to the order $(\theta^+)^4$. It should be noted that the approximation for the phase difference is better if the anchoring W is low, i.e., $q\xi \gg 1$ or $W \ll \sqrt{A_1 M_0^2 K}$.

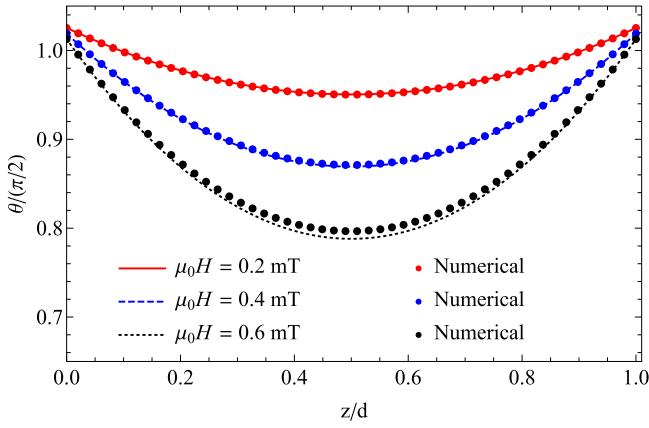


FIG. 3. For low magnetic fields, the numerically calculated polar angle of the director is in agreement with Eq. (50).

In the large-magnetic-field limit, where $qd \gg 1$, and if $q\xi \gg 1$ in addition, one can study asymptotic behavior of Eqs. (60) and (61):

$$r^+(H) \asymp r^+(\infty) - \frac{f^+(q_0)}{\mu_0 |H|}, \quad (62)$$

$$\frac{M_z^+}{M_0} \asymp 1 - \frac{h^+(q_0)}{(\mu_0 H)^2}, \quad (63)$$

where f^+ and h^+ are functions of static parameters for positive magnetic fields and $r^+(\infty) = \lim_{\mu_0 H \rightarrow \infty} r^+(H)$. The behavior of the magnetization M_z , Fig. 2, may at a first glance look like the Langevin function, often observed in magnetic systems. Equation (63) tells us that this is not the case, since the Langevin function saturates with the first power in magnetic field, whereas here the saturation Eq. (63) is of second order in H .

C. Comparison of analytic approximations with numerics

A comparison of analytic and numeric results for the director polar angle $\theta(z)$ is made in Figs. 3 and 4 for small and large magnetic fields, respectively. We find a good agreement for small magnetic fields up to 0.7 mT and for large magnetic fields above 4 mT. It should be emphasized that the values

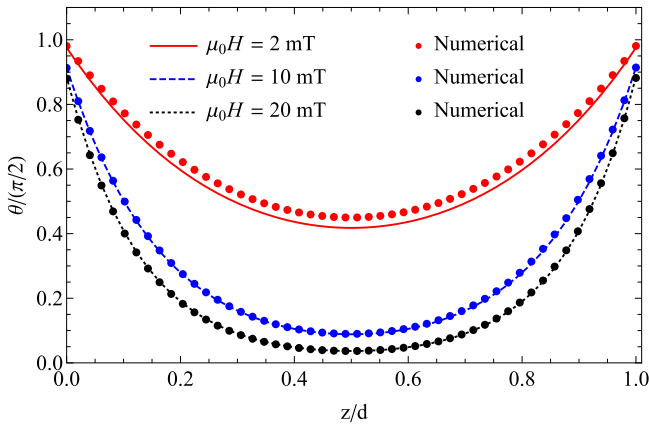


FIG. 4. For large magnetic fields, the numerically calculated polar angle of the director is in agreement with Eq. (57).

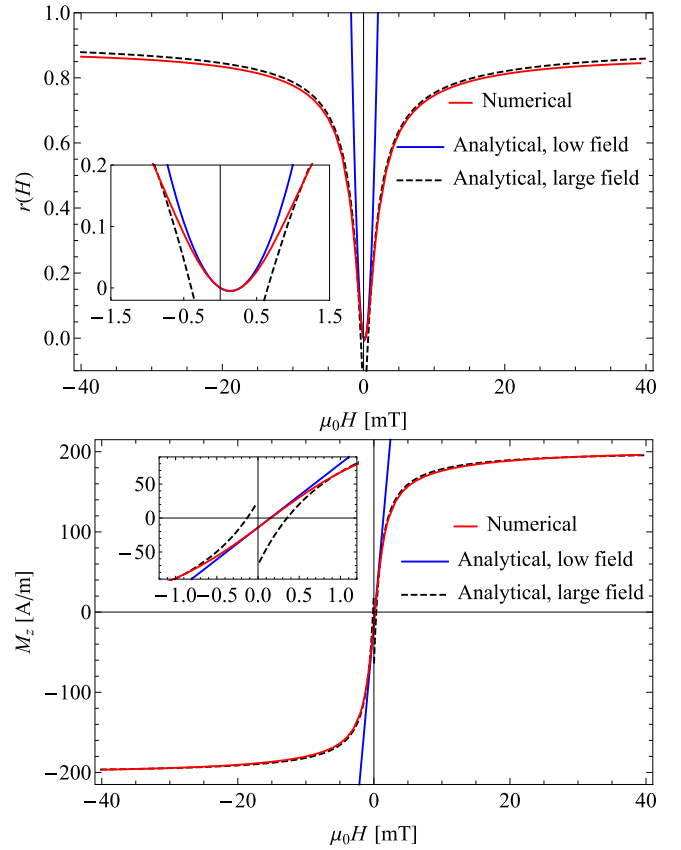


FIG. 5. Comparison of numeric and analytic results at low and high values of the applied magnetic field. Top: Magnetic field dependence of the normalized phase difference for small magnetic fields is in agreement with Eq. (52) below 0.5 mT, whereas the approximation for large magnetic fields, Eq. (61), is within 1% of the numerical value already when above 0.8 mT. Bottom: Magnetic field dependence of the z component of the magnetization for small magnetic fields is in agreement with Eq. (55) below 0.5 mT, whereas the approximation for large magnetic fields, Eq. (60), is within 1% of the numerical value already when above 0.8 mT.

of the magnetic fields at which the approximations become valid depend on the values of the static parameters. We use the values Eqs. (44)–(47) extracted from the fits to the macroscopic model.

In Fig. 5 we compare analytic and numeric results for the z component of the magnetization and the normalized phase difference. Again we find a good agreement between the results at similar ranges of the magnetic field. From the insets of Fig. 5 one can conclude that for our system a magnetic field as small as 1 mT can be considered as large already. The notable discrepancy of the numeric and analytic normalized phase difference at large magnetic fields is due to the fact that one has expanded the expression for the phase difference, Eq. (23), up to the order θ^4 . Since θ does not saturate to zero, this means that the constant term of Eq. (61) is slightly different from the actual value determined numerically.

The agreement between experimental data and the model for two key static properties underscores that we have solid ground for the analysis of the dynamic results which now follows.

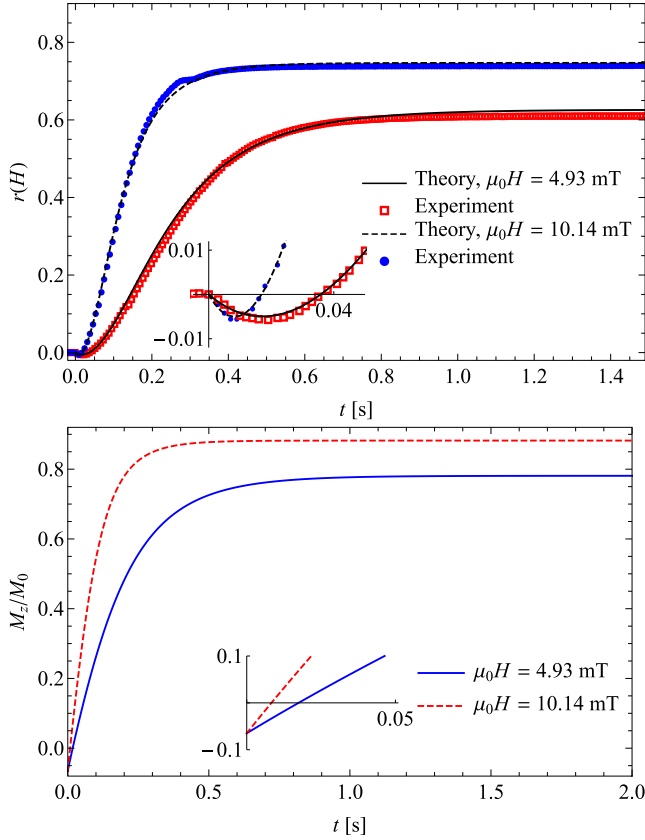


FIG. 6. Top: Time evolution of the measured normalized phase difference, $r(H)$, fitted by the dynamic model Eqs. (1)–(11). The linear-quadratic onset of $r(H)$ is in accord with the analytic result given in Eq. (79). Bottom: The corresponding theoretical time evolution of M_z/M_0 , initially growing linearly as given in Eq. (85).

VI. SWITCH-ON DYNAMICS

In this section we present the experimental and theoretical results of the dynamics that takes place when the magnetic field is switched on.

In Fig. 6 we plot the comparison of experimental and theoretical data for the dynamics of the normalized phase difference (top) as well as the theoretical results for the normalized z component of the magnetization (bottom) for two values of the applied magnetic field. As an inset we show that for small times the magnetization grows linearly, which is also obtained analytically in Sec. VIA. As expected the rise time for the magnetization is reduced as the applied magnetic field is increased. The inset for the top graph shows that the initial phase difference is quadratic in time, which is again obtained also analytically, see Sec. VIA.

The fits for the comparison of the experimental and theoretical normalized phase difference are performed by varying the dynamic parameters taking into account the fundamental restrictions [30] on their values, at fixed values of the static parameters Eqs. (44)–(47). The model captures the dynamics very well for all times from the onset to the saturation. The extracted values of the dynamic parameters are

$$\gamma_1 \sim 0.13 \text{ Pa s}, \quad (64)$$

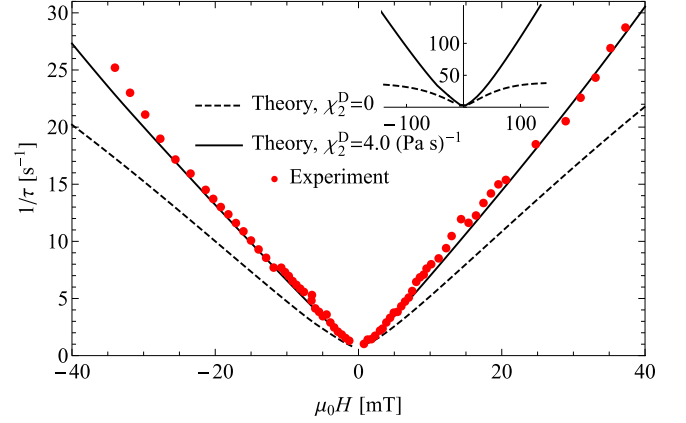


FIG. 7. The overall relaxation rate, $1/\tau(H)$, as a function of the magnetic field $\mu_0 H$, extracted from the experimental data and the theoretical results using the fitting function Eq. (68). Inset: Without the dynamic cross-coupling, the relaxation rate levels off already at low fields (dashed).

$$b_{\perp}^D \sim 1.5 \times 10^5 \text{ Am/V s}^2, \quad (65)$$

$$\chi_2^D \sim 4 (\text{Pa s})^{-1}. \quad (66)$$

The dissipative cross-coupling coefficient χ_2^D is within the allowed interval determined by the restriction [30]

$$|\chi_2^D| < \sqrt{\frac{b_{\perp}^D}{\gamma_1 M_0^2}} \approx 5.4 (\text{Pa s})^{-1}. \quad (67)$$

The remaining two dynamic parameters do not affect the dynamics significantly and are set to $b_{\parallel} = b_{\perp}$ and $\chi_1^D = 0$.

To extract from the time evolution of the normalized phase difference, Fig. 6 (top), a switching time τ as a measure of an overall relaxation rate of the dynamics, we use a squared sigmoidal model function,

$$f(t) = C' \left[1 - \frac{1 + C}{1 + C \exp(-2t/\tau)} \right]^2. \quad (68)$$

Remarkably, the relaxation rate, $1/\tau(H)$, shows a linear dependence on H , Fig. 7. We were first interested in the effect of the dissipative cross-coupling on $1/\tau(H)$. We find that a reasonably strong dynamic cross-coupling χ_2^D is needed in order to obtain the observed linear magnetic field dependence of the relaxation rate. In the absence of this dynamic cross-coupling, Fig. 7, the relaxation rate levels off already at low fields as expected since the transient angle between \mathbf{M} and \mathbf{n} gets larger and starts to decrease for even higher magnetic fields.

The best match of the relaxation rates $1/\tau(H)$ extracted from the experimental data and the model, Fig. 7, allows for a robust evaluation of the dissipative cross-coupling between the magnetization and the director:

$$\chi_2^D = (4.0 \pm 0.7) (\text{Pa s})^{-1}. \quad (69)$$

A. Initial dynamics

We investigate the initial dynamics of the normalized phase difference and magnetization on application of the magnetic

field. Up to linear order we also take into account the pretilt. Initially, \mathbf{n} and \mathbf{M} are parallel to \mathbf{n}_s . Keeping the modulus of the magnetization exactly fixed, the initial thermodynamic forces Eqs. (6) and (7) are

$$\mathbf{h}^n = 0, \quad \mathbf{h}^{\perp M} = \mu_0 H(\varphi_s, 0, -1). \quad (70)$$

where $\mathbf{h}^{\perp M}$ is the projection of \mathbf{h}^M perpendicular to \mathbf{M} . With that, the initial quasicharges are

$$Y_i = \chi_{ij}^D h_j^{\perp M} + \chi^R \epsilon_{ijk} n_j h_k^{\perp M} \Rightarrow \mathbf{Y} = \mu_0 H(\chi_2^D M_0 \varphi_s, \chi^R, -\chi_2^D M_0), \quad (71)$$

$$X_i = b_{ij}^D h_j^{\perp M} + b_{ij}^R h_j^{\perp M} \Rightarrow \mathbf{X} = \mu_0 H(b_{\perp}^D \varphi_s, -(b_1^R + b_2^R) M_0, -b_{\perp}^D). \quad (72)$$

At finite χ_2^D and zero χ^R it follows from Eq. (71) that the z component of the director field responds linearly in time as well as linearly in the magnetic field for small times:

$$n_z(t) \approx \varphi_s + \chi_2^D M_0 \mu_0 H t. \quad (73)$$

As a contrast, if χ_2^D is zero, then the director responds through the nonzero molecular field h_z^n due to the static coupling A_1 ,

$$h_z^n = -A_1 M_0 M_z(t) = -A_1 M_0 b_{\perp}^D \mu_0 H t, \quad (74)$$

where $M_z(t) = b_{\perp}^D \mu_0 H t$ is the initial response of the z component of the magnetization, Eq. (72). The z component of the director field thus responds quadratically in time rather than linearly,

$$n_z(t) \approx \varphi_s + \frac{A_1 M_0 b_{\perp}^D \mu_0 H}{2\gamma_1} t^2. \quad (75)$$

For small times t we can express the refractive index Eq. (20) as

$$n_e(t) \approx n_{e0} \left[1 - \frac{n_{e0}^2 - n_o^2}{2n_o^2} (\varphi_s + \chi_2^D M_0 \mu_0 H t)^2 \right]. \quad (76)$$

The coefficients a and b from Eq. (34) are then

$$a \approx \frac{k_0 d}{2} [n_e(t) - n_o] [1 - 2(\chi^R \mu_0 H)^2 t^2],$$

$$b \approx \frac{k_0 d}{2} [n_e(t) - n_o] (-2\chi^R \mu_0 H) t \quad (77)$$

and the normalized intensity of the transmitted light for small times is

$$\frac{I}{I_0} \approx \sin^2 \left(\frac{\phi_0}{2} \right) - r_0 \varphi_s \chi_2^D \mu_0 H M_0 \phi_0 \sin(\phi_0) t - \left[\frac{r_0}{2} (\chi_2^D \mu_0 H M_0)^2 \phi_0 \sin(\phi_0) + 4(\chi^R \mu_0 H)^2 \sin^2 \left(\frac{\phi_0}{2} \right) \right] t^2. \quad (78)$$

In the lowest order of t , for the phase difference, one gets a linear term that is also linear in pretilt and a quadratic term which does not vanish if the pretilt is zero:

$$r(H) \approx r_0 [(\chi_2^D M_0 \mu_0 H)^2 t^2 + 2\varphi_s \chi_2^D M_0 \mu_0 H t] \equiv k^2 t^2 + pt. \quad (79)$$

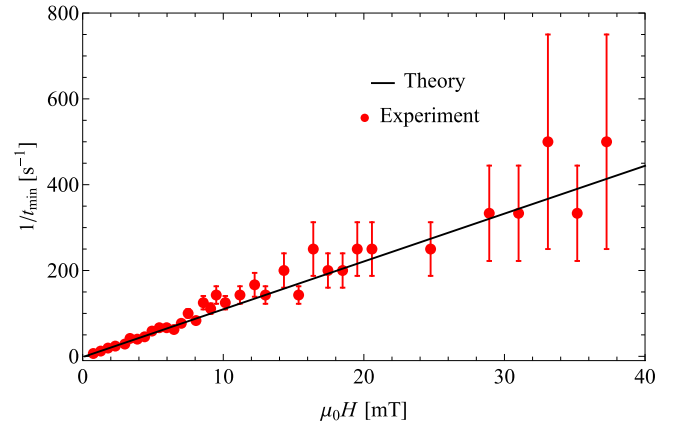


FIG. 8. Inverse of the time of the minimum determined from the measured normalized phase difference as a function of the magnetic field. The linear behavior in magnetic field is in agreement with Eq. (80).

Equation (79) will be used to extract the dissipative cross-coupling coefficient χ_2^D and the pretilt φ_s from the experimental data. Furthermore, from Eq. (79) one can see that in the case of positive (negative) pretilt the normalized phase difference has a minimum at negative (positive) magnetic fields. By measuring the time of this minimum, Fig. 8,

$$t_{\min} = -\frac{\varphi_s}{\chi_2^D \mu_0 H M_0}, \quad (80)$$

one can calculate the ratio of the pretilt and the dissipative cross-coupling. If $\chi_2^D = 0$, then the time of the minimum decreases more slowly with increasing magnetic field:

$$t_{\min} = \sqrt{-\frac{2\gamma_1 \varphi_s}{A_1 b_{\perp}^D \mu_0 H M_0}}. \quad (81)$$

The normalized phase difference evaluated at t_{\min} is of second order in the pretilt:

$$r(H)_{\min} = -r_0 \varphi_s^2. \quad (82)$$

The minimum value Eq. (82) is independent of the applied magnetic field. This can be explained by the fact that the director field goes through an intermediate state which is approximately aligned with the glass plates of the cell.

We note that if both the dissipative cross-coupling coefficient χ_2^D and the pretilt φ_s are zero, the normalized phase difference initially grows as t^4 .

Assuming a negative pretilt, Eq. (79) predicts a minimum for positive magnetic fields, which is also seen in experiments, Fig. 6 (top). In Fig. 8 we show experimental inverse times of the minima. The large error at high magnetic fields is due to the time resolution limitations (1 ms). From the linear behavior predicted by Eq. (80) we can extract the ratio between the dissipative cross-coupling and the pretilt. Independently, we can extract the pretilt by measuring the values of the minima, Fig. 9.

Fitting Eq. (79) to the initial time evolution of measured normalized phase differences (like those presented in Fig. 6) for several values of the magnetic field $\mu_0 H$, we determine the parameters k and p shown in Figs. 10 and 11, respectively.

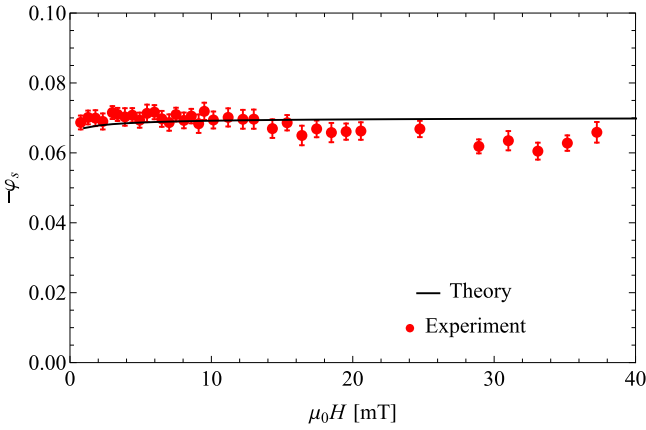


FIG. 9. Pretilt, determined from experimental data using Eq. (82).

Therefrom we extract the value of the dissipative cross-coupling parameter χ_2^D between director and magnetization,

$$\chi_2^D \sim (4.0 \pm 0.5) (\text{Pa s})^{-1}, \quad (83)$$

and from the parameter p of Eq. (79) we extract the pretilt,

$$\varphi_s \sim -0.065 \pm 0.01. \quad (84)$$

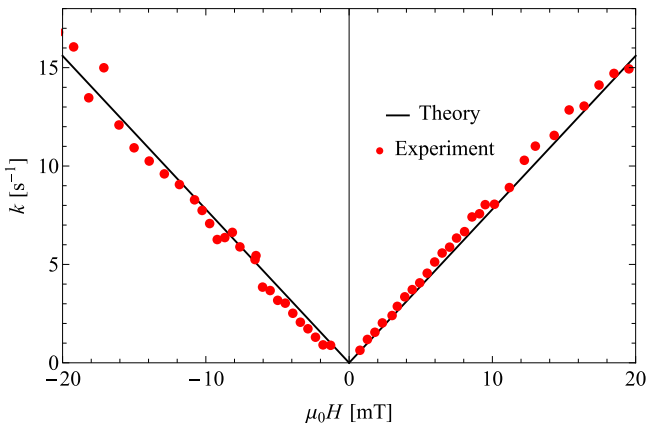
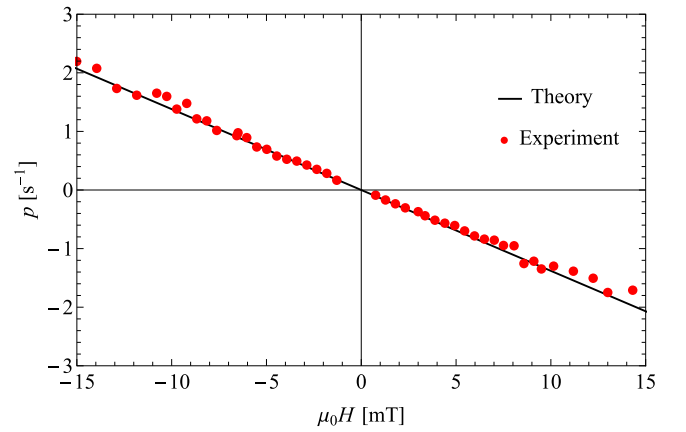
The normalized z component of the magnetization Eq. (18) is linear in t :

$$\frac{M_z}{M_0} = \varphi_s + \frac{b_{\perp}^D}{M_0} \mu_0 H t, \quad (85)$$

which is in accord with Fig. 6 (bottom). From the initial behavior one can therefore directly determine the dissipative coefficient b_{\perp}^D .

Let us define the initial rate of the director reorientation as the time derivative of the director z component at $t = 0$,

$$\frac{1}{\tau_d} = \left. \frac{\partial n_z}{\partial t} \right|_{t=0}. \quad (86)$$

FIG. 10. The coefficient k of Eq. (79) as a function of the magnetic field μ_0H . The straight line fits are used to extract χ_2^D .FIG. 11. The coefficient p of Eq. (79) as a function of the magnetic field μ_0H . The straight line fit is used to extract φ_s .

For a nonzero dissipative cross-coupling coefficient χ_2^D the initial rate, Eq. (73), is

$$\frac{1}{\tau_d} = \chi_2^D M_0 \mu_0 |H|. \quad (87)$$

However, if $\chi_2^D = 0$, then the initial rate of the director reorientation is proportional to the z component of the magnetization, Eq. (74),

$$\frac{1}{\tau_s} = \frac{A_1 M_0}{\gamma_1} |M_z(t)|. \quad (88)$$

The relaxation rates Eqs. (87) and (88) describe two different mechanisms of the director reorientation. The former is associated with the dynamic coupling of the director and the magnetization, whereas the latter is governed by the static coupling A_1 of the director and the magnetization. Here a deviation of the magnetization from the director is needed to exert a torque on the director.

B. Dissipative cross-coupling

We have demonstrated that the dissipative cross-coupling of the director and the magnetization, i.e., the χ_{ij}^D terms of Eqs. (8) and (9), affects the dynamics decisively and is crucial to explain the experimental results. It is described by the parameters χ_1^D and χ_2^D of Eq. (10). Here we check the sensitivity of the dynamics to the values of these two parameters. Varying χ_1^D while keeping $\chi_2^D = 0$, Fig. 12, we see that the influence of χ_1^D is rather small and is not substantial. Moreover, the initial dynamics is not affected, Fig. 12 (inset).

On the other hand, increasing χ_2^D strongly reduces the rise time of the normalized phase difference, Fig. 13, and also strongly affects the initial behavior (inset). For large values of χ_2^D one also observes an overshoot in the normalized phase difference.

By inspecting Eq. (10) one sees that the influence of χ_1^D is largest when $\mathbf{M} \perp \mathbf{n}$, $\mathbf{h}^n \parallel \mathbf{M}$, and $\mathbf{h}^M \parallel \mathbf{n}$. On the other hand, the influence of χ_2^D is largest when $\mathbf{M} \parallel \mathbf{n}$. Since \mathbf{M} and \mathbf{n} are initially parallel and, moreover, the transient angle between them never gets large due to the strong static coupling compared to the magnetic fields applied, it is understandable that χ_2^D affects the dynamics more than χ_1^D .

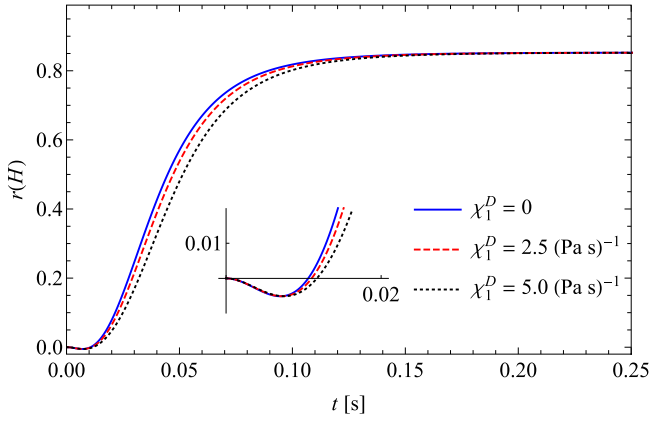


FIG. 12. Normalized phase difference at different values of the dissipative cross-coupling parameter χ_1^D , $\chi_2^D = 0$, $\mu_0 H = 50$ mT. Inset: The initial behavior is not affected.

C. Reversible cross-coupling

The reversible cross-coupling of the director and the magnetization, described by the χ^R terms of Eqs. (12) and (13), has not been considered up to this point. We focus on the reversible cross-coupling coefficient χ^R and put both reversible tensors b_{ij}^R and $(\gamma^{-1})_{ij}^R$ of Eqs. (14) and (15) to zero.

If the reversible currents are included, then both variables wander out of the xz plane dynamically, which will be described by the azimuthal angles δ and φ of the magnetization and the director, respectively, defined by $\mathbf{M} = M_0(\cos \delta \sin \psi, \sin \delta \sin \psi, \cos \psi)$, $\mathbf{n} = (\cos \varphi \sin \theta, \sin \varphi \sin \theta, \cos \theta)$. The dynamic behavior of both azimuthal angles is shown in Fig. 14.

Contrary to the polar angles we find that the response of the azimuthal angle of the director is faster than that of the magnetization. From Fig. 14, we read off that the maximum azimuthal angles increase with χ^R , being higher for the magnetization than for the director.

We note again that here we only included the reversible cross-coupling χ^R . From the initial quasicharges Eqs. (71) and (72) one can see that the initial azimuthal response of

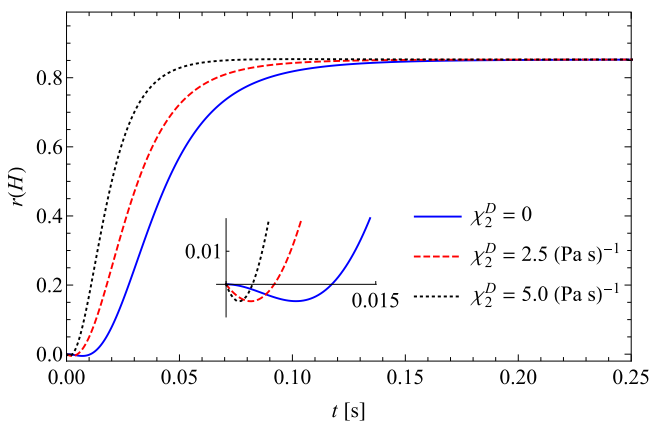


FIG. 13. Normalized phase difference at different values of the dissipative cross-coupling parameter χ_2^D , $\chi_1^D = 0$, $\mu_0 H = 50$ mT. Inset: The initial behavior is strongly affected as well.

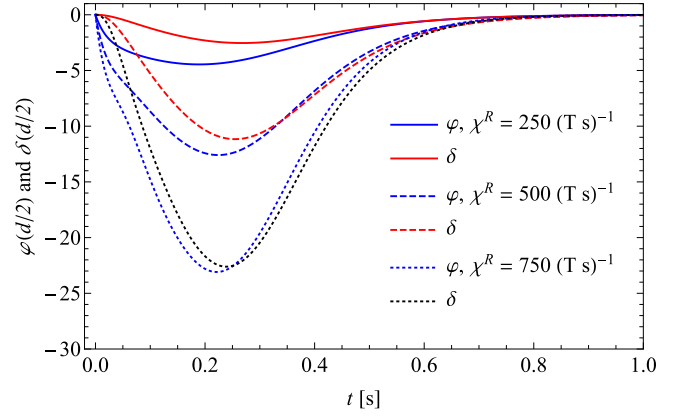


FIG. 14. The time dependencies of the azimuthal angles (degrees) of the director (φ) and the magnetization (δ) at $z = d/2$ for different values of χ^R , $\chi_1^D = \chi_2^D = 0$, $\mu_0 H = 10$ mT.

the magnetization can be faster than that of the director if the coefficients of the tensor b_{ij}^R are sufficiently large,

$$|b_1^R + b_2^R| > |\chi^R|/M_0. \quad (89)$$

There exists a direct way of detecting the possible dynamics in the xy plane. The intensity of the transmitted light in the experiments with crossed polarizers at 45° and -45° is given by Eq. (37),

$$\frac{I}{I_0} = \frac{a^2}{c^2} \sin^2(c). \quad (90)$$

It is this quantity that is typically measured. On the other hand, crossed polarizers at 0° and 90° give us the intensity

$$\frac{I}{I_0} = \frac{b^2}{c^2} \sin^2(c), \quad (91)$$

with a and b given by Eq. (34). This method is better suited for detecting the xy dynamics, since b is more sensitive to the deviation of the director field from the xz plane.

Our numerical calculations have revealed that, due to the reversible dynamics, the magnetization and the director are not confined to the xz plane. As a consequence, the maxima of the time-dependent intensity of transmitted light are lower than unity, Fig. 15, in contrast to the case of a purely in-plane (dissipative) dynamics. Observation of the lower maxima could thus be an indication of the azimuthal dynamics. This effect is more prominent at higher magnetic fields and at higher values of the reversible cross-coupling coefficients.

In recent experiments no clear-cut consequences of the azimuthal dynamics have been found using crossed polarizers at 0° and 90° . In the following we will therefore discard the reversible dynamics.

VII. SWITCH-OFF DYNAMICS

Dynamics of the normalized phase difference after switching off the magnetic field has been also measured. In experiments, the initial state is obtained by switching on the desired magnetic field and waiting for a couple of seconds. Contrary to the previous experiments, here the initial state is not homogeneous.

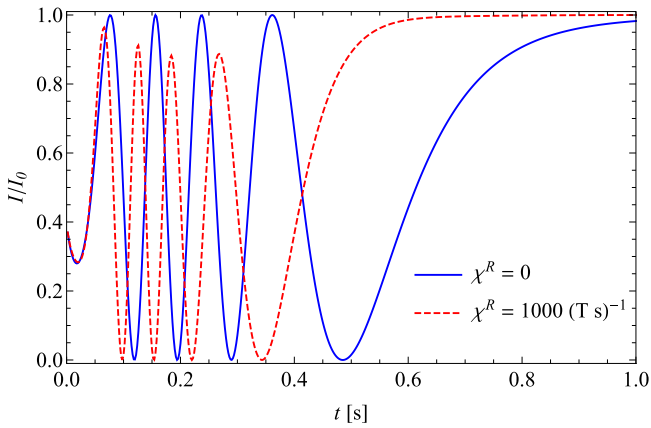


FIG. 15. Time dependence of the normalized intensity of transmitted light for zero and nonzero values of the reversible cross-coupling coefficient χ^R ; $\mu_0 H = 5$ mT.

In Fig. 16 we compare the experimental and numerical normalized phase difference at two different fields. We observe, similarly to the switch-on case, that the normalized phase difference goes through a minimum. This is again explained by the fact that the director field goes through a state, which is approximately aligned with the surfaces of the glass plates. Numerical calculations reveal that a strong dissipative cross-coupling causes the initial behavior of the normalized phase difference to be a linear function in time, Fig. 17, as found experimentally, Fig. 16.

To extract a relaxation time τ of the normalized phase difference, we use an exponential function

$$f(t) = f(0)e^{-t/\tau}. \quad (92)$$

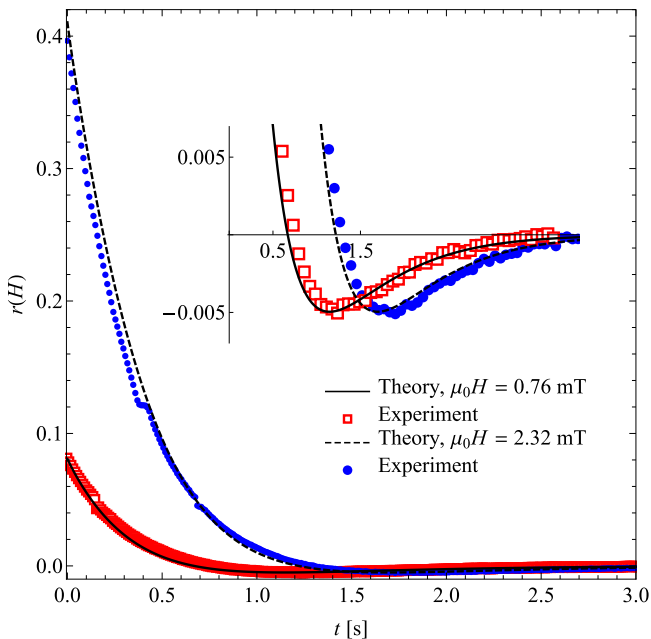


FIG. 16. Experimental and numerical normalized phase difference as a function of time at different values of the applied magnetic field.

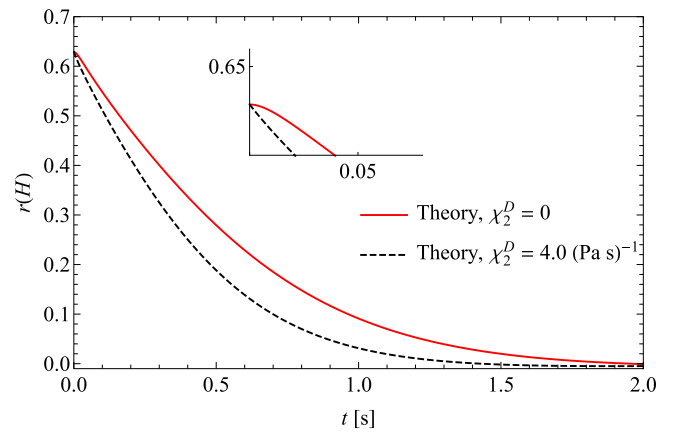


FIG. 17. Normalized phase difference as a function of time at 5 mT, calculated with $\chi_2^D = 0$ and $\chi_2^D = 4.0$ (Pa s) $^{-1}$.

The relaxation rate $1/\tau$ for the experimental data is shown in Fig. 18. It saturates at a finite value as one increases the magnetic field. This is expected since the initial director and magnetization fields do not change much with magnetic field any more when the field is large. In Fig. 19 the relaxation rate of both the computed phase difference and the magnetization is shown. One can see that the relaxation rate of the magnetization is smaller than that of the normalized phase difference, due to the fact that it is the director that is driven by the nonzero elastic force, while the magnetization only follows. This is true for all allowed values of the dynamic cross-coupling parameters.

One can derive analytic formulas for the relaxation rate in the limit of low magnetic fields. With the assumption that the relaxation follows a simple exponential function, it is possible to extract the relaxation rate $1/\tau^{\text{off}}$ from the initial time derivative of the normalized phase difference,

$$r(H, t) \approx r(H, t = 0) \left(1 - \frac{t}{\tau^{\text{off}}} \right). \quad (93)$$

Note that Eq. (93) is defined only when $r(H, t = 0) \neq 0$.

One starts with the director quasicurrent \mathbf{Y} , Eq. (9). The response of the z component of the director field is

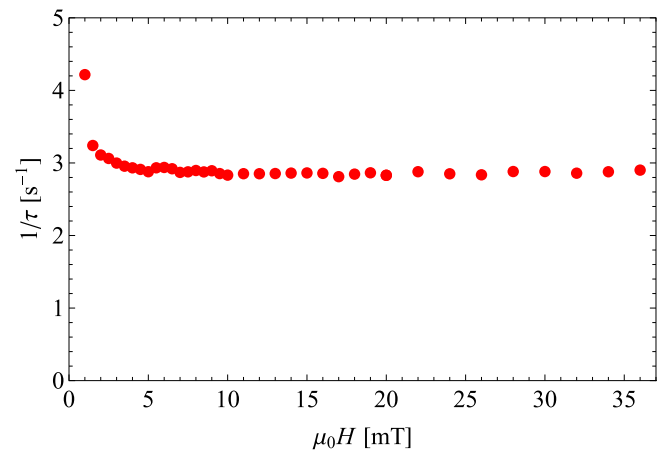


FIG. 18. Experimental switch-off relaxation rate of the normalized phase difference as a function of the applied magnetic field.

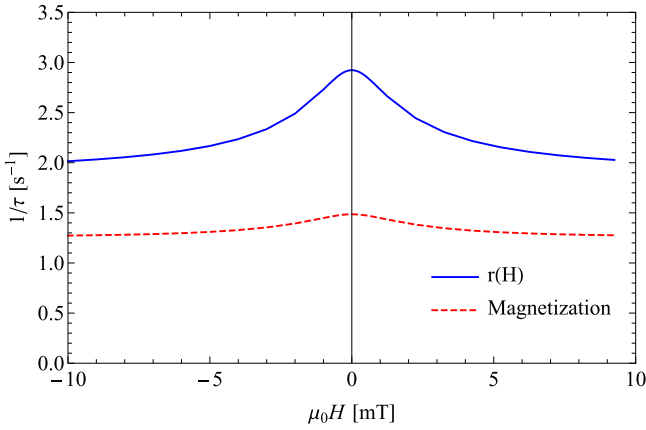


FIG. 19. Relaxation rate of the normalized phase difference and z component of the magnetization after switching off the magnetic field of strength $\mu_0 H$ at $\chi_2^D = 4 \text{ (Pa s)}^{-1}$ and $\varphi_s = 0$.

$n_z \approx n_z(z, t = 0) - Y_z(z, t = 0)t$, which one uses in Eq. (23) for the phase difference,

$$\frac{1}{\tau^{\text{off}}} = \frac{2k_0 r_0 (n_{e0} - n_o)}{\phi_0 r(H, t = 0)} \int_0^d dz \frac{n_z(z) Y_z(z)}{\left[1 + \frac{n_{e0}^2 - n_o^2}{n_o^2} n_z^2(z)\right]^{3/2}}, \quad (94)$$

where all z -dependent quantities are evaluated at $t = 0$. In the last step the integrand is expanded up to linear order in time and the relaxation rate in the low-magnetic-field limit is finally expressed as

$$\frac{1}{\tau^{\text{off}}} = \frac{(1 + r_0 \varphi_s^2) [\mu_0 H M_0 (1 + 6 \frac{\xi}{d}) + 12 \frac{K_1 \varphi_s}{d^2}] \chi_2^D}{\frac{\mu_0 H M_0 d^2}{20 K_1} (1 + 10 \frac{\xi}{d} + 30 \frac{\xi^2}{d^2}) + (1 + 6 \frac{\xi}{d}) \varphi_s}, \quad (95)$$

which is linear in the dissipative cross-coupling coefficient χ_2^D .

Not only does the dissipative cross-coupling make the switching process faster when switching on the field, this can be also true for switching off the field, Figs. 17 and 20. Figure 20 shows the relaxation rate of the normalized phase difference at a high magnetic field as a function of the dissipative cross coupling coefficient χ_2^D . As expected, the

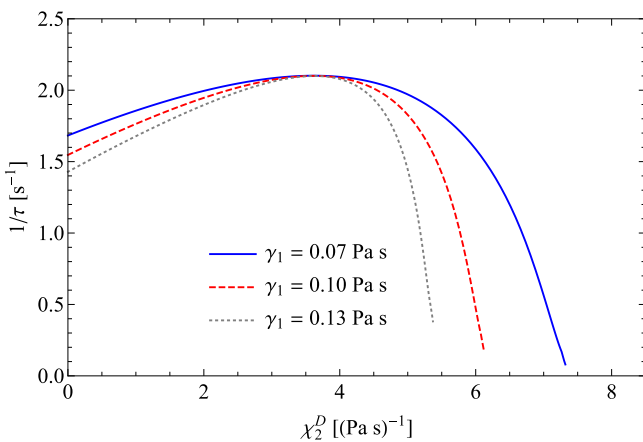


FIG. 20. Relaxation rate at $\mu_0 H = 50 \text{ mT}$ as a function of the dissipative coefficient χ_2^D for different values of the director rotational viscosity γ_1 .

relaxation rate decreases with increasing rotational viscosity γ_1 . The relaxation rate at first increases with increasing values of χ_2^D , which seems also to be the case for small magnetic fields described by Eq. (95). For values above approximately $\chi_2^D = 3.5 \text{ (Pa s)}^{-1}$, the relaxation rate starts to decrease rather rapidly. This is in contrast with the field switch-on case, where the response is faster for increasing values of χ_2^D .

The increasing part of the dependence $\tau^{-1}(\chi_2^D)$ in Fig. 20 is due to the director elastic forces, which drive the switch-off dynamics and also enter Eq. (4) through the dissipative cross-coupling governed by χ_2^D . At higher values of χ_2^D one must, however, also consider the part of the thermodynamic forces corresponding to the static (A_1) coupling between the director and the magnetization. Focusing only on the director equation Eq. (5), one sees that the director relaxes towards the magnetization with a characteristic time set by the rotational viscosity and the static coupling (A_1). On the other hand, the positive value of χ_2^D has the opposite effect. While both fields eventually relax to the ground state parallel to x , the angle between them is decreasing slower and slower as the dynamic cross-coupling (χ_2^D) gets larger. For small magnetic fields one can study the relaxation rate of the dynamic eigenmodes [Eq. (122)] of the next section. The value of χ_2^D above which the relaxation rate starts to decrease then reads

$$\chi_2^D = \begin{cases} \frac{A_1 b_{\perp}^D}{A_1 M_0^2 + K(\pi/d)^2} & \text{if } \frac{1}{\gamma_1} > \frac{b_{\perp}^D}{M_0^2}, \\ \frac{1}{\gamma_1} & \text{if } \frac{1}{\gamma_1} < \frac{b_{\perp}^D}{M_0^2}. \end{cases} \quad (96)$$

In our case $\frac{1}{\gamma_1} > \frac{b_{\perp}^D}{M_0^2}$ holds and the maximum is at $\chi_2^D \approx 3.5 \text{ (Pa s)}^{-1}$.

The switch-on case is different in that the dynamics is driven by the external magnetic field. If the external field is sufficiently high (large compared to $A_1 M_0$), the static cross-coupling effects, which decrease the relaxation rate in the switch-off case through the increasing dynamic cross-coupling χ_2^D , can be neglected and hence the relaxation rate is monotonically increasing with χ_2^D .

VIII. FLUCTUATIONS AND LIGHT SCATTERING

Nematic liquid crystals appear turbid in sufficiently thick layers [32]. The scattering of light is caused by strong director fluctuations which cause fluctuations in the dielectric tensor

$$\varepsilon_{ij} = \varepsilon_{\perp} \delta_{ij}^{\perp} + \varepsilon_{\parallel} n_i n_j, \quad (97)$$

where ε_{\perp} and ε_{\parallel} are dielectric susceptibilities for the electric field perpendicular and parallel to the director, respectively. Fluctuations are easy to observe experimentally and are used to determine the viscoelastic properties of liquid crystals [36].

In this paper we derive the relaxation rates of the fluctuations without taking into account the effects of flow. Since the director is coupled to the magnetization, we now have two fluctuation modes for each director fluctuation mode of the usual nematic [22].

The fluctuating director and magnetization fields are linearized as

$$\mathbf{n} = \mathbf{n}_0 + \delta \mathbf{n}, \quad \mathbf{M} = \mathbf{M}_0 + M_0 \delta \mathbf{m}, \quad (98)$$

where the equilibrium director \mathbf{n}_0 and magnetization \mathbf{M}_0 fields point in x direction in which a magnetic field is applied, whereas fluctuations $\delta\mathbf{n}$ and $\delta\mathbf{m}$ are perpendicular, $\mathbf{n}_0 \cdot \delta\mathbf{n} = \mathbf{M}_0 \cdot \delta\mathbf{m} = 0$. The ansatz for the director fluctuations is

$$\delta\mathbf{n}(\mathbf{r}) = \frac{1}{V} \sum_{\mathbf{q}} \delta\mathbf{n}(\mathbf{q}) e^{i\mathbf{q}\cdot\mathbf{r}}, \quad (99)$$

where $\mathbf{q} = q_x \hat{\mathbf{e}}_x + q_y \hat{\mathbf{e}}_y + q_z \hat{\mathbf{e}}_z$ is the wave vector of the fluctuation. A similar ansatz is used for the fluctuations of the magnetization. In a confined system, the fluctuation spectrum generally depends on the interaction of the nematic with the surface [36]. For simplicity we will use the infinite anchoring limit, so that $q_z = n\pi/d, n \in \mathbb{N}$, while q_x and q_y are in principle arbitrary. For details regarding the anchoring effect we refer to Ref. [36].

To understand the static light-scattering experiments one must determine thermal averages of the fluctuations. This is done by finding linear combinations of the variables in terms of which the free energy functional Eq. (1) is expressed as a sum of quadratic terms and making use of equipartition. Such linear combinations are uncorrelated (statistically independent). A systematic way to perform this decomposition is to write the free energy of a fluctuation \mathbf{q} -mode as a quadratic form and find the corresponding eigenvalues and eigenvectors,

$$F(\mathbf{q}) = \frac{1}{2} \delta\mathbf{x}(\mathbf{q})^H \mathbf{E}(\mathbf{q}) \delta\mathbf{x}(\mathbf{q}), \quad (100)$$

where $\delta\mathbf{x}(\mathbf{q}) = \{\delta n_z(\mathbf{q}), \delta m_z(\mathbf{q}), \delta n_y(\mathbf{q}), \delta m_y(\mathbf{q})\}$, in short $\delta\mathbf{x}(\mathbf{q}) \equiv \{n_z, m_z, n_y, m_y\}$, is the vector of the fluctuation amplitudes, $\mathbf{E}(\mathbf{q})$ is a self-adjoint matrix, and superscript H is the conjugate transpose.

In lowest order of fluctuations, the contributions Eq. (100) of the free energy Eq. (1) are [32]

$$\begin{aligned} F(\mathbf{q}) = & \frac{1}{2V} [(K_1 q_y^2 + K_2 q_z^2 + K_3 q_x^2 + A_1 M_0^2) |n_y|^2 \\ & + (K_1 q_z^2 + K_2 q_y^2 + K_3 q_x^2 + A_1 M_0^2) |n_z|^2 \\ & + (K_1 - K_2) q_z q_y (n_y n_z^* + n_y^* n_z) \\ & + (\mu_0 H M_0 + A_1 M_0^2) (|m_y|^2 + |m_z|^2) \\ & - A_1 M_0^2 (n_y m_y^* + n_y^* m_y + n_z m_z^* + n_z^* m_z)]. \end{aligned} \quad (101)$$

For completeness (not needed here), the volume-integrated free energy is $F = \sum_{\mathbf{q}} F(\mathbf{q})$.

Before giving the eigenvectors of the quadratic form \mathbf{E} , we perform a rotation in the yz plane, $(n_y, n_z) \rightarrow (n_1, n_2)$ and $(m_y, m_z) \rightarrow (m_1, m_2)$, where the new bases in this plane are $\{\hat{\mathbf{e}}_1^n, \hat{\mathbf{e}}_2^n\}$ and $\{\hat{\mathbf{e}}_1^M, \hat{\mathbf{e}}_2^M\}$. Vectors $\hat{\mathbf{e}}_2^n$ and $\hat{\mathbf{e}}_2^M$ are normal to the $(\mathbf{q}, \mathbf{n}_0)$ and $(\mathbf{q}, \mathbf{m}_0)$ plane, respectively, and vectors $\hat{\mathbf{e}}_1^n$ and $\hat{\mathbf{e}}_1^M$ are normal to $\hat{\mathbf{e}}_2^n$ and $\hat{\mathbf{e}}_2^M$, respectively. It should be emphasized that we are studying the case $\mathbf{n}_0 \parallel \mathbf{m}_0$, so the planes $(\mathbf{q}, \mathbf{n}_0)$ and $(\mathbf{q}, \mathbf{m}_0)$ are identical. In the confined system, this would not be the case if the external magnetic field were applied in any direction other than parallel to the initial homogeneous state.

A general fluctuation $\delta\mathbf{x}(\mathbf{q})$ can be written as

$$\delta\mathbf{x} = t_1 \mathbf{t}_1 + p_1 \mathbf{p}_1 + t_2 \mathbf{t}_2 + p_2 \mathbf{p}_2, \quad (102)$$

where $\mathbf{t}_1, \mathbf{t}_2, \mathbf{p}_1, \mathbf{p}_2$ are the eigenvectors of the quadratic form \mathbf{E} and t_1, t_2, p_1, p_2 are the amplitudes of these uncorrelated

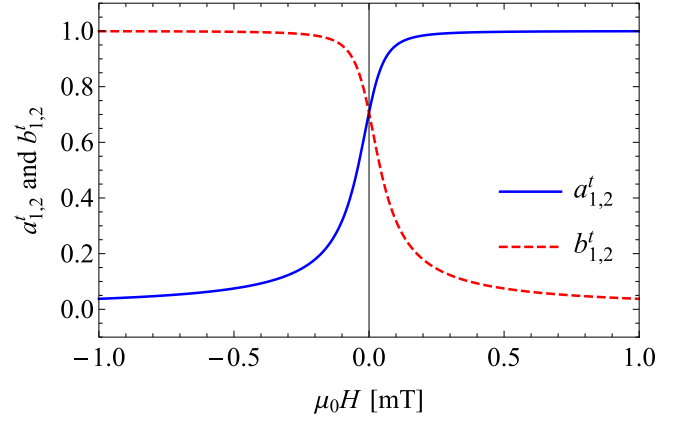


FIG. 21. The normalized coefficients Eq. (103) of the eigenvectors \mathbf{t}_1 and \mathbf{t}_2 as a function of the applied magnetic field with $q_x = 0$ and $q_\perp = \pi/2$; $K_1 = K_2$.

excitations. The eigenvectors are

$$\begin{aligned} \mathbf{t}_\alpha &= a'_\alpha \hat{\mathbf{e}}_\alpha^n + b'_\alpha \hat{\mathbf{e}}_\alpha^M \\ &= \frac{Z_\alpha^-}{\sqrt{1 + (Z_\alpha^-)^2}} \hat{\mathbf{e}}_\alpha^n - \frac{1}{\sqrt{1 + (Z_\alpha^-)^2}} \hat{\mathbf{e}}_\alpha^M, \end{aligned} \quad (103)$$

$$\begin{aligned} \mathbf{p}_\alpha &= a''_\alpha \hat{\mathbf{e}}_\alpha^n + b''_\alpha \hat{\mathbf{e}}_\alpha^M \\ &= \frac{Z_\alpha^+}{\sqrt{1 + (Z_\alpha^+)^2}} \hat{\mathbf{e}}_\alpha^n - \frac{1}{\sqrt{1 + (Z_\alpha^+)^2}} \hat{\mathbf{e}}_\alpha^M, \end{aligned} \quad (104)$$

where

$$Z_\alpha^\pm = \frac{-\mu_0 H M_0 + K_\alpha q_\perp^2 + K_3 q_x^2 \pm s_\alpha}{2A_1 M_0^2}, \quad (105)$$

with $q_\perp^2 = q_y^2 + q_z^2$ and

$$s_\alpha^2 = 4A_1^2 M_0^4 + (K_\alpha q_\perp^2 + K_3 q_x^2 - \mu_0 H M_0)^2. \quad (106)$$

The excitation modes \mathbf{t}_1 and \mathbf{p}_1 are the analogues of the splay-bend mode in the usual NLCs, whereas \mathbf{t}_2 and \mathbf{p}_2 are the analogues of the twist-bend mode.

It is found that in the limit of large magnetic fields these excitations become decoupled, i.e., one eigenvector only contains the fluctuation of the director field and the other the fluctuation of the magnetization field, Figs. 21 and 22.

The thermal averages of the squared amplitudes of the independent excitations read

$$\langle |t_\alpha(\mathbf{q})|^2 \rangle = \frac{k_B T V}{\frac{1}{2} (2A_1 M_0^2 + \mu_0 H M_0 + K_\alpha q_\perp^2 + K_3 q_x^2 - s_\alpha)}, \quad (107)$$

$$\langle |p_\alpha(\mathbf{q})|^2 \rangle = \frac{k_B T V}{\frac{1}{2} (2A_1 M_0^2 + \mu_0 H M_0 + K_\alpha q_\perp^2 + K_3 q_x^2 + s_\alpha)}, \quad (108)$$

with k_B the Boltzmann constant and T the temperature, whereas their thermal cross-correlations are zero.

If $K_1 = K_2$, then the splay-bend ($\alpha = 1$) and the twist-bend ($\alpha = 2$) excitation modes have the same structure [Eqs. (105) and (106)] (Figs. 21 and 22), as well as the same energy

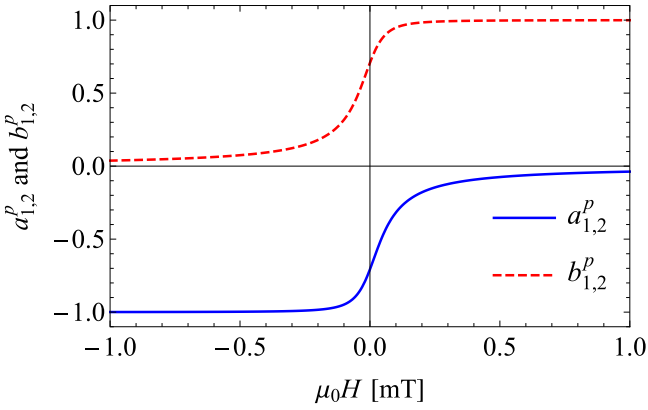


FIG. 22. The normalized coefficients Eq. (104) of the eigenvectors \mathbf{p}_1 and \mathbf{p}_2 as a function of the applied magnetic field with $q_x = 0$ and $q_\perp = \pi/2$; $K_1 = K_2$.

and thermal amplitude [Eqs. (107) and (108)]. The same is true in the degenerate case when $\mathbf{q} = q \hat{\mathbf{e}}_x$, i.e., for a pure bend excitation (in an unconfined system), where there is no difference between the modes $\alpha = 1, 2$ and the bases $\{\hat{\mathbf{e}}_1^n, \hat{\mathbf{e}}_2^n\}$ and $\{\hat{\mathbf{e}}_1^M, \hat{\mathbf{e}}_2^M\}$ are chosen arbitrarily in the yz plane.

The space correlations are expressed as

$$\begin{aligned} \langle t_\alpha(\mathbf{r}) t_{\alpha'}(\mathbf{r}') \rangle &= \frac{1}{V^2} \sum_{\mathbf{q}, \mathbf{q}'} \langle t_\alpha(\mathbf{q}) t_{\alpha'}(\mathbf{q}') \rangle e^{-i(\mathbf{q} \cdot \mathbf{r} + \mathbf{q}' \cdot \mathbf{r}')} \\ &= \frac{\delta_{\alpha, \alpha'}}{V^2} \sum_{\mathbf{q}} \langle t_\alpha(\mathbf{q}) t_\alpha(-\mathbf{q}) \rangle e^{-i\mathbf{q} \cdot (\mathbf{r} - \mathbf{r}')}, \end{aligned} \quad (109)$$

and similarly for $\langle p_\alpha(\mathbf{r}) p_{\alpha'}(\mathbf{r}') \rangle$, whereas $\langle t_\alpha(\mathbf{r}) p_{\alpha'}(\mathbf{r}') \rangle = 0$. In the large magnetic field limit these correlations are

$$\langle t_\alpha(\mathbf{r}) t_\alpha(\mathbf{r}') \rangle \approx \frac{k_B T}{4\pi K r} e^{-q_0 r}, \quad (110)$$

$$\langle p_\alpha(\mathbf{r}) p_\alpha(\mathbf{r}') \rangle \approx \frac{k_B T}{(2\pi)^3 \mu_0 H M_0} \delta(r), \quad (111)$$

where $r = |\mathbf{r} - \mathbf{r}'|$ and $q_0 = \sqrt{A_1 M_0^2 / K}$.

In experiments one measures the intensity of the scattered light. To calculate this intensity, we need an expression for the amplitude of the outgoing electric field. We start with an incident electric field \mathbf{E}_i , described by a plane wave: $\mathbf{E} = E_0 \hat{\mathbf{i}} e^{i(\mathbf{k}_i \cdot \mathbf{r} - \omega t)}$, where \mathbf{k}_i is the wave vector, E_0 the amplitude, and ω the frequency of the incident light. We then proceed with a summation of the electric field contributions of the scattered light through the whole cell, treating every point \mathbf{r} as a radiating dipole. Last, we project the electric field on the axis $\hat{\mathbf{f}}$ of the analyzer. The electric field amplitude of the scattered light is [32]

$$\begin{aligned} E_f(\mathbf{q}, t) &= \frac{E_0 \omega^2}{c^2 R} e^{i(\mathbf{k}_f \cdot \mathbf{r}' - \omega t)} \int_V d^3 r e^{-i\mathbf{q} \cdot \mathbf{r}} \hat{\mathbf{f}}_i [\varepsilon_{ij}(\mathbf{r}, t) - \delta_{ij}] \hat{\mathbf{i}}_j \\ &= \frac{E_0 \omega^2}{c^2 R} e^{i(\mathbf{k}_f \cdot \mathbf{r}' - \omega t)} \hat{\mathbf{f}}_i \varepsilon_{ij}(\mathbf{q}, t) \hat{\mathbf{i}}_j, \end{aligned} \quad (112)$$

where \mathbf{k}_f is the wave vector of the scattered light, R is the distance from the sample to the detector at \mathbf{r}' , and $\mathbf{q} = \mathbf{k}_f - \mathbf{k}_i$ is the fluctuation wave vector. In the last line of Eq. (112) we

discarded the Fourier contribution of δ_{ij} , since it is nonzero only if $\mathbf{q} = 0$. We have assumed that R is large compared to the size of the scattering region, which in turn is much larger than the wave length of the light, and that we are in the limit of small dielectric anisotropy.

In our calculations below, we will be using details of an experimental setup usually used for measuring splay-bend fluctuations in a NLC, which in our geometry have $\delta \mathbf{n} = \delta n_z \hat{\mathbf{e}}_z$, $q_y = 0$, $\hat{\mathbf{e}}_2^{n,M} = \hat{\mathbf{e}}_y$, and $\hat{\mathbf{e}}_1^{n,M} = \hat{\mathbf{e}}_z$. In this case we have a polarizer and an analyzer that are both in the xz plane. The polarizer $\hat{\mathbf{i}}$ is parallel to the x axis, whereas the analyzer $\hat{\mathbf{f}}$ is at an angle ζ from the x axis. In Eq. (112), the projection of the fluctuating part of the dielectric tensor Eq. (97) reads

$$\hat{\mathbf{f}}_i \varepsilon_{ij}(\mathbf{q}, t) \hat{\mathbf{i}}_j = \varepsilon_a f_z \delta n_z, \quad (113)$$

where $f_z = \hat{\mathbf{f}} \cdot \hat{\mathbf{e}}_z$. Using the expansion

$$\delta n_z = (t_1 \mathbf{t}_1 + p_1 \mathbf{p}_1) \cdot \hat{\mathbf{e}}_1^n, \quad (114)$$

the scattering cross section $\sigma = \langle E_f^*(\mathbf{q}, t) E_f(\mathbf{q}, t) \rangle$ with $\mathbf{q} \cdot \hat{\mathbf{e}}_y = 0$ is

$$\begin{aligned} \sigma &= \frac{\varepsilon_a^2 \omega^4}{c^4} \langle |\delta n_z(\mathbf{q})|^2 \rangle f_z^2 \\ &= \frac{\varepsilon_a^2 \omega^4}{c^4} (C_1^+ \langle |t_1(\mathbf{q})|^2 \rangle + C_1^- \langle |p_1(\mathbf{q})|^2 \rangle) f_z^2, \end{aligned} \quad (115)$$

with the coefficient

$$C_1^\pm = \frac{(Z_1^\mp)^2}{1 + (Z_1^\mp)^2}. \quad (116)$$

In the usual experimental setup one observes two splay-bend modes, \mathbf{t}_1 and \mathbf{p}_1 , as opposed to the usual NLC, where one observes only one splay-bend mode.

Asymptotic behaviors of the coefficients C_1^+ and C_1^- at large magnetic fields,

$$C_1^+ \asymp 1 - \frac{A_1^2 M_0^4}{(\mu_0 H M_0)^2}, \quad (117)$$

$$C_1^- \asymp \frac{2(K_\alpha q_\perp^2 + K_3 q_x^2) - 3A_1^2 M_0^4}{(\mu_0 H M_0)^2}, \quad (118)$$

reveal that in the large-magnetic-field limit only the eigenmode \mathbf{t}_1 contributes to the scattering cross section [Eq. (115)].

The dynamics of the fluctuations is probed by dynamic light scattering, where one measures the time correlation of the light intensity $I(t)$,

$$g^{(2)}(t) = \frac{\langle I(0)I(t) \rangle}{\langle I(0) \rangle^2}. \quad (119)$$

Assuming Gaussian fluctuations it follows that

$$g^{(2)}(t) = 1 + |g^{(1)}(t)|^2, \quad (120)$$

where

$$g^{(1)}(t) = \frac{\langle E_f^*(\mathbf{q}, 0) E_f(\mathbf{q}, t) \rangle}{\langle |E_f(\mathbf{q}, 0)|^2 \rangle} \quad (121)$$

is the time correlation of the scattered light electric field.

To calculate the time dependence of the fluctuations, we first linearize the system of dynamic equations and determine the dynamic eigenmodes. Considering only the dissipative

dynamics, Eqs. (8) and (9), and using $\delta \mathbf{n} = \delta n_1 \hat{\mathbf{e}}_1^n + \delta n_2 \hat{\mathbf{e}}_2^n$, $\delta \mathbf{m} = \delta m_1 \hat{\mathbf{e}}_1^M + \delta m_2 \hat{\mathbf{e}}_2^M$, we find a 2×2 homogeneous system for each $\alpha = 1, 2$,

$$\begin{aligned} \frac{1}{\tau} \delta n_\alpha &= \left[\frac{1}{\gamma_1} (K_\alpha q_\perp^2 + K_3 q_x^2 + A_1 M_0^2) - \chi_2^D A_1 M_0^2 \right] \delta n_\alpha \\ &+ \left[A_1 M_0^2 \left(\chi_2^D - \frac{1}{\gamma_1} \right) + \chi_2^D \mu_0 H M_0 \right] \delta m_\alpha, \\ \frac{1}{\tau} \delta m_\alpha &= \left[-b_\perp^D A_1 + \chi_2^D (K_\alpha q_\perp^2 + K_3 q_x^2 + A_1 M_0^2) \right] \delta n_\alpha \\ &+ \left[b_\perp^D A_1 \left(1 + \frac{\mu_0 H M_0}{A_1 M_0^2} \right) - \chi_2^D A_1 M_0^2 \right] \delta m_\alpha, \end{aligned} \quad (122)$$

which can be rewritten as

$$\left(\mathbf{A} - \frac{1}{\tau} \mathbf{l} \right) \begin{pmatrix} \delta n_\alpha \\ \delta m_\alpha \end{pmatrix} = \mathbf{0} \quad (123)$$

and has nontrivial solutions if $\det(\mathbf{A} - \frac{1}{\tau} \mathbf{l}) = 0$. The dynamic eigenmodes are the eigenvectors of the matrix \mathbf{A} ,

$$\mathbf{t}_\alpha^h = c_\alpha^t \hat{\mathbf{e}}_\alpha^n + d_\alpha^t \hat{\mathbf{e}}_\alpha^M, \quad (124)$$

$$\mathbf{p}_\alpha^h = c_\alpha^p \hat{\mathbf{e}}_\alpha^n + d_\alpha^p \hat{\mathbf{e}}_\alpha^M, \quad (125)$$

where the components $c_\alpha^t, c_\alpha^p, d_\alpha^t, d_\alpha^p$ are functions of the static and dynamic material parameters and will not be given explicitly. It is important to realize that the dynamic fluctuation modes [Eqs. (124) and (125)] in general differ from the statistically independent excitation modes [Eqs. (103) and (104)]. If the reversible dynamics [Eqs. (12) and (13)] is included, then a 4×4 eigensystem is obtained coupling both α 's. In that case, splay-bend and twist-bend dynamic modes are no longer decoupled and each eigenmode spans all directions $\{\hat{\mathbf{e}}_1^{n,M}, \hat{\mathbf{e}}_2^{n,M}\}$.

The time dependence of a fluctuation is first expressed in terms of the dynamic eigenmodes [Eqs. (124) and (125)], which are then further expressed by the uncorrelated excitation modes [Eqs. (103) and (104)]. Using Eqs. (112) and (113) and expressing $\delta n_z(t)$ of the splay-bend fluctuation as just explained, the electric field time correlation [Eq. (121)] becomes

$$|g^{(1)}(t)| = \frac{D_1^+(t) \langle |t_1(\mathbf{q}, 0)|^2 \rangle + D_1^-(t) \langle |p_1(\mathbf{q}, 0)|^2 \rangle}{C_1^+ \langle |t_1(\mathbf{q}, 0)|^2 \rangle + C_1^- \langle |p_1(\mathbf{q}, 0)|^2 \rangle}, \quad (126)$$

where

$$\begin{aligned} D_1^+(t) &= (\mathbf{t}_1 \cdot \hat{\mathbf{e}}_1^n)^2 f_1(t) + (\mathbf{t}_1 \cdot \hat{\mathbf{e}}_1^M) (\mathbf{t}_1 \cdot \hat{\mathbf{e}}_1^M) f_{II}(t), \\ D_1^-(t) &= (\mathbf{p}_1 \cdot \hat{\mathbf{e}}_1^n)^2 f_1(t) + (\mathbf{p}_1 \cdot \hat{\mathbf{e}}_1^n) (\mathbf{p}_1 \cdot \hat{\mathbf{e}}_1^M) f_{II}(t). \end{aligned} \quad (127)$$

The functions $f_1(t)$ and $f_{II}(t)$ are expressed using the components $c_1^t, c_1^p, d_1^t, d_1^p$ and the relaxation times of the dynamic eigenmodes denoted by τ_1^t and τ_1^p :

$$f_1(t) = \frac{c_1^t d_1^p e^{-t/\tau_1^t} - c_1^p d_1^t e^{-t/\tau_1^p}}{c_1^t d_1^p - c_1^p d_1^t}, \quad (128)$$

$$f_{II}(t) = \frac{d_1^t d_1^p (e^{-t/\tau_1^t} - e^{-t/\tau_1^p})}{c_1^t d_1^p - c_1^p d_1^t}. \quad (129)$$

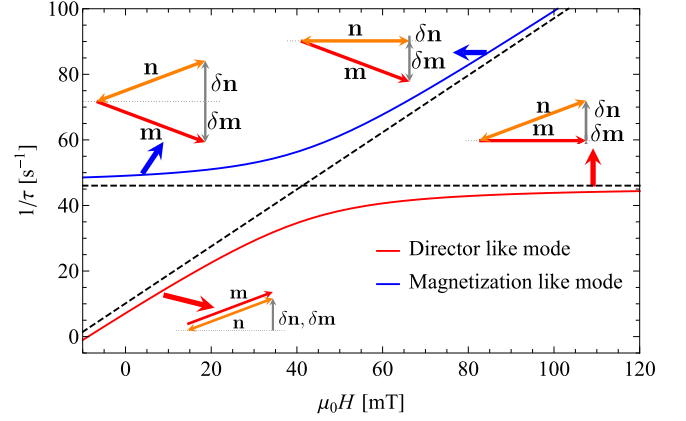


FIG. 23. Relaxation rates of almost pure bend fluctuations ($q_x \gg q_\perp$) and the corresponding dynamic eigenmodes as a function of the applied magnetic field. The dashed lines represent the limiting behavior of the relaxation rates, described by Eqs. (132) and (133). For clarity, a smaller value of the rotational viscosity was used to make the asymptotic behavior set in sooner.

In the limit of large magnetic fields one gets $D_1^\pm \rightarrow C_1^\pm e^{-t/\tau_1^t}$. Taking into account also the large-magnetic-field dependence of the coefficients C_1^\pm , Eqs. (117) and (118), the intensity correlation function Eq. (120) is a single exponential

$$g^{(2)}(t) = 1 + e^{-2t/\tau_1^t}. \quad (130)$$

It is found that the dynamics of the eigenmodes \mathbf{t}_α^h slows down ($\tau_\alpha^t \rightarrow \infty$) at a negative critical magnetic field, here given for $\mathbf{q} = q_z \hat{\mathbf{e}}_z$:

$$\mu_0 H_c^{(\alpha)} = - \frac{A_1 M_0 K_\alpha q_z^2}{K_\alpha q_z^2 + A_1 M_0^2}. \quad (131)$$

The negative value of the critical magnetic field means that it is pointing in the direction opposite to the magnetization. If the applied magnetic field is more negative than the critical field, then the magnetization starts to reverse. In NLCs, $K_2 < K_1$ usually holds and it is the twist mode \mathbf{t}_2^h that slows down at a less-negative magnetic field. With the smallest wave number $q_z = \pi/d$ we get $\mu_0 H_c^{(2)} = -2.5$ mT.

In Fig. 23 we present the magnetic field dependence of the relaxation rate of almost pure bend ($q_x \gg q_\perp$) fluctuations. We also depict the corresponding eigenmodes at a small positive field and at large magnetic fields.

For a general fluctuation, in the limit of large magnetic fields the relaxation rate of the faster (magnetization-like) \mathbf{p}_α^h mode is proportional to the applied magnetic field (Fig. 23 presents the bend fluctuation as an example),

$$\begin{aligned} \frac{1}{\tau_\alpha^p} &= \frac{A_1 (b_\perp^D - \chi_2^D M_0)^2 + (\chi_2^D M_0)^2 (K_\alpha q_\perp^2 + K_3 q_x^2)}{b_\perp^D} \\ &+ \frac{b_\perp^D}{M_0} \mu_0 H. \end{aligned} \quad (132)$$

The relaxation rate of the slower (director-like) \mathbf{t}_α^h mode saturates at a finite value (Fig. 23 presents the bend fluctuation

as an example),

$$\frac{1}{\tau_\alpha^t} = \frac{A_1 M_0^2 + (K_\alpha q_\perp^2 + K_3 q_x^2)}{\gamma_1} \left[1 - \frac{(\chi_2^D M_0)^2 \gamma_1}{b_\perp^D} \right]. \quad (133)$$

It is also illuminating to study the relaxation rates of general fluctuations at zero magnetic field, $H = 0$. Expanding the relaxation rates to second order in q_x and q_\perp one gets

$$\frac{1}{\tau_\alpha^p} = \frac{A_1 M_0^2}{\gamma_1} \left(1 - 2\chi_2^D \gamma_1 + \frac{b_\perp^D \gamma_1}{M_0^2} \right) + \frac{(K_\alpha q_\perp^2 + K_3 q_x^2) \Xi_p}{\gamma_1}, \quad (134)$$

$$\frac{1}{\tau_\alpha^t} = \frac{(K_\alpha q_\perp^2 + K_3 q_x^2) \Xi_t}{\gamma_1}, \quad (135)$$

where

$$\Xi_p = \frac{(\chi_2^D \gamma_1 - 1)^2 M_0^2}{b_\perp^D \gamma_1 + (1 - 2\chi_2^D \gamma_1) M_0^2}, \quad (136)$$

$$\Xi_t = \frac{\gamma_1 (b_\perp^D - (\chi_2^D M_0)^2 \gamma_1)}{b_\perp^D \gamma_1 + (1 - 2\chi_2^D \gamma_1) M_0^2}. \quad (137)$$

From Eqs. (134) and (135) one can see that the relaxation rate $1/\tau_\alpha^p$ of the faster (optic) mode \mathbf{p}_α^h stays finite in the limit $\mathbf{q} \rightarrow 0$. The slower mode \mathbf{t}_α^h is, on the other hand, acoustic, i.e., $1/\tau_\alpha^t \rightarrow 0$ as $\mathbf{q} \rightarrow 0$.

IX. SUMMARY AND PERSPECTIVE

In the present extensive study we have presented detailed experimental and theoretical investigations of the dynamics of the magnetization and the director in a ferromagnetic liquid crystal in the absence of flow. We have shown that a dissipative cross-coupling between these two macroscopic variables, which has been determined quantitatively, is essential to account for the experimental results also for the compound E7 as a nematic solvent for the ferromagnetic nematic phase. Before, this was demonstrated for 5CB as a nematic solvent [30]. We also find that all the experimental results presented here for E7 complement well and are consistent with the previous ones using 5CB as the nematic component. Remarkably, the dissipative cross-coupling (χ_2^D) found for the E7-based ferromagnetic nematic liquid crystal is about a factor of 5 smaller than that of the 5CB based, while the dissipative coefficient of the magnetization (b_\perp^D) is (only) twice as large. This leads to an interesting suggestion for future experimental work, namely to address the question of which molecular features determine the strength of this dissipative cross-coupling. The nematic phases of 5CB and E7, respectively, show one qualitatively different feature: The nematic phase of 5CB is well known to favor the formation of transient pairlike aggregates [37] because of its nitrile group, while such tendencies are reduced in E7 since it is mixture of four different compounds and

also contains a terphenyl. A natural experiment to study these features in more detail would be to investigate the dependence of the dissipative cross-coupling on the magnetic particle concentration on one hand and to investigate mixtures of the nematic solvents 5CB and E7 on the other to learn more about the coupling mechanisms between the nematic order and the magnetic order.

We have also analyzed the consequences of an out-of-plane dynamics, i.e., out of the plane spanned by the magnetic field and the spontaneous magnetization. We give predictions for both the azimuthal angles of director and magnetization as well as for the intensity change related to the reversible dynamic cross-coupling terms between the two order parameters, the magnetization and the director. We find that from both measurements a value for the reversible cross-coupling terms can be extracted.

From the present analysis the next steps in this field appear to be quite well defined. First, the incorporation of flow effects appears to be highly desirable both from a theoretical as well as from an experimental point of view. Early experimental results in this direction have been described in Ref. [38], where it has been shown that viscous effects can be tuned by an external magnetic field of about 10^{-2} T by more than a factor of two. From a theoretical perspective, questions like the analogs of the Miesowicz viscosities and flow alignment are high on the priority list [39].

Moreover, it will be important to realize, although perhaps experimentally challenging, a nematic or cholesteric liquid crystalline version of uniaxial magnetic gels and rubbers [40,41]. Cross-linking a ferromagnetic nematic would give rise to the possibility to obtain a soft ferromagnetic gel, opening the door to a new class of magnetic complex fluids. This way, one could combine the macroscopic degrees of freedom of the first liquid multiferroic, namely the ferromagnetic nematic liquid crystal, with the strain field as well as with relative rotations. In a step towards this goal, we will derive macroscopic dynamic equations generalizing those for uniaxial magnetic gels and ferronematics to obtain the macroscopic dynamics for ferromagnetic nematic and cholesteric gels [42].

ACKNOWLEDGMENTS

Partial support of this work by H.R.B., H.P., T.P., and D.S. through the Schwerpunktprogramm SPP 1681 ‘‘Feldgesteuerte Partikel-Matrix-Wechselwirkungen: Erzeugung, skalenbergreifende Modellierung und Anwendung magnetischer Hybridmaterialien’’ of the Deutsche Forschungsgemeinschaft is gratefully acknowledged, as well as the support of the Slovenian Research Agency, Grants No. N1-0019, J1-7435 (D.S.), No. P1-0192 (A.M. and N.O.), and No. P2-0089 (D.L.). N.S. thanks the ‘‘EU Horizon 2020 Framework Programme for Research and Innovation’’ for its support through the Marie Curie Individual fellowship (Grant No. 701558) (MagNem). We thank the CENN Nanocenter for use of the LakeShore 7400 Series VSM vibrating-sample magnetometer.

[1] F. Brochard and P. G. de Gennes, *J. Phys. (France)* **31**, 691 (1970).

[2] J. Rault, P. E. Cladis, and J. Burger, *Phys. Lett. A* **32**, 199 (1970).

[3] S.-H. Chen and N. M. Amer, *Phys. Rev. Lett.* **51**, 2298 (1983).

- [4] T. Kroin and A. M. F. Neto, *Phys. Rev. A* **36**, 2987 (1987).
- [5] F. L. S. Cuppo, S. L. Gómez, and A. M. F. Neto, *Eur. Phys. J. E* **13**, 327 (2004).
- [6] P. Kopčanský, N. Tomašovičová, M. Koneracká *et al.*, *Phys. Rev. E* **78**, 011702 (2008).
- [7] E. Ouskova, O. Buluy, C. Blanc, H. Dietsch, and A. Mertelj, *Mol. Cryst. Liq. Cryst.* **525**, 104 (2010).
- [8] O. Buluy, S. Nepijko, V. Reshetnyak *et al.*, *Soft Matter* **7**, 644 (2011).
- [9] N. Podoliak, O. Buchnev, D. V. Bavykin, A. N. Kulak, M. Kaczmarek, and T. J. Sluckin, *J. Colloid Interface Sci.* **386**, 158 (2012).
- [10] R. E. Rosensweig, *Ferrohydrodynamics* (Cambridge University Press, Cambridge, 1985).
- [11] S. Odenbach, *J. Phys. Condens. Matter* **16**, R1135 (2004).
- [12] H.-W. Müller and M. Liu, *Phys. Rev. E* **64**, 061405 (2001).
- [13] B. Huke and M. Lücke, *Rep. Prog. Phys.* **67**, 1731 (2004).
- [14] P. Ilg, E. Coquelle, and S. Hess, *J. Phys. Condens. Matter* **18**, S2757 (2006).
- [15] V. I. Zadorozhnyi, A. N. Vasilev, V. Yu. Reshetnyak, K. S. Thomas, and T. J. Sluckin, *Europhys. Lett.* **73**, 408 (2006).
- [16] S. Mahle, P. Ilg, and M. Liu, *Phys. Rev. E* **77**, 016305 (2008).
- [17] S. D. Peroukidis and S. H. L. Klapp, *Phys. Rev. E* **92**, 010501 (2015).
- [18] E. Jarkova, H. Pleiner, H.-W. Müller, A. Fink, and H. R. Brand, *Eur. Phys. J. E* **5**, 583 (2001).
- [19] E. Jarkova, H. Pleiner, H.-W. Müller, and H. R. Brand, *J. Chem. Phys.* **118**, 2422 (2003).
- [20] H. R. Brand, A. Fink, and H. Pleiner, *Eur. Phys. J. E* **38**, 65 (2015).
- [21] H. Pleiner, E. Jarkova, H.-W. Müller, and H. R. Brand, *Magneto-hydrodynamics* **37**, 254 (2001).
- [22] A. Mertelj, D. Lisjak, M. Drogenik, and M. Čopič, *Nature* **504**, 237 (2013).
- [23] M. Shuai, A. Klittnick, Y. Shen *et al.*, *Nat. Commun.* **7**, 10394 (2016).
- [24] Q. Liu, P. J. Ackerman, T. C. Lubensky, and I. I. Smalyukh, *Proc. Natl. Acad. Sci. USA* **113**, 10479 (2016).
- [25] A. Mertelj, N. Osterman, D. Lisjak, and M. Čopič, *Soft Matter* **10**, 9065 (2014).
- [26] Q. Zhang, P. J. Ackerman, Q. Liu, and I. I. Smalyukh, *Phys. Rev. Lett.* **115**, 097802 (2015).
- [27] P. J. Ackerman and I. I. Smalyukh, *Nat. Mater.* **16**, 426 (2017).
- [28] P. M. Rupnik, D. Lisjak, M. Čopič, S. Čopar, and A. Mertelj, *Sci. Adv.* **3**, e1701336 (2017).
- [29] A. Mertelj and D. Lisjak, *Liq. Cryst. Rev.* **5**, 1 (2017).
- [30] T. Potisk, D. Svenšek, H. R. Brand, H. Pleiner, D. Lisjak, N. Osterman, and A. Mertelj, *Phys. Rev. Lett.* **119**, 097802 (2017).
- [31] H. Hakemi, E. F. Jagodzinski, and D. B. Dupré, *Mol. Cryst. Liq. Cryst.* **91**, 129 (1983).
- [32] P. G. de Gennes and J. Prost, *The Physics of Liquid Crystals* (Clarendon Press, Oxford, 1995).
- [33] A. Rapini and M. Papoular, *J. Phys. Coll.* **30**, C4-54 (1969).
- [34] H. Pleiner and H. R. Brand, in *Hydrodynamics and Electrohydrodynamics of Nematic Liquid Crystals, in Pattern Formation in Liquid Crystals*, edited by A. Buka and L. Kramer (Springer, New York, 1996).
- [35] E. Hecht, *Optics*, 5th ed. (Addison-Wesley, Boston, MA, 2016).
- [36] M. Čopič, M. Vilfan, and A. Mertelj, *Liq. Cryst.* **40**, 1646 (2013).
- [37] P. E. Cladis, *Mol. Cryst. Liq. Cryst.* **67**, 177 (1981).
- [38] R. Sahoo, M. V. Rasna, D. Lisjak, A. Mertelj, and S. Dahra, *Appl. Phys. Lett.* **106**, 161905 (2015).
- [39] T. Potisk, D. Svenšek, H. Pleiner, and H. R. Brand (unpublished).
- [40] D. Collin, G. K. Auernhammer, O. Gavat, P. Martinoty, and H. R. Brand, *Macromol. Rapid Commun.* **24**, 737 (2003).
- [41] S. Bohlius, H. R. Brand, and H. Pleiner, *Phys. Rev. E* **70**, 061411 (2004).
- [42] T. Potisk, D. Svenšek, H. Pleiner, and H. R. Brand (unpublished).

Publication 3

Effects of flow on the dynamics of a ferromagnetic nematic liquid crystal

T. Potisk, H. Pleiner, D. Svenšek, and H.R. Brand
Phys. Rev. E **97**, 042705 (2018).

Effects of flow on the dynamics of a ferromagnetic nematic liquid crystalTilen Potisk,^{1,2,*} Harald Pleiner,³ Daniel Svenšek,² and Helmut R. Brand¹¹*Department of Physics, University of Bayreuth, 95440 Bayreuth, Germany*²*Department of Physics, Faculty of Mathematics and Physics, University of Ljubljana, SI-1000 Ljubljana, Slovenia*³*Max Planck Institute for Polymer Research, 55021 Mainz, Germany*

(Received 1 March 2018; published 26 April 2018)

We investigate the effects of flow on the dynamics of ferromagnetic nematic liquid crystals. As a model, we study the coupled dynamics of the magnetization, \mathbf{M} , the director field, \mathbf{n} , associated with the liquid crystalline orientational order, and the velocity field, \mathbf{v} . We evaluate how simple shear flow in a ferromagnetic nematic is modified in the presence of small external magnetic fields, and we make experimentally testable predictions for the resulting effective shear viscosity: an increase by a factor of 2 in a magnetic field of about 20 mT. Flow alignment, a characteristic feature of classical uniaxial nematic liquid crystals, is analyzed for ferromagnetic nematics for the two cases of magnetization in or perpendicular to the shear plane. In the former case, we find that small in-plane magnetic fields are sufficient to suppress tumbling and thus that the boundary between flow alignment and tumbling can be controlled easily. In the latter case, we furthermore find a possibility of flow alignment in a regime for which one obtains tumbling for the pure nematic component. We derive the analogs of the three Miesowicz viscosities well-known from usual nematic liquid crystals, corresponding to nine different configurations. Combinations of these can be used to determine several dynamic coefficients experimentally.

DOI: [10.1103/PhysRevE.97.042705](https://doi.org/10.1103/PhysRevE.97.042705)**I. INTRODUCTION**

Many complex fluids show anisotropic and/or non-Newtonian behavior in their flow properties. A class of anisotropic complex fluids for which the flow behavior has been studied in some detail because of their wide-ranging applications are liquid crystals, in particular nematic liquid crystals [1]. Uniaxial nematics are uniaxially anisotropic liquid systems that find applications, for example, in large area displays. Clearly the flow properties of the uniaxial nematic phase are the most studied and best understood among all liquid crystalline phases [1].

In parallel, the field of magnetic liquids, i.e., suspensions of magnetic monodomain particles, has developed [2]. Various aspects of their characterization as well as of their macroscopic and microscopic properties are addressed in Refs. [3–8].

There has been considerable recent interest in a novel type of nematic phase, namely ferromagnetic nematics, showing simultaneously nematic as well as ferromagnetic order. While such a phase was predicted and investigated theoretically almost 50 years ago [9], its synthesis was reported experimentally only recently [10,11].

The ferromagnetic nematic is a room-temperature liquid multiferroic system. The only other liquid multiferroic systems known earlier are the superfluid phases of ^3He [12,13]. Two of them, namely $^3\text{He-A}$ and $^3\text{He-A}_1$, are also uniaxial and show spontaneously broken orientational order as well as (anti)ferromagnetism. Besides superfluidity, both phases show rich macroscopic behavior including spin waves [14–18].

We also note that in the meantime ferromagnetic cholesteric phases have been described and characterized [19–21], thus complementing the abundant usual cholesteric phases, which break parity symmetry, because they are composed of chiral molecules: left- and right-handed helices differ from their mirror image in a nontrivial way, i.e., they cannot be brought to coincidence by mere rotations. The macroscopic behavior of ferrocholesterics has been elucidated in Ref. [22].

As for ferromagnetic nematics, most studies focused on their synthesis, their characterization, and their static properties [10,11,23]. There is also early work discussing a Landau description of phase transitions involving a ferromagnetic nematic phase [24]. A systematic investigation of their dynamic properties was initiated only quite recently [25,26]. These first two publications focused on the coupled dynamics of the two order parameters, namely the magnetization, \mathbf{M} , characterizing spontaneously broken rotational symmetry in spin space, and the director, \mathbf{n} , characteristic for systems with spontaneously broken rotational symmetry [27].

In this paper, we analyze the coupling of these two order parameters to flows generalizing simple flow situations for uniaxial nematics to ferromagnetic nematics. For the new liquid multiferroic system, we include a discussion of the analogs of effective viscosity, Miesowicz viscosities, flow alignment, as well as transient backflow [28,29] and kickback [30] effects, all familiar from usual nematics [1]. The main goal of this study is to make concrete experimentally testable predictions.

The paper is organized as follows. In Sec. II, we present the macroscopic model used throughout the present paper. In Sec. III, we discuss simple shear flow and its experimentally accessible consequences. Section IV is dedicated to a characterization of the analogs of the Miesowicz viscosities for ferromagnetic nematic liquid crystals leading to many

*tilen.potisk@uni-bayreuth.de

predictions. In Sec. V, we consider the analog of flow alignment and show how the transition to tumbling can be shifted by small external magnetic fields. In Sec. VI, we sketch out the effects of flow on the the dynamic behavior when an external magnetic field is switched on. In the brief last section, we conclude and give a perspective.

II. MACROSCOPIC MODEL

Throughout the present paper, we take into account the magnetization \mathbf{M} , the director field \mathbf{n} , and the velocity field \mathbf{v} as macroscopic variables. For a complete set of macroscopic dynamic equations for ferronematics, we refer the reader to Refs. [31,32].

The static behavior is described by the free-energy density $f(\mathbf{M}, \mathbf{n}, \nabla \mathbf{n})$,

$$f = -\mu_0 \mathbf{M} \cdot \mathbf{H} - \frac{1}{2} A_1 (\mathbf{M} \cdot \mathbf{n})^2 + \frac{1}{2} A_2 (|\mathbf{M}| - M_0)^2 + f^F, \quad (1)$$

where μ_0 is the magnetic constant, \mathbf{H} is the applied magnetic field, and $A_{1,2} > 0$ will be assumed constant. The first term represents the coupling of the magnetization and the external magnetic field. The second term describes the static coupling between the director field and the magnetization (originating from the magnetic particles). The third term describes the energy connected with the deviation of the modulus of the magnetization from M_0 . The last term is the Frank elastic energy associated with director distortions [1]

$$f^F = \frac{1}{2} K_1 (\nabla \cdot \mathbf{n})^2 + \frac{1}{2} K_2 [\mathbf{n} \cdot (\nabla \times \mathbf{n})]^2 + \frac{1}{2} K_3 [\mathbf{n} \times (\nabla \times \mathbf{n})]^2, \quad (2)$$

with positive elastic constants for splay (K_1), twist (K_2), and bend (K_3). Throughout this paper, a one-constant approximation will be used, i.e., $K_1 = K_2 = K_3 = K$. While it is a good approximation to assume that $|\mathbf{M}| = M_0$, we will take into account small variations of $|\mathbf{M}|$ (corresponding to large values of A_2).

The total free energy is $F = \int f \, dV$ and the equilibrium condition requires $\delta F = 0$. The macroscopic dynamic equations for the magnetization, the director field, and the velocity field read [32,33]

$$\left(\frac{\partial}{\partial t} + v_j \nabla_j \right) M_i + \epsilon_{ijk} M_j \omega_k + X_i^R + X_i^D = 0, \quad (3)$$

$$\left(\frac{\partial}{\partial t} + v_j \nabla_j \right) n_i + \epsilon_{ijk} n_j \omega_k + Y_i^R + Y_i^D = 0, \quad (4)$$

$$\rho \left(\frac{\partial}{\partial t} + v_j \nabla_j \right) v_i + \nabla_j (\sigma_{ij}^R + \sigma_{ij}^D + \sigma_{ij}^{\text{th}}) - \nabla_i p = 0, \quad (5)$$

where $\omega_i = \frac{1}{2} \epsilon_{ijk} \nabla_j v_k$ is the vorticity and ρ is the density. The (quasi)currents have been split into reversible ($X_i^R, Y_i^R, \sigma_{ij}^R$) and irreversible, dissipative ($X_i^D, Y_i^D, \sigma_{ij}^D$) parts. In Eq. (5), the reversible part of the stress tensor has been further split to include a thermodynamic part σ_{ij}^{th} ,

$$\sigma_{ij}^{\text{th}} = -B_j H_i - \frac{1}{2} (h_i^n n_j - h_j^n n_i) - \frac{1}{2} (h_i^M M_j - h_j^M M_i) + K_{kjmp} \nabla_p n_m \nabla_i n_k, \quad (6)$$

and the thermodynamic pressure

$$p = -\varepsilon + T\sigma + \mu\rho + \mathbf{g} \cdot \mathbf{v} + \mathbf{B} \cdot \mathbf{H}, \quad (7)$$

with temperature T , entropy density σ , chemical potential μ , density of linear momentum \mathbf{g} , and magnetic flux density \mathbf{B} . The reversible (dissipative) parts of the (quasi)currents have the same (opposite) behavior under time reversal as the time derivatives of the corresponding variables, i.e., Eqs. (3)–(5) are invariant under time reversal only if the dissipative (quasi)currents vanish.

The (quasi)currents are expressed as linear combinations of conjugate quantities (thermodynamic forces)

$$h_i^M \equiv \frac{\delta f}{\delta M_i} = \frac{\partial f}{\partial M_i}, \quad (8)$$

$$h_i^n \equiv \delta_{ik}^\perp \frac{\delta f}{\delta n_k} = \delta_{ik}^\perp \left(\frac{\partial f}{\partial n_k} - \partial_j \Phi_{kj} \right), \quad (9)$$

$$A_{ij} \equiv \frac{1}{2} (\partial_i v_j + \partial_j v_i), \quad (10)$$

with $\Phi_{kj} = \delta f / \partial (\nabla_j n_k)$ and where the transverse Kronecker delta $\delta_{ik}^\perp = \delta_{ik} - n_i n_k$ projects onto the plane perpendicular to the director due to the constraint $\mathbf{n}^2 = 1$.

In Ref. [25], only the dissipative quasicurrents X_i^D and Y_i^D were taken into account as they had a direct relevance for the explanation of the experimental results discussed there. The effects of the reversible quasicurrents X_i^R and Y_i^R were modeled in Ref. [26]. In the present paper, we also include the velocity variable in the approximation of an incompressible flow, $\nabla_i v_i = 0$.

The dissipative quasicurrents take the form [32]

$$X_i^D = b_{ij}^D h_j^M + \chi_{ij}^D h_j^n + c_{ijk}^D A_{jk}, \quad (11)$$

$$Y_i^D = \frac{1}{\gamma_1} \delta_{ik}^\perp h_k^n + \chi_{ij}^D h_j^M + \lambda_{ijk}^D A_{jk}, \quad (12)$$

$$\sigma_{ij}^D = -v_{ijkl}^D A_{kl} - \lambda_{kij}^D h_k^n - c_{kij}^D h_k^M, \quad (13)$$

with

$$\chi_{ij}^D = \chi_1^D \delta_{ik}^\perp M_k n_j + \chi_2^D \delta_{ij}^\perp M_k n_k, \quad (14)$$

$$b_{ij}^D = b_{\parallel}^D n_i n_j + b_{\perp}^D \delta_{ij}^\perp, \quad (15)$$

$$v_{ijkl}^D = 2(v_1 + v_2 - 2v_3) n_i n_j n_k n_l + (v_3 - v_2) (n_j n_l \delta_{ik} + n_j n_k \delta_{il} + n_i n_k \delta_{jl} + n_i n_l \delta_{jk}) + (v_4 - v_2) \delta_{ij} \delta_{kl} + v_2 (\delta_{jl} \delta_{ik} + \delta_{il} \delta_{jk}) + (v_5 - v_4 + v_2) (\delta_{ij} n_k n_l + \delta_{kl} n_i n_j), \quad (16)$$

$$\lambda_{ijk}^D = \lambda_1^D (\delta_{iq}^\perp \epsilon_{pqj} M_p n_k + \delta_{iq}^\perp \epsilon_{pkq} M_p n_j) + \lambda_2^D (\delta_{ik}^\perp \epsilon_{pqj} M_p n_q + \delta_{ij}^\perp \epsilon_{pkq} M_p n_q) + \lambda_3^D (\epsilon_{ipk} M_j n_p + \epsilon_{ipj} M_k n_p) + \lambda_4^D M_q n_q (\epsilon_{ipk} n_j n_p + \epsilon_{ipj} n_k n_p) + \lambda_5^D \epsilon_{piq} M_p n_q n_j n_k + \lambda_6^D \epsilon_{piq} M_p n_q \delta_{jk}^\perp, \quad (17)$$

$$c_{ijk}^D = c^D (\epsilon_{imk} n_m n_j + \epsilon_{imj} n_m n_k). \quad (18)$$

The tensor χ_{ij}^D describes the dissipative cross-coupling between the director and the magnetization. In Refs. [25] and [26] it was shown that it is of major importance for the dynamics and was crucial to explain the presented experiments. The viscosity tensor v_{ijkl}^D is the same as for usual nematic liquid crystals (in the Appendix, the connection with the Leslie viscosity coefficients is reviewed). The existence of the magnetization gives rise to an additional dissipative coupling of the velocity with the director, described by the tensor λ_{ijk}^D , which is not present in usual nematics. Moreover, there exists also a direct dissipative coupling of the velocity and the magnetization, described by the tensor c_{ijk}^D . Throughout the present paper, we will discard the biaxiality of the material that arises for $\mathbf{n} \parallel \mathbf{M}$.

The reversible quasicurrents [32] are obtained by requiring that the entropy production $Y_i h_i^n + X_i h_i^M + \sigma_{ij} A_{ji}$ is zero. They are

$$X_i^R = b_{ij}^R h_j^M + \chi^R \epsilon_{ijk} n_j h_k^n - c_{ijk}^R A_{jk}, \quad (19)$$

$$Y_i^R = (\gamma_1^{-1})_{ij}^R h_j^n + \chi^R \epsilon_{ijk} n_j h_k^M - \frac{1}{2} \lambda_{ijk}^R A_{jk}, \quad (20)$$

$$\sigma_{ij}^R = -v_{ijkl}^R A_{kl} - \frac{1}{2} \lambda_{kji}^R h_k^n - c_{kij}^R h_k^M. \quad (21)$$

In Eqs. (20) and (21), the reversible couplings between the velocity field on the one hand and the director field and the magnetization are described by the flow alignment tensor

$$\lambda_{ijk} = \lambda(\delta_{ij}^\perp n_k + \delta_{ik}^\perp n_j) \quad (22)$$

and by the tensor c_{ijk}^R [32], respectively,

$$\begin{aligned} c_{ijk}^R &= c_1^R M_i n_j n_k + c_2^R (\delta_{ij}^R M_k + \delta_{ik}^R M_j) + c_3^R M_i \delta_{jk} \\ &+ c_4^R n_i M_p n_p \delta_{jk} + c_5^R (n_i M_j n_k + n_i M_k n_j) \\ &+ c_6^R n_i M_p n_p n_j n_k. \end{aligned} \quad (23)$$

In the following, we will discard the contributions of the tensors v_{ijkl}^R , $(\gamma_1^{-1})_{ij}^R$, b_{ij}^R , and χ^R , which can be found in Ref. [32].

A. Geometry and method

In this paper, we study the situation in which a ferromagnetic nematic liquid crystal is confined between a pair of infinite parallel plates separated in the z direction by the cell thickness d . We assume that the fields are functions only of the coordinate z and time t . For solving Eqs. (3)–(5), a simple numerical method is used. We first discretize space into slices of width $\Delta z = d/(N-1)$, where N is the number of discretization points. By varying N , it is found that using $N = 50$ is already sufficient. We use a variant of the so called staggered grid, Fig. 1, to avoid possible numerical instabilities. The velocity field is defined in the middle of the slices, while the stress tensor, the director field, and the magnetization field are defined at the edges of the slices. The velocity field at these edges can be calculated simply by averaging the neighboring points,

$$v_i(j\Delta z) = 0.5\{v_i[(j-1/2)\Delta z] + v_i[(j+1/2)\Delta z]\}, \quad (24)$$

where Δz is the step size and $j \in \{0, 1, \dots, N-1\}$ is an integer.

After discretizing space, one obtains N ordinary differential equations. For the second derivative in the bulk of the liquid-

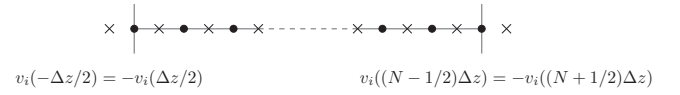


FIG. 1. A schematic representation of the staggered grid used to solve Eqs. (3)–(5). The director field, the magnetization field, and the (quasi)currents are defined on the points (black circles), while the velocity field is defined on the crosses located between the points. There are two crosses outside of the physical space, which are present in order to satisfy the boundary condition for the velocity field.

crystal cell, we used the usual central finite-difference scheme,

$$f''(z) \approx \frac{f(z+\Delta z) - 2f(z) + f(z-\Delta z)}{(\Delta z)^2} + O[(\Delta z)^2]. \quad (25)$$

At the boundaries, we use an asymmetric finite-difference scheme for the derivatives.

Due to its simplicity, we use the Euler method for our analysis. An example for one step of the Euler method for the i th component of the director field at coordinate z is

$$n_i(t+\delta t, z) = n_i(t, z) - \delta t Y_i(t, z) + O(\delta t^2), \quad (26)$$

where δt is the time step. An analogous equation holds for the magnetization field, and the equations are solved simultaneously. Since the numerical scheme for the director field is not norm-preserving, we normalize the director field after each time step: $n_i \rightarrow n_i/(n_j n_j)^{1/2}$.

The velocity field relaxes on time scales much shorter than the director field or the magnetization, and thus Eq. (5) can be simplified to

$$\nabla_j \sigma_{ij}^R + \nabla_j \sigma_{ij}^D + \nabla_j \sigma_{ij}^{\text{th}} - \nabla_i p = 0. \quad (27)$$

The equation for the pressure field can be obtained by taking the divergence of Eq. (27). The boundary conditions for the pressure are obtained by taking the inner product of Eq. (27) with the surface normals, pointing up (down) at the top (bottom) plate. The resulting pressure field is

$$p(z) = p_0 + \sigma_{zz}(z), \quad (28)$$

where p_0 is an arbitrary constant and σ_{zz} includes all the stresses $\sigma_{zz} = \sigma_{zz}^R + \sigma_{zz}^D + \sigma_{zz}^{\text{th}}$. Since p is only a function of z , it only shows up in the dynamic equation for the z component of the velocity field, where it exactly cancels out the contributions of all the stresses. The z component of the velocity field is therefore independent of time, i.e., $\partial v_z / \partial t = 0$, and is zero, $v_z = 0$, due to the boundary condition.

Given the director and the magnetization field, we solve Eq. (27) on a staggered grid for the velocity field, as shown in Fig. 1.

For the director field, we assume infinitely strong (planar) anchoring at the boundaries, $\mathbf{n} = \hat{\mathbf{e}}_x$ at $z = 0$ and $z = d$. For the velocity field, we assume the no-slip condition $\mathbf{v} = \mathbf{0}$ at $z = 0$ and $z = d$. In the case of shear experiments, $\mathbf{v} = v_{0x} \hat{\mathbf{e}}_x$ at $z = d$, where v_{0x} is the velocity of the upper plate. The lower

plate is fixed. We define the shear rate

$$\Gamma_x = \frac{v_{0x}}{d}. \quad (29)$$

B. Material parameters

Throughout this study, we will be using similar values of the static and the dynamic coefficients as determined in Ref. [25]. Therein, a ferromagnetic nematic using 5CB as a nematic solvent was studied. For the static coefficients, we used $A_1 = 130\mu_0$, $A_2 = 1000A_1$, $K = 7$ pN, $M_0 = 50$ A/m, and $d = 50$ μm and for the dynamic ones we used $\chi_2^D = 20$ (Pa s) $^{-1}$, $\chi_1^D = 0$, and $b_{\perp}^D = b_{\parallel}^D = 1.5 \times 10^5$ A m/V s 2 . For the coefficients of the viscosity tensor, the rotational viscosity γ_1 , and the flow alignment parameter λ , we used $\nu_1 = 0.092$ Pa s, $\nu_2 = 0.038$ Pa s, $\nu_3 = 0.045$ Pa s, $\gamma_1 = 0.081$ Pa s, and $\lambda = 1.05$; see the data for 5CB in Ref. [34]. For the remaining coefficients of v_{ijk}^D , we chose $\nu_4 = \nu_2$ and $\nu_5 = 0$. In the literature, one often encounters the so called Ericksen-Leslie viscosities, which are related to the set of viscosities used here (compare the Appendix for the detailed relations). For the reversible coupling c_{ijk}^R between the magnetization and the velocity field in Eqs. (19) and (21), which is the analog of the flow alignment tensor λ_{ijk} of Eqs. (20) and (21), we use the coefficient c_2^R , Eq. (23), as a representative, since it has the same structure as λ in Eq. (22). We choose the value $c_2^R = 0.55$ so that its effects on the magnetization are comparable to the effects of λ on the director field. It should be noted that for simple shear flow, the contributions of c_3^R and c_4^R are automatically zero. Furthermore, due to the approximately fixed modulus of the magnetization, the contribution of the coefficient c_1^R is negligible. The effect of c_5^R is biggest when the magnetization (director) is parallel to the velocity field and the director (magnetization) is perpendicular to the velocity field and within the shear plane, which is perpendicular to the vorticity. Lastly, the effect of c_6^R is biggest when the magnetization is either parallel or perpendicular to the velocity field and the director is at 45° with respect to the magnetization while both fields are in the shear plane.

III. SIMPLE SHEAR

A classical approach to study the rheology of simple and complex fluids is the investigation of a simple shear flow. Here we will focus on the changes compared to the case of uniaxial nematics by the application of a magnetic field perpendicular to the plates of a shear cell.

In this section, we discard the dissipative couplings of the director and the magnetization to the velocity field, i.e., the tensors λ_{ijk}^D and c_{ijk}^D of Eqs. (17) and (18) are set to zero. From the form of the tensor λ_{ijk}^D (c_{ijk}^D) one can see that there is, in general, a nonzero coupling between the out-of-shear plane component of the director (magnetization) field with the part of the director (magnetization) molecular field h_i^n (h_i^M), which is within the shear plane. Since we have set these tensors to zero, the velocity points along the x axis everywhere with the director and the magnetization being within the shear plane, which is also confirmed numerically.

In Fig. 2 we present the solutions of v_x/v_{0x} , n_z , and M_z/M_0 as functions of z . A magnetic field $\mathbf{H} = H\hat{e}_z$ of

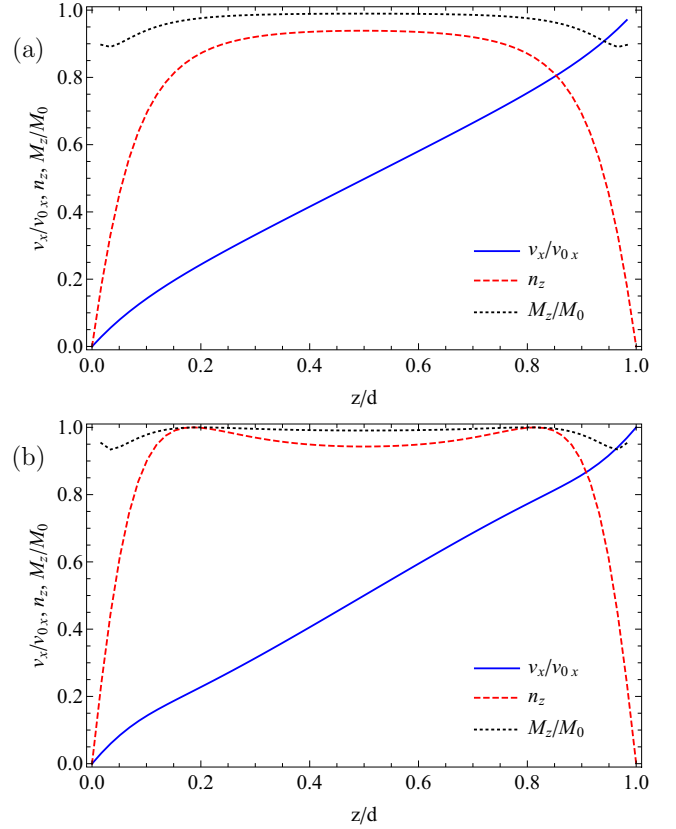


FIG. 2. Profiles of v_x/v_{0x} , M_z/M_0 , and n_z at a shear rate $\Gamma_x = 1$ s $^{-1}$ with (a) $\mu_0 H = 10$ mT and (b) $\mu_0 H = -10$ mT.

$H = 10$ mT [Fig. 2(a)] and $H = -10$ mT [Fig. 2(b)] was applied perpendicularly to the plates, and a shear rate of $\Gamma_x = 1$ s $^{-1}$ was imposed. We observe that for the negative magnetic field, the director in the middle of the cell rotates by an angle of more than $\pi/2$. This is due to the fact that the shear forces, which are described by the tensor λ_{ijk} , change direction at a certain orientation of the director. This orientation is determined by the parameter λ . Secondly, it is more favorable for the director to rotate further, since the coupling energy (A_1) gets lower.

The dependence of the x component of the velocity field on the magnetic field at a shear rate of 1 s $^{-1}$ is shown in Fig. 3. One can see, as expected, that the velocity profile is not linear, and a boundary layer of order 10% of the cell thickness is visible using $\Gamma_x = 1$ s $^{-1}$ and magnetic fields of order 1 mT. The thickness of the boundary layer of the velocity field can be connected with the deformation of the director field, where the boundary layer is determined by the competition of the forces related to the static coupling A_1 and the Frank elastic forces.

The quantity that is normally measured is the effective viscosity of the sheared sample, i.e., the shear force per unit area σ_{xz} exerted by the fluid on the glass plate divided by the shear rate Γ_x . In the present system, one must, however, take into account that the Maxwell stress $-B_j H_i$, unlike all the other contributions to the stress tensor, does not end at the boundary of the fluid as the magnetic flux continues into the glass plate. Consequently, the Maxwell stress does not contribute to the

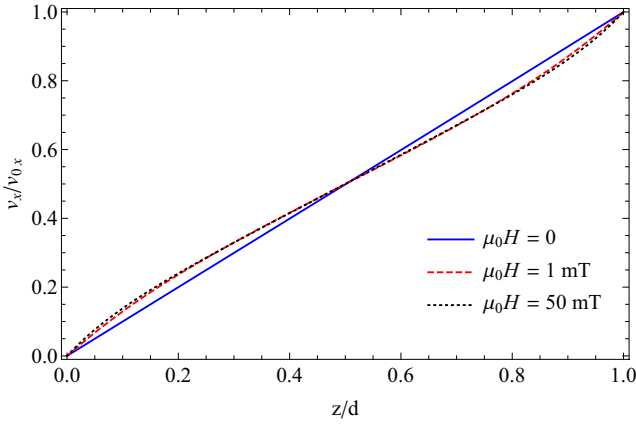


FIG. 3. The normalized x component of the velocity field v_x/v_{0x} for different values of the applied magnetic field at a shear rate $\Gamma_x = 1 \text{ s}^{-1}$.

force on the glass plate. This is best seen by calculating the force as the integral of σ_{xz} over a pair of planes tightly enclosing the $z = d$ interface. In the resulting difference of shear stresses across the interface, $[\sigma_{xz}]$, all contributions to $\sigma_{xz}(z = d)$ are recovered as usual, except the term $-B_j H_i$ of Eq. (6), which cancels out. The effective viscosity is thus

$$\nu^{\text{eff}} = \frac{[\sigma_{xz}]}{\Gamma_x}. \quad (30)$$

In Fig. 4, the effective viscosity is plotted as a function of the magnetic field for two values of the shear rate Γ_x , which are equal in magnitude but opposite in sign.

Most strikingly, a rather large increase in the effective viscosity by about a factor of 2 can be achieved by applying a rather small magnetic field of about 20 mT; see Fig. 4(a). The reason the effective viscosity increases at very low fields is due to the response of the magnetization and the director field in an external magnetic field, which was studied in detail in Ref. [26]. There it was shown analytically that the configuration of the system, i.e., the director and the magnetization field, saturates quickly above a characteristic magnetic field determined by the static coupling, $\mu_0 H \sim A_1 M_0$, which for the parameters used here is approximately 10 mT. The viscosity increases as \mathbf{n} and \mathbf{M} rotate toward getting perpendicular to the velocity field and lying within the shear plane. This opens the door to an easily accessible viscosity control for a nematic fluid system by using small magnetic fields.

In addition, we see that—just as the absolute value of the vertical component of the director—also the effective viscosity is invariant with respect to the transformation $\Gamma_x \rightarrow -\Gamma_x$, $\mu_0 H \rightarrow -\mu_0 H$.

As we increase the magnetic field, we see that the effective viscosity first saturates at fairly low magnetic fields of order 30 mT, Fig. 4(a). A similar effect has been observed in experiments using 8CB [35]. There, a rather complex shear geometry was used, therefore the experimental results cannot be mapped in a straightforward manner onto the results presented here.

It should be noted that we take into account also the diamagnetic contribution, $-\frac{1}{2}\mu_0\chi_a(\mathbf{n} \cdot \mathbf{H})^2$, with a diamagnetic anisotropy, $\chi_a = 5 \times 10^{-6}$. For small magnetic fields, Fig. 4(a),

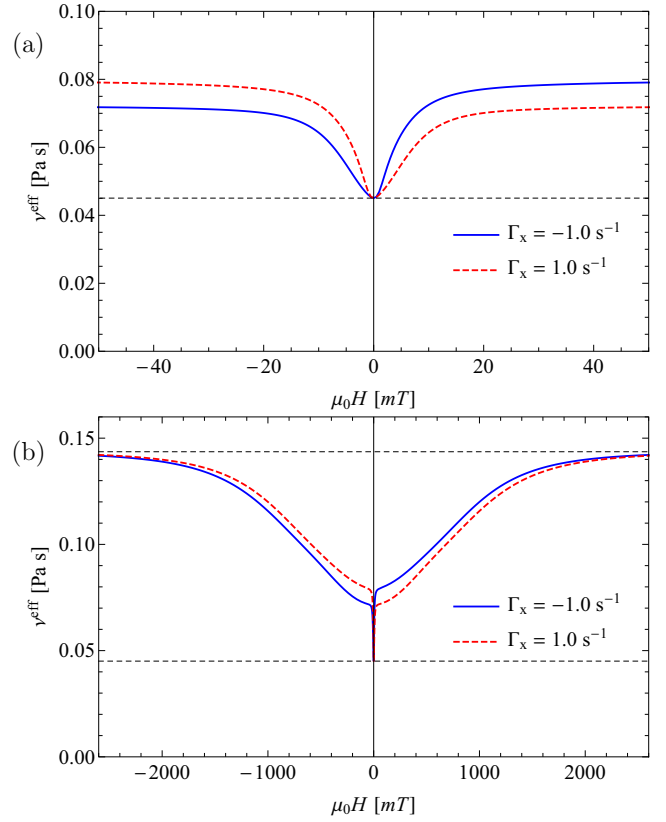


FIG. 4. The behavior of the effective viscosity for (a) small and (b) large values of the applied magnetic field at oppositely equal shear rates. The dashed lines represent two of the Miesowicz viscosities (η_{xx} and η_{zz}), defined in Sec. IV.

the effects of this term are very small, which is verified by comparing the numerical results with $\chi_a = 0$. On the other hand, if we increase the magnetic field further, the viscosity starts to increase again; see Fig. 4(b). This is due to the diamagnetic anisotropy, which tries to align the director along the external magnetic field. The viscosity finally saturates at fields of order 1 T, where the director field along with the magnetization field point approximately along the applied magnetic field. In the limit of large magnetic fields, the director and the magnetization both point along z and, therefore, the effective viscosity converges to one of the Miesowicz viscosities, η_{zz} [dashed line in Fig. 4(b)], defined and calculated in Sec. IV. In the absence of the magnetic field, the director and the magnetization point approximately along the x axis, which means the effective viscosity approaches the value of another Miesowicz viscosity, η_{xx} [dashed line in Fig. 4(a)]. The behavior at larger magnetic fields is a prediction, which can be experimentally tested.

In Fig. 4 one also observes that the effective viscosity strongly increases when one increases the magnetic field from the intermediate saturation region at 50 mT to a large magnetic field of order of 1 T. A possible explanation for such a dramatic increase can be deduced from Fig. 5, where we present the profiles of the fields v_x/v_{0x} , M_z/M_0 , and n_z at these two magnetic fields. For the lower magnetic field, Fig. 5(a), the boundary layer ξ^l of n_z is of order of 10% of the cell thickness,

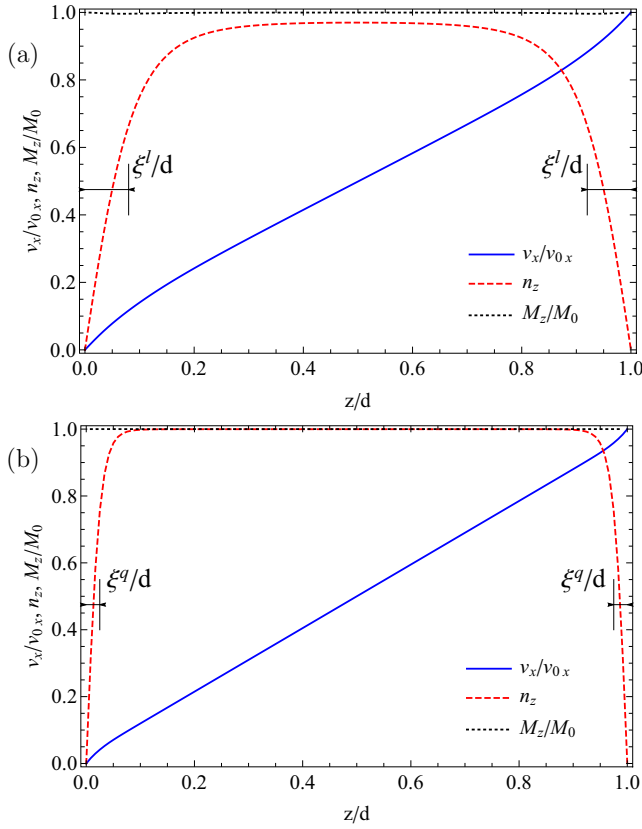


FIG. 5. Profiles of v_x/v_{0x} , M_z/M_0 , and n_z at a shear rate $\Gamma_x = 1 \text{ s}^{-1}$ with (a) $\mu_0 H = 50 \text{ mT}$ and (b) $\mu_0 H = 1 \text{ T}$. The boundary layers for (a) the lower magnetic field, ξ^l , and (b) the higher magnetic field, ξ^q , can be estimated from Eqs. (31) and (32), respectively.

which can be estimated from the parameter q of Eq. (39), discussed in the next subsection:

$$\frac{\xi^l}{d} \sim \sqrt{\frac{K}{A_1 M_0^2 d^2}} \approx 0.1. \quad (31)$$

In the large magnetic-field limit, the diamagnetic energy term is dominant. Equating the typical Frank elastic energy with the typical diamagnetic energy gives us a boundary layer ξ^q of 2% of the cell thickness:

$$\frac{\xi^q}{d} \sim \sqrt{\frac{K}{\mu_0 \chi_a H^2 d^2}} \approx 0.02. \quad (32)$$

Smaller boundary layers for the director field mean stronger elastic forces close to the boundaries. These forces increase the shear stress and therefore also the effective viscosity.

It should be noted that a crossover from a ferromagnetic response linear in H , for small fields, to a regime quadratic in H , for large fields, has also been observed in uniaxial magnetic gels [36], a class of soft matter systems that also shows rich macroscopic behavior [37].

A. Small shear rate behavior

For small shear rates, n_z increases linearly as we increase the shear rate. This can be shown analytically by first assuming that

the velocity profile is linear, i.e., $\mathbf{v} = \Gamma_x z \hat{\mathbf{e}}_x$. We furthermore discard the dissipative cross-couplings between the velocity field and the director or the magnetization, described by the tensors λ_{ijk}^D and c_{ijk}^D , Eqs. (17) and (18). Consequently, there are no terms in the dynamic equations (4) and (3) that couple the thermodynamic forces to the currents in the y direction. The fields thus stay within the shear (xz) plane,

$$\begin{aligned} \mathbf{n} &= \cos \theta \hat{\mathbf{e}}_x + \sin \theta \hat{\mathbf{e}}_z, \\ \mathbf{M}/M_0 &= \cos \psi \hat{\mathbf{e}}_x + \sin \psi \hat{\mathbf{e}}_z. \end{aligned} \quad (33)$$

The dynamic equations for the angles θ and ψ then read

$$\begin{aligned} \frac{\partial \theta}{\partial t} &= -\frac{1}{2} \Gamma_x [1 - \lambda \cos(2\theta)] + \frac{K}{\gamma_1} \frac{\partial^2 \theta}{\partial z^2} \\ &\quad - \frac{A_1 M_0^2}{8} (\chi_1^D + \chi_2^D) \sin[4(\psi - \theta)] \\ &\quad + \mu_0 H M_0 [\chi_2^D \cos^2(\psi - \theta) - \chi_1^D \sin^2(\psi - \theta)] \cos \psi \\ &\quad + \frac{A_1 M_0^2}{4} \left(\frac{2}{\gamma_1} + \chi_1^D - \chi_2^D \right) \sin[2(\psi - \theta)], \quad (34) \\ \frac{\partial \psi}{\partial t} &= -\frac{1}{2} \Gamma_x [1 - 2c_2^R \cos(2\psi)] + \frac{b_{\perp}^D}{M_0^2} \mu_0 H M_0 \cos \psi \\ &\quad + \frac{1}{2} \{ (\chi_1^D + \chi_2^D) \cos[2(\psi - \theta)] - \chi_1^D + \chi_2^D \} K \frac{\partial^2 \theta}{\partial z^2} \\ &\quad + \frac{A_1 M_0^2}{8} (\chi_1^D + \chi_2^D) \sin[4(\psi - \theta)] \\ &\quad - \frac{A_1 M_0^2}{4} \left(\frac{2b_{\perp}^D}{M_0^2} + \chi_1^D - \chi_2^D \right) \sin[2(\psi - \theta)]. \quad (35) \end{aligned}$$

In the small-magnetic-field limit, we can use the small-angle approximation ($\theta, \psi \ll 1$). Setting the time derivatives $\partial \theta / \partial t$ and $\partial \psi / \partial t$ to zero, the solution for the angle θ reads

$$\begin{aligned} \theta(z) &= \frac{\Gamma_x}{4K \left(\frac{b_{\perp}^D}{\gamma_1 M_0^2} - (\chi_2^D)^2 \right)} \left[(\lambda - 1) \left(\chi_2^D - \frac{b_{\perp}^D}{M_0^2} \right) \right. \\ &\quad \left. - (2c_2^R - 1) \left(\frac{1}{\gamma_1} - \chi_2^D \right) \right] z(z - d) \\ &\quad - \frac{\mu_0 H M_0}{2K} z(z - d), \end{aligned} \quad (36)$$

from which one can see that for small magnetic fields and shear rates, n_z is linear in both of them. In the limit $\Gamma_x \rightarrow 0$, one obtains a solution in agreement with the one in Ref. [26]. It is interesting to note that for small shear rates and in the absence of the magnetic field, the angle can decrease as one increases the shear rate, provided that the following inequality is satisfied:

$$2c_2^R > 1 + (\lambda - 1) \frac{\chi_2^D - \frac{b_{\perp}^D}{M_0^2}}{\frac{1}{\gamma_1} - \chi_2^D}. \quad (37)$$

It is rather realistic that this inequality is satisfied using known and/or extracted values of the involved parameters.

In the large magnetic-field limit, the director and the magnetization point approximately along the z axis. The solution for the angles θ^+ (θ^-) for positive (negative) magnetic

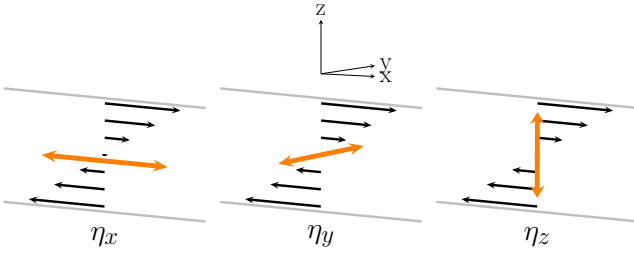


FIG. 6. Miesowicz viscosities in a usual nematic liquid crystal. The director field is indicated in orange.

fields is

$$\theta^\pm(z) = \pm \frac{\pi}{2} - C\Gamma_x \mp \left(\frac{\pi}{2} \mp C\Gamma_x \right) \frac{\cosh[q(z-d/2)]}{\cosh(qd/2)}, \quad (38)$$

where

$$q^2 = q_0^2 \frac{\mu_0 |H| M_0}{A_1 M_0^2 + \mu_0 |H| M_0}, \quad (39)$$

with $q_0 = \sqrt{A_1 M_0^2 / K}$, and C is a constant determined by the dynamic and the static parameters:

$$C = \frac{\gamma_1(1+\lambda)b_\perp^D + (1-d_2)M_0^2}{2\mu_0 |H| M_0 (b_\perp^D - [\chi_2^D]^2 \gamma_1 M_0^2)} + \frac{\gamma_1(1+\lambda)b_\perp^D - (1+2c_2^R)\chi_2^D \gamma_1 M_0^2}{2A_1 M_0^2 (b_\perp^D - [\chi_2^D]^2 \gamma_1 M_0^2)} \quad (40)$$

with the abbreviation $d_2 = 2c_2^R(\chi_2^D \gamma_1 - 1) + \chi_2^D \gamma_1(2 + \lambda)$. We point out that Eq. (38) correctly predicts the fact that the director can rotate by more than $\pi/2$ in the middle of the cell, as is observed in Fig. 2.

IV. MIESOWICZ VISCOSITIES

There exists a number of different ways one can measure viscosities of a nematic liquid crystal. The earliest technique and a particularly useful one is the concept of Miesowicz viscosities, where one fixes by an external magnetic or electric field the director and exposes the system to a shear flow [38,39]. Depending on the relative orientation of the director with respect to the velocity field or the shear plane, Fig. 6, there exist, for sufficiently high external fields, three limiting cases of the measured viscosities: η_x when $\mathbf{n} = \hat{\mathbf{e}}_x$, η_y when $\mathbf{n} = \hat{\mathbf{e}}_y$, and η_z when $\mathbf{n} = \hat{\mathbf{e}}_z$. The shear flow is applied in the xz plane. These Miesowicz viscosities are

$$\eta_x = v_3 + \frac{\gamma_1}{4}(\lambda - 1)^2, \quad (41)$$

$$\eta_y = v_2, \quad (42)$$

$$\eta_z = v_3 + \frac{\gamma_1}{4}(\lambda + 1)^2. \quad (43)$$

Below, we derive analogous viscosities for the ferromagnetic nematic liquid crystal. Since we have the additional variable of magnetization, not only are the expressions for the viscosities different but there are also more possible

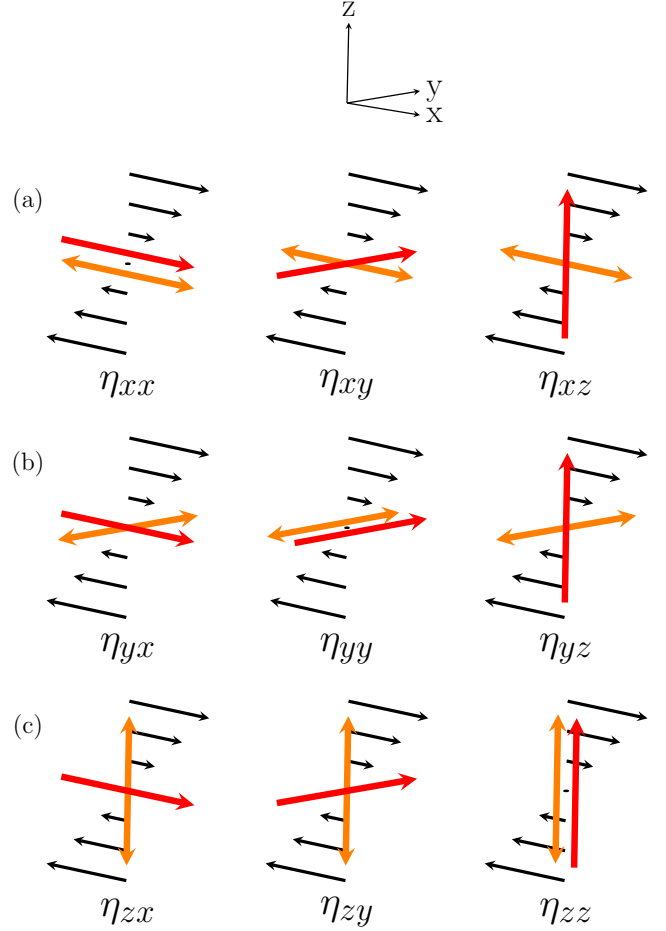


FIG. 7. Analogs of the Miesowicz viscosities in a ferromagnetic nematic liquid crystal, when the director (orange) is along the (a) x , (b) y , and (c) z axis. The magnetization is shown in red.

combinations. We will denote the analogous viscosities by $\eta_{\alpha\beta}$, where $\alpha, \beta \in \{x, y, z\}$ represent the fixed directions of the director and the magnetization, respectively.

A simple shear flow $v_x(z) = \Gamma_x z$, $v_y(z) = 0$, $v_z(z) = 0$ is imposed. The resulting nine independent possible configurations of the magnetization and the director are shown in Fig. 7.

To simplify the expressions, we have set, besides the tensors v_{ijkl}^R , $(\gamma_1^{-1})_{ij}^R$, b_{ij}^R , and χ^R , also the tensors λ_{ijk}^D and χ_1^D to zero, which is the same as in Sec. III, but here we keep c_{ijk}^D , Eq. (18). To derive the Miesowicz viscosities, one first sets the quasicurrents X_i and Y_i to zero. From this one obtains the thermodynamic forces h_i^n and h_i^M , Eqs. (9) and (8), as a function of the shear rate Γ_x . Finally, one uses the thermodynamic forces in the expression for the xz component of the total stress tensor σ_{xz} .

When the director is along the x axis, Fig. 7(a), the three independent viscosities are

$$\eta_{xx} = v_3 + \frac{1}{4} \left(1 - \frac{(\chi_2^D)^2 M_0^2 \gamma_1}{b_\perp^D} \right)^{-1} \left[\gamma_1(1-\lambda)^2 - 4(c^D)^2 + \frac{M_0^2}{b_\perp^D} (1-2c_2^R) [1-2c_2^R - 2\chi_2^D \gamma_1(1-\lambda)] \right], \quad (44)$$

$$\eta_{xy} = \nu_3 + \frac{\gamma_1}{4}(1 - \lambda)^2 - \frac{(c^D)^2}{b_{\perp}^D}, \quad (45)$$

$$\eta_{xz} = \nu_3 + \frac{\gamma_1}{4}(1 - \lambda)^2 - \frac{(c^D)^2}{b_{\perp}^D} + \frac{M_0^2(1 + 2c_2^R + 2c_5^R)^2}{4b_{\parallel}^D}. \quad (46)$$

When the director is along the y axis, Fig. 7(b), the three independent viscosities are

$$\eta_{yx} = \nu_2 + \frac{M_0^2(1 - 2c_2^R)^2}{4b_{\perp}^D}, \quad (47)$$

$$\eta_{yy} = \nu_2, \quad (48)$$

$$\eta_{yz} = \nu_2 + \frac{M_0^2(1 + 2c_2^R)^2}{4b_{\perp}^D}. \quad (49)$$

One can see that in the case in which the director and the magnetization are both perpendicular to the shear plane, the viscosity is $\eta_{yy} = \eta_y = \nu_2$, as in ordinary nematic liquid crystals.

When the director is along the z axis, Fig. 7(c), the viscosities are similar as in the case when the director is along the x axis. One can get the viscosities η_{zi} from η_{xi} by the transformation $\lambda \rightarrow -\lambda$, $c_2^R \rightarrow -c_2^R$, $c_5^R \rightarrow -c_5^R$, and $x \leftrightarrow z$. This can be explained by the fact that the contributions of λ , c_2^R , and c_5^R in the quasicurrents change sign as one rotates the director or the magnetization by 90° within the shear plane. We thus have

$$\eta_{zx} = \nu_3 + \frac{\gamma_1}{4}(1 + \lambda)^2 - \frac{(c^D)^2}{b_{\perp}^D} + \frac{M_0^2(1 - 2c_2^R - 2c_5^R)^2}{4b_{\parallel}^D}, \quad (50)$$

$$\eta_{zy} = \nu_3 + \frac{\gamma_1}{4}(1 + \lambda)^2 - \frac{(c^D)^2}{b_{\perp}^D}, \quad (51)$$

$$\eta_{zz} = \nu_3 + \frac{1}{4} \left(1 - \frac{(\chi_2^D)^2 M_0^2 \gamma_1}{b_{\perp}^D} \right)^{-1} \times \left[\gamma_1(1 + \lambda)^2 - 4(c^D)^2 + \frac{M_0^2}{b_{\perp}^D} (1 + 2c_2^R) [1 + 2c_2^R - 2\chi_2^D \gamma_1(1 + \lambda)] \right]. \quad (52)$$

We observe that the viscosities reduce to Miesowicz viscosities, Eqs. (41)–(43), in the limit $c^D \rightarrow 0$ and $M_0 \rightarrow 0$.

In Refs. [25,26], the value of the dissipative cross-coupling coefficient χ_2^D was shown to be large and thus it should strongly affect the values of the Miesowicz viscosities η_{xx} and η_{zz} as compared with the nematic analogs η_x and η_y .

One notices that the Miesowicz viscosities only contain the coefficients c_2^R and c_5^R of c_{ijk}^R . As discussed in Sec. III, for simple shear the coefficients c_3^R and c_4^R do not contribute. The coefficient c_1^R is irrelevant due to the fixed modulus M_0 . The contributions of c_6^R are zero in the chosen configurations, which is due to either the fixed modulus or the perpendicular orientations of the director and the magnetization.

We emphasize that important relations between the nine Miesowicz viscosities exist, e.g.,

$$\eta_{yz} - \eta_{yx} = \frac{M_0^2 c_2^R}{b_{\perp}^D}, \quad (53)$$

$$\eta_{zz} - \eta_{xx} = \frac{b_{\perp}^D \gamma_1 \lambda - [2c_2^R (\chi_2^D \gamma_1 - 1) + \chi_2^D \gamma_1 \lambda] M_0^2}{b_{\perp}^D - (\chi_2^D)^2 M_0^2 \gamma_1}, \quad (54)$$

$$\eta_{zx} - \eta_{xz} = \gamma_1 \lambda - \frac{M_0^2 (c_2^R + c_5^R)}{b_{\parallel}^D}, \quad (55)$$

which can be used to determine certain combinations of dynamic coefficients experimentally.

V. FLOW ALIGNMENT

In this section, we study the flow alignment in a ferromagnetic nematic. For usual uniaxial nematics, this is a well-known phenomenon, where under the influence of a simple shear flow the director is tilted by a finite angle with respect to the velocity field. In the case of uniaxial nematics, this angle is determined by the flow alignment parameter λ , which is a reversible transport coefficient and not associated with any dissipation. For biaxial nematics and for mixtures of uniaxial nematics, various aspects of flow alignment have also been addressed [40–44]. In ferromagnetic nematic liquid crystals, we have to take into account also the dynamics of the magnetization. This means that in simple shear flow, generally, the director and the magnetization are not parallel.

We investigate the case in which the shear flow is imposed with the external magnetic field pointing along the x axis, $\mathbf{H} = H \hat{\mathbf{e}}_x$, as opposed to the case in Sec. III in which the magnetic field points in z direction. This direction of the magnetic field is chosen to ensure that the director and the magnetization field are in the presence of a magnetic field homogeneous across the cell. The homogeneous response makes it convenient to analyze the ferromagnetic nematic flow alignment as a function of the applied magnetic field. The contribution of the Frank elastic term, Eq. (2), can thus be discarded. Generally, there exists a boundary layer with thickness

$$\xi^v \sim \sqrt{\frac{K}{\gamma_1 \Gamma_x}}, \quad (56)$$

which decreases with increasing shear rate. This boundary layer is defined by a competition between the viscous forces and the elastic forces. In the limit $\xi^v/d \ll 1$, the velocity profile is linear, $\mathbf{v} = \Gamma_x z \hat{\mathbf{e}}_x$. For the parameters used in this study, this limit can be achieved using shear rates $\Gamma_x \gg 0.03 \text{ s}^{-1}$. We remind the reader that two different boundary layers, corresponding to the deformation of the director field in a magnetic field, are defined in Sec. III, Eqs. (31) and (32). Since we discard the elastic forces, these boundary layers are zero.

As is done in Sec. III, we again discard the dissipative cross-couplings between the velocity field and the director or the magnetization, Eqs. (17) and (18). In this case, the director and the magnetization both stay in the shear (xz) plane and can be described by Eq. (33), as discussed in Sec. III.

The dynamic equations for the angles θ and ψ are then similar to those presented in Sec. III, Eqs. (34) and (35), with the difference being in the term describing the magnetic field

and in the absence of elastic forces:

$$\begin{aligned} \frac{\partial \theta}{\partial t} = & -\frac{1}{2}\Gamma_x[1 - \lambda \cos(2\theta)] - \frac{A_1 M_0^2}{8}\chi_2^D \sin[4(\psi - \theta)] \\ & - \chi_2^D \mu_0 H M_0 \cos^2(\psi - \theta) \sin(\psi) \\ & + \frac{A_1 M_0^2}{4}\left(\frac{2}{\gamma_1} - \chi_2^D\right) \sin[2(\psi - \theta)], \end{aligned} \quad (57)$$

$$\begin{aligned} \frac{\partial \psi}{\partial t} = & -\frac{1}{2}\Gamma_x[1 - 2c_2^R \cos(2\psi)] + \frac{A_1 M_0^2}{8}\chi_2^D \sin[4(\psi - \theta)] \\ & - \frac{b_\perp^D}{M_0^2} \mu_0 H M_0 \sin(\psi) \\ & - \frac{A_1 M_0^2}{4}\left(\frac{2b_\perp^D}{M_0^2} - \chi_2^D\right) \sin[2(\psi - \theta)], \end{aligned} \quad (58)$$

where, for simplicity, c_2^R is taken as a representative of c_{ijk}^R , and χ_1^D is set to zero. A stationary solution exists if $\partial\theta/\partial t = 0$ and $\partial\psi/\partial t = 0$.

In the limit of large shear rates ($\Gamma_x \gg \frac{A_1 M_0^2}{\gamma_1}$) and in zero magnetic field, we obtain

$$\cos(2\theta) = \frac{1}{\lambda}, \quad (59)$$

$$\cos(2\psi) = \frac{1}{2c_2^R}. \quad (60)$$

The solutions of Eqs. (59) and (60) are $\theta = \pm \frac{1}{2} \arccos(1/\lambda)$ and $\psi = \pm \frac{1}{2} \arccos(1/2c_2^R)$. A linear stability analysis of Eqs. (57) and (58) has been done, where the angles are perturbed from their stationary values θ_0 and ψ_0 , i.e., $\theta = \theta_0 + \delta\theta$ and $\psi = \psi_0 + \delta\psi$. We find that for positive (negative) shear rates, the positive (negative) angle is the stable solution.

In the large magnetic-field limit, $\frac{b_\perp^D}{M_0^2} \mu_0 H M_0 \gg \frac{A_1 M_0^2}{\gamma_1}$, while still assuming that the effects of the diamagnetic anisotropy are negligible, stationary solutions ψ^\pm for the magnetization angle are

$$\sin \psi^\pm = -\frac{\Gamma_x^H}{\Gamma_x} \pm \sqrt{\left(\frac{\Gamma_x^H}{\Gamma_x}\right)^2 + \frac{2c_2^R - 1}{4c_2^R}}, \quad (61)$$

where

$$\Gamma_x^H = \frac{b_\perp^D}{4c_2^R M_0^2} \mu_0 H M_0 \quad (62)$$

is the characteristic ‘‘magnetic’’ shear rate determined by the magnetic field.

It has not been possible to make the analytical solution for the angle θ tractable. We thus only present the asymptotic behavior of this angle and for completeness also the asymptotic behavior of the angle ψ . From Eq. (61) one can see that in the limit $\Gamma_x/\Gamma_x^H \ll 1$ one finds, to first order,

$$\psi^+ = \frac{2c_2^R - 1}{8c_2^R} \frac{\Gamma_x}{\Gamma_x^H}, \quad (63)$$

$$\begin{aligned} \tan \theta^+ = & \sqrt{\frac{b_\perp^D(\lambda - 1) - (2c_2^R - 1)\chi_2^D M_0^2}{b_\perp^D(1 + \lambda)}} \\ & - \frac{(2c_2^R - 1)^2 \chi_2^D M_0^2}{8b_\perp^D c_2^R (1 + \lambda)} \frac{\Gamma_x}{\Gamma_x^H}, \end{aligned} \quad (64)$$

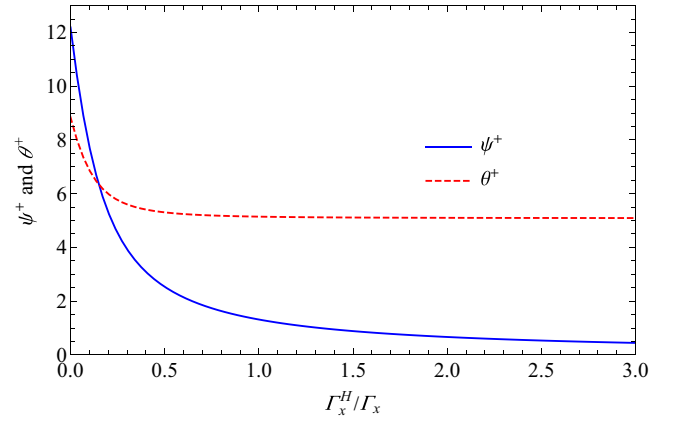


FIG. 8. The theoretical dependence of the magnetization ψ^+ (blue curve) and director θ^+ (red dashed curve) angles in degrees as functions of the dimensionless ratio of the characteristic magnetic shear rate [Eq. (62)] and the applied shear rate, Γ_x^H/Γ_x .

while ψ^- does not exist and $\tan \theta^+$ is calculated by inserting the solution for the angle ψ^+ from Eq. (61) into Eq. (57). It is tractable to perform a linear stability analysis of the solution Eq. (58) analytically, finding the stability condition

$$\pm c_2^R \Gamma_x \sqrt{\left(\frac{\Gamma_x^H}{\Gamma_x}\right)^2 + \frac{2c_2^R - 1}{4c_2^R}} > 0, \quad (65)$$

where the sign \pm corresponds to the solutions ψ^\pm . From Eq. (65) we see that the solution ψ^+ (ψ^-) is stable if the product $c_2^R \Gamma_x$ is positive (negative).

In Fig. 8 we present the numerical solutions of Eqs. (57) and (58) for the angles ψ^+ and θ^+ as functions of Γ_x^H/Γ_x . As predicted in Eqs. (63) and (64), we see that the angle ψ^+ decreases to zero, while the angle θ^+ saturates at a finite value as the field is increased.

In the absence of the magnetic field and in the large shear rate limit, the stationary solution exists if $|\lambda| \geq 1$ and $|c_2^R| \geq \frac{1}{2}$. In usual nematic liquid crystals, if $|\lambda| < 1$ holds, the system shows a tumbling behavior. In such a system flow alignment can be recovered if a sufficiently large electric field is applied; see Refs. [45,46]. In our system, this could be achieved with the use of low magnetic fields.

To check this possibility, one must first ensure the existence of the solutions Eq. (61). Secondly, we are only interested in the stable solutions, i.e., Eq. (65) must hold. We find that the required magnetic field depends on four different ranges of the c_2^R values:

$$c_2^R < 0, \quad \pm \Gamma_x < 0, \quad \frac{\Gamma_x^H}{\Gamma_x} > \mp \frac{1 + 2c_2^R}{8c_2^R}, \quad (66)$$

$$0 < c_2^R < \frac{1}{6}, \quad \pm \Gamma_x > 0, \quad \frac{\Gamma_x^H}{\Gamma_x} > \pm \frac{1 + 2c_2^R}{8c_2^R}, \quad (67)$$

$$\frac{1}{6} < c_2^R < \frac{1}{2}, \quad \pm \Gamma_x > 0, \quad \frac{\Gamma_x^H}{\Gamma_x} > \pm \sqrt{\frac{1 - 2c_2^R}{4c_2^R}}, \quad (68)$$

$$c_2^R > \frac{1}{2}, \quad \pm \Gamma_x > 0, \quad \frac{\Gamma_x^H}{\Gamma_x} > \mp \frac{1 + 2c_2^R}{8c_2^R}, \quad (69)$$

where the signs \pm correspond to the two solutions Eq. (61).

Another stationary solution of the dynamic equations is found when the director is in the shear plane, while the magnetization is perpendicular to this plane,

$$\mathbf{n} = \cos \theta \hat{\mathbf{e}}_x + \sin \theta \hat{\mathbf{e}}_z, \quad (70)$$

$$\mathbf{M} = M_0 \hat{\mathbf{e}}_y. \quad (71)$$

In this case, we do not discard any dynamic coefficients. The solution for the angle θ is

$$\tan(\theta) = \frac{\lambda_{\text{eff}}^D M_0}{\lambda + 1} \pm \sqrt{\left(\frac{\lambda_{\text{eff}}^D M_0}{\lambda + 1}\right)^2 + \frac{\lambda - 1}{\lambda + 1}}, \quad (72)$$

where $\lambda_{\text{eff}}^D = 2\lambda_1^D + 2\lambda_2^D - \lambda_5^D + \lambda_6^D$. A solution exists if the term under the square root is positive, leading to the condition

$$\lambda^2 \geq 1 - (\lambda_{\text{eff}}^D M_0)^2. \quad (73)$$

This means that one can observe flow alignment in a ferromagnetic nematic, even if the pure nematic solvent shows tumbling behavior.

We investigated the stability of the solution Eq. (72) numerically. We find that it is stable in the absence of a magnetic field if the static coupling (A_1) between the director and the magnetization is negative, because in that case $\mathbf{n} \perp \mathbf{M}$ is the equilibrium orientation. For a positive A_1 , even the slightest perturbation in the magnetization field drives the director toward it, since it is favorable for them to be parallel rather than perpendicular. The solution Eq. (72) can nevertheless be made stable for ferromagnetic nematics with positive A_1 , provided one uses a large magnetic field in the y direction and the diamagnetic anisotropy χ_a is negative. This is to ensure that the director stays within the shear plane and the magnetization is perpendicular to it.

The case discussed above, in which the magnetization is perpendicular to the shear plane and the director is in the shear plane at an angle θ with respect to the velocity field, most closely resembles one of the possible stationary solutions of a biaxial nematic liquid crystal exposed to a shear flow; see Ref. [43]. In the latter system, the angle of one of the preferred directions with respect to the velocity field is given by the reversible coupling of the corresponding variable to the velocity field. In contrast, in ferromagnetic nematic liquid crystals this angle is determined by both the reversible and the dissipative coupling of the director to the velocity field.

VI. SWITCH-ON DYNAMICS

In this section, we study the reorientation of the director and the magnetization in an external magnetic field applied perpendicularly to the glass plates, $\mathbf{H} = H \hat{\mathbf{e}}_z$. We are particularly interested in the influence of flow on this transient dynamics. Unlike in the previous sections, flow is not externally imposed, but is generated by the reorientation dynamics itself, i.e., by backflow. Throughout this section, the dissipative cross-coupling between the magnetization and the velocity c_{ijk}^D , Eq. (18), is set to zero.

As a first step, we take into account only the reversible cross-coupling λ_{ijk} between the director and the velocity, Eqs. (20)–(22), while the analog cross-coupling c_{ijk}^R between

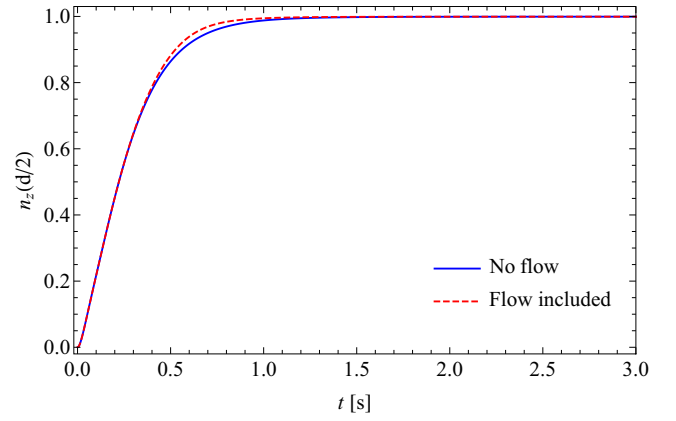


FIG. 9. The theoretical time dependence of n_z in the middle of the cell, for the cases with and without inclusion of flow, $\mu_0 H = 5$ mT. In the former case, only the flow alignment tensor λ_{ijk} and the viscous tensor v_{ijkl}^D are taken into account in the dynamics.

the magnetization and the velocity, Eqs. (19), (21), and (23), is set to zero. Figure 9 shows the time dependence of n_z in the midplane of the cell ($z = \frac{d}{2}$). A comparison is made between cases with and without inclusion of flow. We find that the influence of the reversible director–flow coupling is small and makes the transient dynamics a little faster; see Fig. 9. This has also been readily encountered in usual nematic liquid crystals [28,29]. We find furthermore that a strong dissipative cross-coupling between the director and the magnetization makes these backflow effects even less visible. To isolate them, we have set the tensor χ_{ij}^D , Eq. (14), to zero.

When the term c_2^R of the cross-coupling c_{ijk}^R , Eq. (23), is included in addition to λ_{ijk} , the backflow effects are similar, i.e., the dynamics is only slightly faster. This is not surprising, since the tensor λ_{ijk} and the term c_2^R have a similar form.

On the other hand, we find that the dissipative cross-coupling between the director and the velocity λ_{ijk}^D , Eq. (17), which is absent in usual nematics, can have a somewhat larger influence, Fig. 10. In our numerical calculations, we used the coefficient λ_3^D as the representative of the tensor λ_{ijk}^D , i.e., $\lambda_{ijk}^D = \lambda_3^D (\epsilon_{ipk} M_j n_p + \epsilon_{ipj} M_k n_p)$.

The reason for this choice is that at $t = 0$, when both \mathbf{n} and \mathbf{M} are parallel and within the xz plane, λ_3^D provides a nonzero contribution to the director quasicurrent component Y_y . The same is true for the coefficients λ_1^D and λ_4^D , while the initial contributions of λ_2^D , λ_5^D , and λ_6^D are zero. It should be noted that, due to the additional dissipative cross-coupling λ_{ijk}^D , the velocity field has a general orientation somewhere in the xy plane and hence \mathbf{n} and \mathbf{M} wander out of the xz plane, Fig. 10(b). This is in contrast to the case in Sec. III, where the velocity points along the x direction throughout the cell, and \mathbf{n} and \mathbf{M} stay in the shear plane.

The v_x and v_y profiles at four different moments are presented in Fig. 11 in terms of the Ericksen number, defined as the ratio of viscous and elastic forces on the director,

$$\text{Er}_i = \frac{\gamma_1 v_i d}{K}, \quad (74)$$

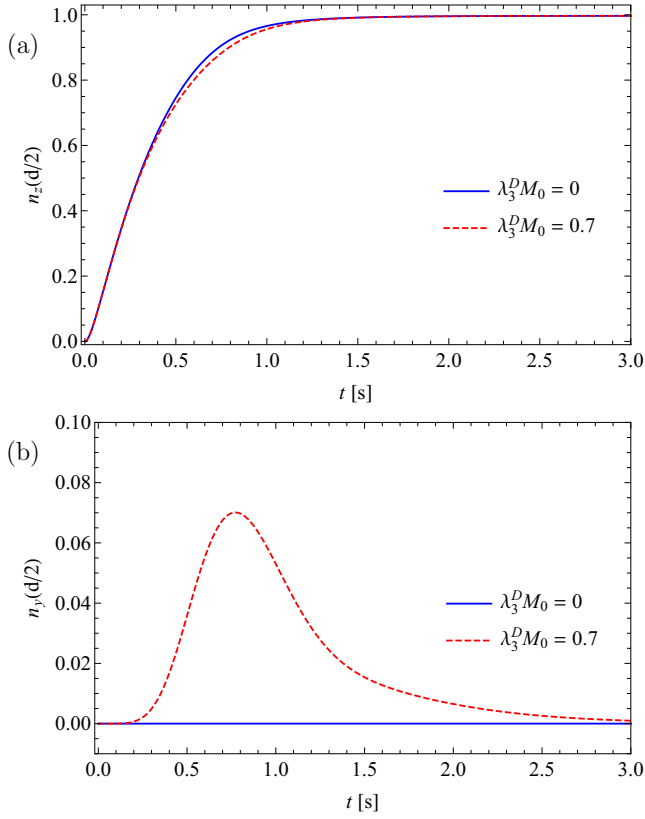


FIG. 10. The theoretical time dependence of the (a) z and (b) y component of the director field at $\mu_0 H = 5$ mT for two different values of λ_3^D .

with i corresponding to either the x or y velocity component. For the chosen value of λ_3^D , the maximum values in both directions are comparable, $Er_x \sim Er_y \sim 2$.

It should be noted that the values of the dissipative cross-coupling coefficients are fundamentally restricted by the positivity of the entropy production. In our case (zero χ_1^D , χ_2^D ,

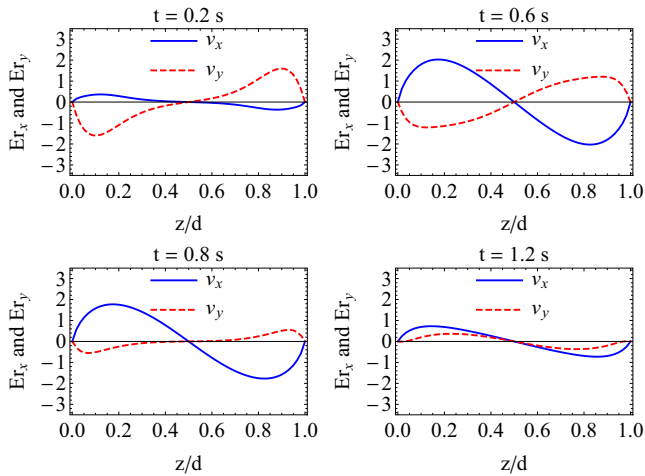


FIG. 11. Backflow profiles in terms of the Ericksen numbers Er_x and Er_y , Eq. (74), at four moments of time; $\mu_0 H = 5$ mT, $\lambda_3^D M_0 = 0.7$.

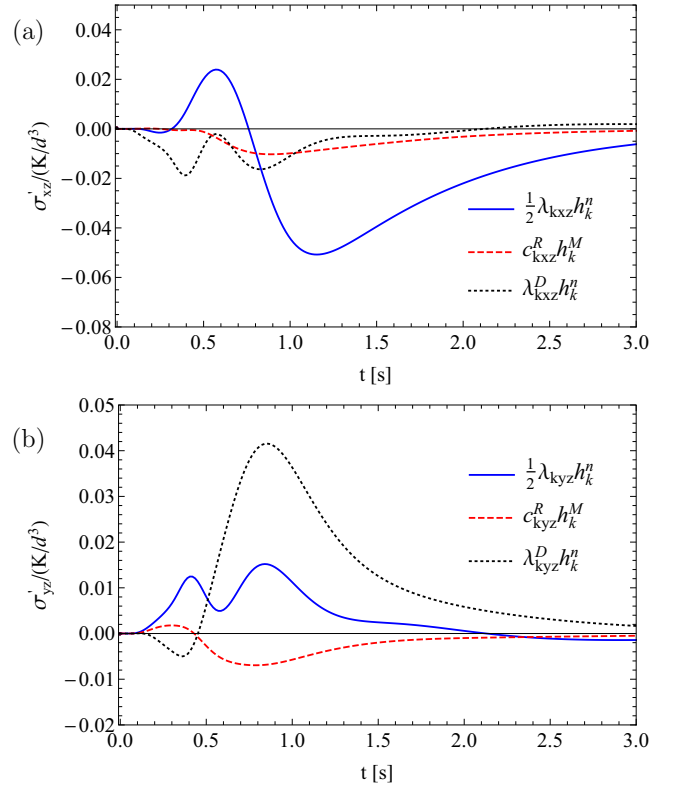


FIG. 12. The x and y components of the stress tensor divergence (a) $\sigma'_{xz} = \partial\sigma_{xz}/\partial z$ and (b) $\sigma'_{yz} = \partial\sigma_{yz}/\partial z$, at $z = d/2$, in units of characteristic divergence of the elastic stress K/d^3 for each of the three different backflow-driving stress tensor contributions explained in the text.

and c^D), the restriction is

$$|\lambda_3^D M_0| \leq \sqrt{\frac{v_3}{\gamma_1}} \sim 0.75, \quad (75)$$

where v_3 is chosen as the representative of the tensor v_{ijkl} .

We are interested in the importance of specific contributions to components σ_{xz} and σ_{yz} of the stress tensor. These are the usual nematic backflow-driving stress $\frac{1}{2}\lambda_{kij}h_k^n$, the analogous stress corresponding to the dynamics of the magnetization, $c_{kij}^R h_k^M$, and the stress from the dissipative director-velocity cross-coupling, $\lambda_{kij}^D h_k^n$. The divergence of these stresses has nonzero x and y components that are individually presented in Fig. 12.

We first analyze the σ_{xz} component, Fig. 12(a). The contributions of $c_{kxz}^R h_k^M$ and $\lambda_{kxz}^D h_k^n$ are smaller than those of $\frac{1}{2}\lambda_{kxz}h_k^n$. This can be explained by two facts. First, at any moment the director field is much more deformed than the magnetization field, which means that the thermodynamic force h_i^n , Eq. (9), will have a much bigger impact on the divergence of the stress than the thermodynamic force h_i^M , Eq. (8). This automatically explains that the backflow from the director field $\frac{1}{2}\lambda_{kxz}h_k^n$ is bigger than that from the magnetization $c_{kxz}^R h_k^M$. Secondly, the contribution $\lambda_{kxz}^D h_k^n$ is proportional to $\lambda_3^D n_y M_z h_z^n$. Since n_y is never large [Fig. 10(b)], neither is the contribution of $\lambda_{kxz}^D h_k^n$.

The situation is different for the σ_{yz} component. Figure 12(b) reveals that the contribution of $\lambda_{kyz}^D h_k^n$ is the biggest. This can be explained by writing its leading term as $\lambda_3^D n_x M_z h_z^n$, which does not contain n_y . The leading terms of the backflow contributions, $\frac{1}{2}\lambda_{kyz} h_k^n$ and $c_{kyz}^R h_k^n$, are smaller in comparison, since they are always proportional to either n_y and M_y , or to h_y^n and h_y^M .

Next, we are interested in the magnitude of the flow generated when a magnetic field is applied perpendicularly to the plates in one case and a voltage difference is applied across the plates in the other case. The magnitude of the flow is measured using the Ericksen number Er_x , Eq. (74), which we have calculated using the maximum magnitude of the velocity across the cell. We find that $Er_x \sim 1$ can be achieved using either a rather small magnetic field of 3 mT or a voltage difference of 2.5 V.

We conclude this section by pointing out that there are no effects of flow on the initial dynamics, at least up to first order in time. This can be shown by expanding the currents in Eqs. (3)–(5). Since the initial thermodynamic forces h_i^n and h_i^M are homogeneous, the generated stress σ_{ij} in Eq. (5) is also homogeneous. Its divergence, which generates flow, is thus absent initially. Consequently, Eqs. (3) and (5) are initially also unaffected by flow. It is the dissipative cross-coupling coefficient χ_2^D between the director and the magnetization that gives a linear time dependence of n_z , as was shown in Ref. [25] and discussed in Ref. [26].

VII. CONCLUSIONS AND PERSPECTIVE

In this paper, we have analyzed the consequences of some simple flows on various configurations of ferromagnetic nematic liquid crystals. These flows include simple shear flow, the determination of transport coefficients in the spirit of Miesowicz, and the analog of flow alignment for ferromagnetic nematics.

For the case of simple shear, we find that the effective viscosity can be increased by a factor of about 2 for rather small magnetic fields of about 20 mT. This effect can be tuned continuously in magnitude simply by varying the external magnetic field. For the determination of transport coefficients, we analyze the analog of the three Miesowicz configurations well-known from usual uniaxial nematics. Since one can fix the director and the direction of the spontaneous magnetization by external electric and magnetic fields, it is now possible to analyze nine independent different geometries. We find that these various geometries can be used to determine experimentally combinations of coefficients including dissipative and reversible terms characteristic of a system with a director, a magnetization, and a velocity field as macroscopic variables.

For the analog of flow alignment in usual uniaxial nematics, we find simple stationary solutions without an external magnetic field involving an orientation of both the director and the magnetization for the case in which both of these variables are in the shear plane in the limit of sufficiently large shear. In addition, we show that a small external magnetic field can shift the boundary between tumbling and flow alignment. For the case in which the magnetization \mathbf{M}_0 is perpendicular to the shear plane and the director \mathbf{n} is lying in the shear plane, we find for a range of parameters that a ferromagnetic nematic can

reveal flow alignment, although the nematic solvent by itself shows tumbling.

As a perspective, we point out that we are aware of only one experimental publication investigating the effect of flow on ferromagnetic nematics, namely the effects of shear flow in a rather complicated geometry [35]. These experimental results are compatible with our theoretical results in the sense that they show qualitatively similar behavior as a function of an external magnetic field and a viscosity enhancement effect of comparable magnitude. In a next step, it is highly desirable to compare experimental and theoretical results quantitatively for a simple and well-controlled geometry. There appear to be no experimental results available so far for the question of flow alignment and the evaluation of transport coefficients, parallel to the Miesowicz concept, for ferromagnetic nematics. Clearly, any experimental results in these two directions will stimulate refinement of the modeling of this exciting first liquid multiferroic system at room temperatures.

ACKNOWLEDGMENTS

Partial support of this work through the Schwerpunktprogramm SPP 1681 ‘‘Feldgesteuerte Partikel-Matrix-Wechselwirkungen: Erzeugung, skalenbergreifende Modellierung und Anwendung magnetischer Hybridmaterialien’’ of the Deutsche Forschungsgemeinschaft is gratefully acknowledged, as well as the support of the Slovenian Research Agency, Grants No. J1-7435 and No. J1-7441 (D.S.).

APPENDIX: LESLIE COEFFICIENTS

In the Ericksen-Leslie formulation of nematodynamics, a different set of coefficients is used. The Leslie coefficients are defined [1] by the symmetrized stress tensor

$$\sigma_{ij}^{\text{EL}} = \alpha_1 n_i n_j n_k n_p A_{kp} + (\alpha_2 + \alpha_3)(n_i N_j + n_j N_i) + \alpha_4 A_{ij} + (\alpha_5 + \alpha_6)(n_i n_k A_{jk} + n_j n_k A_{ik}), \quad (\text{A1})$$

and the molecular field

$$h_i^{\text{EL}} = \gamma_1 N_i + \gamma_2 n_j A_{ij}, \quad (\text{A2})$$

with $\gamma_2 = \alpha_3 + \alpha_2$ being a reversible transport parameter, not a viscosity. Here, the superscript EL denotes Ericksen-Leslie, $N_i = \partial n_i / \partial t - \omega_{ij} n_j$ is the corotational time derivative of the director—or rather its dissipative quasicurrent, $-Y_i^D$ [Eq. (4)], and $\omega_{ij} = \frac{1}{2}(\partial v_i / \partial x_j - \partial v_j / \partial x_i)$ is the vorticity tensor.

The set of Leslie coefficients is related to the coefficients of the tensor v_{ijkl}^D [33]:

$$\alpha_1 = 2(v_1 + v_2 - 2v_3) - \gamma_1 \lambda^2, \quad (\text{A3})$$

$$\alpha_2 + \alpha_3 = -\gamma_1 \lambda, \quad (\text{A4})$$

$$\alpha_4 = 2v_2, \quad (\text{A5})$$

$$\alpha_5 + \alpha_6 = 4(v_3 - v_2) + \gamma_1 \lambda^2. \quad (\text{A6})$$

The flow alignment parameter $\lambda = -\gamma_2 / \gamma_1$ is expressed as the ratio of reversible transport parameter γ_2 and the rotational viscosity γ_1 .

- [1] P. G. de Gennes and J. Prost, *The Physics of Liquid Crystals* (Clarendon Press, Oxford, 1995).
- [2] R. E. Rosensweig, *Ferrohydrodynamics* (Cambridge University Press, Cambridge, 1985).
- [3] S. Odenbach, *J. Phys.: Condens. Matter* **16**, R1135 (2004).
- [4] H.-W. Müller and M. Liu, *Phys. Rev. E* **64**, 061405 (2001).
- [5] B. Huke and M. Lücke, *Rep. Prog. Phys.* **67**, 1731 (2004).
- [6] P. Ilg, E. Coquelle, and S. Hess, *J. Phys.: Condens. Matter* **18**, S2757 (2006).
- [7] S. Mahle, P. Ilg, and M. Liu, *Phys. Rev. E* **77**, 016305 (2008).
- [8] S. D. Peroukidis and S. H. L. Klapp, *Phys. Rev. E* **92**, 010501 (2015).
- [9] F. Brochard and P. G. de Gennes, *J. Phys. (France)* **31**, 691 (1970).
- [10] A. Mertelj, D. Lisjak, M. Drogenik, and M. Čopič, *Nature (London)* **504**, 237 (2013).
- [11] A. Mertelj and D. Lisjak, *Liq. Cryst. Rev.* **5**, 1 (2017).
- [12] A. J. Leggett, *Rev. Mod. Phys.* **47**, 331 (1975).
- [13] J. C. Wheatley, *Rev. Mod. Phys.* **47**, 415 (1975).
- [14] R. Graham, *Phys. Rev. Lett.* **33**, 1431 (1974).
- [15] R. Graham and H. Pleiner, *Phys. Rev. Lett.* **34**, 792 (1975).
- [16] M. Liu, *Phys. Rev. Lett.* **43**, 1740 (1979).
- [17] H. Brand, M. Dorfle, and R. Graham, *Ann. Phys. (NY)* **119**, 434 (1979).
- [18] H. Brand and H. Pleiner, *J. Phys. (France)* **43**, 369 (1982).
- [19] Q. Zhang, P. J. Ackerman, Q. Liu, and I. I. Smalyukh, *Phys. Rev. Lett.* **115**, 097802 (2015).
- [20] P. J. Ackerman and I. I. Smalyukh, *Nat. Mater.* **16**, 426 (2017).
- [21] P. Medle Rupnik, D. Lisjak, M. Čopič, S. Čopar, and A. Mertelj, *Sci. Adv.* **3**, e1701336 (2017).
- [22] H. R. Brand, A. Fink, and H. Pleiner, *Eur. Phys. J. E* **38**, 65 (2015).
- [23] A. Mertelj, N. Osterman, D. Lisjak, and M. Čopič, *Soft Matter* **10**, 9065 (2014).
- [24] H. Pleiner, E. Jarkova, H.-W. Müller, and H. R. Brand, *Magnetohydrodynamics* **37**, 254 (2001).
- [25] T. Potisk, D. Svenšek, H. R. Brand, H. Pleiner, D. Lisjak, N. Osterman, and A. Mertelj, *Phys. Rev. Lett.* **119**, 097802 (2017).
- [26] T. Potisk, A. Mertelj, N. Sebastián, N. Osterman, D. Lisjak, H. R. Brand, H. Pleiner, and D. Svenšek, *Phys. Rev. E* **97**, 012701 (2018).
- [27] D. Forster, *Hydrodynamic Fluctuations, Broken Symmetries and Correlation Functions* (Benjamin, Reading, MA, 1995).
- [28] D. Svenšek and S. Žumer, *Liq. Cryst.* **28**, 1389 (2001).
- [29] D. Svenšek and S. Žumer, *Continuum Mech. Thermodyn.* **14**, 231 (2002).
- [30] J. Turk and D. Svenšek, *Phys. Rev. E* **89**, 032508 (2014).
- [31] E. Jarkova, H. Pleiner, H.-W. Müller, A. Fink, and H. R. Brand, *Eur. Phys. J. E* **5**, 583 (2001).
- [32] E. Jarkova, H. Pleiner, H.-W. Müller, and H. R. Brand, *J. Chem. Phys.* **118**, 2422 (2003).
- [33] H. Pleiner and H. R. Brand, in *Pattern Formation in Liquid Crystals*, edited by A. Buka and L. Kramer (Springer, New York, 1996).
- [34] L. M. Blinov and V. G. Chigrinov, *Electrooptic Effects in Liquid Crystal Materials* (Springer, New York, 1996).
- [35] R. Sahoo, M. V. Rasna, D. Lisjak, A. Mertelj, and S. Dahra, *Appl. Phys. Lett.* **106**, 161905 (2015).
- [36] D. Collin, G. K. Auernhammer, O. Gavot, P. Martinoty, and H. R. Brand, *Macromol. Rapid Commun.* **24**, 737 (2003).
- [37] S. Bohlius, H. R. Brand, and H. Pleiner, *Phys. Rev. E* **70**, 061411 (2004).
- [38] M. Miesowicz, *Nature (London)* **136**, 261 (1935).
- [39] M. Miesowicz, *Nature (London)* **158**, 27 (1946).
- [40] H. Brand and H. Pleiner, *Phys. Rev. A* **24**, 2777 (1981).
- [41] M. Liu, *Phys. Rev. A* **24**, 2720 (1981).
- [42] A. Saupe, *J. Chem. Phys.* **75**, 5118 (1981).
- [43] H. Brand and H. Pleiner, *J. Phys.* **43**, 853 (1982).
- [44] H. Pleiner and H. R. Brand, *J. Phys.* **46**, 615 (1985).
- [45] K. Skarp and T. Carlsson, *Mol. Cryst. Liq. Cryst.* **49**, 75 (1978).
- [46] T. Carlsson and K. Skarp, *Mol. Cryst. Liq. Cryst.* **78**, 157 (1981).

Publication 4

Dynamic interplay of nematic, magnetic, and tetrahedral order
in ferromagnetic nematic phases

T. Potisk, H. Pleiner, and H.R. Brand
Phys. Rev. E **98**, 042703 (2018).

Dynamic interplay of nematic, magnetic, and tetrahedral order in ferromagnetic nematic phasesTilen Potisk,^{1,*} Harald Pleiner,² and Helmut R. Brand¹¹*Department of Physics, University of Bayreuth, 95440 Bayreuth, Germany*²*Max Planck Institute for Polymer Research, 55021 Mainz, Germany*

(Received 30 August 2018; published 25 October 2018)

We consider the influence of tetrahedral (octupolar) order on ferromagnetic nematic liquid-crystalline phases. The presence of tetrahedral order leads to broken parity symmetry in an achiral liquid-crystalline system, in addition to broken time-reversal symmetry associated with the existence of a spontaneous magnetization. As a consequence, we find static as well as reversible and irreversible dynamic cross-coupling terms absent in usual ferromagnetic nematics. Several static and dynamic experiments are suggested to detect possible tetrahedral order. We predict that linear gradient terms in the generalized energy involving the ferromagnetic magnetization and the nematic director field lead to chiral domains of ambidextrous helicity. As a characteristic dissipative dynamic cross coupling we point out that the rotation of the magnetization can be driven by temperature and/or concentration gradients. Conversely, heat and concentration currents can be generated by rotations of the magnetization. As a characteristic example for reversible cross-coupling terms we analyze the consequences of the coupling between the molecular field of the nematic director and temperature and concentration gradients.

DOI: [10.1103/PhysRevE.98.042703](https://doi.org/10.1103/PhysRevE.98.042703)**I. INTRODUCTION**

Following the pioneering work of Fel [1,2] on tetrahedral (octupolar) order in liquid crystals the theoretical investigations of the physical consequences of this type of nonpolar order associated with broken parity symmetry focused on applications in liquid crystals: phase transitions [1,3–5], microscopic models, and phase diagrams [6–8] as well as the macroscopic properties of liquid-crystalline phases involving tetrahedral order [9–15]. Most of the experimental work on the question of tetrahedral order concentrated on the influence on phase transitions and on macroscopic properties of liquid-crystalline phases formed by bent-core molecules [16–28]. In addition, there were experimental reports indicating the presence of tetrahedral order in another class of compounds, namely, ferrocenomesogens [29,30]. Most of these observations and experimental results such as ambidextrous helicity and ambidextrous chirality [16,19,26] and unusual behavior near the isotropic–liquid-crystal phase transitions including shifts of the phase transition temperature by up to 10 K linear in electric fields, two optically isotropic phases in magnetic fields, and reentrant isotropic phases [17,18,20,23,25,27,28] could be interpreted successfully in terms of the occurrence of tetrahedral order [12,14,15,31,32]. In parallel, tetrahedral order has been incorporated into the dynamic description of movable and deformable active particles which are used as models for self-propelled microorganisms in biological applications [33–35]. Quite recently there is also growing interest in clarifying various mathematical aspects of tetrahedral order in two and three spatial dimensions [36–38]. Last year it has been pointed out [31] that the observed macroscopic chiral domains in optically isotropic, partially fluid systems [39–41]

can be interpreted naturally in terms of tetrahedral order provided a transient network is assumed. For a recent review of tetrahedral order in liquid crystals we refer to [32].

An important issue so far not considered is the influence of a magnetization on tetrahedral liquid-crystalline phases. This influence is interesting from a symmetry point of view, because the magnetization is odd under time reversal, and in a ferromagnet with a spontaneous magnetization the ground state breaks time-reversal symmetry.

In the magnetic domain of soft matter physics Brochard and de Gennes predicted in their seminal work [42], the existence of ferromagnetic nematics and ferromagnetic cholesterics in the domain of liquid crystals. Simultaneously, first experimental efforts along these lines started immediately [43], but they were not leading to ferromagnetic nematic phases, since suitably characterized and uniform magnetic nanoparticles did not exist in 1970. Only about five years ago the group around Lisjak and Mertelj reported the successful synthesis and characterization of a homogeneous phase of a truly ferromagnetic nematic [44]. This is of particular interest, since this material represents the first liquid multiferroic system at room temperature. In addition to the director characterizing spontaneously broken rotational symmetry, a truly ferromagnetic phase breaks time-reversal symmetry and rotational symmetry in spin space. Several synthetic and static investigations also involving the phase transition to the isotropic phase followed quickly [45–48]. Biaxial ferromagnetic nematics have also been reported quite recently [49]. An earlier Landau investigation of the phase transitions involved [50] could be used to interpret some of the experimental results [44]. Building on the macroscopic dynamic work of Jarkova *et al.* [51,52], the approach of macroscopic dynamics for truly ferromagnetic nematics has been used successfully recently to describe quantitatively dynamic experimental results [53,54] and to make further experimentally testable predictions [55]. For a

*tilen.potisk@uni-bayreuth.de

recent review on truly ferromagnetic nematics we refer to Ref. [56].

More recently, ferromagnetic cholesterics, for which a nematic containing chiral molecules has been used as the liquid-crystalline solvent, have been synthesized and characterized [57–59]. While ferromagnetic cholesterics turn out to have many different textures and defects depending on the ratio of cholesteric pitch and sample thickness, also simple textures could be obtained recently [59]. The latter observation will open the door to apply a recent macroscopic description of ferrocholesterics [60] to this rather complex system.

Our goal in the present paper is to analyze how to detect the possible presence of tetrahedral (octupolar) order in ferromagnetic nematics, a system composed of nonchiral molecules. We focus our investigations on macroscopic properties in the static as well as in the dynamic domain.

The paper is organized as follows. In Sec. II we give a Landau analysis and determine the macroscopic variables. In Sec. III we present the thermodynamics and the static properties of ferromagnetic nematics followed in Sec. IV by the derivation of the macroscopic dynamic equations. In Sec. V we make suggestions on how to detect the presence of tetrahedral order statically and dynamically followed by brief conclusions and a perspective.

II. LANDAU ENERGIES AND MACROSCOPIC VARIABLES

In this section we discuss the properties of a phase, for which one allows for the additional presence of a tetrahedral order parameter in a ferromagnetic nematic phase. We use a Landau energy approach to discuss the possible ground states. We then identify all macroscopic variables for a selected ground state.

A. Landau energy considerations

As variables in a Landau expansion we take into account, in addition to the magnetization, M_i , and the quadrupolar order parameter, Q_{ij} , the tetrahedral order parameter, T_{ijk} , a fully symmetric third-rank tensor [1]

$$T_{ijk} = T_0 \sum_{\zeta=1}^4 n_i^\zeta n_j^\zeta n_k^\zeta, \quad (1)$$

where the vectors \mathbf{n}^ζ ($\zeta = 1, 2, 3, 4$) span a tetrahedron and the order parameter T_0 describes the strength of the tetrahedral order. We assume the strength of the tetrahedral order, T_0 , as constant, which is a good approximation far away from a phase transition, where the tetrahedral order vanishes.

Tetrahedral order fully breaks rotational symmetry of isotropic space. However, in the absence of any orienting external field or boundary the actual orientation of the tetrahedron is arbitrary: Any homogeneous rotation of the tetrahedron leads to a distinct, but energetically identical equilibrium state. These are the three Goldstone modes that appear as (symmetry) variables in the hydrodynamic description. In that respect, tetrahedral order is analogous to the case of biaxial nematic liquid crystals [61,62].

The nematic (quadrupolar) order parameter is described by a symmetric traceless second-rank tensor $Q_{ij} = \frac{1}{2}S(3n_i n_j - \delta_{ij})$ [63]. The quantity S is a scalar order parameter, which describes the strength of the orientational ordering. It is zero in the isotropic phase, where the molecules are randomly oriented, while it is equal to 1 if on average all the molecules point in the same direction. The unit vector \mathbf{n} is the director field and describes the orientation of the nematic ordering. Without loss of generality one can assume $n_i n_i = 1$. It should be emphasized that due to the equivalence $\mathbf{n} \rightarrow -\mathbf{n}$ all of the equations should be invariant with respect to this transformation.

The Landau energy has, in addition to the terms already present in a magnetic tetrahedral phase [64], also the Landau energy expressions for a pure nematic phase and the various coupling terms between the magnetization, the quadrupolar, and the tetrahedral order parameters. These coupling terms read

$$F^C = F^{QM} + F^{QT} + F^{MT} + F^{QTM}, \quad (2)$$

with F^{QM} being the same as for the ferromagnetic nematic phase (see Ref. [50]):

$$F^{QM} = \frac{\gamma}{2} M_i M_j Q_{ij} + \frac{\delta_1}{2} M_k M_k Q_{ij} Q_{ji} + \frac{\delta_2}{2} M_i M_k Q_{ij} Q_{kj}. \quad (3)$$

The second term in Eq. (2) was investigated in Ref. [14]:

$$F^{QT} = d_1 Q_{il} Q_{jm} T_{ilk} T_{jmk} + \frac{d_2}{2} (Q_{im} Q_{jl} + Q_{ij} Q_{lm}) T_{ilk} T_{jmk}. \quad (4)$$

There it was found that if $d_1 + d_2 > 0$, the phase is of D_{2d} symmetry where the director points along one of the improper $\bar{4}$ axes, whereas if $d_1 + d_2 < 0$, the phase is of C_{3v} symmetry and the director points along one of the tetrahedral vectors. The cross-coupling terms between the magnetization, the quadrupolar, and the tetrahedral order parameters, F^{QTM} , are of quintic order:

$$F^{QTM} = c_1 Q_{il} M_j M_m T_{ilk} T_{jmk} + \frac{c_2}{2} (Q_{ij} M_m + Q_{im} M_j) M_l T_{ilk} T_{jmk}. \quad (5)$$

One can see the similarities of Eqs. (5) and (4). This is due to the fact that the free energy should be even in the magnetization to ensure invariance with respect to time-reversal symmetry.

As a first step we assume the director is fixed with respect to the tetrahedral structure and points along the z axis, $\mathbf{n} = \hat{\mathbf{e}}_z$. To find the orientation of \mathbf{M} in the ground state, we vary the azimuthal and the polar angle, defined by $\mathbf{M} = M_0(\cos \varphi \sin \psi, \sin \varphi \sin \psi, \cos \psi)$. There are five different solutions of the angles that correspond to a minimum of the free energy. The first solution is where the magnetization points along the director field $\mathbf{M} \parallel \mathbf{n}$.

Next, also the energy term coupling the magnetization and the tetrahedral order parameter enters the picture:

$$F^{MT} = a T_{ilk} T_{jmk} M_i M_l M_j M_m. \quad (6)$$

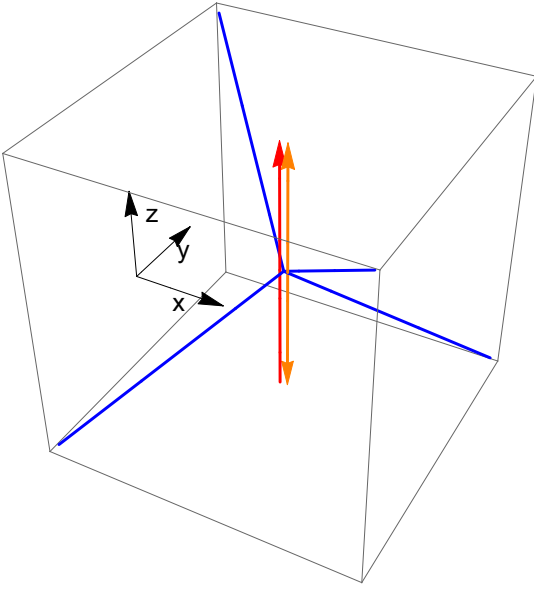


FIG. 1. The ground state of the system showing the magnetization (red) and the director (shown as a double-headed arrow in orange) along one of the improper $\bar{4}$ axes of the tetrahedron (blue).

Two of the other solutions correspond to the magnetization lying in the plane perpendicular to the director. One of these solutions is stable if $a > 0$ and the magnetization points along one of the other two improper $\bar{4}$ axes. The other solution is stable if $a < 0$ and the magnetization lies within one of the mirror planes. For the last two solutions the angle ψ depends on the value of coefficients in the expression for the free energy, Eq. (2).

In the following we focus on the solution where the director and the magnetization are parallel in the ground state as depicted in Fig. 1.

B. Macroscopic variables

To derive the macroscopic equations of a particular macroscopic system one must first identify the relevant macroscopic variables based on a specific ground state as input. In addition to the conserved variables characteristic of an isotropic fluid—the mass density ρ , the energy density ε , and the density of linear momentum \mathbf{g} —one must address the issue of variables associated with spontaneously broken continuous symmetries and of macroscopic variables, which relax on a long, but finite timescale [65–67].

Inspired by the experimental results available on ferromagnetic nematic liquid-crystalline phases [44–48,53,54,56], we will assume that in the ground state the director \mathbf{n} and the magnetization \mathbf{M} are parallel. In addition, we assume that $a > 0$ and that the magnetization points along one of the improper $\bar{4}$ axes of the tetrahedron. Thus the situation considered in the following is that of a nematic phase with D_{2d} symmetry [14] with an additional spontaneous magnetization parallel to the nematic director in the ground state.

Rotations of the tetrahedral structure can be described by a projection, $\delta\Gamma_i$, with [14]

$$\delta\Gamma_i = \frac{1}{4\tilde{\alpha}} \epsilon_{ipq} T_{pkl} \delta T_{qkl}, \quad (7)$$

where δT_{qkl} is the deviation of the tetrahedral order parameter from the equilibrium one, $\delta T_{qkl} = T_{qkl} - T_{qkl}^{\text{eq}}$. We use the normalization [14,32] $T_{ikl} T_{jkl} = \tilde{\alpha} \delta_{ij}$, with $\tilde{\alpha} = (32/27)T_0^2$. This relation can be inverted [14,32] to yield

$$\delta T_{qkl} = 2\epsilon_{ipq} T_{pkl} \delta\Gamma_i. \quad (8)$$

In this paper we focus on the importance and influence of tetrahedral order on a ferromagnetic nematic phase. The hydrodynamic orientational degrees of freedom associated with the director are characterized by the variations of the director field, δn_i , with $\delta n_i n_i = 0$. The magnetic order is due to the existence of a spontaneous magnetization, \mathbf{M} . It describes the strength of magnetic order by the order parameter $M \equiv |\mathbf{M}|$, and its orientation by the unit vector $\mathbf{m} = \mathbf{M}/M$. The former is neither connected to a Goldstone mode, nor to a conservation law, and therefore does not give rise to a genuine hydrodynamic variable. Nevertheless, its relaxation time can be large enough to be relevant in the hydrodynamic regime, and we will keep $\delta M \equiv M - M_0$, with M_0 the equilibrium magnetization, as a macroscopic variable.

Since we will assume a rigid coupling between the director, the tetrahedral order, and the magnetization in the ground state, we have as hydrodynamic variables the director variations δn_i and the quantity $\delta\Omega \equiv n_i \delta\Gamma_i$, with $\delta\Gamma_i$ given by Eq. (7), which describes a rotation of the tetrahedral structure about the equilibrium director and thus also about the magnetization in equilibrium. In addition, we have as macroscopic variables δm_i and δM .

III. THERMODYNAMICS AND STATIC PROPERTIES

To describe the statics of the tetrahedral ferromagnetic nematic phase we proceed along the same lines as for ferromagnets [51,52] and ferromagnetic nematics [53–55]. We use the conservation laws for density ρ , energy density ε , density of linear momentum \mathbf{g} , and particle concentration c . For the magnetic degrees of freedom we have the variation of the modulus δM and the variations of the magnetic unit vector \mathbf{m} , δm_i . In addition, we have the director degrees of freedom, δn_i . As discussed above there is now the additional variable $\delta\Omega$ describing rotations of the tetrahedral structure about the equilibrium director. To satisfy Maxwell's equations the magnetic induction \mathbf{B} must be considered as well.

Throughout this paper we assume local thermodynamic equilibrium. Changes of the macroscopic variables listed above are then related to changes of the total energy density via the Gibbs relation, which is the local formulation of the first law of thermodynamics:

$$\begin{aligned} df = & T d\sigma + \mu d\rho + v_i d g_i + \mu_c d c + h^M d M \\ & + h_i^m d m_i + \Psi_{ij}^m d \nabla_j m_i + h^\Omega d \Omega + \Psi_i^\Omega d \nabla_i \Omega \\ & + h_i^n d n_i + \Phi_{ij}^n d \nabla_j n_i. \end{aligned} \quad (9)$$

In Eq. (9), h_i^m , h^Ω , and h_i^n are the thermodynamic conjugate forces to m_i , Ω , and n_i and are given explicitly in Eqs. (37), (42), and (39).

In the static behavior only the combinations

$$\begin{aligned} h_i^M &= h_i^{M'} - \nabla_j \Psi_{ij}^M, \\ h_i^n &= h_i^{n'} - \nabla_j \Phi_{ij}^n, \quad \text{and} \\ h_i^\Omega &= h_i^{\Omega'} - \nabla_j \Psi_i^\Omega \end{aligned} \quad (10)$$

enter the picture. In addition, in the absence of boundaries or orienting fields, $h_i^{M'} = h_i^{n'} = h_i^{\Omega'} = 0$ to guarantee that changes in the orientation do not change the energy.

The thermodynamic conjugates are prefactors of the differentials in Eq. (9), i.e., temperature T , chemical potential μ , velocity v_i , osmotic pressure (divided by the pressure) μ_c , so-called molecular fields of the magnetic order h^M , of the magnetization rotations h_i^m , of rotations about the director h^Ω , and of director rotations h_i^n . They (or their gradients) act as thermodynamic forces in the dynamics (depending on whether they are zero or finite in equilibrium).

Rotational invariance leads, for Eq. (9), to the additional requirement

$$\begin{aligned} 0 &= \epsilon_{ijk} (h_i^m m_j + h_i^{n'} n_j + \Psi_i^\Omega \nabla_j \Omega + \Psi_{ii}^m \nabla_j m_l \\ &\quad + \Psi_{ii}^n \nabla_l m_j + \Phi_{ii}^n \nabla_j n_l + \Phi_{ii}^n \nabla_l n_j) - h^\Omega m_k, \end{aligned} \quad (11)$$

where the last term is due to the fact that Ω is not a scalar quantity and is not invariant under rotations. For details, cf. [14,64].

The material tensors will be constructed using the invariants n_i , $\delta_{ij}^{\perp n} = \delta_{ij} - n_i n_j$, ϵ_{ijk} , and T_{ijk} . The magnetization M_i does not define an extra, independent preferred direction, and will occur only when its specific time-reversal behavior is crucial. Since all material parameters can be arbitrary functions of M^2 , only linear contributions of M_i will explicitly show up in the material tensors. This is in the same spirit as for the case without tetrahedral order [51–54].

The thermodynamic conjugates are defined as partial derivatives of the total energy density with respect to the appropriate variable. Thus they follow from a total energy functional that can be written as

$$f = f_0 + f_{\text{el}} + f_M + f_{M\text{grad}} + f_{\text{lin}}, \quad (12)$$

where f_0 is the total energy of an isotropic liquid mixture; f_{el} contains the gradient terms associated with the director, the orientation of the magnetization, and with Ω ; f_M is the spatially homogeneous magnetic energy including external magnetic fields; and $f_{M\text{grad}}$ contains gradients of M while f_{lin} is linear in gradients.

When constructing the explicit forms of the various energy contributions one can make use of the totally antisymmetric symbol ϵ_{ijk} , the tetrahedral structure T_{ijk} , and the director n_i . One has to note that T_{ijk} is odd under spatial inversion and n_i is even under time reversal, while m_i is odd under time reversal. In particular, we find [67]

$$\begin{aligned} f_0 &= \frac{T}{2C_V} (\delta\sigma)^2 + \frac{1}{2\rho^2 \kappa_s} (\delta\rho)^2 + \frac{\gamma}{2} (\delta c)^2 + \frac{1}{\rho \alpha_s} (\delta\sigma)(\delta\rho) \\ &\quad + \beta_\sigma (\delta c)(\delta\sigma) + \beta_\rho (\delta c)(\delta\rho) + \frac{g_i^2}{2\rho} \end{aligned} \quad (13)$$

containing the standard thermodynamic susceptibilities, such as specific heat C_V , compressibility κ_s , thermal expansion α_s , etc.

In general, inhomogeneous rotations of n_i , m_i , and Ω must increase the total energy

$$\begin{aligned} f_{\text{el}} &= \frac{1}{2} K_{ijkl}^m (\nabla_j m_i)(\nabla_l m_k) + \frac{1}{2} K_{ijkl} (\nabla_j n_i)(\nabla_l n_k) \\ &\quad + K_{ijkl}^{nm} (\nabla_i n_j)(\nabla_k m_l) + \frac{1}{2} K_{ij}^\Omega (\nabla_i \Omega)(\nabla_j \Omega) \\ &\quad + C_{ijk}^{n\Omega} (\nabla_i \Omega)(\nabla_k n_j) + C_{ijk}^{M_i \Omega} (\nabla_i \Omega)(\nabla_k m_j) \\ &\quad + \Pi_{ijk}^c (\nabla_i c)(\nabla_k n_j) + \Pi_{ijk}^\sigma (\nabla_i \sigma)(\nabla_k n_j) \\ &\quad + \Pi_{ijk}^\rho (\nabla_i \rho)(\nabla_k n_j) \\ &\quad + \Pi_{ijk}^{M_i c} (\nabla_i c)(\nabla_k m_j) + \Pi_{ijk}^{M_i \sigma} (\nabla_i \sigma)(\nabla_k m_j) \\ &\quad + \Pi_{ijk}^{M_i \rho} (\nabla_i \rho)(\nabla_k m_j) \\ &\quad + (\nabla_i \Omega)(C_{ij}^{c\Omega} \nabla_j c + C_{ij}^{\sigma\Omega} \nabla_j \sigma + C_{ij}^{\rho\Omega} \nabla_j \rho) \end{aligned} \quad (14)$$

with the rotational stiffness (or rotational elastic) tensors

$$\begin{aligned} K_{ijkl}^m &= K_1^m \delta_{ij}^\perp \delta_{kl}^\perp + K_2^m n_p n_q \epsilon_{ijp} \epsilon_{klq} \\ &\quad + K_3^m n_j n_l \delta_{ik}^\perp + K_4^m n_p n_q T_{ijp} T_{klq}, \end{aligned} \quad (15)$$

$$\begin{aligned} K_{ijkl} &= K_1 \delta_{ij}^\perp \delta_{kl}^\perp + K_2 n_p n_q \epsilon_{ijp} \epsilon_{klq} \\ &\quad + K_3 n_j n_l \delta_{ik}^\perp + K_4 n_p n_q T_{ijp} T_{klq}, \end{aligned} \quad (16)$$

$$K_{ijkl}^{mn} = K^{mn} \delta_{ij}^\perp (n_i M_k + n_k M_i), \quad (17)$$

$$K_{ij}^\Omega = K_\perp^\Omega \delta_{ij}^\perp + K_\parallel^\Omega n_i n_j, \quad (18)$$

$$C_{ijk}^{n\Omega} = C_\perp (\epsilon_{jkp} n_i + \epsilon_{jip} n_k) n_p, \quad (19)$$

$$\begin{aligned} C_{ijk}^{M_i \Omega} &= C_2^{M_i \Omega} (\epsilon_{jkp} n_i + \epsilon_{jip} n_k) M_p \\ &\quad + C_3^{M_i \Omega} (\epsilon_{jkp} M_i + \epsilon_{jip} M_k) n_p, \end{aligned} \quad (20)$$

$$\Pi_{ijk}^\lambda = \Pi^\lambda (n_i \delta_{jk}^\perp + n_k \delta_{ij}^\perp), \quad (21)$$

$$\Pi_{ijk}^{M_i \lambda} = \Pi^{M_i \lambda} (M_i \delta_{jk}^\perp + M_k \delta_{ij}^\perp), \quad (22)$$

$$C_{ij}^{\lambda\Omega} = C_\perp^\lambda n_k T_{kps} (\epsilon_{irs} T_{jpr} + \epsilon_{jrs} T_{ipr}), \quad (23)$$

where $\lambda \in \{\sigma, \rho, c\}$.

The structure of f_{el} bears some similarity with the gradient energy in the D_{2d} phase [68] and contains four coefficients each related to bending distortions of the orientation of the magnetization and the director. In addition there are two coefficients related to inhomogeneous rotations about the director and one mixed one. We emphasize that there is only one gradient term coupling the gradients of the director with those of m_i . In addition, there are cross couplings of the inhomogeneous rotations of Ω with gradients of the scalar conserved variables. Also note that the contribution $\sim C_\perp$ [69], which couples gradients of n_i and of Ω is associated with $\nabla \times \mathbf{n}$.

The magnetic part of the free energy homogeneous in the magnetization in Eq. (12) reads

$$f_M = -M_i H_i - \frac{1}{2} A_1 (m_i n_i)^2 + \frac{1}{2} \alpha M^2 + \frac{1}{4} \beta M^4. \quad (24)$$

This expression is derived taking into account the static magnetic Maxwell equations. α and β are expansion coefficients in a Landau expansion for M and where the contribution $\sim A_1$ describes the coupling between m_i and n_i . The derivation parallels very closely that given in Ref. [52] and quite recently in Ref. [64]. f_M is the Legendre transformed magnetic energy containing the magnetic field \mathbf{H} . The ferromagnetic coupling in f_M leads to the parallel equilibrium orientation of the magnetization along an external magnetic field. As a result, a homogeneous external field is compatible with a homogeneous combined magnetization and tetrahedral structure in the phase considered here: ferromagnetic nematic with additional tetrahedral order. However, the degeneracy of the (combined) orientation of the magnetization and the tetrahedral structure is partially lifted and only the orientation of the structure perpendicular to the field (and \mathbf{m}) is still arbitrary.

For the magnetic gradient energy we find

$$\begin{aligned} f_{M\text{grad}} = & \frac{1}{2} K_{ij}^M (\nabla_i M)(\nabla_j M) + C_{ij}^{M\Omega} (\nabla_i M)(\nabla_j \Omega) \\ & + K_{ijk}^{Mm} (\nabla_i M)(\nabla_j m_k) + K_{ijk}^{Mn} (\nabla_i M)(\nabla_j n_k) \\ & + (\nabla_i M)(\Pi_{ij}^{cM} \nabla_j c + \Pi_{ij}^{\sigma M} \nabla_j \sigma + \Pi_{ij}^{\rho M} \nabla_j \rho) \end{aligned} \quad (25)$$

with

$$K_{ij}^M = K_{\perp}^M \delta_{ij}^{\perp} + K_{\parallel}^M n_i n_j, \quad (26)$$

$$C_{ij}^{M\Omega} = C_{\parallel} n_k T_{kps} (\epsilon_{irs} T_{jpr} + \epsilon_{jrs} T_{ipr}), \quad (27)$$

$$K_{ijk}^{Mm} = K^{Mm} (M_j \delta_{ik}^{\perp} + M_i \delta_{jk}^{\perp}), \quad (28)$$

$$K_{ijk}^{Mn} = K^{Mn} (n_j \delta_{ik}^{\perp} + n_i \delta_{jk}^{\perp}), \quad (29)$$

$$\Pi_{ij}^{\lambda M} = \Pi_{\perp}^{\lambda M} \delta_{ij}^{\perp} + \Pi_{\parallel}^{\lambda M} n_i n_j, \quad (30)$$

where $\lambda \in \{\sigma, \rho, c\}$. There are two stiffness coefficients ($K_{\perp}^M, K_{\parallel}^M$) related to distortions of M . Cross couplings between distortions of M and inhomogeneous rotations of and about the director, are described by one coefficient each (K^{Mn} and C_{\parallel} , respectively), while there are in total six coefficients ($\Pi_{\perp, \parallel}^{\lambda M}$) connected to the coupling of gradients of M with gradients of the scalar conserved variables. Finally we note that we have kept in Eq. (25) one term linear in the magnetization M_i : K^{Mm} .

The last energy contribution we are discussing here is the linear gradient energy

$$f_{\text{lin}} = \xi^M T_{ijk} M_i (\nabla_j m_k) + \xi^n T_{ijk} n_i (\nabla_j n_k). \quad (31)$$

This expression is identical to the linear gradient term in the D_{2d} phase [14] for the director n_i . In addition, it also contains the analogous linear gradient term, when one uses m_i instead of the director n_i . These two linear gradient terms are allowed due to the presence of tetrahedral order, which breaks parity. The present system appears to be the first one for which two of these linear gradient terms exist: one associated with the nematic director and one associated with the direction of the magnetization. As a consequence, the ground state might not be homogeneous, resembling the case of added chirality to nematic liquid crystals. In fact, these terms are well known by now to give rise to ambidextrous helicity [14,15,31,32]. In the case in which one can obtain sufficiently large domains of either handedness in a ferromagnetic nematic liquid crystal composed of nonchiral constituents, this would be rather obvious evidence of the presence of tetrahedral order. Naturally, an observation in the visible range would be most attractive.

For completeness we list the expressions for the thermodynamic conjugates that follow from the energy contributions introduced above:

$$v_i = \frac{1}{\rho} g_i, \quad (32)$$

$$\delta T = \frac{T}{C_V} \delta \sigma + \frac{1}{\rho \alpha_s} \delta \rho + \beta_{\sigma} \delta c - \nabla_i (\Pi_{ijk}^{\sigma} \nabla_k n_j + \Pi_{ij}^{\sigma M} \nabla_j M + C_{ij}^{\sigma \Omega} \nabla_j \Omega) - \nabla_i (\Pi_{ijk}^{M_i \sigma} \nabla_k m_j), \quad (33)$$

$$\delta \mu = \frac{1}{\rho^2 \kappa_s} \delta \rho + \frac{1}{\rho \alpha_s} \delta \sigma + \beta_{\rho} \delta c - \nabla_i (\Pi_{ijk}^{\rho} \nabla_k n_j + \Pi_{ij}^{\rho M} \nabla_j M + C_{ij}^{\rho \Omega} \nabla_j \Omega) - \nabla_i (\Pi_{ijk}^{M_i \rho} \nabla_k m_j), \quad (34)$$

$$\delta \mu_c = \gamma \delta c + \beta_{\sigma} \delta \sigma + \beta_{\rho} \delta \rho - \nabla_i (\Pi_{ijk}^c \nabla_k n_j + \Pi_{ij}^{cM} \nabla_j M + C_{ij}^{c\Omega} \nabla_j \Omega) - \nabla_i (\Pi_{ijk}^{M_i c} \nabla_k m_j), \quad (35)$$

$$\begin{aligned} h^M = & -m_i H_i + \alpha M + \beta M^3 - \nabla_i (K_{ij}^M \nabla_j M + C_{ij}^{M\Omega} \nabla_j \Omega + K_{ijk}^{Mm} \nabla_j m_k) - \nabla_i (K_{ijk}^{Mn} \nabla_j n_k) \\ & - \nabla_i (\Pi_{ij}^{\sigma M} \nabla_j \sigma + \Pi_{ij}^{\rho M} \nabla_j \rho + \Pi_{ij}^{cM} \nabla_j c) + [C_2^{M_i \Omega} (\epsilon_{jkp} n_i + \epsilon_{jip} n_k) m_p + C_3^{M_i \Omega} (\epsilon_{jkp} m_i + \epsilon_{jip} m_k) n_p] (\nabla_i \Omega) (\nabla_k m_j) \\ & + [\Pi^{M_i \rho} \nabla_i \rho + \Pi^{M_i \sigma} \nabla_i \sigma + \Pi^{M_i c} \nabla_i c] (m_i \delta_{jk}^{\perp} + m_k \delta_{ij}^{\perp}) (\nabla_k m_j), \end{aligned} \quad (36)$$

$$h_i^{m'} = -M H_i - A_1 (m_j n_j) n_i, \quad (37)$$

$$\Psi_{ij}^m = K_{ijkl}^m \nabla_l m_k + K_{jikl}^{nm} \nabla_l n_k + K_{kji}^{Mm} \nabla_k M + \Pi_{kji}^{M_i \sigma} (\nabla_k \sigma) + \Pi_{kji}^{M_i \rho} (\nabla_k \rho) + \Pi_{kji}^{M_i c} (\nabla_k c) + C_{kji}^{M_i \Omega} (\nabla_k \Omega), \quad (38)$$

$$h_i^{n'} = -A_1 (m_j n_j) m_i, \quad (39)$$

$$\Phi_{ij}^n = K_{ijkl}^n \nabla_l n_k + C_{kij}^{n\Omega} \nabla_k \Omega + K_{kji}^{Mn} \nabla_k M + \Pi_{kij}^{\sigma} \nabla_k \sigma + \Pi_{kij}^{\rho} \nabla_k \rho + \Pi_{kij}^c \nabla_k c + K_{jikl}^{nm} \nabla_k m_l, \quad (40)$$

$$\Psi_i^{\Omega} = K_{ij}^{\Omega} \nabla_j \Omega + C_{ijk}^{n\Omega} \nabla_k n_j + C_{ij}^{M\Omega} \nabla_j M + C_{ij}^{\sigma \Omega} \nabla_j \sigma + C_{ij}^{\rho \Omega} \nabla_j \rho + C_{ij}^{c\Omega} \nabla_j c + C_{ijk}^{M_i \Omega} \nabla_k m_j, \quad (41)$$

$$h^{\Omega'} = 0. \quad (42)$$

Since the δ 's in Eqs. (33)–(35) describe deviations from the constant equilibrium values of the appropriate variable, all expressions on the left-hand side of Eqs. (32)–(42) are zero in equilibrium and can act as thermodynamic forces that drive the dynamics of the system. On the other hand, the right-hand sides of all these equations have to be zero in equilibrium (Euler conditions). Note that the energy f_{lin} does not enter any Euler condition (except for $\nabla_i T_{ijk} \neq 0$), since it is linear in gradients of m_i .

IV. DYNAMICS OF FERROMAGNETIC NEMATICS WITH TETRAHEDRAL ORDER

A. Dynamic equations

The hydrodynamic variables can be put into two different classes. There are conserved variables, like the mass density, energy density, and momentum density \mathbf{g} , which are governed by conservation laws. The second class of variables corresponds to the variables associated with spontaneously broken continuous symmetries. Their dynamics is governed by balance laws. In our case we have from this class the director variations, δn_i , and the rotation around the director, $\delta\Omega$. There are some macroscopic variables that relax on a finite but very long timescale and it is therefore sensible to include them into the macroscopic description, Ref. [67]. In our case we will consider the magnitude of the magnetization, M , as well as the orientational variations of the magnetization, M_i : δm_i .

The dynamic equations read (including the dynamic equations already given in Ref. [52])

$$\frac{\partial}{\partial t} f + \nabla_i ([f + p]v_i + j_i^f) = 0, \quad (43)$$

$$\frac{\partial}{\partial t} \rho + \nabla_i g_i = 0, \quad (44)$$

$$\frac{\partial}{\partial t} g_i + \nabla_j (g_i v_j + p\delta_{ij} + \sigma_{ij}^{th} + \sigma_{ij}) = 0, \quad (45)$$

$$\frac{\partial}{\partial t} \sigma + \nabla_i (\sigma v_i + j_i^\sigma) = \frac{2R}{T}, \quad (46)$$

$$\rho \left(\frac{\partial}{\partial t} + v_j \nabla_j \right) c + \nabla_i j_i^c = 0, \quad (47)$$

$$\left(\frac{\partial}{\partial t} + v_j \nabla_j \right) M + X^M = 0, \quad (48)$$

$$\left(\frac{\partial}{\partial t} + v_j \nabla_j \right) m_i - \epsilon_{ijk} \omega_j m_k + X_i^m = 0, \quad (49)$$

$$\left(\frac{\partial}{\partial t} + v_j \nabla_j \right) \Omega - m_i \omega_i + Z = 0, \quad (50)$$

$$\left(\frac{\partial}{\partial t} + v_j \nabla_j \right) n_i - \epsilon_{ijk} \omega_j n_k + Y_i^n = 0, \quad (51)$$

with the vorticity $\omega_i = (1/2)\epsilon_{ijk}\nabla_j v_k$ and the pressure p .

The vorticity contributions are due to the fact that m_i and n_i transform under spatial rotations as a vector, and Ω as a special component of a vector [32]. These terms ensure that only those rotations enter hydrodynamics that go beyond the global rotation (e.g., of the coordinate system).

In Eq. (45) we have explicitly written down the nonphenomenological part of the stress tensor, σ_{ij}^{th} , which is given by

$$\begin{aligned} \sigma_{ij}^{th} = & \frac{1}{2}(m_i h_j^m - m_j h_i^m) + \Psi_{kj}^m \nabla_i m_k + \Psi_j^\Omega \nabla_i \Omega \\ & - h^\Omega \epsilon_{ijk} m_k + \frac{1}{2}(n_i h_j^n - n_j h_i^n) + \Phi_{kj}^n \nabla_i n_k. \end{aligned} \quad (52)$$

Using the condition of a rotational invariant free energy, Eq. (11), it can be brought into the form [67]

$$\begin{aligned} 2\sigma_{ij}^{th} = & \Psi_{kj}^m \nabla_i m_k + \Psi_{ki}^m \nabla_j m_k + \Psi_j^\Omega \nabla_i \Omega + \Psi_i^\Omega \nabla_j \Omega \\ & + \Phi_{ki}^n \nabla_j n_k + \Phi_{kj}^n \nabla_i n_k \\ & + \nabla_k (m_j \Psi_{ik}^m - m_i \Psi_{jk}^m + n_j \Phi_{ik}^n - n_i \Phi_{jk}^n) \end{aligned} \quad (53)$$

that guarantees angular momentum conservation [65].

The source term in the dynamic evolution equation for the entropy density, Eq. (46), is proportional to the dissipation function R representing (half of) the rate at which the heat is transferred to the microscopic degrees of freedom. The second law of thermodynamics requires $R > 0$ for dissipative processes, while $R = 0$ holds for the reversible parts of the currents, in which case Eq. (46) is a conservation law. Splitting the phenomenological currents (j_i^f , σ_{ij} , j_i^σ , j_i^c , X^M , X_i^m , Z , Y_i^n) into the dissipative part (superscript D) and the reversible one (superscript R) the Gibbs relation Eq. (9) then leads to the condition

$$\begin{aligned} 2R = & -\nabla_i j_i^{fD} - j_i^{\sigma D} \nabla_i T - j_i^{cD} \nabla_i \mu_c - \sigma_{ij}^D A_{ij} \\ & + X^{MD} h^M + X_i^{mD} h_i^m + Z^D h^\Omega + Y_i^{nD} h_i^{nD} > 0 \end{aligned} \quad (54)$$

for dissipative processes, where only the symmetrized velocity gradient $2A_{ij} = \nabla_i v_j + \nabla_j v_i$ enters, in order to prevent solid body rotations to produce entropy. For reversible currents, the condition

$$\begin{aligned} -\nabla_i j_i^{fR} - j_i^{\sigma R} \nabla_i T - j_i^{cR} \nabla_i \mu_c - \sigma_{ij}^R A_{ij} \\ + X^{MR} h^M + X_i^{mR} h_i^m + Z^R h^\Omega + Y_i^{nR} h_i^{nR} = 0 \end{aligned} \quad (55)$$

applies. Possible pure divergence contributions (surface terms) are put into j_i^f , but are not needed in the following. The various transport contributions in the time derivatives of Eqs. (43)–(50) are all reversible. Their zero entropy production is ensured by the nonphenomenological parts of the stress tensor σ_{ij}^{th} and by the pressure p .

A current is reversible, if it transforms under time reversal in the same way as the time derivative of the appropriate variable, while the dissipative part of a current has the opposite time-reversal behavior. In the following we will discuss the dissipative and reversible dynamics separately.

To derive the dissipative parts of the phenomenological currents one first writes the dissipation function as a positive quadratic form in the thermodynamic forces taking into account that R has to be a time-reversal-symmetric, scalar quantity. By taking the variational derivative of this function with respect to the chosen thermodynamic force one gets the corresponding dissipative current.

B. Dissipation function and dissipative currents

The dissipation function reads

$$\begin{aligned}
 R = & \frac{1}{2}\kappa_{ij}(\nabla_i T)(\nabla_j T) + \frac{1}{2}D_{ij}(\nabla_i \mu_c)(\nabla_j \mu_c) + D_{ij}^T(\nabla_i T)(\nabla_j \mu_c) + \frac{1}{2}v_{ijkl}^D A_{ij} A_{kl} + \frac{1}{2}b_{ij}^D h_i^m h_j^m + \frac{1}{2}b^M h^M h^M + \frac{1}{2}b^\Omega h^\Omega h^\Omega \\
 & + \frac{1}{2\gamma_1} h_i^n \delta_{ij}^\perp h_j^n + \tau_{ij} A_{ij} h^\Omega + c_{ij}^M A_{ij} h^M + \chi_{ij}^D h_j^m h_i^n + c_{ijk}^D A_{jk} h_i^m + \lambda_{ijk}^D A_{jk} h_i^n \\
 & + \Gamma_{ijk}^{(2)} A_{ij} \nabla_k T + \Gamma_{ijk}^{(3)} A_{ij} \nabla_k \mu_c + T_{ijk} M_j (\tilde{\psi}^{TD} \nabla_k T + \tilde{\psi}^{cD} \nabla_k \mu) h_i^m + T_{ijk} n_j \delta_{iq}^\perp (\psi^{TD} \nabla_k T + \psi^{cD} \nabla_k \mu) h_q^n
 \end{aligned} \quad (56)$$

and the dissipative parts of the currents are

$$j_i^{\sigma D} = -\kappa_{ij} \nabla_j T - D_{ij}^T \nabla_j \mu_c - \tilde{\psi}^{TD} M_j T_{kji} h_k^m - \psi^{TD} n_j \delta_{kq}^\perp T_{kji} h_q^n - \Gamma_{kji}^{(2)} A_{kj}, \quad (57)$$

$$j_i^{cD} = -D_{ij} \nabla_j \mu_c - D_{ji}^T \nabla_j T - \tilde{\psi}^{cD} M_j T_{kji} h_k^m - \psi^{cD} n_j \delta_{kq}^\perp T_{kji} h_q^n - \Gamma_{kji}^{(3)} A_{kj}, \quad (58)$$

$$\sigma_i^D = -v_{ijkl}^D A_{kl} - c_{kji}^D h_k^m - c_{ij}^M h^M - \tau_{ij} h^\Omega - \Gamma_{ijk}^{(2)} \nabla_k T - \Gamma_{ijk}^{(3)} \nabla_k \mu_c - \lambda_{kij}^D h_k^n, \quad (59)$$

$$X_i^{mD} = b_\perp^D \delta_{ij}^\perp h_j^m + c_{ijk}^D A_{jk} + \chi_{ji}^D h_i^n + M_j T_{ijk} (\tilde{\psi}^{TD} \nabla_k T + \tilde{\psi}^{cD} \nabla_k \mu_c), \quad (60)$$

$$X^{MD} = b^M h^M + c_{ij}^M A_{ij}, \quad (61)$$

$$Z^D = b^\Omega h^\Omega + \tau_{ij} A_{ij}, \quad (62)$$

$$Y_i^{nD} = \frac{1}{\gamma_1} \delta_{ij}^\perp h_j^n + \chi_{ij}^D h_j^m + \lambda_{ijk}^D A_{jk} + T_{qjk} n_j \delta_{iq}^\perp (\psi^{TD} \nabla_k T + \psi^{cD} \nabla_k \mu_c), \quad (63)$$

where the tensors κ_{ij} , D_{ij} , D_{ij}^T , and b_{ij}^D are of the usual uniaxial form

$$\zeta_{ij}^D = \zeta_1^D \delta_{ij}^\perp + \zeta_2^D n_i n_j. \quad (64)$$

while the others read

$$\Gamma_{ijk}^{(2)} = \Gamma_{21}^D \epsilon_{kpr} T_{ijp} M_r + \Gamma_{22}^D (\epsilon_{ipr} T_{kjp} M_r + \epsilon_{jpr} T_{kip} M_r), \quad (65)$$

$$\Gamma_{ijk}^{(3)} = \Gamma_{31}^D \epsilon_{kpr} T_{ijp} M_r + \Gamma_{32}^D (\epsilon_{ipr} T_{kjp} M_r + \epsilon_{jpr} T_{kip} M_r), \quad (66)$$

$$\begin{aligned}
 v_{ijkl}^D = & v_1 \delta_{ij}^\perp \delta_{kl}^\perp + v_2 (\delta_{jl}^\perp \delta_{ik}^\perp + \delta_{il}^\perp \delta_{jk}^\perp) + v_3 n_i n_j n_k n_l + v_4 (\delta_{ij}^\perp n_k n_l + \delta_{kl}^\perp n_i n_j) \\
 & + v_5 (\delta_{ik}^\perp n_j n_l + \delta_{jk}^\perp n_i n_l + \delta_{il}^\perp n_j n_k + \delta_{jl}^\perp n_i n_k) + v_6 n_p n_q T_{ijp} T_{klq},
 \end{aligned} \quad (67)$$

$$c_{ijk}^D = c_1^D (\epsilon_{imk} n_j + \epsilon_{imj} n_k) n_m, \quad (68)$$

$$\tau_{ij} = \tau (n_i M_j + n_j M_i), \quad (69)$$

$$c_{ij}^M = c_2^D (\epsilon_{irs} T_{jpr} + \epsilon_{jrs} T_{ipr}) M_k T_{kps}, \quad (70)$$

$$\chi_{ij}^D = \chi_2^D \delta_{ij}^{tr} M_k n_k, \quad (71)$$

$$\lambda_{ijk}^D = \lambda_1^D (\delta_{iq}^{tr} \epsilon_{pj} M_p n_k + \delta_{iq}^{tr} \epsilon_{pk} M_p n_j) + \lambda_2^D (M_j \epsilon_{ipk} n_p + M_k \epsilon_{ipj} n_p) + \lambda_3^D (M_q n_q n_j \epsilon_{ipk} n_p + M_q n_q n_k \epsilon_{ipj} n_p). \quad (72)$$

C. Reversible currents

The reversible parts of the currents do not follow from any potential, but can be derived by requiring that the entropy production R in Eq. (54) is zero:

$$j_i^{\sigma R} = -\kappa_{ij}^R \nabla_j T - D_{ij}^{TR} \nabla_j \mu_c + \psi_{ij}^T h_j^m + \Gamma_{kji}^T A_{jk} + \xi_{ij}^{Tn} h_j^n, \quad (73)$$

$$j_i^{cR} = -D_{ij}^R \nabla_j \mu_c + D_{ij}^{TR} \nabla_j T + \psi_{ij}^c h_j^m + \Gamma_{kji}^c A_{jk} + \xi_{ij}^{cn} h_j^n, \quad (74)$$

$$\begin{aligned}
 \sigma_{ij}^R = & -\frac{1}{2} \lambda_{kji} h_k^n - v_{ijkl}^R A_{kl} - c_{kij}^R h_k^m - c_{ij}^R h^M \\
 & - \Gamma_{ijk}^T \nabla_k T - \Gamma_{ijk}^c \nabla_k \mu_c - \tau_{ij} h^\Omega,
 \end{aligned} \quad (75)$$

$$\begin{aligned}
 X_i^{mR} = & b_{ij}^R h_j^m - c_{ijk}^R A_{jk} + \psi_{ji}^T \nabla_j T + \psi_{ji}^c \nabla_j \mu_c \\
 & + \chi^R (\mathbf{n} \times \mathbf{h}^n)_i,
 \end{aligned} \quad (76)$$

$$X^{MR} = -c_{ij}^R A_{ij}, \quad (77)$$

$$Z^R = -\tau_{ij}^R A_{ij}, \quad (78)$$

$$Y_i^{nR} = (\gamma_1^{-1})_{ij}^R h_j^n + \lambda_{ijk} A_{jk} + \xi_{ji}^{Tn} \nabla_j T + \xi_{ji}^{cn} \nabla_j c + \chi^R (\mathbf{n} \times \mathbf{h}^m)_i, \quad (79)$$

where the tensors κ_{ij}^R , D_{ij}^{TR} , D_{ij}^R , b_{ij}^R , and $(\gamma_1^{-1})_{ij}$ are all of the form

$$\kappa_{ij}^R = \kappa_1^R \epsilon_{ijk} M_k + \kappa_2^R \epsilon_{ijk} n_k n_p M_p \quad (80)$$

and the other tensors read

$$\psi_{ij}^{c,T} = \psi^{c,T} \epsilon_{ipr} T_{jpk} n_k n_r, \quad (81)$$

$$c_{ijk}^R = c_1^R (M_j \delta_{ik}^\perp + M_k \delta_{ij}^\perp), \quad (82)$$

$$c_{ij}^R = c_\perp^R \delta_{ij}^\perp + c_\parallel^R n_i n_j, \quad (83)$$

$$\tau_{ij}^R = \tau^R (\epsilon_{irs} T_{jpr} + \epsilon_{jrs} T_{ipr}) n_k T_{kps}, \quad (84)$$

$$\xi_{ij}^{Tn} = \xi^{Tn} M_k n_r \epsilon_{ipr} T_{jpk}, \quad (85)$$

$$\xi_{ij}^{cn} = \xi^{cn} M_k n_r \epsilon_{ipr} T_{jpk}, \quad (86)$$

$$\lambda_{ijk} = \lambda (\delta_{ij}^\perp n_k + \delta_{ik}^\perp n_j), \quad (87)$$

$$\Gamma_{kji}^{T,c} = T_{qjk} (\Gamma_1^{TR,cR} \delta_{qi}^\perp + \Gamma_2^{TR,cR} n_q n_i). \quad (88)$$

It is straightforward to check that there is no linearly independent reversible coupling of n_i and m_i containing T_{ijk} quadratically in addition to the contribution $\sim \chi^R$. We note that ξ_{ij}^{Tn} and ξ_{ij}^{cn} are odd under parity, time-reversal, and $\mathbf{n} \rightarrow -\mathbf{n}$ symmetry. This type of coupling has not been given before and its possible experimental consequences will be discussed in the next section.

The reversible analog of the viscosity tensor has five components:

$$\begin{aligned} v_{ijkl}^R &= v_1^R [\epsilon_{ikp} n_j n_l + \epsilon_{ilp} n_j n_k \\ &\quad + \epsilon_{jlp} n_i n_k + \epsilon_{jkp} n_i n_l] n_p n_m M_m \\ &\quad + v_2^R [\epsilon_{ikp} n_j n_l + \epsilon_{ilp} n_j n_k \\ &\quad + \epsilon_{jlp} n_i n_k + \epsilon_{jkp} n_i n_l] M_p \\ &\quad + v_3^R [\epsilon_{ikp} \delta_{jl} + \epsilon_{ilp} \delta_{jk} + \epsilon_{jlp} \delta_{ik} + \epsilon_{jkp} \delta_{il}] n_p n_m M_m \\ &\quad + v_4^R [\epsilon_{ikp} \delta_{jl} + \epsilon_{ilp} \delta_{jk} + \epsilon_{jlp} \delta_{ik} + \epsilon_{jkp} \delta_{il}] M_p \\ &\quad + v_5^R [\epsilon_{ikp} (M_j n_l + M_l n_j) + \epsilon_{ilp} (M_j n_k + M_k n_j) \\ &\quad + \epsilon_{jlp} (M_i n_k + M_k n_i) + \epsilon_{jkp} (M_i n_l + M_l n_i)] n_p. \end{aligned} \quad (89)$$

This fourth-order tensor is antisymmetric in the exchange of the first pair of indices with the second one, thus guaranteeing zero entropy production.

Due to the presence of a tetrahedral order parameter, one has dissipative dynamic cross couplings of the temperature and the concentration gradients with the magnetization or the director field. This is, in principle, also possible in the ferromagnetic cholesteric phase.

If one applies a temperature or a concentration gradient to the sample of a tetrahedral ferromagnetic nematic phase, one can induce flow via both the dissipative and reversible currents.

V. SUGGESTIONS FOR EXPERIMENTS

In this section we discuss various experimental setups that can reveal selected static and dynamic cross-coupling effects due to the presence of tetrahedral order in ferromagnetic nematics.

A. Ambidextrous helical domains

In Sec. III we already briefly discussed the linear gradient energy

$$f_{\text{lin}} = \xi^M T_{ijk} M_i (\nabla_j m_k) + \xi^n T_{ijk} n_i (\nabla_j n_k). \quad (90)$$

We note that these two terms can only arise for a system with broken parity. In addition, ξ^M and ξ^n can have either sign, since they are linear gradient terms. To study their consequences we perform an analysis, which closely resembles that for D_{2d} nematics given in Ref. [14]. That is, we look for a helical state, which has lower energy than the homogeneous state. As a result of this analysis we obtain an energy reduction due to the two linear gradient terms, which takes the form

$$\Delta f = \frac{8}{27} T_0^2 \frac{(\xi^n + \xi^M M_0)^2}{K_2 + K_2^m}, \quad (91)$$

which yields for the helical wave vector

$$q_0 = -\frac{4}{3\sqrt{3}} T_0 \frac{(\xi^n + \xi^M M_0)}{K_2 + K_2^m}. \quad (92)$$

We point out that the cross-coupling term $\sim K^{mn}$ between gradients of the director and the magnetization does not enter the picture, since the components of the director and the magnetization along the helical axis are zero. From Eqs. (91) and (92) two important conclusions follow immediately. First of all the system can gain energy by generating a helical state. Surely the system will also generate defects, which cost energy. Provided the helical domains obtained are large enough, this result leads to a straightforward way to detect the presence of octupolar order in a ferromagnetic nematic: the optical observation of domains of opposite handedness. The other conclusion is closely tied to the fact that we have two linear gradient terms. The sign and magnitudes of ξ^n and ξ^M are material properties that are fixed. In the case in which the signs of ξ^n and ξ^M are opposite, but their magnitude is comparable, the expectation is to have a small value of the net wave vector or a large wavelength for the ambidextrous helical domains.

B. Temperature gradients can drive reversible director rotations

As a reversible cross-coupling term characteristic of ferromagnetic nematics with octupolar order we consider coupling terms involving temperature, concentration, and the director field. For heat and concentration currents we get a coupling to the molecular field of the director (compare Sec. IV C):

$$j_i^{\sigma R} = \dots + \xi_{ij}^{Tn} h_j^n, \quad (93)$$

$$j_i^{cR} = \dots + \xi_{ij}^{cn} h_j^n \quad (94)$$

or, explicitly for σ and for $m_i \parallel \hat{z}$ and $n_i \parallel \hat{z}$:

$$j_x^{\sigma R} = \dots + \xi^{Tn} M_0 \tilde{T}_0 h_x^n, \quad (95)$$

$$j_y^{\sigma R} = \dots - \xi^{Tn} M_0 \tilde{T}_0 h_y^n, \quad (96)$$

$$j_z^{\sigma R} = \dots + 0, \quad (97)$$

where $\tilde{T}_0 = \frac{4}{3\sqrt{3}} T_0$.

From inspection of Eqs. (85) and (86) we see that the cross coupling $\sim \xi_{ij}^{Tn}$ and $\sim \xi_{ij}^{cn}$ is linear in \mathbf{M} , T_{ijk} , and \mathbf{n} . Thus the coupling is mediated by making use of the odd behavior under parity and time reversal of the ground state. And the physics is quite apparent: director rotations drive heat and concentration currents without generating entropy.

As a complement we find that temperature gradients and concentration gradients applied externally generate director rotations

$$\dot{n}_i \sim Y_i^{nR} = \dots + \xi_{ji}^{Tn} \nabla_j T + \xi_{ji}^{cn} \nabla_j c \quad (98)$$

or, explicitly for $m_i \parallel \hat{z}$ and $n_i \parallel \hat{z}$:

$$Y_x^{nR} = \dots + \xi^{Tn} M_0 \tilde{T}_0 \nabla_x T + \xi^{cn} M_0 \tilde{T}_0 \nabla_x c, \quad (99)$$

$$Y_y^{nR} = \dots - \xi^{Tn} M_0 \tilde{T}_0 \nabla_y T - \xi^{cn} M_0 \tilde{T}_0 \nabla_y c, \quad (100)$$

$$Y_z^{nR} = \dots + 0. \quad (101)$$

C. Magnetization rotations can drive heat currents

Here we present an example of a dissipative effect, which requires a magnetization as well as tetrahedral order. From Sec. IV B we have for the parts of the heat and concentration current coupling to magnetization rotations

$$j_i^{\sigma D} = \dots - \tilde{\psi}^{TD} M_j T_{kji} h_k^m, \quad (102)$$

$$j_i^{cD} = \dots - \tilde{\psi}^{cD} M_j T_{kji} h_k^m \quad (103)$$

or, explicitly for the concentration c and for $m_i \parallel \hat{z}$ and $n_i \parallel \hat{z}$:

$$j_x^{cD} = \dots - \tilde{\psi}^{cD} M_0 \tilde{T}_0 h_y^m, \quad (104)$$

$$j_y^{cD} = \dots - \tilde{\psi}^{cD} M_0 \tilde{T}_0 h_x^m, \quad (105)$$

$$j_z^{cD} = \dots + 0. \quad (106)$$

Inspecting Eqs. (102) and (103) we see that heat currents as well as concentration currents are induced by rotations of

the magnetization for ferromagnetic nematics with tetrahedral order, since such a rather unique system breaks both time-reversal and parity symmetry. Conversely, temperature gradients as well as concentration gradients drive the dynamics of the magnetization via

$$\dot{m}_i \sim X_i^{mD} = \dots + M_j T_{ijk} (\tilde{\psi}^{TD} \nabla_k T + \tilde{\psi}^{cD} \nabla_k \mu_c) \quad (107)$$

or, explicitly for $m_i \parallel \hat{z}$ and $n_i \parallel \hat{z}$:

$$X_x^{mD} = \dots + M_0 \tilde{T}_0 (\tilde{\psi}^{TD} \nabla_y T + \tilde{\psi}^{cD} \nabla_y \mu_c), \quad (108)$$

$$X_y^{mD} = \dots + M_0 \tilde{T}_0 (\tilde{\psi}^{TD} \nabla_x T + \tilde{\psi}^{cD} \nabla_x \mu_c), \quad (109)$$

$$X_z^{mD} = \dots + 0. \quad (110)$$

VI. SUMMARY AND PERSPECTIVE

In this paper we have analyzed how the macroscopic properties of ferromagnetic nematic liquid crystals are influenced by the presence of parity breaking octupolar order. It turns out that many additional cross-coupling terms arise in statics and dynamics, since now one has a ground state that breaks both time-reversal and inversion symmetry. Clearly the hallmark for the presence of octupolar order will be the detection of chiral domains of both hands in a ferromagnetic nematic compound composed of nonchiral molecules: ambidextrous helicity. Since there are two linear gradient terms in the system investigated here, one associated with the nematic director and one associated with ferromagnetic order, one can tune the helical pitch by changing the magnitude of the spontaneous magnetization, M_0 .

As a perspective it will be most interesting to investigate how tetrahedral order will influence ferromagnetic cholesteric liquid crystals, since in such a system parity symmetry breaking is achieved by two different mechanisms: a pseudoscalar quantity associated with the chirality of the molecules of at least one of the constituents as well as with octupolar order. Such a system represents also a challenge for its mathematical description in three spatial dimensions, when both parity breaking mechanisms are at work.

ACKNOWLEDGMENTS

Partial support of this work by H.R.B., H.P., and T.P. through the Schwerpunktprogramm SPP 1681 ‘‘Feldgesteuerte Partikel-Matrix-Wechselwirkungen: Erzeugung, skalenübergreifende Modellierung und Anwendung magnetischer Hybridmaterialien’’ of the Deutsche Forschungsgemeinschaft is gratefully acknowledged.

- [1] L. G. Fel, *Phys. Rev. E* **52**, 702 (1995).
- [2] L. G. Fel, *Phys. Rev. E* **52**, 2692 (1995).
- [3] L. Radzihovsky and T. C. Lubensky, *Europhys. Lett.* **54**, 206 (2001).
- [4] T. C. Lubensky and L. Radzihovsky, *Phys. Rev. E* **66**, 031704 (2002).
- [5] B. Mettout, *Phys. Rev. E* **74**, 041701 (2006).

- [6] L. Longa, G. Pajak, and T. Wydro, *Phys. Rev. E* **79**, 040701 (2009).
- [7] K. Trojanowski, G. Pajak, L. Longa, and T. Wydro, *Phys. Rev. E* **86**, 011704 (2012).
- [8] L. Longa and K. Trojanowski, *Acta. Phys. Pol. B* **44**, 1201 (2013).
- [9] H. R. Brand, H. Pleiner, and P. E. Cladis, *Eur. Phys. J. E* **7**, 163 (2002).

- [10] P. E. Cladis, H. Pleiner, and H. R. Brand, *Eur. Phys. J. E* **11**, 283 (2003).
- [11] H. R. Brand, P. E. Cladis, and H. Pleiner, *Ferroelectrics* **315**, 165 (2005).
- [12] H. R. Brand, H. Pleiner, and P. E. Cladis, *Physica A* **351**, 189 (2005).
- [13] H. Pleiner, P. E. Cladis, and H. R. Brand, *Eur. Phys. J. E* **20**, 257 (2006).
- [14] H. R. Brand and H. Pleiner, *Eur. Phys. J. E* **31**, 37 (2010).
- [15] H. Pleiner and H. R. Brand, *Eur. Phys. J. E* **37**, 11 (2014).
- [16] G. Pelzl, A. Eremin, S. Diele, H. Kresse, and W. Weissflog, *J. Mat. Chem.* **12**, 2591 (2002).
- [17] V. Bourny, V. Lorman, J. Pavel, B. Mettout, and H. T. Nguyen, *Ferroelectrics* **276**, 127 (2002).
- [18] W. Weissflog, M. W. Schröder, S. Diele, and G. Pelzl, *Adv. Mater.* **15**, 630 (2003).
- [19] T. Niori, J. Yamamoto, and H. Yokoyama, *Mol. Cryst. Liq. Cryst.* **409**, 475 (2004).
- [20] M. W. Schroeder, S. Diele, G. Pelzl, and W. Weissflog, *ChemPhysChem* **5**, 99 (2004).
- [21] D. Wiant, J. T. Gleeson, N. Eber, K. Fodor-Csorba, A. Jakli, and T. Toth-Katona, *Phys. Rev. E* **72**, 041712 (2005).
- [22] J. Harden, B. Mbang, N. Eber, K. Fodor-Csorba, S. Sprunt, J. T. Gleeson, and A. Jakli, *Phys. Rev. Lett.* **97**, 157802 (2006).
- [23] D. Wiant, S. Stojadinovic, K. Neupane, S. Sharma, K. Fodor-Csorba, A. Jakli, J. T. Gleeson, and S. Sprunt, *Phys. Rev. E* **73**, 030703 (2006).
- [24] D. Wiant, K. Neupane, S. Sharma, J. T. Gleeson, S. Sprunt, A. Jakli, N. Pradhan, and G. Iannacchione, *Phys. Rev. E* **77**, 061701 (2008).
- [25] T. Ostapenko, D. B. Wiant, S. N. Sprunt, A. Jakli, and J. T. Gleeson, *Phys. Rev. Lett.* **101**, 247801 (2008).
- [26] Y. Jang, R. Balachandran, C. Keith, A. Lehmann, C. Tschierske, and J. K. Vij, *Soft Matter* **8**, 10479 (2012).
- [27] F. Vita, I. F. Placentino, C. Ferreo, G. Singh, E. T. Samulski, and O. Francescangeli, *Soft Matter* **9**, 6475 (2013).
- [28] M. Jasinski, D. Pocięcha, H. Monobe, J. Szczytko, and P. Kaszynski, *J. Am. Chem. Soc.* **136**, 14658 (2014).
- [29] O. N. Kadkin, E. H. Kim, Y. J. Rha, S. Y. Kim, J. Taem, and M.-G. Choi, *Chem. Eur. J.* **15**, 10343 (2009).
- [30] E. H. Kim, O. N. Kadkin, S. Y. Kim, J. Taem, and M.-G. Choi, *Eur. J. Inorg. Chem.* **2011**, 2933 (2011).
- [31] H. R. Brand and H. Pleiner, *Eur. Phys. J. E* **40**, 34 (2017).
- [32] H. Pleiner and H. R. Brand, *Braz. J. Phys.* **46**, 565 (2016).
- [33] T. Ohta, T. Ohkuma, and K. Shitara, *Phys. Rev. E* **80**, 056203 (2009).
- [34] M. Tarama and T. Ohta, *Phys. Rev. E* **87**, 062912 (2013).
- [35] T. Hiraiwa, M. Y. Matsuo, T. Ohkuma, T. Ohta, and M. Sano, *Europhys. Lett.* **91**, 20001 (2010).
- [36] E. G. Virga, *Eur. Phys. J. E* **38**, 63 (2015).
- [37] G. Gaeta and E. G. Virga, *Eur. Phys. J. E* **39**, 113 (2016).
- [38] Y. Chen, L. Qi, and E. G. Virga, *J. Phys. A* **51**, 025206 (2018).
- [39] C. Dressel, T. Reppe, M. Prehm, M. Brautzsch, and C. Tschierske, *Nat. Chem.* **6**, 971 (2014).
- [40] C. Dressel, W. Weissflog, and C. Tschierske, *Chem. Commun.* **51**, 15850 (2015).
- [41] M. Alaasar, M. Prehm, Y. Cao, F. Liu, and C. Tschierske, *Angew. Chem., Int. Ed.* **55**, 312 (2016).
- [42] F. Brochard and P. G. de Gennes, *J. Phys. (France)* **31**, 691 (1970).
- [43] J. Rault, P. E. Cladis, and J. Burger, *Phys. Lett. A* **32**, 199 (1970).
- [44] A. Mertelj, D. Lisjak, M. Drogenik, and M. Čopič, *Nature (London)* **504**, 237 (2013).
- [45] A. Mertelj, N. Osterman, D. Lisjak, and M. Čopič, *Soft Matter* **10**, 9065 (2014).
- [46] R. Sahoo, M. V. Rasna, D. Lisjak, A. Mertelj, and S. Dahra, *Appl. Phys. Lett.* **106**, 161905 (2015).
- [47] A. J. Hess, Q. Liu, and I. I. Smalyukh, *Appl. Phys. Lett.* **107**, 071906 (2015).
- [48] M. Shuai *et al.*, *Nat. Commun.* **7**, 10394 (2016).
- [49] Q. Liu, P. J. Ackerman, T. C. Lubensky, and I. I. Smalyukh, *Proc. Natl. Acad. Sci. USA* **113**, 10479 (2016).
- [50] H. Pleiner, E. Jarkova, H.-W. Müller, and H. R. Brand, *Magnetohydrodynamics* **37**, 254 (2001).
- [51] E. Jarkova, H. Pleiner, H.-W. Müller, A. Fink, and H. R. Brand, *Eur. Phys. J. E* **5**, 583 (2001).
- [52] E. Jarkova, H. Pleiner, H.-W. Müller, and H. R. Brand, *J. Chem. Phys.* **118**, 2422 (2003).
- [53] T. Potisk, D. Svenšek, H. R. Brand, H. Pleiner, D. Lisjak, N. Osterman, and A. Mertelj, *Phys. Rev. Lett.* **119**, 097802 (2017).
- [54] T. Potisk, A. Mertelj, N. Sebastián, N. Osterman, D. Lisjak, H. R. Brand, H. Pleiner, and D. Svenšek, *Phys. Rev. E* **97**, 012701 (2018).
- [55] T. Potisk, H. Pleiner, D. Svenšek, and H. R. Brand, *Phys. Rev. E* **97**, 042705 (2018).
- [56] A. Mertelj and D. Lisjak, *Liq. Cryst. Rev.* **5**, 1 (2017).
- [57] Q. Zhang, P. J. Ackerman, Q. Liu, and I. I. Smalyukh, *Phys. Rev. Lett.* **115**, 097802 (2015).
- [58] P. J. Ackerman and I. I. Smalyukh, *Nat. Mater.* **16**, 426 (2017).
- [59] P. Medle Rupnik, D. Lisjak, M. Čopič, S. Čopar, and A. Mertelj, *Sci. Adv.* **3**, e1701336 (2017).
- [60] H. R. Brand, A. Fink, and H. Pleiner, *Eur. Phys. J. E* **38**, 65 (2015).
- [61] H. Brand and H. Pleiner, *Phys. Rev. A* **24**, 2777 (1981).
- [62] M. Liu, *Phys. Rev. A* **24**, 2720 (1981).
- [63] P. G. de Gennes and J. Prost, *The Physics of Liquid Crystals* (Clarendon Press, Oxford, 1995).
- [64] T. Potisk, H. Pleiner, and H. R. Brand (unpublished).
- [65] P. C. Martin, O. Parodi, and P. S. Pershan, *Phys. Rev. A* **6**, 2401 (1972).
- [66] D. Forster, *Hydrodynamic Fluctuations, Broken Symmetry and Correlation Functions* (Benjamin, Reading, MA, 1975).
- [67] H. Pleiner and H. R. Brand, *Hydrodynamics and Electrohydrodynamics of Liquid Crystals*, edited by A. Buka and L. Kramer, Pattern Formation in Liquid Crystals (Springer, New York, 1996), p. 15 ff.
- [68] W. P. Mason, *Physical Acoustics and the Properties of Solids* (D. Van Nostrand, New York, 1958).
- [69] We note that the term $\sim C_{\perp}$ is different from the K_7 term in Ref. [32], Eq. (74): the C_{\perp} is correctly symmetrized in the gradients, while the K_7 term is antisymmetric and therefore does not exist.

Publication 5

Influence of Tetrahedral Order on Ferromagnetic Gel Phases

T. Potisk, H. Pleiner, and H.R. Brand
Eur. Phys. J. E **42**, 35 (2019).

Influence of tetrahedral order on ferromagnetic gel phases

Tilen Potisk^{1,a}, Harald Pleiner^{2,b}, and Helmut R. Brand¹

¹ Department of Physics, University of Bayreuth, 95440 Bayreuth, Germany

² Max Planck Institute for Polymer Research, 55021 Mainz, Germany

Received 10 January 2019

Published online: 25 March 2019

© The Author(s) 2019. This article is published with open access at Springerlink.com

Abstract. We investigate the macroscopic dynamics of gels with tetrahedral/octupolar symmetry, which possess in addition a spontaneous permanent magnetization. We derive the corresponding static and dynamic macroscopic equations for a phase, where the magnetization is parallel to one of the improper fourfold tetrahedral symmetry axes. Apart from elastic strains, we take into account relative rotations between the magnetization and the elastic network. The influence of tetrahedral order on these degrees of freedom is investigated and some experiments are proposed that are specific for such a material and allow to indirectly detect tetrahedral order. We also consider the case of a transient network and predict that stationary elastic shear stresses arise when a temperature gradient is applied.

1 Introduction

Ferrofluids are a well-established subfield of complex fluids [1, 2] showing a strong response to small external magnetic fields since they contain magnetic monodomain particles in a solvent. They have numerous applications including seals, dampers, loud speakers etc. They are strictly speaking super-paramagnetic and have no spontaneous magnetization in contrast to, for example, ferromagnetic solids. Their description on many length and time scales is well established [3–8]. Truly ferromagnetic fluids have not yet been reported for room temperature and ambient conditions.

More recently isotropic magnetic gels have been investigated for a number of polymeric systems containing magnetic particles and combining the properties of a ferrofluid with those of a polymeric gel [9–13]. Also their macroscopic and mesoscopic properties have been analyzed in some detail [14–16]. Synthesizing ferrogels in the presence of an external magnetic field has led to uniaxial magnetic gels [10, 17] with a finite magnetization M_0 in the absence of a magnetic field, which is implemented during the cross-linking process. This property is of high physical significance, since such systems show a linear response in a magnetic field [17], in addition to the usual quadratic field response. For both, isotropic ferrogels [14] and uniaxial [18] ferromagnetic gels, dynamic macroscopic descriptions are available.

We derive the hydrodynamics of tetrahedral ferromagnetic gels. They can be viewed as (uniaxial) magnetic gels

with an additional tetrahedral order. Uniaxial magnetic gels have been described theoretically in ref. [18] and are investigated experimentally in ref. [17]. Here we are interested in finding new effects that would hallmark the presence of an additional tetrahedral order. We consider predominantly the case of permanent gels, where elastic strains do not relax. As before, we will assume that the magnetic preferred direction is along one of the $\bar{4}$ axes of the tetrahedral order and that this coupling is rigid.

Here we investigate macroscopically the influence of octupolar/tetrahedral order on the physical properties of ferromagnetic gels. This issue is important, because the presence of octupolar order is associated with spontaneously broken inversion (parity) symmetry and can thus lead to static and dynamic cross-coupling effects absent otherwise. For gelled magnetic systems we are not aware of any previous study in this direction.

The major part of the investigations on the influence of octupolar order for fluid and gel-like systems has been in the field of liquid crystals [19–33] starting with the pioneering papers of Fel [19, 20]. From an experimental point of view the systems of interest have been liquid-crystalline phases derived from bent-core or ferrocene-type molecules [34–48]. For a recent review of the field of tetrahedral order in liquid crystals we refer to ref. [49]. Quite recently, the hydrodynamics of tetrahedral ferromagnetic nematic fluids has been discussed [50]. Only rather recently the presence of octupolar order has been suggested as an explanation [51] for the observation of macroscopic chiral domains of either hand in some optically isotropic phases [52–54]. In ref. [51] it has been shown in the framework of macroscopic dynamics that the simultane-

^a e-mail: tilen.potisk@uni-bayreuth.de

^b e-mail: pleiner@mpip-mainz.mpg.de

ous presence of octupolar order and a transient network is sufficient to produce ambidextrous helicity and thus to the possibility to obtain macroscopic chiral domains of either hand in compounds composed of non-chiral molecules.

The present paper is organized as follows. In sect. 2 we discuss the macroscopic dynamic description of ferromagnetic gel phases with octupolar order. This is followed in sect. 3 by suggestions of possible static and dynamic experiments that are specific for such phases including elasticity, tetrahedral and magnetic order. In sect. 4 we consider the case of a transient network and propose an experiment to study its influence. A summary and perspective, sect. 5, concludes the main text. In appendix A we list the full expressions for the thermodynamic conjugate forces and in appendix B we present the explicit expressions for the dissipative parts of the currents.

2 Ferromagnetic gel phases with tetrahedral order

2.1 Macroscopic variables

To derive the macroscopic equations of a particular macroscopic system one must first identify the relevant macroscopic variables. In addition to the conserved variables characteristic of an isotropic fluid, the mass density ρ , the energy density ε , the density of linear momentum \mathbf{g} , and the concentration c , related to an additional mass conservation law in binary mixtures, tetrahedral phases are described by a fully symmetric third rank tensor $T_{ijk} = T_0 \sum_{\beta=1}^4 n_i^\beta n_j^\beta n_k^\beta$ [19], where the vectors \mathbf{n}^β ($\beta = 1, 2, 3, 4$) span a tetrahedron and the order parameter T_0 (or rather $\tilde{T}_0 \equiv 4T_0/3\sqrt{3}$) describes the strength of the tetrahedral order, which we take as constant. Tetrahedral order breaks spatial inversion symmetry, but does not imply polar order, nor chirality. It fully breaks (spontaneously) rotational symmetry of isotropic space and its three independent rotations are the symmetry or Goldstone variables [49].

In ferromagnetic systems the spontaneous magnetization, \mathbf{M} , describes the strength of magnetic order by the order parameter $M \equiv |\mathbf{M}|$, and its orientation by the unit vector $\mathbf{m} = \mathbf{M}/M$. The former is neither connected to a Goldstone mode, nor to a conservation law, and therefore does not give rise to a genuine hydrodynamic variable. Nevertheless, its relaxation time can be large enough to be relevant in the hydrodynamic regime, and we will keep $\delta M \equiv M - M_0$, with M_0 the equilibrium magnetization, as a macroscopic variable.

The orientation of the magnetization breaks rotational symmetry of isotropic space partially twice, but is arbitrary in the absence of any orienting external field or boundary, constituting two Goldstone or symmetry variables $\delta \mathbf{m}$ with $\mathbf{m} \cdot \delta \mathbf{m} = 0$. In this respect they are equivalent to director rotations in uniaxial nematic liquid crystals. However, in the present system, where rotational symmetry is already broken by the tetrahedral order, magnetic orientation does not give rise to additional

independent Goldstone modes, and only the (three) combined (rigid) rotations of tetrahedral and magnetic orientations give rise to hydrodynamic degrees of freedom. Obviously, there must be an energetic penalty for rotations of the magnetization relative to the tetrahedral orientation.

Indeed, a simple Landau free energy argument shows that there are two energetic minima (stable thermodynamic phases), either with the magnetization pointing along one of the tetrahedral vectors, or along one of the improper 4 axes of the tetrahedron. The former is a phase of C_{3v} symmetry, which we will not consider here. The latter is a D_{2d} symmetric phase, similar to the tetrahedral nematic liquid crystal phase D_{2d} [49]. Nevertheless, the hydrodynamics of the ferromagnetic tetrahedral gel phase (called D_{2d}^{mg} in the following) is quite different from that of a D_{2d} phase, since the magnetization is a variable that changes sign under time reversal (in contrast to the nematic director) and since the D_{2d} phase is fluid. The static and the dynamic behavior of the D_{2d}^{mg} phase is also quite different from that of a tetrahedral ferromagnetic nematic phase [50], where the magnetization and the director field point both along one of the improper 4 axes. This phase includes as an example a dynamic interaction of the magnetization and the director field, which is different from the interplay of the magnetization and the strain field (defined at the end of this subsection). Furthermore, in a D_{2d}^{mg} phase one can induce an inhomogeneous rotation of the magnetization by application of an external strain, which, of course, has no effect in a tetrahedral ferromagnetic nematic phase, since the latter is fluid.

As hydrodynamic variables one can use the (three) combined rigid rotations of the tetrahedral structure together with the magnetization. An alternative possibility, more appropriate to the magnetic nature of the phase (and the application of external magnetic fields) is the use of the two magnetization rotations $\delta \mathbf{m}$ (implying an appropriate co-rotation of the tetrahedral structure to preserve rigidly the combined structure) and a rotation of the tetrahedral structure about the magnetization, $\delta \Omega$. The latter is not just a scalar variable, but has rather unusual rotational properties [32, 49].

We describe the elastic properties of a gel by the linearized version of the strain field $\varepsilon_{ij} = \frac{1}{2}(\nabla_i u_j + \nabla_j u_i)$ with u_i the displacement field of the network. Note that ε_{ij} is invariant under time reversal and spatial inversion. For a hydrodynamic implementation of nonlinear elasticity, see refs. [55, 56]. We also consider as macroscopic variables the relative rotations between the preferred direction m_i and the polymer network, defined linearly as $\tilde{O}_i = \delta m_i - \frac{1}{2}m_j(\nabla_i u_j - \nabla_j u_i)$. The relative rotations are transverse to the magnetization by construction ($m_i \tilde{O}_i = 0$), invariant under spatial inversion, but change sign under time reversal. For a nonlinear description of relative rotations we refer the reader to ref. [57]. From uniaxial nematic gels (with the director as preferred direction) it is well known that those relative rotations play a crucial role in the static and dynamic behavior of nematic gels [58, 59], and we expect similar importance for the magnetic case.

2.2 Thermodynamics and statics

In this section we deal with static deviations from the equilibrium state. Changes of the variables introduced above are related to changes of the total energy density f by the Gibbs relation, which is the local formulation of the first law of thermodynamics

$$\begin{aligned} df = & T d\sigma + \mu d\rho + v_i dg_i + \mu_c dc + h^M dM \\ & + h_i^{m'} dm_i + \Psi_{ij}^m d\nabla_j m_i + h^{\Omega'} d\Omega + \Psi_i^{\Omega} d\nabla_i \Omega \\ & + \Psi_{ij} d\varepsilon_{ij} + W_i d\tilde{O}_i, \end{aligned} \quad (1)$$

where we have explicitly considered gradients of the rotational degrees of freedom, since they are symmetry variables and, in the absence of any orienting fields or boundaries, changes of their orientations must not change the energy ($h_i^{m'} = 0 = h^{\Omega'}$). In the statics only the combinations

$$h_i^M = h_i^{M'} - \nabla_j \Psi_{ij}^M \quad \text{and} \quad h^\Omega = h^{\Omega'} - \nabla_i \Psi_i^\Omega \quad (2)$$

do occur.

The thermodynamic conjugates are the prefactors of the differentials in eq. (1), *i.e.* temperature T , chemical potential μ , velocity v_i , osmotic pressure (divided by the pressure) μ_c , so-called molecular fields of the magnetic order h^M , of the magnetization rotations h_i^m , of rotations about the magnetization h^Ω and the elastic stress, Ψ_{ij} and the molecular field corresponding to the relative rotations, W_i . They (or their gradients) act as thermodynamic forces in the dynamics (depending whether they are zero or finite in equilibrium).

The energy has to be rotationally invariant. This requires for eq. (1) the condition

$$\begin{aligned} 0 = & \epsilon_{ijk} (h_i^{m'} m_j + \Psi_{li}^m \nabla_j m_l + \Psi_{il}^m \nabla_l m_j + \Psi_i^\Omega \nabla_j \Omega \\ & + \Psi_{il} \varepsilon_{jl} + \Psi_{li} \varepsilon_{lj} + W_i \tilde{O}_j) - h^\Omega m_k, \end{aligned} \quad (3)$$

which will later be used to symmetrize the stress tensor. The last term in this condition is due the fact that Ω is not a scalar, but a component of a vector that is not invariant under rotation. To find its rotational behaviour one can use the fact that δT_{qkl} transforms under rotations like an ordinary vector in each of its indices [32].

Since the energy of the total volume, $F = \int f dV$, has to be a first order Eulerian form of the extensive variables, the thermodynamic pressure, $p \equiv -\partial F / \partial V$, can be written as a bilinear expression of the extensive variables and their thermodynamic conjugates with the final result (Gibbs-Duhem equation)

$$\begin{aligned} dp = & \sigma dT + \rho d\mu + g_i dv_i + c d\mu_c + M dh^M \\ & - h_i^{m'} dm_i - \Psi_{ij}^m d\nabla_j m_i - h^{\Omega'} d\Omega - \Psi_i^\Omega d\nabla_i \Omega \\ & - \varepsilon_{ij} d\Psi_{ij} - \tilde{O}_i dW_i. \end{aligned} \quad (4)$$

The thermodynamic conjugates are defined as partial derivatives of the total energy density with respect to the

appropriate variable. Thus they follow from a total energy functional that can be written as

$$f = f_0 + f_{\text{rotel}} + f_M + f_{\text{lin}} + f_{\text{el}} + f_{\text{rr}}, \quad (5)$$

where f_0 is the total energy of an isotropic liquid, f_{rotel} contains the rotational-elastic energy, f_M is the magnetic energy including external magnetic fields, and f_{el} contains the elastic energy and all cross-couplings of the strain tensor with the other variables (except relative rotations) and finally, f_{rr} , shows all contributions of the relative rotations.

When constructing the explicit forms of the various energy contributions one can make use of the Levi-Civita tensor ϵ_{ijk} , the tetrahedral structure T_{ijk} and the magnetic direction m_i , where the latter two are not really independent. One has to note that T_{ijk} is odd under spatial inversion and m_i is odd under time reversal. In particular we find [60]

$$\begin{aligned} f_0 = & \frac{T}{2C_V} (\delta\sigma)^2 + \frac{1}{2\rho^2 \kappa_s} (\delta\rho)^2 + \frac{\gamma}{2} (\delta c)^2 + \frac{1}{\rho \alpha_s} (\delta\sigma)(\delta\rho) \\ & + \beta_\sigma (\delta c)(\delta\sigma) + \beta_\rho (\delta c)(\delta\rho) + \frac{g_i^2}{2\rho} \end{aligned} \quad (6)$$

containing the standard thermodynamic susceptibilities, like specific heat, compressibility, thermal expansion etc.

Rotations of the magnetization must not increase the total energy of the system, since m_i is a symmetry variable. Therefore, only inhomogeneous rotations enter f_{rotel}

$$\begin{aligned} f_{\text{rotel}} = & \frac{1}{2} K_{ijkl} (\nabla_j m_i)(\nabla_l m_k) + \frac{1}{2} K_{ij}^\Omega (\nabla_i \Omega)(\nabla_j \Omega) \\ & + C_{ijk}^{m\Omega} (\nabla_i \Omega)(\nabla_k m_j) + \Pi_{ijk}^c (\nabla_i c)(\nabla_k m_j) \\ & + \Pi_{ijk}^\sigma (\nabla_i \sigma)(\nabla_k m_j) + \Pi_{ijk}^\rho (\nabla_i \rho)(\nabla_k m_j) \\ & + (\nabla_i \Omega) \left(C_{ij}^{c\Omega} \nabla_j c + C_{ij}^{\sigma\Omega} \nabla_j \sigma + C_{ij}^{\rho\Omega} \nabla_j \rho \right) \end{aligned} \quad (7)$$

with the rotational stiffness (or rotational elastic) tensors

$$\begin{aligned} K_{ijkl} = & K_1 \delta_{ij}^\perp \delta_{kl}^\perp + K_2 m_p m_q \epsilon_{ijp} \epsilon_{klq} \\ & + K_3 m_j m_l \delta_{ik}^\perp + K_4 m_p m_q T_{ikp} T_{jlq}, \end{aligned} \quad (8)$$

$$K_{ij}^\Omega = K_\perp^\Omega \delta_{ij}^\perp + K_\parallel^\Omega m_i m_j, \quad (9)$$

$$C_{ijk}^{m\Omega} = C_\perp (\epsilon_{jkp} m_i + \epsilon_{jip} m_k) m_p, \quad (10)$$

$$\Pi_{ijk}^\lambda = \Pi^\lambda (m_i \delta_{jk}^\perp + m_k \delta_{ij}^\perp), \quad (11)$$

$$C_{ij}^{\lambda\Omega} = C_\perp^\lambda m_k T_{kps} (\epsilon_{irs} T_{jpr} + \epsilon_{jrs} T_{ipr}), \quad (12)$$

where $\lambda \in \{\sigma, \rho, c\}$. The structure of f_{el} is isomorphic to the gradient energy in the D_{2d} phase and contains 4 coefficients related to bending distortions of the magnetization, 2 related to inhomogeneous rotations about the magnetization and 1 mixed one. In addition there are cross-couplings of those inhomogeneous rotations with gradients of the scalar conserved variables. We note that the contribution $\sim C_\perp$ is associated with $\nabla \times \mathbf{m}$; while this quantity typically vanishes statically, this need not be the case dynamically¹.

¹ The appropriate term $\sim K_7$ in refs. [49] and [32] should have the form of eq. (11)

The magnetic part of the free energy in eq. (5) reads

$$f_M = -M_i H_i + \frac{1}{2} \alpha M^2 + \frac{1}{4} \beta M^4 + f_{gM}, \quad (13)$$

where f_{gM} contains gradients of the magnetic order parameter M , which are often neglected, but come here in parallel to gradients of the magnetic direction m_j . The homogeneous part of f_M is derived in sect. 2.4 taking into account the static magnetic Maxwell equations. f_M is the Legendre transformed magnetic energy containing the magnetic field \mathbf{H} . The ferromagnetic coupling in f_M leads to the parallel equilibrium orientation of the magnetization along an external magnetic field. As a result a homogeneous external field is compatible with a homogeneous combined magnetization/tetrahedral structure in the D_{2d}^m phase. However, the degeneracy of the (combined) orientation of the magnetization and the tetrahedral structure is partially lifted and only the orientation of the structure perpendicular to the field (and \mathbf{m}) is still arbitrary. A discussion on how the degeneracy can completely be eliminated by additional (*e.g.*, electric fields) is discussed below.

For the magnetic gradient energy we find

$$\begin{aligned} f_{gM} = & \frac{1}{2} K_{ij}^M (\nabla_i M) (\nabla_j M) + C_{ij}^{M\Omega} (\nabla_i M) (\nabla_j \Omega) \\ & + K_{ijk}^{Mm} (\nabla_i M) (\nabla_j m_k) \\ & + (\nabla_i M) \left(\Pi_{ij}^{cM} \nabla_j c + \Pi_{ij}^{\sigma M} \nabla_j \sigma + \Pi_{ij}^{\rho M} \nabla_j \rho \right) \end{aligned} \quad (14)$$

with

$$K_{ij}^M = K_{\perp}^M \delta_{ij}^{\perp} + K_{\parallel}^M m_i m_j, \quad (15)$$

$$C_{ij}^{M\Omega} = C_{\parallel} m_k T_{kps} (\epsilon_{irs} T_{jpr} + \epsilon_{jrs} T_{ipr}), \quad (16)$$

$$K_{ijk}^{Mm} = K^{Mm} (m_j \delta_{ik}^{\perp} + m_i \delta_{jk}^{\perp}), \quad (17)$$

$$\Pi_{ij}^{\lambda M} = \Pi_{\perp}^{\lambda M} \delta_{ij}^{\perp} + \Pi_{\parallel}^{\lambda M} m_i m_j, \quad (18)$$

where $\lambda \in \{\sigma, \rho, c\}$. There are two stiffness coefficients ($K_{\perp}^M, K_{\parallel}^M$) related to distortions of M . Cross-couplings between distortions of M and inhomogeneous rotations of, and about the magnetization, are described by one coefficient each (K^{Mm} and C_{\parallel} , respectively), while there are in total six coefficients ($\Pi_{\perp, \parallel}^{\lambda M}$) connected to the coupling of gradients of M with gradients of the scalar conserved variables.

The next energy contribution we are discussing here is the linear gradient energy

$$f_{\text{lin}} = \xi T_{ijk} m_i (\nabla_j m_k). \quad (19)$$

This expression is identical to the linear gradient term in the D_{2d} phase [32], when m_i is replaced by the director n_i . This linear gradient term is allowed due to the presence of tetrahedral order, which breaks parity. As a consequence, the ground state might not be homogeneous, resembling the case of added chirality to nematic liquid crystals. However, here is no chirality involved and helices of both rotation sense are equally well possible (ambidextrous chirality) [49]. This is further investigated in appendix A.

The elastic part of the energy reads

$$\begin{aligned} f_{\text{el}} = & \frac{1}{2} c_{ijkl} \varepsilon_{ij} \varepsilon_{kl} - \gamma_{ij} \varepsilon_{ij} M_0 \delta M \\ & + (\chi_{ij}^{\sigma} \delta \sigma + \chi_{ij}^{\rho} \delta \rho + \chi_{ij}^c \delta c) \varepsilon_{ij} \\ & + \left(\tau_{ijk}^{\sigma} \nabla_k \sigma + \tau_{ijk}^c \nabla_k c + \tau_{ijk}^{\rho} \nabla_k \rho + \tau_{ijk}^M \nabla_k M \right) \varepsilon_{ij} \\ & + \chi_{ijk}^{\Omega} \varepsilon_{ij} \nabla_k \Omega + \chi_{ijkl}^m \varepsilon_{ij} \nabla_l m_k. \end{aligned} \quad (20)$$

The first two lines of f_{el} are known from uniaxial magnetic gels [18]. The elastic tensor c_{ijkl} is of the form of the viscosity tensor, eq. (46), and has six elastic moduli, $c_{1, \dots, 6}$, one more than in uniaxial magnetic gels due to the tetrahedral order. The rank-2 tensors are of the standard uniaxial form, eq. (15), and describe magnetostriction as well as elastic deformations due to changes in temperature, density or concentration. The third line describes static couplings between gradients of temperature, density, concentration or magnitude of the magnetization with elastic deformations with the tensors

$$\tau_{ijk}^{\lambda} = \left(\tau_{\perp}^{\lambda} \delta_{kl}^{\perp} + \tau_{\parallel}^{\lambda} m_k m_l \right) T_{ijl} \quad (21)$$

containing two coefficients for each $\lambda \in \{\sigma, \rho, c, M\}$. In ref. [51] such a coupling is also present, but shows only one coefficient for each λ due to the optically isotropic nature of the T_d phase. The fourth line contains couplings genuine for the D_{2d}^{mg} phase between elastic deformations and inhomogeneous rotations of the tetrahedral/magnetization structure with the material tensors

$$\chi_{ijk}^{\Omega} = \chi_1^{\Omega} (\epsilon_{ipr} T_{jkp} + \epsilon_{jpr} T_{ikp}) m_r + \chi_2^{\Omega} \epsilon_{kpr} T_{ijp} m_r, \quad (22)$$

$$\chi_{ijkl}^m = \delta_{kp}^{\perp} (\chi_1^m [T_{ipl} m_j + T_{jpl} m_i] + \chi_2^m T_{ijp} m_l). \quad (23)$$

Finally, the energy containing relative rotations

$$\begin{aligned} f_{\text{rr}} = & \frac{1}{2} D_1 \tilde{O}_i \tilde{O}_i + D_2 (m_j \delta_{ik}^{\perp} + m_k \delta_{ij}^{\perp}) \tilde{O}_i \varepsilon_{jk} \\ & + (\psi_{ij}^c \nabla_i c + \psi_{ij}^{\rho} \nabla_i \rho + \psi_{ij}^{\sigma} \nabla_i \sigma + \psi_{ij}^M \nabla_i M) \tilde{O}_j \end{aligned} \quad (24)$$

contains the stiffness of relative rotations, D_1 , and the standard uniaxial coupling between elasticity and relative rotations, D_2 , well known from nematic and magnetic gels. The second line describes the genuine couplings of gradients of temperature, density, concentration, and magnitude of the magnetization with relative rotations in the D_{2d}^{mg} phase by

$$\psi_{ij}^{\lambda} = \psi^{\lambda} m_k T_{ijk}. \quad (25)$$

The expressions for the thermodynamic conjugates that follow from the energy contributions introduced above are listed in appendix A.

2.3 Dynamic equations

The hydrodynamic variables can be put into two different classes. There are conserved variables, like the mass density, energy density and momentum density \mathbf{g} , which are

governed by conservation laws. The second class of variables corresponds to the variables associated with spontaneously broken continuous symmetries. Their dynamics is governed by balance laws. In our case we have from this class the magnetization and the rotation around the magnetization Ω . There are some variables, that relax on a finite but very long time scale and it is therefore sensible to include them into the macroscopic description, ref. [60]. In our case we will consider the relative rotations \tilde{O}_i , which are important, if the magnetization and the strain are weakly coupled.

The dynamic equations read

$$\frac{\partial}{\partial t} f + \nabla_i ([f + p]v_i + j_i^f) = 0, \quad (26)$$

$$\frac{\partial}{\partial t} \rho + \nabla_i g_i = 0, \quad (27)$$

$$\frac{\partial}{\partial t} g_i + \nabla_j (g_i v_j + p \delta_{ij} + \sigma_{ij}^{th} + \sigma_{ij}) = 0, \quad (28)$$

$$\frac{\partial}{\partial t} \sigma + \nabla_i (\sigma v_i + j_i^\sigma) = \frac{2R}{T}, \quad (29)$$

$$\rho \left(\frac{\partial}{\partial t} + v_j \nabla_j \right) c + \nabla_i j_i^c = 0, \quad (30)$$

$$\left(\frac{\partial}{\partial t} + v_j \nabla_j \right) M + X^M = 0, \quad (31)$$

$$\left(\frac{\partial}{\partial t} + v_j \nabla_j \right) m_i - \epsilon_{ijk} \omega_j m_k + X_i^m = 0, \quad (32)$$

$$\left(\frac{\partial}{\partial t} + v_j \nabla_j \right) \Omega - m_i \omega_i + Z = 0, \quad (33)$$

$$\left(\frac{\partial}{\partial t} + v_k \nabla_k \right) \epsilon_{ij} + Y_{ij}^{th} + Y_{ij} = 0, \quad (34)$$

$$\left(\frac{\partial}{\partial t} + v_j \nabla_j \right) \tilde{O}_i + \epsilon_{ijk} \tilde{O}_j \omega_k + Y_i^O = 0 \quad (35)$$

with the vorticity $\omega_i = (1/2)\epsilon_{ijk}\nabla_j v_k$. The vorticity contributions are due to the fact that m_i and \tilde{O}_i transform under spatial rotations as vectors, and Ω as a special component of a vector [49]. These terms ensures that only those rotations enter hydrodynamics that go beyond the global rotation (*e.g.*, of the coordinate system). In eq. (33) the $m_i \omega_i$ term shows again that Ω is not a scalar quantity.

In eq. (34) we have introduced the non-phenomenological current of the strain as

$$Y_{ij}^{th} = -A_{ij} + \epsilon_{kj} \nabla_i v_k + \epsilon_{ki} \nabla_j v_k \quad (36)$$

containing $A_{ij} = (1/2)(\nabla_i v_j + \nabla_j v_i)$ due to the translational nature of the displacement field, as well as the rotational part of the time derivative of the strain tensor.

In eq. (28) we have explicitly written down the non-phenomenological part of the stress tensor $\nabla_i p$, the pressure gradient given by eq. (4), and σ_{ij}^{th} given by

$$2\sigma_{ij}^{th} = \Psi_{kj}^m \nabla_i m_k + \Psi_{ki}^m \nabla_j m_k + \Psi_j^\Omega \nabla_i \Omega + \Psi_i^\Omega \nabla_j \Omega + \nabla_k (m_j \Psi_{ik}^m - m_i \Psi_{jk}^m) - 2\Psi_{ij} + \Psi_{ik} \epsilon_{kj} + \Psi_{jk} \epsilon_{ki}, \quad (37)$$

which has been brought, using eq. (3), into the form [61] that guarantees angular momentum conservation [62]. The three last terms describe linear and nonlinear elastic stresses.

The source term in the dynamic evolution equation for the entropy density, eq. (29), is proportional to the dissipation function R representing (half of) the rate at which the heat is transferred to the microscopic degrees of freedom. The second law of thermodynamics requires $R > 0$ for dissipative processes, while $R = 0$ holds for the reversible parts of the currents, in which case eq. (29) is a conservation law. Splitting the phenomenological currents ($j_i^f, \sigma_{ij}, j_i^\sigma, j_i^c, X^M, X_i^m, Z, Y_{ij}, Y_i^O$) into the dissipative part (superscript D) and the reversible one (superscript R) the Gibbs relation eq. (1) then leads to the condition

$$2R = -\nabla_i j_i^{fD} - j_i^{\sigma D} \nabla_i T - j_i^{cD} \nabla_i \mu_c - \sigma_{ij}^D A_{ij} + X_i^{mD} h_i^m + X^{MD} h^M + Z^D h^\Omega + Y_{ij}^D \Psi_{ij} + Y_i^{OD} W_i > 0 \quad (38)$$

for dissipative processes, where only the symmetrized velocity gradient A_{ij} enters, in order to prevent solid body rotations to produce entropy.

For reversible currents, the condition

$$0 = -\nabla_i j_i^{fR} - j_i^{\sigma R} \nabla_i T - j_i^{cR} \nabla_i \mu_c - \sigma_{ij}^R A_{ij} + X^{MR} h^M + X_i^{mR} h_i^m + Z^R h^\Omega + Y_{ij}^R \Psi_{ij} + Y_i^{OR} W_i \quad (39)$$

applies. Possible pure divergence contributions (surface terms) are put into j_i^f , but are not needed in the following. The various transport contributions in the time derivatives of eqs. (26)–(35) are all reversible. Their zero entropy production is ensured by the non-phenomenological parts of the stress tensor σ_{ij}^{th} and by the pressure p . Similarly, Y_{ij}^{th} compensates the linear and nonlinear elastic stresses in σ_{ij}^{th} to give $R = 0$.

A current is reversible, if it transforms under time reversal in the same way as the time derivative of the appropriate variable, while the dissipative part of a current has the opposite time reversal behavior. In the following we will discuss the dissipative and reversible dynamics separately.

To derive the dissipative parts of the phenomenological currents one first writes the dissipation function as a positive quadratic form in the thermodynamic forces taking into account that R has to be a time reversal symmetric, scalar quantity. By taking the variational derivative of this function with respect to the chosen thermodynamic force one gets the corresponding dissipative current. The dissipation function reads

$$R = \frac{1}{2} \kappa_{ij} (\nabla_i T) (\nabla_j T) + \frac{1}{2} D_{ij} (\nabla_i \mu_c) (\nabla_j \mu_c) + D_{ij}^T (\nabla_i T) (\nabla_j \mu_c) + \Gamma_{ijk}^{(2)} A_{ij} \nabla_k T + \Gamma_{ijk}^{(3)} A_{ij} \nabla_k \mu_c + \frac{1}{2} \nu_{ijkl}^D A_{ij} A_{kl} + c_{ijk}^D A_{ij} h_k^m + c_{ij}^M A_{ij} h^M + \tau_{ij} A_{ij} h^\Omega + T_{ijk} m_j (\psi^{TD} \nabla_k T + \psi^{cD} \nabla_k \mu) h_i^m$$

$$\begin{aligned}
& + \frac{1}{2} b_{ij}^D h_i^m h_j^m + \frac{1}{2} b^M h^M h^M + \frac{1}{2} b^\Omega h^\Omega h^\Omega \\
& + \frac{1}{2} D_{ij}^\Psi (\nabla_k \Psi_{ik}) (\nabla_l \Psi_{jl}) + \frac{1}{2} \tau^W W_i W_i \\
& + (\xi_{ij}^T \nabla_i T + \xi_{ij}^c \nabla_i \mu_c + \xi_{ij}^M \nabla_i h^M) (\nabla_k \Psi_{jk}) \\
& + \xi_{ijk}^A A_{ij} W_k + T_{ijk} m_k (p^W W_i + p^m h_i^m) \nabla_l \Psi_{jl} \\
& + T_{ijk} m_k (p^T \nabla_j T + p^c \nabla_j \mu_c + p^M \nabla_j h^M) W_i \\
& + f_{ijk}^D A_{ij} \nabla_l \Psi_{kl} + \xi^{Wm} \delta_{ij}^\perp W_i h_j^m. \quad (40)
\end{aligned}$$

Note that we have used the divergence of the elastic stress, $\nabla_j \Psi_{ij}$, as the thermodynamic force, rather than the elastic stress tensor itself, Ψ_{ij} . Using the latter there are additional contributions to the dissipation function, which will be discussed in detail in sect. 4 on transient networks. Since we assume in this section that the network of the gel is permanent, elastic strains can only diffuse, but not relax. Therefore we discard the part of the dissipation function associated with transient networks, eq. (87), and write in the following the elastic currents in the form

$$Y_{ij}^{D,R} = -\frac{1}{2} \left(\nabla_j F_i^{D,R} + \nabla_i F_j^{D,R} \right), \quad (41)$$

which reflects the definition of the linear strain tensor. In terms of the displacement vector. The dissipative expression F_i^D follows from eq. (40) by $F_i^D = \partial R / (\partial \nabla_k \Psi_{ik})$.

The dissipative currents for permanent networks will be given explicitly in appendix B.

The dissipative material tensors κ_{ij} , D_{ij} , D_{ij}^T , τ_{ij} , D_{ij}^Ψ , ξ_{ij}^T , ξ_{ij}^c and ξ_{ij}^M are of the standard uniaxial form

$$\zeta_{ij}^D = \zeta_1^D \delta_{ij}^\perp + \zeta_2^D m_i m_j \quad (42)$$

with a perpendicular and a parallel component, while the others read

$$\Gamma_{ijk}^{(2)} = \Gamma_{21}^D \epsilon_{kpr} T_{ijp} m_r + \Gamma_{22}^D (\epsilon_{ipr} T_{kjp} m_r + \epsilon_{jpr} T_{kip} m_r), \quad (43)$$

$$\Gamma_{ijk}^{(3)} = \Gamma_{31}^D \epsilon_{kpr} T_{ijp} m_r + \Gamma_{32}^D (\epsilon_{ipr} T_{kjp} m_r + \epsilon_{jpr} T_{kip} m_r), \quad (44)$$

$$f_{ijk}^D = f_1^D \epsilon_{kpr} T_{ijp} m_r + f_2^D (\epsilon_{ipr} T_{kjp} m_r + \epsilon_{jpr} T_{kip} m_r), \quad (45)$$

$$\begin{aligned}
\nu_{ijkl}^D &= \nu_1 \delta_{ij}^\perp \delta_{kl}^\perp + \nu_2 (\delta_{ji}^\perp \delta_{ik}^\perp + \delta_{il}^\perp \delta_{jk}^\perp) \\
&+ \nu_3 m_i m_j m_k m_l + \nu_4 (\delta_{ij}^\perp m_k m_l + \delta_{kl}^\perp m_i m_j) \\
&+ \nu_5 (\delta_{ik}^\perp m_j m_l + \delta_{jk}^\perp m_i m_l + \delta_{il}^\perp m_j m_k + \delta_{jl}^\perp m_i m_k) \\
&+ \nu_6 m_p m_q T_{ijp} T_{klq}, \quad (46)
\end{aligned}$$

$$c_{ijk}^D = c_1^D (\epsilon_{ikp} m_j + \epsilon_{jkp} m_i) m_p, \quad (47)$$

$$\xi_{ijk}^A = \xi^A (\epsilon_{ikp} m_j + \epsilon_{jkp} m_i) m_p, \quad (48)$$

$$c_{ij}^M = c_2^D (\epsilon_{irs} T_{jpr} + \epsilon_{jrs} T_{ipr}) m_k T_{kps}. \quad (49)$$

The reversible parts of the currents do not follow from any potential, but can be derived by requiring that the

entropy production R in eq. (38) is zero. Replacing there $Y_{ij}^R \Psi_{ij}$ by $F_i^R \nabla_k \Psi_{ik}$ one gets

$$j_i^{\sigma R} = -\kappa_{ij}^R \nabla_j T - D_{ij}^{TR} \nabla_j \mu_c + \psi_{ij}^T h_j^m + \Gamma_{kji}^T A_{jk} - d_{ij}^T W_j - f^T \epsilon_{ijk} m_j \nabla_l \Psi_{kl}, \quad (50)$$

$$j_i^{cR} = -D_{ij}^R \nabla_j \mu_c + D_{ij}^{TR} \nabla_j T + \psi_{ij}^c h_j^m + \Gamma_{kji}^c A_{jk} - d_{ij}^c W_j - f^c \epsilon_{ijk} m_j \nabla_l \Psi_{kl}, \quad (51)$$

$$\begin{aligned}
\sigma_{ij}^R &= -\nu_{ijkl}^R A_{kl} - c_{kij}^R h_k^m - c_{ij}^R h^M - \tau_{ij}^R h^\Omega \\
&+ d^A (m_i \delta_{kj}^\perp + m_j \delta_{ki}^\perp) W_k + f_{kji}^A \nabla_l \Psi_{kl} \\
&- \Gamma_{ijk}^T \nabla_k T - \Gamma_{ijk}^c \nabla_k \mu_c, \quad (52)
\end{aligned}$$

$$X_i^{mR} = b_{ij}^R h_j^m - c_{ijk}^R A_{jk} + \psi_{ji}^T \nabla_j T + \psi_{ji}^c \nabla_j \mu_c + d^{m\epsilon} \epsilon_{ijk} m_j W_k, \quad (53)$$

$$X^{MR} = -c_{ij}^R A_{ij}, \quad (54)$$

$$Z^R = -\tau_{ij}^R A_{ij} + f_{ij}^\Omega \nabla_j \nabla_k \Psi_{ik}, \quad (55)$$

$$F_i^R = d_{ki}^\Psi W_k + f^T \epsilon_{ijk} m_j \nabla_k T + f^c \epsilon_{ijk} m_j \nabla_k \mu_c + f^\Psi \epsilon_{ijk} m_j \nabla_l \Psi_{kl} + f_{ij}^\Omega \nabla_j h^\Omega + f_{ijk}^A A_{jk}, \quad (56)$$

$$Y_i^{OR} = d_{ij}^T \nabla_j T + d_{ij}^c \nabla_j \mu_c + d_{ij}^\Psi \nabla_k \Psi_{jk} + d^W \epsilon_{ijk} m_j W_k + d^m \epsilon_{ijk} m_j h_k^m + d^A (m_k \delta_{il}^\perp + m_l \delta_{ik}^\perp) A_{kl}, \quad (57)$$

where the tensors f_{ij}^Ω and c_{ij}^R are of the standard uniaxial form, eq. (15) with two coefficients $f_{\perp,\parallel}^\Omega$ and $c_{\perp,\parallel}^R$, respectively. The antisymmetric tensors κ_{ij}^R , D_{ij}^{TR} , D_{ij}^R , and b_{ij}^R have only one coefficients and are of the form

$$\kappa_{ij}^R = \kappa^R \epsilon_{ijk} m_k, \quad (58)$$

while for the other tensors we find

$$\psi_{ij}^{c,T} = \psi^{c,T} \epsilon_{ipr} T_{jpk} m_k m_r, \quad (59)$$

$$d_{ij}^{T,c,\Psi} = d^{T,c,\Psi} \epsilon_{ipr} T_{jpk} m_k m_r, \quad (60)$$

$$\begin{aligned}
\nu_{ijkl}^R &= \nu_1^R (\epsilon_{ikp} \delta_{jl}^\perp + \epsilon_{jkp} \delta_{il}^\perp + \epsilon_{ilp} \delta_{jk}^\perp + \epsilon_{jlp} \delta_{ik}^\perp) m_p \\
&+ \nu_2^R (\epsilon_{ikp} m_j m_l + \epsilon_{jlp} m_i m_k + \epsilon_{ilp} m_j m_k \\
&+ \epsilon_{jkp} m_i m_l) m_p + \nu_3^R T_{ijp} T_{klr}, \epsilon_{prs} m_s, \quad (61)
\end{aligned}$$

$$c_{ijk}^R = c_1^R (m_j \delta_{ik}^\perp + m_k \delta_{ij}^\perp), \quad (62)$$

$$\tau_{ij}^R = \tau^R (\epsilon_{irs} T_{jpr} + \epsilon_{jrs} T_{ipr}) m_k T_{kps}, \quad (63)$$

$$\Gamma_{kji}^{T,c} = T_{qjk} \left(\Gamma_{\perp}^{T,c} \delta_{qi}^\perp + \Gamma_{\parallel}^{T,c} m_q m_i \right), \quad (64)$$

$$f_{ijk}^A = T_{qjk} \left(f_{\perp}^A \delta_{qi}^\perp + f_{\parallel}^A m_q m_i \right). \quad (65)$$

The dissipative coupling between flow and gradients of temperature and concentration, described by Γ_{21}^D , Γ_{22}^D , Γ_{31}^D and Γ_{32}^D in eqs. (43) and (44), is genuine for magnetic tetrahedral fluids, while their reversible counterparts, $\Gamma_{\perp}^{T,c}$ and $\Gamma_{\parallel}^{T,c}$ and in eqs. (50) and (51), are already known from the nematic tetrahedral D_{2d} phase, refs. [32, 49], and for $\Gamma_{\perp}^{T,c} = \Gamma_{\parallel}^{T,c}$ from the isotropic T_d phase, refs. [27, 49]. Similarly, for the reversible cross-coupling between rotations of the magnetization and gradients of temperature and concentration, $\psi_{ij}^{c,T}$, eq. (59), are already found

in D_{2d} . Their dissipative counterparts, ψ^{TD} and ψ^{cD} , eqs. (B.1), (B.2) and (B.4), are genuine for a tetrahedral ferromagnetic (fluid) phase. This is also true for the dissipative coupling between flow and changes of M , provided by c_{ij}^M , eq. (49), and the reversible coupling between flow and rotations about the magnetization, τ_{ij}^R , eq. (63). Couplings provided by f_1^D , f_2^D , p^W , p^m , p^T , p^c are genuine for the D_{2d}^{mg} phase and require the simultaneous presence of tetrahedral and magnetic order and of elasticity.

2.4 External fields

In the case that we have not only an external magnetic, but also an electric field, there are many competing orienting energy contributions

$$\begin{aligned} f_{\text{fields}} = & -M_i H_i + a T_{ilk} T_{jmk} M_i M_l M_j M_m \\ & -\zeta_1 T_{ijk} E_i E_j E_k - \zeta_2 T_{ijk} E_i H_j H_k \\ & -\zeta_3 T_{ijk} E_i M_j H_k - \zeta_4 T_{ijk} E_i M_j M_k, \end{aligned} \quad (66)$$

which we discuss in the spirit of a Landau description. The first term, the ferromagnetic coupling between the magnetization and the external magnetic field, aligns the magnetization along the field and the second one governs the relative orientation of the magnetization with the tetrahedron, which for $a > 0$, leads to the D_{2d}^{mg} structure. The terms $\sim \zeta_{1,2}$ are the typical couplings of external fields with the tetrahedral orientation, present in any tetrahedral phase. The last two terms $\sim \zeta_{3,4}$ are specific for the magnetic tetrahedral phase.

A full minimization of f_{fields} is beyond the scope of this work. We look for some special cases. First, we assume that the energy contribution $\sim a$, which defines the structure of the D_{2d}^{mg} phase, is the dominant one ($a \rightarrow \infty$). In that case the energy contribution $\sim \zeta_4$ is identically zero for all orientations of the fields. The ferromagnetic energy is minimal for the magnetization (and thus the $\bar{4}$ axis of the tetrahedron) to be parallel with the magnetic field (z -axis), while the cubic electric field contribution is minimal, if the electric field is parallel (for $\zeta_1 > 0$) or antiparallel (for $\zeta_1 < 0$) to one of the tetrahedral axes. However, the tetrahedral vectors make a finite angle $\theta_T/2$ (with $\cos(\theta_T/2) = \pm 1/\sqrt{3}$) with the $\bar{4}$ axes, leading to frustration (except for the very special case that the two external fields make an angle of $\theta_T/2$). Since the magnetic field does not fix the transverse structure, the energy $\sim \zeta_1$ can be minimized independently with regard to this transverse direction. As a result, the directions $\hat{e}_x \pm \hat{e}_y$ are given by (the tilt direction of) the electric field (the $\zeta_{2,3}$ energies do not change that statement).

The frustration of the orientation of the magnetization (or $\bar{4}$ axis) with respect to the orientation of the external fields, can be discussed along the lines of the liquid crystal case [32]. For strong magnetic and weak electric fields the ferromagnetic energy will win, while for weak magnetic and strong electric fields the magnetization will approach the orientation of the electric field. The transition process

is governed by the parameters $\beta_{1,2,3}$, indicating the balance of ferromagnetic energy to those including electric fields, $\sim \zeta_{1,2,3}$, respectively

$$\beta_1 = \frac{M_0 H_0}{\zeta_1 T_0 E_0^3}, \quad (67)$$

$$\beta_2 = \frac{M_0}{\zeta_2 T_0 E_0 H_0}, \quad (68)$$

$$\beta_3 = \frac{1}{\zeta_3 T_0 E_0}. \quad (69)$$

Qualitatively, a large β_1 leads to an orientation of the magnetization close to that of the magnetic field, while a small β_1 results in an orientation close to the electric field. The parameters $\beta_{2,3}$ come into play only for orientations in-between, neither very close to the magnetic, nor very close to the electric field.

If there is only an electric, but no magnetic field, the former fixes the orientation of the tetrahedron according to the ζ_1 energy. In the case of the D_{2d}^{mg} phase, where the magnetization is along one of the $\bar{4}$ axes, however, the ζ_1 energy vanishes and the electric field does not orient the tetrahedron. But the electric field induces elastic deformations according to the energy

$$f_{\text{elast}} = -\zeta_\varepsilon T_{ijk} E_i \varepsilon_{jk} \quad (70)$$

that leads to elastic stresses

$$\begin{aligned} \Psi_{xy}^{es} &= \zeta_\varepsilon \tilde{T}_0 E_{\parallel}, \\ \sqrt{(\Psi_{xz}^{es})^2 + (\Psi_{yz}^{es})^2} &= \zeta_\varepsilon \tilde{T}_0 E_{\perp} \end{aligned} \quad (71)$$

for the field parallel to the magnetization (E_{\parallel}) and perpendicular to it (E_{\perp}), respectively. The elastic stresses are compensated by appropriate deformations in the equilibrium state. This constitutes *linear electrostriction* in a magnetic phase that does not possess a permanent electric polarization.

On the other hand, there is a permanent magnetization and therefore magnetostriction

$$f_{\text{mstrict}} = -\frac{1}{2} \gamma_{ijkl} M_k M_l \varepsilon_{ij} \quad (72)$$

leading to elastic strains of a completely different form

$$\begin{aligned} \Psi_{xx}^{ms} &= \Psi_{yy}^{ms} = -\gamma_{\perp} M_0^2, \\ \Psi_{zz}^{ms} &= -\gamma_{\parallel} M_0^2. \end{aligned} \quad (73)$$

In equilibrium they are compensated by appropriate deformations, and hydrodynamic deviations are described by the energy $\sim \gamma_{ij}$ in eq. (20), with $\gamma_{ij} = \gamma_{ijzz}$. In the case of an additional external magnetic field (but without an electric one) M_0 is replaced by $M_0 + H_0$. In the presence of both external fields the striction deformations are extremely complicated due to the complicated orientation of the tetrahedron.

From eqs. (71) and (73) we read off immediately that external electric and magnetic fields lead to an anisotropy

of the stresses and thus also of the associated strains. This anisotropy, which is probably very small, is neglected. We note that the coefficient α in eq. (13) is also modified by external fields due to the effects of the equilibrium strains ε_{ij}^0 . The corresponding anisotropy will be neglected as well.

3 Suggestions for experiments involving elasticity

In this section we discuss experiments that are specific for the ferromagnetic tetrahedral gel phases. In particular, we consider experiments in the homogeneous state with a constant orientation of the preferred direction. We propose experiments that probe static couplings specific for the presence of tetrahedral order in sect. 3.1. In particular, we consider static external strains applied to the gel that affect the magnitude and the orientation of the magnetization and the relative rotations. In addition, we show, how relative rotations can induce gradients of density, concentration, or temperature perpendicular to the magnetization. In sect. 3.2 we discuss strains induced dynamically by temperature gradients, as well as reversible and irreversible heat or concentration currents induced by relative rotations.

3.1 Static experiments

There is a static coupling between elastic stresses and the orientation of the magnetization in eq. (20) provided by the material tensor χ_{ijkl}^m with two coefficients $\chi_{1,2}^m$ in eq. (23). Together with the rotational stiffness energy of the magnetization in eq. (7), given by the Frank-type tensor K_{ijkl} , eq. (8), and neglecting other cross-couplings, the stationarity condition, $\Psi_{ij}^m = 0$, leads, for linear deviations from $\mathbf{m} = \mathbf{e}_z$, to

$$\nabla_z m_y = A \varepsilon_{xz}^0 \quad \text{and} \quad \nabla_z m_x = A \varepsilon_{yz}^0 \quad (74)$$

with $A = (\chi_1^m + \chi_2^m) \tilde{T}_0 / K_3$. This describes an inhomogeneous rotation of the magnetization out of the shear plane of the external strain ε_{xz}^0 or ε_{yz}^0 . This effect only occurs when tetrahedral order is present.

Similarly, a uniaxial compression along the preferred axis leads to linear deviations of the magnetization in the transverse plane given by

$$\nabla_x m_y = \nabla_y m_x = \frac{\chi_1^m}{2K_4 \tilde{T}_0} \varepsilon_{zz}^0. \quad (75)$$

This solution describes a spatial pattern, where the induced transverse magnetization is of constant magnitude ($m_x^2 + m_y^2 = \text{const}$) on circles around the z -axis, but changes its direction by 2π , when moving along the circle. This pattern has no splay, bend or twist character, but is quite special for tetrahedral order.

External strains (ε_{xz}^0 , ε_{yz}^0 , and $\varepsilon_{xx}^0 - \varepsilon_{yy}^0$) create spatial patterns of relative rotations, due to the $\chi_{1,2}^m$ coupling in eq. (22), which, however, might be difficult to observe.

A well-known effect of external strains applied to ferromagnetic gels is magnetostriction, the change of the magnitude of the magnetization. Using the magnetostrictive coupling, described by γ_{ij} in eq. (20), the homogeneous changes induced by compressional strains have the uniaxial form

$$M_0 \delta M = -\frac{\alpha}{\gamma_{\parallel}} \varepsilon_{zz}^0 - \frac{\alpha}{\gamma_{\perp}} (\varepsilon_{xx}^0 + \varepsilon_{yy}^0), \quad (76)$$

where α is the magnetic stiffness coefficient.

In ferromagnetic gels with tetrahedral structure, in addition, external shear strains change the magnitude of the magnetization

$$\alpha \delta M = -2\tau_{\parallel} \tilde{T}_0 \nabla_z \varepsilon_{xy}^0 - 2\tau_{\perp} \tilde{T}_0 (\nabla_y \varepsilon_{xz}^0 + \nabla_x \varepsilon_{yz}^0) \quad (77)$$

although the inhomogeneous external shear strains are probably not easy to apply.

Another possibility to probe magnetic and tetrahedral order is the application of a static relative rotation, \tilde{O}_i . Due to the coupling provided by ψ_{ij}^{λ} in eq. (24) or (A.11), this results in gradients of the scalar variables $\lambda \in \{\sigma, \rho, c, M\}$ perpendicular to m_i and \tilde{O}_i

$$\nabla_y \lambda = \frac{D_1}{\psi^{\lambda} \tilde{T}_0} \tilde{O}_x, \quad (78)$$

$$\nabla_x \lambda = \frac{D_1}{\psi^{\lambda} \tilde{T}_0} \tilde{O}_y \quad (79)$$

with ψ^{λ} defined in eq. (25).

3.2 Dynamic experiments

As an example for a dynamic coupling, we discuss induced stresses due to an external temperature gradient perpendicular to the direction of the magnetization. Such couplings are specific for tetrahedral order. Already in the fluid case, there is a dissipative, $\Gamma_{ijk}^{(2)}$, and reversible, Γ_{ijk}^T , coupling according to eqs. (B.3) and (52), respectively,

$$\sigma_{ij} = -\Gamma_{ijk}^{(2)} \nabla_k T - \Gamma_{ijk}^T \nabla_k T. \quad (80)$$

With the explicit form of the material tensors, eqs. (43) and (64), one gets for the temperature gradient applied along the x -axis, $\nabla_x T = \beta_0$ (and the magnetization along the z -axis) the induced stresses

$$\sigma_{xz} = \sigma_{zx} = \beta_0 \tilde{T}_0 (\Gamma_{21}^D + \Gamma_{22}^D), \quad (81)$$

$$\sigma_{yz} = \sigma_{zy} = \beta_0 \tilde{T}_0 \Gamma_{\perp}^T, \quad (82)$$

where the in-plane shear stresses are due to the dissipative coupling, while the shear stresses perpendicular to the temperature gradient result from the reversible coupling.

If the temperature gradient is along the y -axis, equivalent expressions for the appropriate induced stresses are found, with the same prefactor for the reversible coupling and opposite sign in the dissipative case. This reflects the

breaking of transverse isotropy by the tetrahedral order. A temperature gradient along the magnetic field does not induce any stresses.

In a fluid phase such constant stresses only act as possible boundary conditions for flow and are difficult to measure. In a gel phase the stress tensor also comprises the elastic stresses, which are easier measurable by mechanical means. However, in the gel case there are additional couplings that effectively add to the response of stresses on external temperature gradients. In particular, temperature gradients induce non-zero values of W_i , the molecular field of relative rotations, due to the stationary condition $Y_i^O = 0$. The couplings described by p^T and d^W in eqs. (B.8) and (57) are provided by the tetrahedral order. On the other hand, those induced non-zero values of W_i act as forces that give rise to additional stresses via ξ^A and d^A in eqs. (B.3) and (52). As a result, induced elastic stresses $\Psi_{xz} = \Psi_{zx}$ and $\Psi_{yz} = \Psi_{zy}$ are obtained that are proportional to $\beta_0 \tilde{T}_0$. The proportionality factors are lengthy expressions containing static susceptibilities and (in both cases) reversible and irreversible transport coefficients, which we will not show in detail here.

Applying a thermodynamic force W_i , by means of a relative rotation $W_i = D_1 \tilde{O}_i$, eq. (A.11), heat and concentration currents, both reversibly, eqs. (50) and (51), as well as irreversibly, eqs. (B.1) and (B.2) are triggered of the form

$$j_x^{(\sigma,c)R} = d^{(T,c)} \tilde{T}_0 W_x, \quad (83)$$

$$j_y^{(\sigma,c)R} = -d^{(T,c)} \tilde{T}_0 W_y, \quad (84)$$

and

$$j_x^{(\sigma,c)D} = p^{(T,c)} \tilde{T}_0 W_y, \quad (85)$$

$$j_y^{(\sigma,c)D} = p^{(T,c)} \tilde{T}_0 W_x, \quad (86)$$

where $d^{(T,c)}$ is defined in eq. (60).

4 On the influence of transient elasticity

If the elastic network is not permanent, but transient, strains are relaxing (rather than diffusing). This means that elastic stresses Ψ_{ij} act as thermodynamic forces (rather than $\nabla_j \Psi_{ij}$) and the dissipation function acquires additional contributions

$$R_{\text{relax}} = \frac{1}{2} \tau_{ijkl}^{\Psi} \Psi_{ij} \Psi_{kl} + \xi^{T\Psi} T_{ijk} \Psi_{ij} \nabla_k T + \xi^{c\Psi} T_{ijk} \Psi_{ij} \nabla_k c + \xi^{M\Psi} T_{ijk} \Psi_{ij} \nabla_k h^M. \quad (87)$$

The strain relaxation tensor τ_{ijkl}^{Ψ} has the same form as the viscosity tensor ν_{ijkl} in eq. (46) containing six relaxation times $\tau_1^{\Psi} - \tau_6^{\Psi}$. There are dissipative cross-couplings between the elastic stresses and temperature, concentration gradients and gradients of M . The form of the dissipative currents is given in appendix B.

The reversible currents have to fulfil the proper time-reversal symmetry requirements and must not increase the

entropy, *i.e.* they must fulfil eq. (39). Under that proviso we find

$$j_i^{\sigma R} = \xi^{TR} T_{jkm} \epsilon_{iml} m_l \Psi_{jk}, \quad (88)$$

$$j_i^{cR} = \xi^{cR} T_{jkm} \epsilon_{iml} m_l \Psi_{jk}, \quad (89)$$

$$X^{MR} = \xi^{MR} \epsilon_{klm} \nabla_k (m_l T_{ijk} \Psi_{ij}), \quad (90)$$

$$Y_{ij}^R = \tau_{ijkl}^R \Psi_{kl} + \xi^{TR} T_{ijk} \epsilon_{klm} m_l \nabla_m T + \xi^{cR} \epsilon_{klm} m_l \nabla_m c + \xi^{MR} T_{ijk} \epsilon_{klm} m_l \nabla_m h^M, \quad (91)$$

where the tensor τ_{ijkl}^R has the same form as ν_{ijkl}^R in eq. (61) with three parameters $\tau_1^R, \tau_2^R, \tau_3^R$. All the cross-couplings are possible due to the simultaneous presence of magnetic and tetrahedral order.

As far as static deformations are concerned, there is no difference between permanent and relaxing elasticity, and sect. 2.2 applies here as well.

If the elasticity is transient, one can induce elastic shear stresses directly using a temperature gradient. From eqs. (B.12) and (91) we get

$$Y_{ij} = (\tau_{ijkl}^{\Psi} + \tau_{ijkl}^R) \Psi_{kl} + (\xi^{TR} T_{ijk} \epsilon_{klm} m_l + \xi^{T\Psi} T_{ijm}) \nabla_m T. \quad (92)$$

A stationary solution for the elastic stress is then obtained by setting all components $Y_{ij} = 0$. These induced stresses are constant, and so are the additions to the heat current, eq. (B.9), preserving the stationarity of such solutions.

For a temperature gradient in the direction of the magnetization, shear stresses in the perpendicular plane are induced

$$\Psi_{xy} = \frac{\tilde{T}_0 \xi^{T\Psi} \nabla_z T}{2(\tau_2^{\Psi} + \tilde{T}_0^2 \tau_6^{\Psi}) + 8(\tau_1^R)^2 / \tau_2^{\Psi}} \quad (93)$$

involving dissipative as well as reversible transport parameters. The reversible couplings have also the effect of creating compressive stresses

$$\Psi_{xx} = -\Psi_{yy} = -\frac{2\tau_1^R}{\tau_2^{\Psi}} \Psi_{xy}, \quad \Psi_{zz} = 0. \quad (94)$$

The result given in eq. (94) demonstrates the significant difference between reversible dynamic effects studied here and static magnetostriction presented in eq. (73).

If the external temperature gradient is perpendicular to the magnetization, it defines a preferred direction in this plane, which we will take without loss of generality as the x -axis, $\nabla_x T \equiv \Delta$. Then, of course, the y -direction is fixed by $\mathbf{m} \times \nabla \mathbf{T}$. The orientation of the tetrahedron in the x/y -plane is arbitrary and the x, y, z components of the four tetrahedral vectors can be written as

$$T_{ijk} = \frac{T_0}{\sqrt{3}} \begin{pmatrix} C + S & -C - S & C - S & -C + S \\ -C + S & C - S & C + S & -C - S \\ 1 & 1 & -1 & -1 \end{pmatrix} \quad (95)$$

with $C = \cos \varphi$ and $S = \sin \varphi$. For $\varphi = 0$ the projections of the four tetrahedral vectors are along the bisections $(1/\sqrt{2})(\hat{e}_x \pm \hat{e}_y)$, while for $\varphi = \pi/4$ they are along the x - and y -axis, cf. fig. 1.

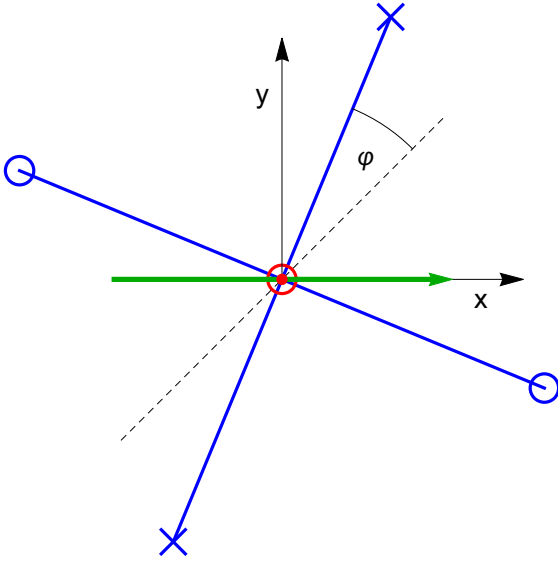


Fig. 1. The red circle in the middle indicates the magnetization perpendicular to the drawing plane, while the temperature gradient (green arrow) is along the x -axis. The blue lines show the projections of the tetrahedral vectors (where circles and the crosses represent vectors pointing out or into the plane, respectively).

Disregarding the reversible contributions in eq. (92) for the moment, we get the induced stresses

$$\Psi_{xz} = -\frac{\xi^{T\Psi} \tilde{T}_0 \Delta}{2\tau_5^{\Psi}} \sin(2\varphi), \quad (96)$$

$$\Psi_{yz} = \frac{\xi^{T\Psi} \tilde{T}_0 \Delta}{2\tau_5^{\Psi}} \cos(2\varphi). \quad (97)$$

As a result, the shear stresses are perpendicular to the temperature gradient for $\varphi = 0$, while for $\varphi = \pi/4$ the induced shear stress is in the x/z plane given by the magnetization and the temperature gradient. In the general case, both types of stresses are present. By measuring Ψ_{xz}/Ψ_{yz} one can determine the angle φ and therefore the orientation of the tetrahedron. Alternatively, one could change the orientation of the temperature gradient to find one of the two special cases discussed above.

Taking into account also the reversible couplings, the results get more complicated, but the general features are similar

$$\Psi_{xz} = \frac{Aa - Bb}{a^2 + b^2} \tilde{T}_0 \Delta, \quad (98)$$

$$\Psi_{yz} = \frac{Ba + Ab}{a^2 + b^2} \tilde{T}_0 \Delta \quad (99)$$

with

$$A = -\xi^{T\Psi} \sin(2\varphi) + \xi^{TR} \cos(2\varphi), \quad (100)$$

$$B = \xi^{T\Psi} \cos(2\varphi) + \xi^{TR} \sin(2\varphi), \quad (101)$$

$$a = 2\tau_5^{\Psi}, \quad (102)$$

$$b = 2\tau_2^R - 2\tau_3^R \tilde{T}_0^2. \quad (103)$$

The orientation of the tetrahedral vectors, for which the resulting shear stress is perpendicular to the temperature gradient, *i.e.* $\Psi_{xz} = 0$, is now given by

$$\tan(2\varphi) = -\frac{b\xi^{T\Psi} - a\xi^{TR}}{a\xi^{T\Psi} + b\xi^{TR}}. \quad (104)$$

The other special case, $\Psi_{yz} = 0$, is still obtained by $\varphi \rightarrow \varphi + \pi/4$.

5 Summary and perspective

The macroscopic dynamics of ferromagnetic gels with tetrahedral order is rather peculiar due to two aspects. First, the permanent magnetization that spontaneously breaks part of rotational symmetry, is a variable that changes sign under time reversal. Second, the tetrahedral order, not only lifts the transverse isotropy perpendicular to the magnetization, but also breaks inversion symmetry already of the ground state. For the D_{2d}^{mg} phase, where the orientation of the magnetization is rigidly coupled to one of the tetrahedral $\bar{4}$ directions, we have discussed in detail, in the statics as well as in the reversible and irreversible dynamics, the possible cross-couplings among the three rotational symmetry variables, the strain tensor, relative rotations between the elastic network and the magnetization, and the usual fluid degrees of freedom.

We describe experimentally accessible effects that are specific for the D_{2d}^{mg} phase. In particular, we show that static external deformations lead to spatial patterns in the orientation of the magnetization. Shear deformations with the preferred direction in the shear plane trigger rotations of the magnetization direction out of the shear plane, while longitudinal compressions along the preferred direction result in a complicated, characteristic spatial pattern of the magnetization in the transverse plane. Both effects are only possible due to the tetrahedral order. In addition to the standard linear magnetostriction effects in ferromagnetic gels, the D_{2d}^{mg} phase also shows a kind of linear electrostriction, where the application of an electric field results in elastic *shear* stresses. Although there is no polarization present in the ground state of this phase, the necessary breaking of inversion symmetry is provided by the tetrahedral order. Another consequence of the tetrahedral order is a change of the magnitude of the magnetization due to external distortional deformation. Finally, relative rotations lead to gradients in the temperature, density, concentration, and the magnitude of the magnetization.

From the dynamics of tetrahedral fluids it is well known that, *e.g.* temperature gradients give rise to constant shear stresses. In a gel phase the stress tensor comprises also elastic stresses, which are easier measurable by mechanical means. In addition, in D_{2d}^{mg} there are additional couplings, mediated by relative rotations, that effectively add to the response of elastic stresses on external temperature gradients. Conversely, relative rotations trigger heat (and concentration) currents in the plane perpendicular to the magnetization. In the case of transient elasticity the elasticity is not permanent, but can relax

either simply in the course of time (like polymers) or due to external (generalized) forces (eventually above a certain threshold value like in magneto-rheological systems). Here, the relaxation of strains can be compensated by *e.g.* external temperature gradients, such that stationary elastic stresses result. For gradients along the magnetization, elastic shear stresses, but also compressional ones (due to a specific reversible dynamic coupling), occur in the perpendicular plane. If the temperature gradient is perpendicular to the magnetization the resulting elastic shear stresses (in a plane that contains the magnetization direction) allow the identification of the transverse orientation of the tetrahedron relative to the gradient direction. This finding opens the door for the experiments investigating the orientation of the tetrahedron without the need of both magnetic and electric fields.

As a perspective it would be interesting to investigate the effects of dynamic (*e.g.*, oscillatory) shear experiments on the orientation of the tetrahedral structure. Since several variables couple to the velocity field, both reversibly and dissipatively, one might expect a rich behavior depending on the amplitude as well as the frequency of the oscillations. Of special interest are also the rotations around the magnetization, which couple dynamically (neglecting the inhomogeneous stress forces) only to flow. It would also be important to investigate how the additional elastic network will influence the recently investigated tetrahedral ferromagnetic nematic liquid crystals.

Open Access funding provided by Max Planck Society. Partial support of this work by HRB, HP and TP through the Schwerpunktprogramm SPP 1681 ‘‘Feldgesteuerte Partikel-Matrix-Wechselwirkungen: Erzeugung, skalenübergreifende Modellierung und Anwendung magnetischer Hybridmaterialien’’ of the Deutsche Forschungsgemeinschaft is gratefully acknowledged.

Author contribution statement

The authors have contributed equally to this paper.

Publisher’s Note The EPJ Publishers remain neutral with regard to jurisdictional claims in published maps and institutional affiliations.

Appendix A. Conjugate quantities

For convenience we give the explicit form of the conjugate quantities that follow from the energy functional f , eq. (5), by partial derivation

$$v_i \equiv \frac{\partial f}{\partial g_i} = \frac{1}{\rho} g_i, \quad (\text{A.1})$$

$$\begin{aligned} \delta T \equiv \frac{\partial f}{\partial \sigma} &= \frac{T}{C_V} \delta \sigma + \frac{1}{\rho \alpha_s} \delta \rho + \beta_\sigma \delta c - \nabla_i (\Pi_{ijk}^\sigma \nabla_k m_j \\ &+ \Pi_{ij}^{\sigma M} \nabla_j M + C_{ij}^{\sigma \Omega} \nabla_j \Omega) + \chi_{ij}^\sigma \varepsilon_{ij} - \tau_{ijk}^\sigma \nabla_k \varepsilon_{ij} \\ &- \psi_{ij}^\sigma \nabla_i \tilde{O}_j, \end{aligned} \quad (\text{A.2})$$

$$\begin{aligned} \delta \mu \equiv \frac{\partial f}{\partial \rho} &= \frac{1}{\rho^2 \kappa_s} \delta \rho + \frac{1}{\rho \alpha_s} \delta \sigma + \beta_\rho \delta c - \nabla_i (\Pi_{ijk}^\rho \nabla_k m_j \\ &+ \Pi_{ij}^{\rho M} \nabla_j M + C_{ij}^{\rho \Omega} \nabla_j \Omega) + \chi_{ij}^\rho \varepsilon_{ij} - \tau_{ijk}^\rho \nabla_k \varepsilon_{ij} \\ &- \psi_{ij}^\rho \nabla_i \tilde{O}_j, \end{aligned} \quad (\text{A.3})$$

$$\begin{aligned} \delta \mu_c \equiv \frac{\partial f}{\partial c} &= \gamma \delta c + \beta_\sigma \delta \sigma + \beta_\rho \delta \rho - \nabla_i (\Pi_{ijk}^c \nabla_k m_j \\ &+ \Pi_{ij}^{cM} \nabla_j M + C_{ij}^{c\Omega} \nabla_j \Omega) + \chi_{ij}^c \varepsilon_{ij} - \tau_{ijk}^c \nabla_k \varepsilon_{ij} \\ &- \psi_{ij}^c \nabla_i \tilde{O}_j, \end{aligned} \quad (\text{A.4})$$

$$\begin{aligned} h^M \equiv \frac{\partial f}{\partial M} &= -m_i H_i + \alpha M + \beta M^3 - \gamma_{ij} M_0 \varepsilon_{ij} \\ &- \tau_{ijk}^M \nabla_k \varepsilon_{ij} - \psi_{ij}^M \nabla_i \tilde{O}_j \\ &- \nabla_i (K_{ij}^M \nabla_j M + C_{ij}^{M\Omega} \nabla_j \Omega + K_{ijk}^{Mm} \nabla_j m_k \\ &+ \Pi_{ij}^{\sigma M} \nabla_j \sigma + \Pi_{ij}^{\rho M} \nabla_j \rho + \Pi_{ij}^{cM} \nabla_j c), \end{aligned} \quad (\text{A.5})$$

$$h_i^{m'} \equiv \frac{\partial f}{\partial m_i} = -M H_i, \quad (\text{A.6})$$

$$\begin{aligned} \Psi_{ij}^m \equiv \frac{\partial f}{\partial \nabla_j m_i} &= K_{ijkl} \nabla_l m_k + C_{kij}^{m\Omega} \nabla_k \Omega + K_{kji}^{Mm} \nabla_k M \\ &+ \chi_{klij}^m \varepsilon_{kl} + \Pi_{kij}^\sigma \nabla_k \sigma + \Pi_{kij}^\rho \nabla_k \rho + \Pi_{kij}^c \nabla_k c, \end{aligned} \quad (\text{A.7})$$

$$h_i^{\Omega'} \equiv \frac{\partial f}{\partial \Omega} = 0, \quad (\text{A.8})$$

$$\begin{aligned} \Psi_i^\Omega \equiv \frac{\partial f}{\partial \nabla_i \Omega} &= K_{ij}^\Omega \nabla_j \Omega + C_{ijk}^{m\Omega} \nabla_k m_j + C_{ij}^{M\Omega} \nabla_j M \\ &+ \chi_{kji}^\Omega \varepsilon_{kj} + C_{ij}^{\sigma\Omega} \nabla_j \sigma + C_{ij}^{\rho\Omega} \nabla_j \rho + C_{ij}^{c\Omega} \nabla_j c, \end{aligned} \quad (\text{A.9})$$

$$\begin{aligned} \Psi_{ij} \equiv \frac{\partial f}{\partial \varepsilon_{ij}} &= c_{ijkl} \varepsilon_{kl} - \gamma_{ij} M_0 \delta M + \chi_{ij}^\sigma \delta \sigma + \chi_{ij}^\rho \delta \rho \\ &+ \chi_{ij}^c \delta c + \tau_{ijk}^\sigma \nabla_k \sigma + \tau_{ijk}^c \nabla_k c + \tau_{ijk}^\rho \nabla_k \rho + \tau_{ijk}^M \nabla_k M \\ &+ \chi_{ijk}^\Omega \nabla_k \Omega + \chi_{ijkl}^m \nabla_l m_k + D_2 (m_i \delta_{kj}^\perp + m_j \delta_{ki}^\perp) \tilde{O}_k, \end{aligned} \quad (\text{A.10})$$

$$\begin{aligned} W_i \equiv \frac{\partial f}{\partial \tilde{O}_i} &= D_1 \tilde{O}_i + D_2 (m_j \delta_{ik}^\perp + m_k \delta_{ij}^\perp) \varepsilon_{jk} + \psi_{ji}^c \nabla_j c \\ &+ \psi_{ji}^\rho \nabla_j \rho + \psi_{ji}^\sigma \nabla_j \sigma + \psi_{ji}^M \nabla_j M. \end{aligned} \quad (\text{A.11})$$

Since the δ 's in eqs. (A.2)–(A.4) describe deviations from the constant equilibrium values of the appropriate variable, all expressions on the left-hand side of the above equations are zero in equilibrium and can act as thermodynamic forces that drive the dynamics of the system. On the other hand, the right-hand sides of all these equations have to be zero in equilibrium (Euler-Lagrange conditions). Note that the energy f_{lin} does not enter any Euler-Lagrange condition (except for $\nabla_l T_{ijk} \neq 0$), since it is linear in gradients of m_i .

Appendix B. Dissipative currents

For permanent elasticity the dissipative parts of the currents follow from the dissipation function R , eq. (40),

$$j_i^{\sigma D} \equiv -\frac{\partial R}{\partial \nabla_i T} = -\kappa_{ij} \nabla_j T - D_{ij}^T \nabla_j \mu_c$$

$$\begin{aligned} & -\psi^{TD} m_j T_{kji} h_k^m - \Gamma_{kji}^{(2)} A_{kj} - p^T T_{ijk} m_k W_j \\ & - \xi_{ij}^T \nabla_k \Psi_{jk}, \end{aligned} \quad (\text{B.1})$$

$$\begin{aligned} j_i^{cD} & \equiv -\frac{\partial R}{\partial \nabla_i \mu_c} = -D_{ij} \nabla_j \mu_c - D_{ji}^T \nabla_j T \\ & - \psi^{cD} m_j T_{kji} h_k^m - \Gamma_{kji}^{(3)} A_{kj} - p^c T_{ijk} m_k W_j \\ & - \xi_{ij}^c \nabla_k \Psi_{jk}, \end{aligned} \quad (\text{B.2})$$

$$\begin{aligned} \sigma_{ij}^D & \equiv -\frac{\partial R}{\partial A_{ij}} = -\nu_{ijkl}^D A_{kl} - c_{ijk}^D h_k^m - c_{ij}^M h^M - \tau_{ij} h^\Omega \\ & - \xi_{ijk}^A W_k - \Gamma_{ijk}^{(2)} \nabla_k T - \Gamma_{ijk}^{(3)} \nabla_k \mu_c - f_{ijk}^D \nabla_l \Psi_{kl}, \end{aligned} \quad (\text{B.3})$$

$$\begin{aligned} X_i^{mD} & \equiv \frac{\partial R}{\partial h_i^m} = b_\perp^D \delta_{ij}^\perp h_j^m + m_j T_{ijk} (\psi^{TD} \nabla_k T \\ & + \psi^{cD} \nabla_k \mu_c) + c_{jki}^D A_{jk} + p^m T_{ijk} m_k \nabla_l \Psi_{jl} \\ & + \delta_{ij}^\perp \xi^{Wm} W_j, \end{aligned} \quad (\text{B.4})$$

$$\begin{aligned} X^{MD} & \equiv \frac{\delta R}{\delta h^M} = b^M h^M + c_{ij}^M A_{ij} + \xi_{ij}^M \nabla_i \nabla_k \Psi_{jk} \\ & - p^M \nabla_i (T_{ijk} m_k W_j), \end{aligned} \quad (\text{B.5})$$

$$Z^D \equiv \frac{\partial R}{\partial h^\Omega} = b^\Omega h^\Omega + \tau_{ij} A_{ij}, \quad (\text{B.6})$$

$$\begin{aligned} F_i^D & \equiv \frac{\partial R}{\partial \nabla_k \Psi_{ik}} = D_{il}^\Psi \nabla_k \Psi_{lk} + \xi_{li}^T \nabla_l T + \xi_{li}^c \nabla_l \mu_c \\ & + f_{kji}^D A_{jk} + T_{ilk} m_k (p^W W_l + p^m h_l^m) \\ & + \xi_{ij}^M \nabla_j h^M, \end{aligned} \quad (\text{B.7})$$

$$\begin{aligned} Y_i^{OD} & \equiv \frac{\partial R}{\partial W_i} = \tau^W W_i + \xi_{kji}^A A_{jk} + p^W T_{ijk} m_k \nabla_l \Psi_{jl} \\ & + \xi^{Wm} \delta_{ij}^\perp h_j^m + T_{ijk} m_k (p^T \nabla_j T + p^c \nabla_j c) \\ & + p^M \nabla_j h^M, \end{aligned} \quad (\text{B.8})$$

where F_i^D is related to the dissipative strain current by $Y_{ij}^D = -\frac{1}{2}(\nabla_j F_i^D + \nabla_i F_j^D)$.

In case of a relaxing elasticity there are additional contributions in the dissipation function R_{relax} , eq. (87), giving rise to the following additional dissipative currents

$$j_i^{\sigma D} \equiv -\frac{\partial R_{\text{relax}}}{\partial \nabla_i T} = -\xi^{T\psi} T_{kji} \Psi_{kj}, \quad (\text{B.9})$$

$$j_i^{cD} \equiv -\frac{\partial R_{\text{relax}}}{\partial \nabla_i \mu_c} = -\xi^{c\psi} T_{kji} \Psi_{kj}, \quad (\text{B.10})$$

$$X^{MD} \equiv -\nabla_k \frac{\partial R_{\text{relax}}}{\partial \nabla_k h^M} = -\xi^{M\psi} \nabla_k (T_{ijk} \Psi_{ij}), \quad (\text{B.11})$$

$$\begin{aligned} Y_{ij}^D & \equiv \frac{\partial R_{\text{relax}}}{\partial \Psi_{ij}} = \tau_{ijk}^\psi \Psi_{kl} + \xi^{T\psi} T_{ijk} \nabla_k T \\ & + \xi^{c\psi} T_{ijk} \nabla_k c + \xi^{M\psi} T_{ijk} \nabla_k h^M \end{aligned} \quad (\text{B.12})$$

that come in addition to those of eqs. (B.1)–(B.8) shown above.

Open Access This is an open access article distributed under the terms of the Creative Commons Attribution

License (<http://creativecommons.org/licenses/by/4.0>), which permits unrestricted use, distribution, and reproduction in any medium, provided the original work is properly cited.

References

1. R.E. Rosensweig, *Ferrohydrodynamics* (Cambridge University Press, Cambridge, 1985).
2. S. Odenbach, J. Phys.: Condens. Matter **16**, R1135 (2004).
3. H.-W. Müller, M. Liu, Phys. Rev. E **64**, 061405 (2001).
4. B. Huke, M. Lücke, Rep. Prog. Phys. **67**, 1731 (2004).
5. P. Ilg, E. Coquelle, S. Hess, J. Phys.: Condens. Matter **18**, S2757 (2006).
6. V.I. Zadorozhnyi, A.N. Vasilev, V.Yu. Reshetnyak, K.S. Thomas, T.J. Sluckin, Europhys. Lett. **73**, 408 (2006).
7. S. Mahle, P. Ilg, M. Liu, Phys. Rev. E **77**, 016305 (2008).
8. S.D. Peroukidis, S.H.L. Klapp, Phys. Rev. E **92**, 010501 (2015).
9. M. Zrinyi, Trends Polym. Sci. **5**, 280 (1997).
10. Z. Varga, J. Fehér, G. Filipcsei, M. Zrinyi, Macromol. Symp. **200**, 93 (2003).
11. M. Zrinyi, L. Barsi, A. Büki, J. Chem. Phys. **104**, 8750 (1996).
12. M. Zrinyi, F. Horkay, J. Intell. Mater. Syst. Struct. **4**, 190 (1993).
13. M. Babincová, D. Leszczynska, P. Sourivong, P. Čičmanec, P. Babinec, J. Magn. & Magn. Mater. **225**, 109 (2001).
14. E. Jarkova, H. Pleiner, H.-W. Müller, H.R. Brand, Phys. Rev. E **68**, 041706 (2003).
15. G. Pessot, P. Cremer, D.Y. Borin, S. Odenbach, H. Löwen, A.M. Menzel, J. Chem. Phys. **141**, 124904 (2014).
16. S. Huang, G. Pessot, P. Cremer, R. Weeber, C. Holm, J. Nowak, S. Odenbach, A.M. Menzel, G.K. Auernhammer, Soft Matter **12**, 228 (2016).
17. D. Collin, G.K. Auernhammer, O. Gavati, P. Martinoty, H.R. Brand, Macromol. Rapid Commun. **24**, 737 (2003).
18. S. Bohlius, H.R. Brand, H. Pleiner, Phys. Rev. E **70**, 061411 (2004).
19. L.G. Fel, Phys. Rev. E **52**, 702 (1995).
20. L.G. Fel, Phys. Rev. E **52**, 2692 (1995).
21. L. Radzihovsky, T.C. Lubensky, Europhys. Lett. **54**, 206 (2001).
22. T.C. Lubensky, L. Radzihovsky, Phys. Rev. E **66**, 031704 (2002).
23. B. Mettout, Phys. Rev. E **74**, 041701 (2006).
24. L. Longa, G. Pajak, T. Wydro, Phys. Rev. E **79**, 040701 (2009).
25. K. Trojanowski, G. Pajak, L. Longa, T. Wydro, Phys. Rev. E **86**, 011704 (2012).
26. L. Longa, K. Trojanowski, Acta. Phys. Pol. B **44**, 1201 (2013).
27. H.R. Brand, H. Pleiner, P.E. Cladis, Eur. Phys. J. E **7**, 163 (2002).
28. P.E. Cladis, H. Pleiner, H.R. Brand, Eur. Phys. J. E **11**, 283 (2003).
29. H.R. Brand, P.E. Cladis, H. Pleiner, Ferroelectrics **315**, 165 (2005).
30. H.R. Brand, H. Pleiner, P.E. Cladis, Physica A **351**, 189 (2005).
31. H. Pleiner, P.E. Cladis, H.R. Brand, Eur. Phys. J. E **20**, 257 (2006).
32. H.R. Brand, H. Pleiner, Eur. Phys. J. E **31**, 37 (2010).

33. H. Pleiner, H.R. Brand, Eur. Phys. J. E **37**, 11 (2014).
34. G. Pelzl, A. Eremin, S. Diele, H. Kresse, W. Weissflog, J. Mater. Chem. **12**, 2591 (2002).
35. V. Bourny, V. Lorman, J. Pavel, B. Mettout, H.T. Nguyen, Ferroelectrics **276**, 127 (2002).
36. W. Weissflog, M.W. Schröder, S. Diele, G. Pelzl, Adv. Mater. **15**, 630 (2003).
37. T. Niori, J. Yamamoto, H. Yokoyama, Mol. Cryst. Liq. Cryst. **409**, 475 (2004).
38. M.W. Schroeder, S. Diele, G. Pelzl, W. Weissflog, ChemPhysChem **2004**, 99 (2004).
39. D. Wiant, J.T. Gleeson, N. Eber, K. Fodor-Csorba, A. Jakli, T. Toth-Katona, Phys. Rev. E **72**, 041712 (2005).
40. J. Harden, B. Mbang, N. Eber, K. Fodor-Csorba, S. Sprunt, J.T. Gleeson, A. Jakli, Phys. Rev. Lett. **97**, 157802 (2006).
41. D. Wiant, S. Stojadinovic, K. Neupane, S. Sharma, K. Fodor-Csorba, A. Jakli, J.T. Gleeson, S. Sprunt, Phys. Rev. E **73**, 030703 (2006).
42. D. Wiant, K. Neupane, S. Sharma, J.T. Gleeson, S. Sprunt, A. Jakli, N. Pradhan, G. Iannacchione, Phys. Rev. E **77**, 061701 (2008).
43. T. Ostapenko, D.B. Wiant, S.N. Sprunt, A. Jakli, J.T. Gleeson, Phys. Rev. Lett. **101**, 247801 (2008).
44. Y. Jang, R. Balachandran, C. Keith, A. Lehmann, C. Tschierske, J.K. Vij, Soft Matter **8**, 10479 (2012).
45. F. Vita, I.F. Placentino, C. Ferreo, G. Singh, E.T. Samulski, O. Francescangeli, Soft Matter **9**, 6475 (2013).
46. M. Jasinski, D. Pocięcha, H. Monobe, J. Szczytko, P. Kaszynski, J. Am. Chem. Soc. **136**, 14658 (2014).
47. O.N. Kadkin, E.H. Kim, Y.J. Rha, S.Y. Kim, J. Taem, M.-G. Choi, Chem. Eur. J. **15**, 10343 (2009).
48. E.H. Kim, O.N. Kadkin, S.Y. Kim, J. Taem, M.-G. Choi, Eur. J. Inorg. Chem. **2011**, 2933 (2011).
49. H. Pleiner, H.R. Brand, Braz. J. Phys. **46**, 565 (2016).
50. T. Potisk, H. Pleiner, H.R. Brand, Phys. Rev. E **98**, 042703 (2018).
51. H.R. Brand, H. Pleiner, Eur. Phys. J. E **40**, 34 (2017).
52. C. Dressel, T. Reppe, M. Prehm, M. Brautzsch, C. Tschierske, Nat. Chem. **6**, 971 (2014).
53. C. Dressel, W. Weissflog, C. Tschierske, Chem. Commun. **51**, 15850 (2015).
54. M. Alaasar, M. Prehm, Y. Cao, F. Liu, C. Tschierske, Angew. Chem. Int. Ed. **55**, 312 (2016).
55. H. Temmen, H. Pleiner, M. Liu, H.R. Brand, Phys. Rev. Lett. **84**, 3228 (2000).
56. H. Pleiner, M. Liu, H.R. Brand, Rheol. Acta **39**, 560 (2000).
57. A.M. Menzel, H. Pleiner, H.R. Brand, J. Chem. Phys. **126**, 234901 (2007).
58. A. Menzel, H. Pleiner, H.R. Brand, J. Appl. Phys. **105**, 013503 (2009).
59. A. Menzel, H. Pleiner, H.R. Brand, Eur. Phys. J. E **30**, 371 (2009).
60. H. Pleiner, H.R. Brand, *Hydrodynamics and Electrohydrodynamics of Nematic Liquid Crystals*, in *Pattern Formation in Liquid Crystals*, edited by A. Buka, L. Kramer (Springer, New York, 1996).
61. H.R. Brand, H. Pleiner, Eur. Phys. J. E **37**, 122 (2014).
62. P.C. Martin, O. Parodi, P.S. Pershan, Phys. Rev. A **6**, 2401 (1972).

Publication 6

Continuum model of magnetic field induced viscoelasticity in magnetorheological fluids

Reproduced from

T. Potisk, D. Svenšek, H. Pleiner, and H.R. Brand
J. Chem. Phys. **150**, 174901 (2019),

with the permission of AIP Publishing.

Continuum model of magnetic field induced viscoelasticity in magnetorheological fluids

Cite as: J. Chem. Phys. **150**, 174901 (2019); <https://doi.org/10.1063/1.5090337>

Submitted: 26 January 2019 . Accepted: 12 April 2019 . Published Online: 06 May 2019

Tilen Potisk , Daniel Švenšek , Harald Pleiner, and Helmut R. Brand



View Online



Export Citation



CrossMark

The Journal
of Chemical Physics

2018 EDITORS' CHOICE

READ NOW!

AIP
Publishing

Continuum model of magnetic field induced viscoelasticity in magnetorheological fluids

Cite as: *J. Chem. Phys.* **150**, 174901 (2019); doi: [10.1063/1.5090337](https://doi.org/10.1063/1.5090337)

Submitted: 26 January 2019 • Accepted: 12 April 2019 •

Published Online: 3 May 2019



View Online



Export Citation



CrossMark

Tilen Potisk,^{1,a)} Daniel Svenešek,² Harald Pleiner,³ and Helmut R. Brand¹

AFFILIATIONS

¹Department of Physics, University of Bayreuth, 95440 Bayreuth, Germany

²Department of Physics, Faculty of Mathematics and Physics, University of Ljubljana, SI-1000 Ljubljana, Slovenia

³Max Planck Institute for Polymer Research, 55021 Mainz, Germany

^{a)}Electronic mail: tilen.potisk@uni-bayreuth.de

ABSTRACT

An effective macroscopic model of magnetorheological fluids in the viscoelastic regime is proposed. Under the application of an external magnetic field, columns of magnetizable particles are formed in these systems. The columns are responsible for solidlike properties, such as the existence of elastic shear modulus and yield stress, and are captured by the strain field, while magnetic properties are described by the magnetization. We investigate the interplay of these variables when static shear or normal pressure is imposed in the presence of the external magnetic field. By assuming a relaxing strain field, we calculate the flow curves, i.e., the shear stress as a function of the imposed shear rate, for different values of the applied magnetic field. Focusing on the small amplitude oscillatory shear, we study the complex shear modulus, i.e., the storage and the loss moduli, as a function of the frequency. We demonstrate that already such a minimal model is capable of furnishing many of the key physical features of these systems, such as yield stress, enhancement of the shear yield stress by pressure, threshold behavior in the spirit of the frequently employed Bingham law, and several features in the frequency dependence of storage and loss moduli.

Published under license by AIP Publishing. <https://doi.org/10.1063/1.5090337>

I. INTRODUCTION

Magnetorheological (MR) fluids are a class of fluids, which experience significant changes upon application of an external magnetic field. Examples of such changes are a fast and reversible acquisition of solidlike properties and a dramatic increase in the viscosity. This makes such systems suitable for many applications such as shock absorbers, clutches, and brakes.

Introduced in Ref. 1, MR fluids are composed of micron sized magnetizable particles, typically suspended in oil. Under the influence of the external magnetic field, gap-spanning chains or columns of the particles in the direction of the field are formed and a finite stress, also called the yield stress, is needed to break these structures and initiate flow. The columnar structure can be explained by the induced dipole interaction between the particles, which is attractive when they are parallel to the magnetic field. The application of the magnetic field also leads to a significant rise in the viscosity. For reviews of general aspects of MR fluids, cf. Refs. 2–6.

Several microscopic and macroscopic models have been developed to predict the column formation and the dependence of the yield stress on the applied magnetic field. Due to the similar form of the interaction between the particles (dipolar), the studies of the electrorheological fluids are also relevant for the description of MR fluids. Microscopic models usually assumed single chain structures, which are deformed in the shear plane,^{7–11} although certain refinements on the electrorheological fluids have been done taking into account the crystal structure of the particle aggregates.¹² Theoretical studies of rheological properties are much less frequent. In Ref. 13, the so-called independent droplet model was used to model the shear-thinning behavior. Other studies focus on single chains^{14,15} or simulations of individual particles.¹⁶

Macroscopic models usually rely on the Maxwell stress tensor and magnetostriction effects.⁹ In the case of electrorheological fluids, the anisotropy caused by the chains was treated using a directorlike degree of freedom known in nematic liquid crystals.^{17–19} In Ref. 20, the static yield stress was calculated for a fluid with lamellar

structure. To predict the rheological properties, the two fluid approach, where the solvent phase and the particle phase are treated separately, has been used.^{21,22} With this approach, various aspects of pattern formation including sheets, disktype structures in a rotating field, etc., have also been analyzed.^{23–25}

The aim of this paper is to construct a minimal macroscopic model for MR fluids, which is capable of capturing the main physical effects found in static as well as dynamic experiments. To derive the static and the dynamic equations, a symmetry based approach is used.²⁶ One of its advantages with respect to microscopic approaches is the applicability to different systems and geometries.

This article is organized as follows: The macroscopic model is introduced in Sec. II, followed by the numerical analysis of the static shear deformation in the external magnetic field in Sec. III A. In Sec. III B, the effects of the normal pressure on the static yield stress are considered. Flow properties are discussed by analyzing shear stresses due to stationary (Sec. IV A) and oscillatory (Sec. IV B) imposed shear flow.

II. MACROSCOPIC MODEL

Generally, in a fluid mixture, the macroscopic variables are mass density ρ , momentum density \mathbf{g} , entropy density σ , and concentration density c . For magnetic fluids, there is, in addition, a magnetization field \mathbf{M} , which is zero in equilibrium in the absence of an external magnetic field. For MR fluids, in particular, an external field triggers columnar structures of the magnetizable particles due to the attractive magnetic forces between the particles that lead to solidlike, elastic properties. Therefore, we introduce a strain field ε_{ij} as a macroscopic variable that is zero in the field-free case and finite in a magnetic field. For the dynamics, we restrict ourselves to the regime, where the viscoelastic nature of the MR fluids can be described by a relaxational dynamics for the strain field.

In order to make the model as simple as possible, we disregard the density ρ , the entropy density σ , and the concentration c as variables, effectively meaning they are constant. This implies incompressibility and the neglect of temperature and concentration gradients (sedimentation). Thus, we deal with elastic deformations and flow, as well as the magnetization. Furthermore, we will consider all material tensors only in their isotropic form. This seems to be a reasonable simplification, since we only consider shear in the plane perpendicular to the magnetization (and compression along the field). It turns out that the static and the dynamic theoretical behavior is in qualitative agreement with experiments. Even the anisotropy of the ultrasound velocity can be explained without invoking anisotropic material tensors.^{27–29} We emphasize that the introduction of a director in the present context is inappropriate, since it has the wrong behavior under time reversal. If anisotropy is taken into account, all the material tensors acquire additional terms due to the lower symmetry. Furthermore, in an elastic system with an orientational order, one must, in principle, consider the additional variable of relative rotations between the network and the preferred direction. These relative rotations play an important role in the description of nematic gels.^{30,31} Throughout most of this paper, we concentrate on the isotropic aspects of material properties and, therefore, discard relative rotations.

A. Statics

The statics of a macroscopic system is best set up by considering its total energy density ϵ . The Gibbs relation, a manifestation of the first law of thermodynamics, relates changes of the macroscopic variables to energy changes

$$d\epsilon = d\epsilon_0 + v_i dg_i + h_i^M dM_i + \psi_{ij} d\varepsilon_{ij}, \quad (1)$$

where $d\epsilon_0$ represents the neglected macroscopic degrees of freedom and is given in Ref. 26. The thermodynamic conjugates to the macroscopic variables considered here are the bulk velocity v_i , the magnetic molecular field h_i^M , and the elastic stress ψ_{ij} .

The statics is described by the energy density $\epsilon(\varepsilon_{ij}, \mathbf{M}, \mathbf{g})$,³²

$$\begin{aligned} \epsilon = & \epsilon_0 - \mu_0 H_i M_i + \frac{1}{2} \alpha \mathbf{M}^2 + \frac{1}{4} \beta (\mathbf{M}^2)^2 \\ & + \frac{1}{2} c_{ijkl} \varepsilon_{ij} \varepsilon_{kl} - \frac{1}{2} \gamma_{ijkl} \varepsilon_{ij} M_k M_l + \frac{1}{2\rho} \mathbf{g}^2, \end{aligned} \quad (2)$$

where the coupling to an external magnetic field, $\sim \mu_0 \mathbf{H}$, ensures the induced magnetization to be parallel to the field, while the next two terms govern the magnitude of the magnetization (modulus) $M \equiv \sqrt{\mathbf{M}^2}$ that is induced by the field. The form given in Eq. (2) is suitable for rather small fields, while in the general case, the α and β terms have to be replaced by a more complicated function $f_1(M^2)$ that can be taken from experimental results.

The material tensors c_{ijkl} and γ_{ijkl} describe elasticity and magnetostriction, respectively. In their standard isotropic form,³²

$$c_{ijkl} = c_1 \mathbf{M}^2 \delta_{ij} \delta_{kl} + c_2 \mathbf{M}^2 (\delta_{ik} \delta_{jl} + \delta_{il} \delta_{kj}), \quad (3)$$

$$\gamma_{ijkl} = \gamma_1 \delta_{ij} \delta_{kl} + \gamma_2 (\delta_{ik} \delta_{jl} + \delta_{il} \delta_{kj}), \quad (4)$$

where we have assumed here that the elastic moduli are proportional to M^2 . This ensures that elasticity, and therefore the elastic tensor c_{ijkl} , vanishes, when there are no columns, i.e., when the magnetization \mathbf{M} is zero. This quadratic dependence is the simplest assumption but can be replaced by a more complicated (even discontinuous) function $f_2(M^2)$, provided $f_2(M^2) \rightarrow 0$ for $M \rightarrow 0$. The dependence on M^2 (rather than M_i) is due to the time reversal behavior of \mathbf{M} .

As usual, the isotropic tensors c_{ijkl} and γ_{ijkl} have two coefficients each, where the terms $\sim c_1$ and $\sim \gamma_1$ describe the energy associated with the compressive or elongational strains, while the coefficients c_2 and γ_2 correspond to the shear strains. In the examples described in Secs. III A and III B we assume that the compression is always parallel to the magnetic field and that for the shear deformation the shear plane contains the magnetic field. For completeness, if uniaxial anisotropy of the system is considered, with the axis along $\mathbf{m} = \mathbf{M}/|\mathbf{M}|$, one gets additional terms in Eqs. (3) and (4)³³

$$\begin{aligned} \tilde{c}_{ijkl} = & \tilde{c}_1 \delta_{ij}^{\perp} \delta_{kl}^{\perp} + \tilde{c}_2 (\delta_{ik}^{\perp} \delta_{jl}^{\perp} + \delta_{il}^{\perp} \delta_{kj}^{\perp} - \delta_{ij}^{\perp} \delta_{kl}^{\perp}) + \tilde{c}_3 m_i m_j m_k m_l \\ & + \tilde{c}_4 (m_i m_j \delta_{kl}^{\perp} + m_k m_l \delta_{ij}^{\perp}) + \tilde{c}_5 (m_i m_k \delta_{jl}^{\perp} + m_i m_l \delta_{jk}^{\perp} \\ & + m_j m_k \delta_{il}^{\perp} + m_j m_l \delta_{ik}^{\perp}), \end{aligned} \quad (5)$$

$$\begin{aligned} \tilde{\gamma}_{ijkl} = & \tilde{\gamma}_1 \delta_{ij}^{\perp} \delta_{kl}^{\perp} + \tilde{\gamma}_2 (\delta_{ik}^{\perp} \delta_{jl}^{\perp} + \delta_{il}^{\perp} \delta_{kj}^{\perp} - \delta_{ij}^{\perp} \delta_{kl}^{\perp}) + \tilde{\gamma}_3 m_i m_j m_k m_l \\ & + \tilde{\gamma}_4 m_i m_j \delta_{kl}^{\perp} + \tilde{\gamma}_5 m_k m_l \delta_{ij}^{\perp} + \tilde{\gamma}_6 (m_i m_k \delta_{jl}^{\perp} + m_i m_l \delta_{jk}^{\perp} \\ & + m_j m_k \delta_{il}^{\perp} + m_j m_l \delta_{ik}^{\perp}), \end{aligned} \quad (6)$$

where $\delta_{ij}^{\perp} = \delta_{ij} - m_i m_j$ and where $\tilde{c}_1, \tilde{c}_2, \tilde{c}_3, \tilde{c}_4$, and \tilde{c}_5 are all proportional to \mathbf{M}^2 . As already mentioned above, here we will not pursue these refinements and will be using the isotropic forms [Eqs. (3) and (4)].

To calculate the equilibrium values of the variables, one must first calculate the thermodynamic forces. These are the thermodynamic conjugates of the macroscopic variables [Eq. (1)] and are derived by taking the variational derivatives of the energy density [Eq. (2)] with respect to the corresponding variables²⁶

$$h_i^M = \frac{\delta \epsilon}{\delta M_i} = (\alpha + \beta \mathbf{M}^2) M_i - \mu_0 H_i - \gamma_1 M_i \epsilon_{kk} - 2\gamma_2 M_j \epsilon_{ij} + (c_1 \epsilon_{kk}^2 + 2c_2 \epsilon_{kj} \epsilon_{jk}) M_i, \quad (7)$$

$$\psi_{ij} = \frac{\delta \epsilon}{\delta \epsilon_{ij}} = c_1 \epsilon_{kk} \mathbf{M}^2 \delta_{ij} + 2c_2 \mathbf{M}^2 \epsilon_{ij} - \frac{1}{2} \gamma_1 \mathbf{M}^2 \delta_{ij} - \gamma_2 M_i M_j, \quad (8)$$

$$v_i = \frac{\delta \epsilon}{\delta g_i} = \frac{1}{\rho} g_i. \quad (9)$$

Thermodynamic equilibrium requires all thermodynamic forces to be zero, i.e., $h_i^M = 0$ and $\psi_{ij} = 0$. For a finite external magnetic field, $H_i = H \delta_{iz}$, the conditions (7)–(9) lead to a finite equilibrium magnetization $M_z^{eq} = \mu_0 H / \alpha$ and a finite equilibrium strain $\epsilon_{zz}^{eq} = (1/2)(\gamma_1 + 2\gamma_2) / (c_1 + 2c_2)$. The latter is independent of the field since the field dependences of the magnetostriction and the elasticity compensate each other. Note that our simplified linear model only applies for finite fields and does not describe the case $H \equiv 0$.

B. Macroscopic dynamics

The dynamic evolution of deviations from the equilibrium state is described by the proper macroscopic equations discussed in the following. The dynamic equations for the momentum density g_i , the magnetization M_i , and the strain field ϵ_{ij} are³²

$$\frac{d}{dt} g_i + \nabla_j (p \delta_{ij} - \psi_{ij} + \sigma_{ij}^{th} + \sigma_{ij}) = 0, \quad (10)$$

$$\frac{d}{dt} M_i + \epsilon_{ijk} M_j \omega_k + X_i = 0, \quad (11)$$

$$\frac{d}{dt} \epsilon_{ij} + \epsilon_{kj} \nabla_i v_k + \epsilon_{ki} \nabla_j v_k - A_{ij} + Y_{ij} = 0, \quad (12)$$

where $d/(dt) \equiv \partial/(\partial t) + v_j \nabla_j$ is the material derivative, $A_{ij} = (\nabla_i v_j + \nabla_j v_i)/2$ is the symmetric gradient of the velocity field, and the vorticity $\omega_i = \epsilon_{ijk} \nabla_j v_k / 2$ corresponds to its antisymmetric gradient.

The thermodynamic pressure, p , is given by²⁶

$$p = -\epsilon + v_i g_i + B_i H_i + \epsilon_0, \quad (13)$$

where $\mathbf{B} = \mu_0(\mathbf{H} + \mathbf{M})$ is the magnetic flux density and ϵ_0 represents the neglected macroscopic degrees of freedom. The nonlinear stress tensor contributions read in symmetrized form³²

$$\sigma_{ij}^{th} = -\frac{1}{2} (B_i H_j + B_j H_i) + \frac{1}{2} (\psi_{jk} \epsilon_{ki} + \psi_{ik} \epsilon_{kj}). \quad (14)$$

The nonphenomenological parts of the currents, shown explicitly in Eqs. (10)–(14), are not related to any phenomenological (transport) parameters and are given by general symmetry and thermodynamic principles.²⁶ We emphasize that their structure, in particular, that of the convective derivative $\epsilon_{kj} \nabla_i v_k + \epsilon_{ki} \nabla_j v_k$ in Eq. (12), is uniquely determined.^{34,35} All those terms are reversible, meaning that they transform under time reversal, $t \rightarrow -t$, in the same way as the time derivative of their appropriate variable. For a general discussion of time reversal symmetry and its importance for macroscopic equations, we refer to Ref. 36.

The phenomenological part of the stress tensor σ_{ij} and the quasicurrents X_i and Y_{ij} describe temporal changes of their corresponding variables and can be written as a sum of a reversible (superscript R) and an irreversible part (superscript D). They are functions of the thermodynamic forces [Eqs. (7)–(9)] (A_{ij} , h_i^M , and ψ_{ij}) involving phenomenological transport parameters. The second law of thermodynamics states that irreversible dynamic processes always dissipate energy (transfer energy to the microscopic degrees of freedom as heat) and therefore increase the entropy. On the contrary, reversible processes are nondissipative and must not increase the entropy.

Within linear irreversible thermodynamics,³⁷ the dissipation function R , which is proportional to the entropy production, can be written as a bilinear form of fluxes and forces, in our case

$$2R = -\sigma_{ij} A_{ij} + X_i h_i^M + Y_{ij} \psi_{ij}. \quad (15)$$

For the reversible parts of the currents $\{\sigma_{ij}^R, X_i^R, Y_{ij}^R\}$, one has to require $R = 0$, while the dissipative ones $\{\sigma_{ij}^D, X_i^D, Y_{ij}^D\}$ fulfill $R > 0$.

To derive the dissipative parts of the (quasi-) currents, one writes the dissipation function R as a quadratic form in the relevant thermodynamic forces. By taking the variational derivative of this function with respect to the chosen thermodynamic force, according to Eq. (15), one gets the corresponding dissipative current. The dissipation function is

$$R = \frac{1}{2} v_{ijkl}^D A_{ij} A_{kl} + \frac{1}{2} b^D h_i^M h_i^M + \frac{1}{2} (1/\tau)_{ijkl} \psi_{ij} \psi_{kl} + d_{ijk} \psi_{jk} h_i^M, \quad (16)$$

leading to

$$\sigma_{ij}^D = -v_{ijkl}^D A_{kl}, \quad (17)$$

$$X_i^D = b^D h_i^M + d_{ijk} \psi_{jk}, \quad (18)$$

$$Y_{ij}^D = (1/\tau)_{ijkl} \psi_{kl} + d_{kij} h_k^M. \quad (19)$$

As in Eqs. (3) and (4), we again assume an isotropic form of the material tensors v_{ijkl}^D and $(1/\tau)_{ijkl}$ describing viscosity and strain relaxation, respectively,

$$v_{ijkl}^D = \nu_1 \delta_{ij} \delta_{kl} + \nu_2 (\delta_{ik} \delta_{jl} + \delta_{jk} \delta_{il}), \quad (20)$$

$$(1/\tau)_{ijkl} = \frac{1}{\tau_1 M_0^2} \delta_{ij} \delta_{kl} + \frac{1}{\tau_2 M_0^2} (\delta_{ik} \delta_{jl} + \delta_{jk} \delta_{il}). \quad (21)$$

Thus, we model the viscoelastic properties of MR fluids^{38–43} by using the strain field as a relaxing variable. When the columns are deformed, the particles experience a drive to redistribute, e.g., by permeation effects, which shows on the macroscopic level

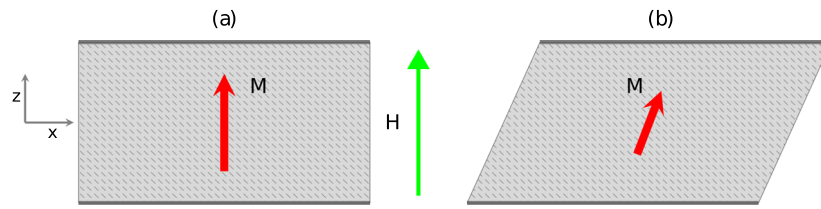


FIG. 1. Sketch of a MR fluid, confined between two parallel plates. (a) The external magnetic field is applied perpendicularly to the plates, which induces a nonzero magnetization (red arrow) along the z axis. (b) MR fluid, when an additional static shear deformation is imposed.

as relaxation of the strain. In addition, we assume that the relaxation coefficients, $\tau_1 M_0^2$ and $\tau_2 M_0^2$, are proportional to M_0^2 , which is motivated by the fact that the elastic network relaxes on longer time scales in larger magnetic fields, i.e., it behaves more elastically. Depending on the type of deformation, either compression or shear, the strain relaxes with a characteristic time proportional to $\tau_1 + 2\tau_2$ or τ_2 , respectively. It should be noted that $\tau_{1,2}$ can still be functions of M^2 , which is also the case for the viscosities $\nu_{1,2}$ and the magnetization relaxation b^D . In the incompressible case, ν_1 drops out and can be put to zero. We discard diffusion-type contributions $\sim \nabla_k \psi_{ij}$.

In Eq. (16), the material tensor

$$d_{ijk} = d_1 M_i \delta_{jk} + d_2 (M_j \delta_{ik} + M_k \delta_{ij}) \quad (22)$$

represents the dissipative coupling of the elastic stress to the magnetization. It is linear in the magnetic field to make sure that the contributions to X_i^D and Y_{ij}^D are irreversible, but an additional M^2 dependence is possible.

The reversible currents cannot be derived from the dissipation function since $R \equiv 0$ for the reversible case. Instead, they are set up by collecting all possible combinations allowed by (e.g., time-reversal) symmetry that leads to a vanishing R in Eq. (15),

$$\sigma_{ij}^R = -\nu_{ijk}^R A_{kl} - c_{kij}^R M_k^M, \quad (23)$$

$$X_i^R = b_{ij}^R M_j^M - c_{ijk}^R A_{jk}, \quad (24)$$

$$Y_{ij}^R = 0. \quad (25)$$

The material tensors in Eqs. (23) and (24) read³²

$$\nu_{ijkl}^R = \nu^R (\epsilon_{ikp} \delta_{jl} + \epsilon_{jkp} \delta_{il} + \epsilon_{ilp} \delta_{jk} + \epsilon_{jlp} \delta_{ik}) M_p, \quad (26)$$

$$c_{ijk}^R = c_1^R M_i \delta_{jk} + c_2^R (M_j \delta_{ik} + M_k \delta_{ij}), \quad (27)$$

$$b_{ij}^R = b^R \epsilon_{ijk} M_k, \quad (28)$$

where c_{ijk}^R has the same form as d_{ijk} in Eq. (22). To make these currents reversible, all three material tensors have to be odd functions in M_i and additional M^2 dependences of the parameters are possible. In the incompressible case, ν^R and c_1^R drop out and can be put to zero.

C. Geometry and material parameters

Throughout this paper, we use the geometry of two parallel plates, as shown in Fig. 1. The macroscopic variables are assumed to

be only a function of the z coordinate. The magnetic field will always be applied normal to the plates (along the z axis). In Secs. III A and IV, we consider shear deformations as shown in Fig. 1(b), while in Sec. III B, a compressive strain (along the field direction) is additionally assumed.

Here, we list the values of the material parameters that we generally use in our numerical calculations (exceptions are indicated in the figure captions). The prefactors of the elastic moduli are $c_1 = c_2 = 10 \text{ Pa A}^{-2} \text{ m}^2$, and the coefficients connected with the modulus of the magnetization are $\alpha = 0.06 \text{ Pa A}^{-2} \text{ m}^2$ and $\beta = 10^{-8} \text{ Pa A}^{-4} \text{ m}^4$. The values for c_2 and α are estimated by comparing the results of Sec. III [Eqs. (34) and (36)] to the measurements of the static (elastic) yield stress and the value of the critical strain in Ref. 44. For the magnetostrictive parameters, we find, by comparison of Eq. (38) with experimental results, $\gamma_2 \approx 0.3 \text{ Pa A}^{-2} \text{ m}^2$, cf. Sec. III A, and $\gamma_1 \approx 1.2 \text{ Pa A}^{-2} \text{ m}^2$, see Eq. (42) in Sec. III B.

Among the transport parameters that we use are $\nu_2 = 0.2 \text{ Pa s}$, $b^D = 40 \text{ A}^2 \text{ Pa}^{-1} \text{ s}^{-1} \text{ m}^{-2}$, and $\tau_2 = 0.1 \text{ Pa s m}^2 \text{ A}^{-2}$ or $\tau_2 = 10 \text{ Pa s m}^2 \text{ A}^{-2}$ in Sec. IV B. The coefficient, τ_2 , corresponding to the strain relaxation, is estimated from viscoelastic measurements, where, under a step shear strain deformation, the shear stress relaxed on the order of 0.01 s⁴⁵ or 1 s.³⁸ This time is then compared to the characteristic time scale that shows up in our model, $\tau_{el} = \tau_2/4c_2$, cf. Sec. IV B. The reversible coupling coefficient, c_2^R , relating the magnetization to the symmetric velocity gradient is already known from the dynamics of magnetic liquids,^{46–48} where it was crucial to explain dynamic experiments.^{49,50} We use a similar value as in Ref. 50, $c_2^R = 0.4$.

III. STATIC DEFORMATIONS

We discuss first the relation between static deformations and elastic stresses for different magnetic field strengths. Since the strains are relaxing, purely static experiments can only be performed on time scales short compared to the strain relaxation time, where strains can effectively be described by the static equations of Sec. II A.

A. Static shear deformation

In this section, we study the static shear deformation, when the MR fluid is confined between two parallel plates and the upper plate is displaced parallel to the x axis. Such a geometry is typically used in experiments to measure the elastic shear stress as a function of the shear strain. Experimental results show that the elastic shear stress first increases linearly with the shear strain, but when

the shear strain is increased further, one typically observes a saturation in the elastic shear stress. The value of the elastic stress, where the stress-strain curve levels off, is known as static yield stress, and it is from the application point of view desirable to have it as large as possible. The value of the static yield stress was measured for many different MR fluids and it increases quadratically with the field for small fields.⁴⁴ For intermediate magnetic fields, the static yield stress increases with the power of 3/2, which was measured experimentally,⁴³ as well as modeled numerically in Ref. 7, taking into account the saturation effects of the magnetization of the particles. The static yield strain does not depend on the magnetic field and is typically around 0.5%.^{42,44}

Throughout this section, we assume that the elastic shear deformation of Fig. 1(b) is constant, $\varepsilon_{xz} = \varepsilon_{zx} = \frac{1}{2}\Gamma$, and all other components are vanishing. This can be achieved by a displacement of the upper plate by $\mathbf{u} = \Gamma\hat{\mathbf{e}}_x$, where Γ is called the shear strain.

The elastic shear stress induced by the shear deformation follows from Eq. (8), which now reads

$$\psi_{xz} = c_2\mathbf{M}^2\Gamma - \gamma_2M_xM_z, \quad (29)$$

while the magnetization follows from Eq. (7)

$$\mu_0H = \alpha M_z + c_2\Gamma^2M_z - \gamma_2\Gamma M_x, \quad (30)$$

$$0 = \alpha M_x + c_2\Gamma^2M_x - \gamma_2\Gamma M_z, \quad (31)$$

where β is neglected here.

These equations can be solved analytically, but the resulting formulas are rather involved. We will discuss and explain the main features either using special cases or show figures of numerical solutions.

In Fig. 2, we present the elastic shear stress as a function of the shear strain at three different values of the applied magnetic field. One can see that the elastic shear stress first increases linearly, then goes through a maximum, and starts to decrease as one increases the shear strain. This can be understood by inspecting Eq. (29) for the elastic shear stress. The applied magnetic field induces a nonzero magnetization, which, in turn, induces a nonzero elastic shear modulus. For small values of the shear strain Γ , in particular, for

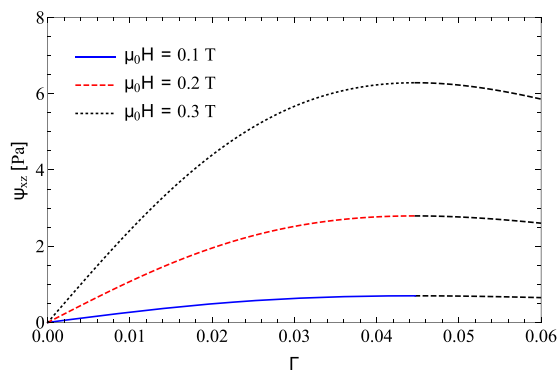


FIG. 2. The elastic shear stress as a function of the shear strain $\gamma_2 = 0$ at three different values of the applied magnetic field. The black dashed parts of the curves represent the unstable regime, where the elastic shear stress decreases with the shear strain.

$\Gamma \ll \alpha/\gamma_2$ and $\Gamma^2 \ll \alpha/c_2$, the elastic shear stress [Eq. (29)] increases linearly with the shear strain

$$\psi_{xz} \approx \frac{\mu_0^2 H^2}{\alpha^2} \left(c_2 - \frac{\gamma_2^2}{\alpha} \right) \Gamma \quad (32)$$

and the initial slope of the elastic shear stress increases quadratically with the applied magnetic field.

As one increases the shear strain, the elastic shear stress saturates and finally decreases (Fig. 2). One reason for this is the magnetization, which decreases for increasing strains (see Fig. 3). Disregarding the magnetostrictive parameter γ_2 for the moment, the induced elastic shear stress reads (for any Γ)

$$\psi_{xz} = \mu_0^2 H^2 \frac{c_2 \Gamma}{(\alpha + c_2 \Gamma^2)^2}. \quad (33)$$

Equation (33) provides a tool to determine the static coefficients c_2 and α from the comparison of the model to the measurements of the stress as a function of the strain. The stress-strain curve indeed has a maximum at

$$\Gamma^c = \sqrt{\frac{\alpha}{3c_2}}, \quad (34)$$

which is called the yield strain. Taking into account γ_2 perturbatively, e.g., for $\gamma_2^2 \ll \alpha c_2$, it is shifted to higher strains (Fig. 4),

$$\Gamma^{yield} \approx \Gamma^c \left(1 + \frac{5}{8} \frac{\gamma_2^2}{\alpha c_2} \right) \quad (35)$$

and does not depend on the magnetic field.

The value of the maximum elastic shear stress, the static yield stress, decreases with increasing γ_2 according to

$$\psi_{xz}^{yield} \approx \frac{3\sqrt{3}}{16} \sqrt{\alpha c_2} \left(1 - \frac{3}{16} \frac{\gamma_2^2}{\alpha c_2} \right) \frac{\mu_0^2 H^2}{\alpha^2}. \quad (36)$$

In addition, the static yield stress scales quadratically with the applied magnetic field (as is also visible in Fig. 2), which is in agreement with experiments.

The magnetostriction is responsible for the tilting of the chains of magnetizable particles. The tilt angle θ can be calculated from Eqs. (30) and (31) and is proportional to γ_2 ,

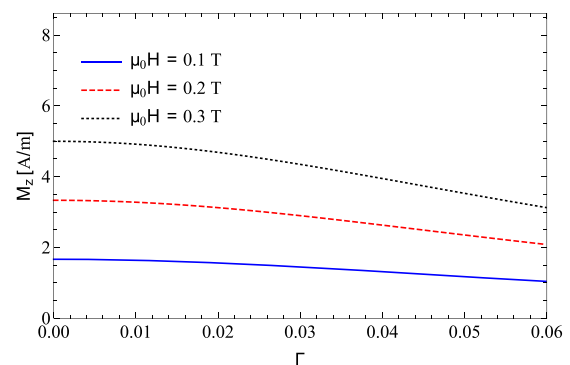


FIG. 3. The z component of the magnetization M_z as a function of the shear strain for $\gamma_2 = 0$ at three different values of the applied magnetic field.

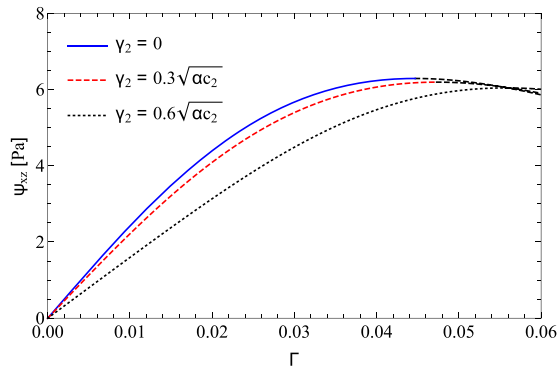


FIG. 4. The elastic shear stress vs shear strain for three different values of the magnetostriction coefficient γ_2 at a magnetic field $\mu_0 H = 0.3$ T. The black dashed parts of the curves represent the unstable regime, where the elastic shear stress decreases with the shear strain.

$$\tan \theta = \frac{M_x}{M_z} = \frac{\gamma_2 \Gamma}{\alpha + c_2 \Gamma^2} \quad (37)$$

with the maximum tilt value

$$\tan \theta^{max} = \frac{\gamma_2}{2\sqrt{\alpha c_2}} \quad (38)$$

which is taken at $\Gamma = \sqrt{\alpha/c_2}$.

We note, in passing, that given Eqs. (33) and (37), it is obvious that $\tan \theta$ and ψ_{xz} do not have their maximum at the same Γ . As a consequence of the tilting of the chains, the elastic stress decreases as has been discussed, above. Experimentally, the maximum tilt angle of the chains with respect to the direction of the magnetic field is on the order of 10° , which implies $\gamma_2 \approx 0.4\sqrt{\alpha c_2} \approx 3.0 \times 10^{-1} \text{ Pa A}^{-2} \text{ m}^2$. This means that the approximation $\gamma_2^2 \ll \alpha c_2$, which we used for some of the analytical results of this section, is quite appropriate.

B. Effects of normal pressure

A desirable property of MR fluids is a high static shear yield stress. This can to some extent be achieved by using a large magnetic field; however, due to the saturation of the magnetization, the static yield stress also saturates as one increases the magnetic field. In Refs. 51–54, it was found that, after the application of a magnetic field, compressing the MR fluid along the field direction strongly increases the static shear yield stress. Moreover, the static yield stress was found to be linearly dependent on the applied pressure P ,

$$\psi_{xz}^{yield}(P) = \psi_{xz}^{yield}(0) + kP, \quad (39)$$

where $\psi_{xz}^{yield}(0)$ is the static yield stress without compression, and the slope k was shown in Ref. 51 to be only very slightly increasing with the magnetic field.

Physically, the increase in the static shear yield stress can be explained by the fact that the compression pushes the chains of magnetizable particles to form thicker columns, which can better resist the shear forces.

We have found that the magnetostriction coefficient $\sim \gamma_1$ accounts for these experimental findings. Since the effect of γ_2

on the elastic shear stress has been discussed in Sec. III A, we will put $\gamma_2 = 0$ here. The external pressure P corresponds to an external stress $\psi_{zz} = +P$, from which a compressive strain ϵ_{zz} is induced via Eq. (8),

$$\epsilon_{zz} = +\frac{P}{\bar{c}_1 M^2}, \quad (40)$$

where the effective longitudinal elastic coefficient is $\bar{c}_1 = c_1 + 2c_2$. This strain comes in addition to the equilibrium compressive strain ϵ_{zz}^{eq} due to the external field, discussed in Sec. II A.

As a result of the compression, the magnetization M_z increases due to the magnetostrictive coupling $\sim \gamma_1$ (M_x vanishes in the $\gamma_2 = 0$ approximation)

$$M_z \approx \frac{\mu_0 H}{(\alpha + c_2 \Gamma^2)} + \frac{\gamma_1}{\bar{c}_1 \mu_0 H} P, \quad (41)$$

which we have linearized in the pressure.

An increase in the magnetization leads, according to Eq. (29), to an enhanced shear yield stress. In Fig. 5, we show the elastic shear stress as a function of the shear strain at three different values of the applied normal pressure.

Indeed, the elastic shear stress and its maximum (the static yield stress) increase linearly with the pressure (Fig. 6). For small values of the applied pressure, this is described by k [Eq. (39)] which takes the form

$$k \approx \frac{9}{32} \frac{\gamma_1}{\bar{c}_1} \sqrt{\frac{3c_2}{\alpha}}. \quad (42)$$

For typical experimental values of $k \approx 1/4$, one finds $\gamma_1 \approx 1.2 \text{ Pa A}^{-2} \text{ m}^2$.

In addition, the static yield stress is shifted to higher strains. This shift of the critical strain is also linear in the pressure and can be observed in Fig. 5 for different values of the field.

For small values of the applied pressure, one gets

$$\Gamma^{yield} \approx \Gamma^c + \frac{1}{2} \frac{\gamma_1 \alpha}{\bar{c}_1 \mu_0^2 H^2} P, \quad (43)$$

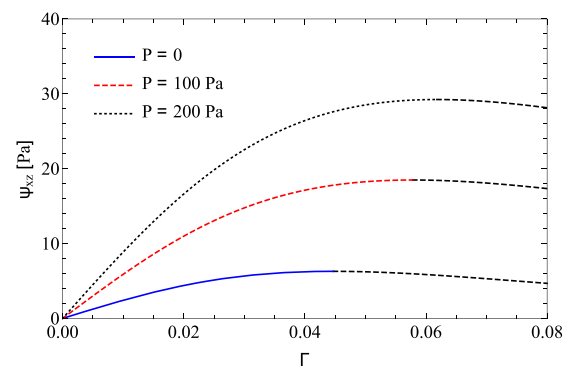


FIG. 5. Elastic shear stress as a function of shear strain using $\mu_0 H = 0.3$ T at three different values of the applied compressive pressure. The black dashed parts of the curves represent the unstable regime, where the elastic shear stress decreases with the shear strain.

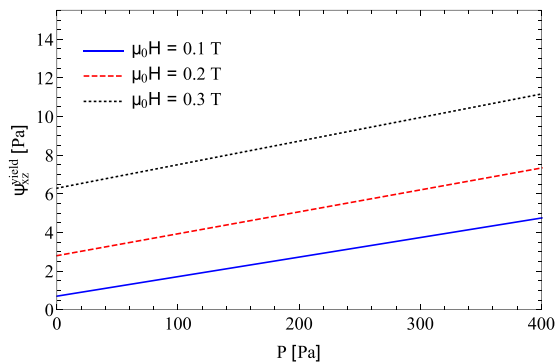


FIG. 6. Static yield stress as a function of the applied compressive pressure at three different values of the applied magnetic field.

showing also the $1/H^2$ field dependence. By measuring the yield stress and the yield strain as a function of the pressure, one could, in principle, determine the coefficients γ_1 and c_1 , while the coefficients c_2 and α could already be determined in the shear strain experiments (see Sec. III A).

IV. DYNAMIC DEFORMATIONS

In this section, we investigate the effect of the magnetic field on the measured viscosities of MR fluids in the presence of an applied shear flow. Experimental results show a threshold behavior, where a finite stress, also called the dynamic shear stress, is needed to sustain a shear flow. In addition, MR fluids are typically found to be slightly shear thinning, which means the viscosity decreases as one increases the shear rate.

We assume simple shear with a linear velocity profile of the form $\mathbf{v} = \dot{\gamma}z\hat{\mathbf{e}}_x$, where the so-called shear rate is constant for a steady shear flow, $\dot{\gamma} = \dot{\gamma}_0$, Sec. IV A, and time-dependent for oscillatory flow, $\dot{\gamma} = \dot{\gamma}_0 \cos(\omega t)$, Sec. IV B, with ω being the oscillatory frequency.

For shear flow, the dynamics of the magnetic degree of freedom, given in Sec. II, reads

$$-\frac{\partial}{\partial t}M_x = b^D M_x (\alpha + \beta \mathbf{M}^2 + 4c_2 \varepsilon_{xz}^2) - \frac{1}{2}(1 + 2c_2^R)M_z \dot{\gamma}, \quad (44)$$

$$-\frac{\partial}{\partial t}M_z = b^D M_z (\alpha + \beta \mathbf{M}^2 + 4c_2 \varepsilon_{xz}^2) - b^D \mu_0 H + \frac{1}{2}(1 - 2c_2^R)M_x \dot{\gamma} = 0, \quad (45)$$

where we have neglected γ_2 , since it provided only corrections to the main results in the static shear strain case, and we expect the same for the presence of a shear flow. The couplings provided by the coefficient d_2 are comparable and are also neglected. We also take $b^R = 0$, which ensures that the orientation of the magnetization (of the chains) does not deviate from the shear plane. Equations (44) and (45) are equivalent to those studied by Liu's group^{47,48} for magnetic liquids (where $\varepsilon_{xz} = 0$), when we use the identification $2c_2^R = \lambda_2$ and take $\beta = 0$.

For the elastic degree of freedom, we get

$$-\frac{\partial}{\partial t}\varepsilon_{xz} = \frac{4c_2}{\tau_2}\varepsilon_{xz} - \frac{1}{2}\dot{\gamma}. \quad (46)$$

Finally, the total stress tensor, the momentum density current in Eq. (10) not only contains the elastic stress tensor ψ_{ij} [Eq. (8)] but also the dissipative and reversible phenomenological parts σ_{ij}^D [Eq. (17)] and σ_{ij}^R [Eq. (23)]. It is given by

$$-\sigma_{xz}^{\text{tot}} = \nu_2 \dot{\gamma} + 2c_2 M^2 \varepsilon_{xz} + \frac{1}{2}(1 - 2c_2^R)\mu_0 H M_x + 2c_2^R M_x M_z (\alpha + \beta \mathbf{M}^2 + 4c_2 \varepsilon_{xz}^2) \quad (47)$$

and will be needed to set up the stress-strain rate relations, i.e., the apparent viscosity in Sec. IV A and the complex shear modulus in Sec. IV B.

A. Steady shear flow

In this section, we are only interested in stationary solutions of the dynamic equations. In that case, the left-hand sides of Eqs. (44)–(46) are zero. This immediately allows us to relate the stationary shear strain to the applied shear flow

$$\varepsilon_{xz} = \varepsilon_{zx} = \frac{\dot{\gamma}\tau_2}{8c_2}. \quad (48)$$

Of course, a stationary strain is only possible for a relaxing strain variable, while for permanent elasticity, the strain would increase indefinitely, when a constant flow is applied. Equation (48) represents the stationary balance between the increasing strain due to the shear flow and its relaxation due to the microscopic redistribution of the particles.

With this result, Eqs. (44) and (45) can be solved for the magnetization components M_x and M_z as functions of $\dot{\gamma}$ and H . This can only be done numerically due to the nonlinearities involved.

In Fig. 7, the shear stress Eq. (47) is plotted as a function of the shear rate for different values of the field. We also study the apparent viscosity, defined by

$$\eta = \frac{-\sigma_{xz}^{\text{tot}}}{\dot{\gamma}}. \quad (49)$$

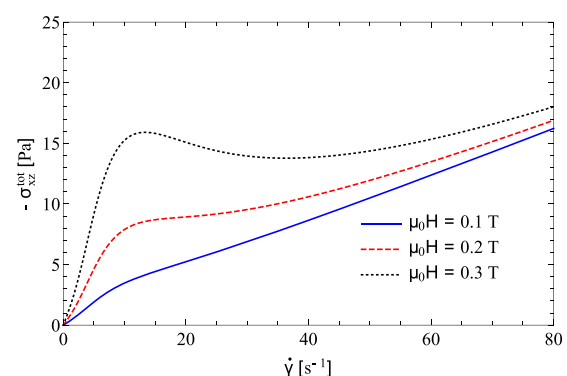


FIG. 7. The shear stress $-\sigma_{xz}^{\text{tot}}$ as a function of the steady shear rate at three different values of the applied magnetic field.

There are basically three regimes. For very small shear rates, there is a steep linear increase in the stress and the slope (apparent viscosity η) strongly depends on the magnetic field. At very high shear rates, there is another (almost) linear stress increase, which is much smaller than in the initial regime and is, for very large shear rates, field independent. In between, the transition region shows a peak structure for higher magnetic fields. Reducing the external field, the peaklike structure diminishes until it simply denotes the transition between the low and high shear rate regimes. A peak structure, which gives rise to a local minimum at intermediate shear rates, can be explained by the induced elastic stress, described by the second term in Eq. (47). Initially, this stress increases linearly with the shear rate, which results in a steep initial slope of the flow curve [Eq. (50)]. At higher shear rates, the magnetization modulus starts to decrease inversely with the square of the shear rate, which decreases the elastic stress contribution toward zero. If the applied magnetic field is large enough, a peak structure will be observed.

The initial slope for small $\dot{\gamma}$ can be written approximately

$$\eta_{in} = \nu_2 + \left(\frac{1}{4} \tau_2 + \frac{(1 + 2c_2^R)^2}{4b^D} \right) M_0^2, \quad (50)$$

where $M_0 = \mu H_0 / \alpha$ and ν_2 is the viscosity (without field) due to the carrier fluid and the magnetizable particles suspended in it. The initial slope η_{in} strongly increases with the external field, which is a prediction that could be tested in experiments. This is because shear flow reorients the columns of magnetizable particles due to the reversible coupling between flow and the magnetization via c_{ijk}^R [Eq. (27)]. The z-component of the magnetization is basically given by the magnetic field resulting in the field dependence of η_{in} . This effect is even bigger for smaller values of b^D , i.e., when the relaxation time of the magnetization is longer. This is the magnetic field dominated regime.

At a very high shear rate, the hydrodynamic regime is reached. Here, the influence of the magnetic field on the slope η diminishes and finally, for $\dot{\gamma} \rightarrow \infty$, the flow curves converge to the same line, $-\sigma_{xz}^{\text{tot}} = \nu_2 \dot{\gamma}$.

In the transition region, the stress obtains its (dynamic) yield stress value, $-\sigma_{xz}^0$, which is the stress needed to sustain flow.

There is some arbitrariness in the definition of the yield stress. Usually, it is read off from stress-strain relations as in Fig. 7 by extrapolating the high strain rate curves to zero strain rate. Or one could use as the yield stress the peak of the shear stress, or the shoulder, where the initial linear behavior turns into the final one. We determine this transition point as the shear rate at which the total shear stress, with the viscous contribution $\sim \nu_2$ subtracted, i.e., $-\sigma_{xz}^{\text{tot}} - \nu_2 \dot{\gamma}$, attains a maximum. The dynamic yield stress is shown in Fig. 8 to be a quadratic function of the external field, $-\sigma_{xz}^0 = \Xi (\mu_0 H)^2$ with $\Xi \approx 150 \text{ A}^2 \text{ Pa}^{-1} \text{ m}^{-2}$.

We have used the same set of parameters as in Sec. III, discussing the static deformations. It should be noted that a higher value of the yield stress may be obtained by using, for example, lower values of α , which as a consequence increases the magnetic susceptibility. This stress also increases with increasing b^D , while the dependence of the yield stress on τ_2 increases for low values and then starts to decrease for larger values of τ_2 .

Beyond the initial steep rise, the shear stress is often described approximately by a Bingham model

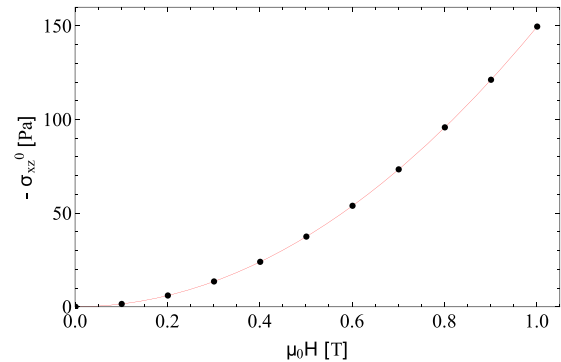


FIG. 8. The yield shear stress $-\sigma_{xz}^0$ as a function of the magnetic field.

$$-\sigma_{xz} = -\sigma_{xz}^0 + \eta_{\infty} \dot{\gamma}, \quad (51)$$

where a Newtonian viscous contribution is combined with the yield stress $-\sigma_{xz}^0$. Real MR fluids generally deviate from the Bingham model, in particular, for higher magnetic fields. Somewhat better fits to the experimental data can be achieved by using the so called Casson or Herschel-Bulkley models,⁵⁵ which are frequently more suitable for flow curves that are not linear. In Fig. 9, it is shown, for the highest field case, that the apparent viscosity in our description is lower than in the Bingham model, demonstrating shear thinning. This effect is smaller for intermediate fields and almost invisible for low fields. This is in accordance with experimental findings, where the Mason number^{40,56} is often found to be slightly lower than 1, indicating shear thinning.⁵⁷⁻⁶³ We mention that a model that takes into account the anisotropy together with the additional dynamic interplay of the relative rotations between the magnetization and the elastic network may produce a stress-strain curve that is closer to the Bingham model, Eq. (51). Another possibility is to consider the 2-fluid description of the magnetizable particulate phase and the solvent, but this is beyond the scope of this work.

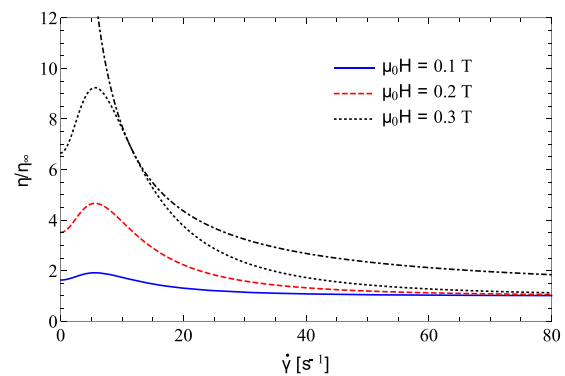


FIG. 9. The apparent viscosity η , scaled by η_{∞} , as a function of the shear rate for three different values of the applied magnetic field. Bingham behavior is shown as a dashed-dotted line for the high field case. The shear thinning of the apparent viscosity at intermediate shear rates compared to the Bingham model is obvious. For $\dot{\gamma} \rightarrow \infty$, all curves converge at $\eta/\eta_{\infty} \rightarrow 1$.

B. Oscillatory shear flow

In this section, we study the viscoelastic properties of MR fluids in the linear response regime. We impose an oscillatory deformation along the x axis, $\mathbf{v}(z) = \dot{\gamma} e^{-i\omega t} z \hat{\mathbf{e}}_x + c.c.$, with ω being the frequency of the oscillation and where $c.c.$ denotes the complex conjugate. A measure of the viscoelastic properties is the complex shear modulus $G = G' + iG''$, defined as the ratio of the shear stress σ_{xz}^{tot} [Eq. (47)] and the imposed strain $-\gamma \equiv \dot{\gamma}/i\omega$, $G = \sigma_{xz}^{tot}/\gamma$. The real, G' , and the imaginary part, G'' , are the storage and the loss modulus, describing the reactive and dissipative response, respectively. We note that γ is not identical to the Γ of Sec. III, as can be seen from Eq. (46).

To calculate the complex shear modulus, we linearize Eqs. (44)–(46) around equilibrium, where the strain field ε_{ij} is zero and the magnetization points along the z axis, $\mathbf{M} = M_0 \hat{\mathbf{e}}_z$, with $M_0 = \mu_0 H/\alpha$ for low magnetic fields. For the relevant variables M_x , M_z , and ε_{xz} , we use the ansatz $M_x = M_x^{(0)} e^{-i\omega t} + c.c.$, $M_z = M_0 + (M_z^{(0)} e^{-i\omega t} + c.c.)$, and $\varepsilon_{xz} = \varepsilon_{xz}^{(0)} e^{-i\omega t} + c.c.$, with $M_x^{(0)}$, $M_z^{(0)}$, and $\varepsilon_{xz}^{(0)}$ being the corresponding amplitudes, which are, in general, complex quantities. The frequency is assumed to be sufficiently small so that the linear velocity profile is established at any time.

The characteristic time scales are $\tau_{el} = \tau_2/(4c_2)$, corresponding to the relaxing strain, and $\tau_m = 1/(b^D \alpha)$, corresponding to the magnetization relaxation. For the parameter values used in this section, the time scales are almost equal, $\tau_{el} \lesssim \tau_m$.

Experimental results^{63–65} show that the storage modulus is considerably larger than the loss modulus at intermediate frequencies and that both increase with increasing magnetic field, which we could qualitatively reproduce (see Fig. 10). This means that the system behaves more like a solid than a liquid, which is expected, since a small amplitude shear oscillation can only slightly influence the strength of the columns. For smaller frequencies, the numerical results show that the system behaves, as expected, more like a liquid than a solid (Fig. 10).

For low frequencies, the storage modulus increases quickly with frequency and then saturates for larger frequencies.^{64,65} This can be seen in Fig. 10. The initial rise of the storage modulus is quadratic in the frequency

$$G' \approx \left(\frac{\alpha}{4} (1 + 2c_2^R)^2 \tau_m^2 + c_2 \tau_{el}^2 \right) M_0^2 \omega^2, \quad (52)$$

while for larger frequencies, the plateau value

$$G'_\infty = \left(\frac{\alpha}{4} (1 + 2c_2^R)^2 + c_2 \right) M_0^2 \quad (53)$$

is reached. The increase in the storage modulus at low frequencies is not reported often, which is either because many of the experiments have not gone quite to the low frequency regime, or the characteristic frequency where one observes such an effect, is not experimentally accessible for many setups. In Ref. 64, a saturation of the storage modulus is observed at a frequency of about 1 Hz.

The loss modulus, on the other hand, has a slightly more complicated behavior. Theoretical results show that the loss modulus increases linearly for low frequencies

$$G'' \approx \eta_{in} \omega, \quad (54)$$

where η_{in} is the initial slope of the steady shear stress [Eq. (50)]. After a maximum, it starts to decrease, and at intermediate frequencies, it

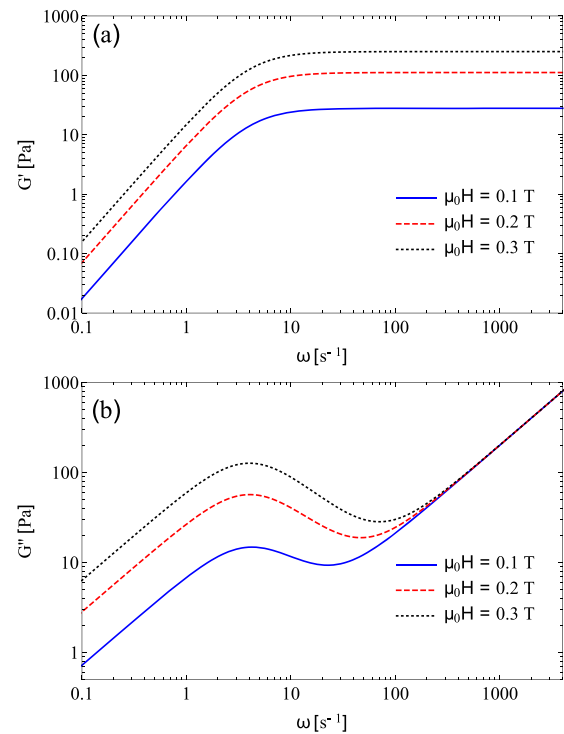


FIG. 10. (a) Storage modulus G' and (b) loss modulus G'' as a function of the frequency at three different values of the applied magnetic field.

passes a minimum before it increases, finally. The location of the maximum is at

$$\omega_{\max} \approx 1/\tau_{el} \quad (55)$$

and is independent of the magnetic field.

The minimum of the loss modulus at intermediate frequencies shifts to larger frequencies as one increases the magnetic field [Fig. 10(b)], which is detected in certain experiments.^{63,64} For $\omega^2 \tau_m^2 \gg 1$ and $\omega^2 \tau_{el}^2 \gg 1$, the minimum is at

$$\omega_{\min} \approx \frac{M_0}{\sqrt{v_2}} \sqrt{\frac{4c_2^2}{\tau_2} + \frac{1}{4} (1 + 2c_2^R)^2 b^D \alpha^2}, \quad (56)$$

where the frequency of the minimum ω_{\min} shifts linearly with the field.

The final, asymptotic behavior of the loss modulus for $\omega \rightarrow \infty$ is described by the viscosity v_2 ,

$$G'' \simeq v_2 \omega. \quad (57)$$

The maximum of the loss modulus at small frequencies has not been reported often, perhaps due to the experimental limitations at lower frequencies. There are certain indications that such a maximum exists.⁶⁵

We found that a simple relation exists for the master curves g' and g'' of G' and G'' , respectively. The storage modulus has to be rescaled by a factor of $\mu_0 H^2$, $g'(\omega) = G'(\omega)/\mu_0 H^2$, while the viscosity term needs to be subtracted first in the loss modulus, $g''(\omega) = (G''(\omega) - v_2 \omega)/\mu_0 H^2$. The storage and the loss moduli can be at any given

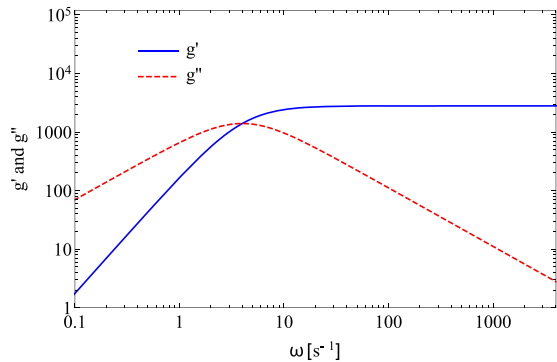


FIG. 11. The master curves g' and g'' as a function of the frequency ω corresponding to the storage G' and the loss modulus G'' , respectively.

magnetic field H reduced exactly to the curves $g'(\omega)$ and $g''(\omega)$, which is not surprising because all contributions in the stress tensor [Eq. (47)] apart from the viscosity term $\sim \nu_2$, are proportional to the square of the magnetic field. Since the characteristic time scales τ_m and τ_{el} are independent of the magnetic field, the master curves are obtained without the need to rescale the frequency variable (Fig. 11).

We now discuss the dependence of the absolute value of the complex shear modulus $|G| = \sqrt{(G')^2 + (G'')^2}$ on the frequency. After the initial linear increase, governed by the loss modulus [Eq. (54)], there is a plateau at intermediate frequencies, which is basically given by the plateau of the storage modulus G'_∞ [Eq. (53)], since the loss modulus G'' is much smaller there. For high frequencies, the loss modulus is dominating again and $|G|$ increases according to Eq. (57). This final increase is best visible in Fig. 12 for low fields.

This scenario applies to the case of (almost) equal elastic and magnetic time scales. If these time scales are sufficiently well separated, a somewhat different behavior of $|G|$ is found (Fig. 13). After the very steep initial rise, a very narrow plateau is found at rather low frequencies, which is approximately of height $c_2 M_0^2$ (for $\tau_{el} \ll \tau_m$) and $\frac{1}{4}(1 + 2c_2^R)^2 \alpha M_0^2$ (for $\tau_{el} \gg \tau_m$). At intermediate frequencies, $|G|$

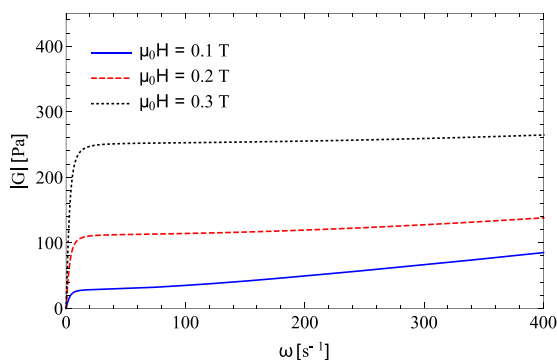


FIG. 12. $|G|$ as a function of the frequency at three different values of the applied magnetic field.

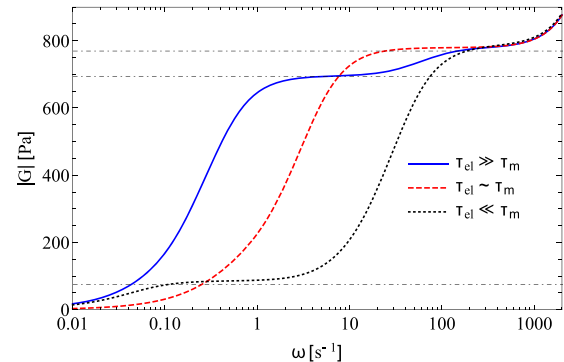


FIG. 13. Shear modulus $|G|$ as a function of the frequency in a semilog plot at $\mu_0 H = 0.5$ T for three different (arbitrary) choices of the time scales τ_{el} and τ_m . The light black dashed horizontal lines denote the values of the plateaus for the different cases. To enhance the visibility of the lowest plateau, $c_2^R = 4$ has been chosen in this plot.

gently increases to the combined plateau G'_∞ [Eq. (53)] and finally converges to the asymptotic behavior independent of the relaxation times.

In polymer dynamics, the empirical Cox-Merz rule is often very well fulfilled. It allows us to estimate shear stresses when a steady shear is imposed from data obtained by small amplitude oscillatory strain rate experiments. This rule states that at a given frequency ω , the modulus $|G|$ is identical to the shear stress, $-\sigma_{xz}^{tot}$, under a steady shear rate $\dot{\gamma} = \omega$. It is trivially fulfilled for $\dot{\gamma} \rightarrow \infty$ and $\omega \rightarrow \infty$, where $|G| \propto \nu_2 \omega$ and $-\sigma_{xz}^{tot} \propto \nu_2 \dot{\gamma}$. Similarly, for very small ω , $|G| \approx G'' \sim \omega$ [Eq. (54)] increases the same way as $-\sigma_{xz}^{tot} \sim \dot{\gamma}$. Applying the Cox-Merz rule to the yield shear stress, however, would lead to

$$-\sigma_{xz}^0 = \left(\frac{(1 + 2c_2^R)^2}{4} + \frac{c_2}{\alpha} \right) \alpha M_0^2 \approx 2800 (\mu_0 H)^2 \quad (58)$$

for the stationary yield stress, which is, though, much larger than the value of $150 (\mu_0 H)^2$ found in Sec. IV A (Fig. 9). This shows that the Cox-Merz rule is not obeyed in MR fluids. This difference is probably due to the columnar structures, which are not destroyed in the small amplitude oscillatory shear, but are destroyed in steady shear. Equations (56) and (58) can be used to determine the dynamic coefficients c_2^R , b^D , and τ_2 or serve as an additional method to determine the static parameter c_2 .

V. SUMMARY AND PERSPECTIVE

In this study, a simple macroscopic model for the MR fluids has been proposed. We tested the model on several simple experimental configurations, such as the influence of a magnetic field or a normal pressure on the static shear deformations as well as simple shear flow in the steady and the oscillatory regime.

In order to model the effects of the chains of magnetizable particles, which are observed in experiments, and to capture the solidlike properties, we included as the macroscopic variables the magnetization and the strain field. We have shown that the inclusion of these variables well explains certain experimental facts, such

as the existence of a static yield stress or the influence of a normal pressure on the static yield stress. We have successfully reproduced the quadratic field dependence of the static yield stress with the appropriate critical strain being independent of the magnetic field. This was made possible by a (quadratic) dependence of the elastic moduli on the magnetization, which is motivated by the fact that the solidlike properties of MR fluids are due to the magnetic field.

Furthermore, we probed the dynamics of our model by investigating the stresses that arise by applying a shear flow. Here, our assumption that the strain relaxation coefficients are proportional to the magnetization squared comes into play, which is motivated by the fact that the elastic network relaxes on longer time scales in larger magnetic fields. First, we applied a stationary shear flow, leading to the flow curves describing the shear stress as a function of the shear rate. For intermediate values of the shear rate, a maximum, the dynamic yield stress, was obtained and the flow curve could almost be described by the Bingham law. However, deviations were found indicating shear thinning, in particular, for higher magnetic fields.

We also studied the effects of an imposed oscillatory shear flow. We showed that the complex shear modulus as a function of the frequency exhibits a plateau. The values of the plateau are related to the elastic shear modulus or to the hydrodynamic coupling between magnetization and flow, or to both, depending on whether the elastic relaxation time is much larger, or much smaller, or almost equal to the magnetic relaxation time, respectively. Applying the Cox-Merz rule, which compares the plateau regime with the dynamic yield stress of the stationary case, revealed that the Cox-Merz rule is not fulfilled by our model.

We derive equations and present expressions that can be used for measuring certain phenomenological coefficients. Examples are the elastic and magnetostriction coefficients, which could be determined from measurements of the stress-strain curves and the maximum tilt angles of the chains. We also discuss the possibilities to determine the dynamic coefficients by measuring, for example, the initial slope of the stress as a function of the shear rate, the shift of the minimum in the loss modulus G'' as a function of the magnetic field, or by measuring the plateau values of the shear modulus $|G|$. We have also shown that a simple master curve may be generated for the storage and the loss modulus.

In the next step, it is desirable to capture various aspects of pattern formation in MR fluids. Examples of these patterns include the formation of the columns themselves, the thickening of the columns under a pressure force,⁶⁶ the stripe formation under shear flow,^{67–69} or structures formed in a rotating magnetic field.⁷⁰ A macroscopic 2-fluid model has been presented in Ref. 71, but has never been applied to magnetic systems such as MR fluids. In this case, one would model the MR fluid with the solvent phase and the particle phase as two separate fluid phases.

As a perspective, we mention the generalizations to large magnetic fields for which the approximation used in the present no longer applies. In addition, the role of relative rotations between the magnetization, M_x , and the elastic matrix should also be investigated. Relative rotations could also contribute to the tilting of the chains, complementing the magnetostrictive effects discussed in Sec. III A.

ACKNOWLEDGMENTS

We thank one of the referees for asking about the existence of the master curve in the dynamic oscillatory shear flow. Partial support of this work through the Schwerpunktprogramm SPP 1681 “Feldgesteuerte Partikel-Matrix-Wechselwirkungen: Erzeugung, skalenübergreifende Modellierung und Anwendung magnetischer Hybridmaterialien” of the Deutsche Forschungsgemeinschaft is gratefully acknowledged, as well as the support of the Slovenian Research Agency, Grant No. P1-0055 (D.S.).

REFERENCES

- 1 J. Rabinow, *Trans. Am. Inst. Electr. Eng.* **67**, 1308 (1948).
- 2 B. J. Park, F. F. Fang, and H. J. Choi, *Soft Matter* **6**, 5246 (2010).
- 3 J. de Vicente, D. Klingenberg, and R. Hidalgo-Alvarez, *Soft Matter* **7**, 3701 (2011).
- 4 A. Zubarev, L. Iskakova, M. T. Lopez-Lopez, P. Kuzhir, and G. Bossis, *J. Rheol.* **58**, 1673 (2014).
- 5 J. A. Ruiz-Lopez, J. C. Fernandez-Toledano, D. J. Klingenberg, R. Hidalgo-Alvarez, and J. de Vicente, *J. Rheol.* **60**, 61 (2016).
- 6 G. Bossis, O. Volkova, Y. Grasselli, and A. Cifreio, *Front. Mater.* **6**, 4 (2019).
- 7 J. M. Ginder and L. C. Davis, *Appl. Phys. Lett.* **65**, 3410 (1994).
- 8 J. M. Ginder, in *Encyclopedia of Applied Physics*, edited by G. L. Trigg (VCH, Weinheim, 1996), Vol. 16, p. 487.
- 9 G. Bossis, E. Lemaire, O. Volkova, and H. Clercx, *J. Rheol.* **41**, 687 (1997).
- 10 G. Bossis, O. Volkova, S. Laci, and A. Meunier, *Lect. Notes Phys.* **594**, 202 (2002).
- 11 D. J. Klingenberg and C. F. Zukoski, *Langmuir* **6**, 15 (1990).
- 12 G. L. Gulley and R. Tao, *Phys. Rev. E* **48**, 2744 (1993).
- 13 T. C. Halsey, J. E. Martin, and D. Adolf, *Phys. Rev. Lett.* **68**, 1519 (1992).
- 14 S. Melle and J. E. Martin, *J. Chem. Phys.* **118**, 9875 (2003).
- 15 J. E. Martin, J. Odinek, T. C. Halsey, and R. Kamien, *Phys. Rev. E* **57**, 756 (1998).
- 16 R. T. Bonnecaze and J. F. Brady, *J. Chem. Phys.* **96**, 2183 (1992).
- 17 P. O. Brunn and B. Abu-Jdayil, *Z. Angew. Math. Mech.* **78**, 97 (1998).
- 18 Y. M. Shkel and D. J. Klingenberg, *J. Rheol.* **43**, 1307 (1999).
- 19 A. T. Horvath, D. J. Klingenberg, and Y. M. Shkel, *Int. J. Mod. Phys. B* **16**, 2690 (2002).
- 20 R. E. Rosensweig, *J. Rheol.* **39**, 179 (1995).
- 21 J. W. Zhang, X. Q. Gong, C. Liu, W. Wen, and P. Sheng, *Phys. Rev. Lett.* **101**, 194503 (2008).
- 22 P. Sheng and W. Wen, *Solid State Commun.* **150**, 1023 (2010).
- 23 K. von Pfeil, M. D. Graham, D. J. Klingenberg, and J. F. Morris, *Phys. Rev. Lett.* **88**, 188301 (2002).
- 24 K. von Pfeil, M. D. Graham, D. J. Klingenberg, and J. F. Morris, *J. Appl. Phys.* **93**, 5769 (2003).
- 25 K. von Pfeil and D. J. Klingenberg, *J. Appl. Phys.* **96**, 5341 (2004).
- 26 H. Pleiner and H. R. Brand, “Hydrodynamics and electrohydrodynamics of nematic liquid crystals,” in *Pattern Formation in Liquid Crystals*, edited by A. Buka and L. Kramer (Springer, New York, 1996).
- 27 W. E. Isler and D. Y. Chung, *J. Appl. Phys.* **49**, 1812 (1978).
- 28 H. Pleiner and H. R. Brand, *J. Magn. Magn. Mater.* **85**, 125 (1990).
- 29 H. R. Brand and H. Pleiner, *Phys. Rev. Lett.* **86**, 1385 (2001).
- 30 A. Menzel, H. Pleiner, and H. R. Brand, *J. Appl. Phys.* **105**, 013503 (2009).
- 31 A. Menzel, H. Pleiner, and H. R. Brand, *Eur. Phys. J. E* **30**, 371 (2009).
- 32 E. Jarkova, H. Pleiner, H.-W. Müller, and H. R. Brand, *Phys. Rev. E* **68**, 041706 (2003).
- 33 S. Bohlius, H. R. Brand, and H. Pleiner, *Phys. Rev. E* **70**, 061411 (2004).
- 34 H. Temmen, H. Pleiner, M. Liu, and H. R. Brand, *Phys. Rev. Lett.* **84**, 3228 (2000).
- 35 H. Pleiner, M. Liu, and H. R. Brand, *Rheol. Acta* **39**, 560 (2000).
- 36 H. R. Brand, H. Pleiner, and D. Savenšek, *Rheol. Acta* **57**, 773 (2018).

- ³⁷S. R. de Groot and P. Mazur, *Nonequilibrium Thermodynamics* (North Holland, Amsterdam, 1962).
- ³⁸W. H. Li, H. Du, G. Chen, and S. H. Yeo, *Mater. Sci. Eng. A* **333**, 368 (2002).
- ³⁹J. Claracq, J. Sarrazin, and J.-P. Montfort, *Rheol. Acta* **43**, 38 (2004).
- ⁴⁰Y. Otsubo and K. Edamura, *J. Rheol.* **38**, 1721 (1994).
- ⁴¹Z. Wang, K. Shahrivar, and J. de Vicente, *J. Rheol.* **58**, 1725 (2014).
- ⁴²K. D. Weiss, J. D. Carlson, and D. A. Nixon, *J. Intell. Mater. Syst. Struct.* **5**, 772 (1994).
- ⁴³B. D. Chin, J. H. Park, M. H. Kwon, and O. O. Park, *Rheol. Acta* **40**, 211 (2001).
- ⁴⁴Y. Yang, L. Li, and G. Chen, *Rheol. Acta* **48**, 457 (2009).
- ⁴⁵S. S. Deshmukh and G. H. McKinley, in Proceedings of XIVth International Congress on Rheology, Seoul, South Korea, August 2004.
- ⁴⁶H. W. Müller and M. Liu, *Phys. Rev. E* **64**, 061405 (2001).
- ⁴⁷O. Müller, D. Hahn, and M. Liu, *J. Phys.: Condens. Matter* **18**, S2623 (2006).
- ⁴⁸S. Mahle, P. Ilg, and M. Liu, *Phys. Rev. E* **77**, 016305 (2008).
- ⁴⁹S. Odenbach and H. W. Müller, *Phys. Rev. Lett.* **89**, 037202 (2002).
- ⁵⁰S. Odenbach and H. W. Müller, *J. Magn. Magn. Mater.* **289**, 242 (2005).
- ⁵¹X. Tang, X. Zhang, R. Tao, and Y. M. Rong, *J. Appl. Phys.* **87**, 2634 (2000).
- ⁵²X. Z. Zhang, X. L. Gong, P. Q. Zhang, and Q. M. Wang, *J. Appl. Phys.* **96**, 2359 (2004).
- ⁵³S. A. Mazlan, N. B. Ekreem, and A. G. Olabi, *J. Mater. Process. Technol.* **201**, 780 (2007).
- ⁵⁴H. Wang, D. Cheng, J. Kan, C. Gao, and W. Ziao, *J. Intell. Mater. Syst. Struct.* **22**, 811 (2011).
- ⁵⁵D. Susan-Resiga, *J. Intell. Mater. Syst. Struct.* **20**, 1001 (2007).
- ⁵⁶D. J. Klingenberg, J. C. Ulicny, and M. A. Golden, *J. Rheol.* **51**, 883 (2007).
- ⁵⁷D. W. Felt, M. Hagenbuchle, J. Liu, and J. Richard, *J. Intell. Mater. Syst. Struct.* **7**, 589 (1996).
- ⁵⁸B. J. de Gans, H. Hoekstra, and J. Mellema, *Faraday Discuss.* **112**, 209 (1999).
- ⁵⁹O. Volkova, G. Bossis, M. Guyot, V. Bashtovoi, and A. Reks, *J. Rheol.* **44**, 91 (2000).
- ⁶⁰Y. D. Liu, F. F. Fang, and H. J. Choi, *Colloid Polym. Sci.* **289**, 1295 (2011).
- ⁶¹Y. Rabbani, M. Ashtiani, and S. H. Hashemabadi, *Soft Matter* **11**, 4453 (2015).
- ⁶²Y. Fu, J. Yao, H. Zhao, G. Zhao, Z. Wan, and Y. Qiu, *Smart Mater. Struct.* **27**, 125001 (2018).
- ⁶³J. H. Lee, Q. Lu, J. Y. Lee, and H. J. Choi, *Polymers* **11**, 219 (2019).
- ⁶⁴G. Wang, Y. Ma, G. H. Cui, N. N. Li, and X. F. Dong, *Soft Matter* **14**, 1917 (2018).
- ⁶⁵I. Arief and P. K. Mukhopadhyay, *J. Alloys Compd.* **696**, 1053 (2017).
- ⁶⁶R. Tao, *J. Phys.: Condens. Matter* **13**, R979 (2001).
- ⁶⁷S. Cutillas and G. Bossis, *Eur. Phys. Lett.* **40**, 465 (1997).
- ⁶⁸S. Cutillas, G. Bossis, and A. Cebers, *Phys. Rev. E* **57**, 804 (1998).
- ⁶⁹O. Volkova, S. Cutillas, P. Carletto, G. Bossis, A. Cebers, and A. Meunier, *J. Magn. Magn. Mater.* **201**, 66 (1999).
- ⁷⁰P. Carletto, G. Bossis, and A. Cebers, *Int. J. Mod. Phys. B* **16**, 2279 (2002).
- ⁷¹H. Pleiner and J. L. Harden, *AIP Conf. Proc.* **708**, 46 (2004); e-print [arXiv:cond-mat/0404134](https://arxiv.org/abs/cond-mat/0404134).

Acknowledgement

- First of all, I would like to thank prof. dr. Helmut Brand for offering me the opportunity to work with him. I appreciate that you always had time and patience to discuss science with me. I thank you for sharing with me your enthusiasm for physics and also for caring for my scientific career. I also thank you for your help with the bureaucracy, especially with all the documents I had to fill in at the beginning of my stay.
- Second, I would like to thank prof. dr. Harald Pleiner. I benefited very much from your constructive comments on the projects we did. They shined a light on the problem from a different perspective, from which I was able to put the missing pieces together. Thank you also for inviting me to the Max Planck Institute in Mainz to give a seminar.
- Third I thank prof. dr. Daniel Svehšek. I feel extremely lucky to have met you already when I was an undergraduate. Each discussion I had with you was very fruitful and after them I always felt more enthusiastic and enlightened on how to see the big picture.
- They say that in science one should stand on the shoulders of giants. I had the privilege to work with three of them.
- I also thank priv.-doz. dr. Andreas Menzel for many stimulating discussions and for being the Zweitgutachter of my thesis. It was always a great pleasure for me to listen to your excellent talks at various conferences.
- Next, I thank the Deutsche Forschungsgemeinschaft for financial support through the Schwerpunktprogramm SPP 1681.
- I thank Claudia Brandt for taking care of the bureaucracy with the trips to various scientific conferences and also with my work contract.
- I have to express my gratitude to my neighbor Lili Mravlja for helping me with the German version of the abstract.
- Finally, I thank my family for their support and understanding. I also thank my wife Jasmina Potisk for her constant encouragement and emotional support.

Erklärung

Hiermit versichere ich an Eides statt, dass ich die vorliegende Arbeit selbständig verfasst und keine anderen als die von mir angegebenen Quellen und Hilfsmittel verwendet habe.

Weiterhin erkläre ich, dass ich die Hilfe von gewerblichen Promotionsberatern bzw. -vermittlern oder ähnlichen Dienstleistern weder bisher in Anspruch genommen habe, noch künftig in Anspruch nehmen werde.

Zusätzlich erkläre ich hiermit, dass ich keinerlei frühere Promotionsversuche unternommen habe.

Bayreuth, den _____

Tilen Potisk